Author:
McCann, Cassandra

Title:
Coordination chemistry and ethene oligomerisation catalysis with new ligands containing a PNP backbone

Coordination chemistry and ethene oligomerisation catalysis with new ligands containing a PNP backbone

By
Cassandra McCann

A thesis submitted to the University of Bristol in accordance with the requirements for the degree of Doctor of Philosophy in the School of Chemistry, Faculty of Science.

September 2004

Abstract

The following series of ligands is reported: $Ph_2PN(Et)PPh_2$ ($\mathbf{L^1}$), $Ph_2PN(n\text{-}Pr)PPh_2$ ($\mathbf{L^2}$) and $Ph_2PN(i\text{-}Pr)PPh_2$ ($\mathbf{L^3}$), which were made from the corresponding $Cl_2PN(R)PCl_2$; a series of ligands with ether groups on the central nitrogen $Ph_2PN(CH_2CH_2OCH_3)PPh_2$ ($\mathbf{L^4}$), $Ph_2PN(CH_2CH_2CH_2OCH_3)PPh_2$ ($\mathbf{L^5}$) and $Ph_2PN(CH_2(2\text{-}OCH_3)C_6H_4)PPh_2$ ($\mathbf{L^6}$); ligands with *ortho*-substituted phenyls $(2\text{-}CF_3C_6H_4)_2PN(Me)P(2\text{-}CF_3C_6H_4)_2$ ($\mathbf{L^7}$), $(2\text{-}ClC_6H_4)_2PN(Me)P(2\text{-}ClC_6H_4)_2$ ($\mathbf{L^8}$), $((o\text{-}OCH_3C_6H_4)(C_6H_5))PN(Me)P((C_6H_5)(o\text{-}OCH_3C_6H_4))$ ($\mathbf{L^9}$); the diphosphoramidites ((*R*)-1,1′-bi-2-naphthoxo)PN(Me)P((*R*)-1,1′-bi-2-naphthoxo) ($\mathbf{L^{10}}$), (*S*)-9,9′-biphenanthryl-10,10′-dioxo)PN(Me)P((*S*)-9,9′-biphenanthryl-10,10′-dioxo) ($\mathbf{L^{11}}$), mixed *rac/meso* (9,9′-biphenanthryl-10,10′-dioxo)PN(Me)P(9,9′-biphenanthryl-10,10′-dioxo) ($\mathbf{L^{12}}$). All of these phosphines are characterised by a combination of NMR, mass spectrometry and elemental analysis. X-ray crystal structures of ($\mathbf{L^4}$), ($\mathbf{L^5}$), ($\mathbf{L^7}$), and ($\mathbf{L^{12}}$) are described.

The diphosphines $(2\text{-}CH_3C_6H_4)_2PCH_nP(2\text{-}CH_3C_6H_4)_2$ n = 1-3 have been reacted with [PtClMe(1,5-COD)] to give four-, five- or six-membered chelates. The phosphines ($\mathbf{L^1}$ – $\mathbf{L^3}$) were reacted with [PtClMe(1,5-COD)], ($\mathbf{L^4}$ – $\mathbf{L^7}$) with [PtClMe(1,5-COD)] and $[PdCl_2(NCPh)]$ and ($\mathbf{L^8}$, $\mathbf{L^{10}}$, $\mathbf{L^{11}}$) with $[PtCl_2(1,5\text{-}COD)]$, to give four-membered chelates. All platinum(II) and palladium(II) complexes were characterised by a combination of NMR, mass spectrometry, elemental analysis and in some cases X-ray crystal structure determination. A DFT study comparing the LUMO of $[NiH(Ph_2PCH_2PPh_2)]^+$ and $[NiH(Ph_2PNMePPh_2)]^+$ is also described.

The ligands ($\mathbf{L^1}$ – $\mathbf{L^{12}}$) were screened for Ni-catalysed ethylene oligomerisation activity using a *GreenHouse* reactor. A more detailed study of Ni-catalysed ethylene oligomerisation using an *Endeavor* reactor was carried out on the most active ligands ($\mathbf{L^8}$) and ($\mathbf{L^{10}}$). These were shown to yield butene and hexene as major products. The effect of adding hydrogen to the system was also investigated.

The ligands ($\mathbf{L^4}$ – $\mathbf{L^7}$, $\mathbf{L^9}$, $\mathbf{L^{10}}$) were tested for Cr-catalysed trimerisation using an *Endeavor* reactor. The results with ($\mathbf{L^9}$) showed 1-hexene to be the major product. With ($\mathbf{L^4}$ – $\mathbf{L^6}$) a Schulz-Flory distribution of oligomer was obtained with high activities. ($\mathbf{L^7}$) and ($\mathbf{L^{10}}$) were shown to be poor catalysts for ethylene trimerisation. The effect of addition of hydrogen was also investigated.

Acknowledgements

First and foremost I would like to thank Prof Paul Pringle for giving me the opportunity to undertake this PhD and all his ideas, help and general advice throughout the past three years. More particularly the lessons in grammar and the humorous storytelling of an evening down the pub.

I would also like to thank the crystallographers Angharad Baber and Katie Heslop for carrying out some of the crystal structures and the rest of the X-ray lab for answering my many simple questions, especially Ang, Mari, Dr John Jeffery and Dr J. Charmant. A thank you must go to Dr Jeremy Harvey for all his help with the molecular modelling. Thanks also to all the technicians who carried out mass specs, elemental analyses and NMR's, in particular Dr. Martin Murray, Rose, Paul, Tony and Adrian.

I am thankful to Dr. Stefan Spitzmesser at BP and Dr. Duncan Wass without whose help and advice the catalytic studies would never have been carried out or analysed. Also thanks to Stefan for the opportunity to visit Brussels and taste the fine selection of beers and chocolates.

The lab deserves a large thank you for keeping me so well entertained for three years, Lee, Matt C, Rich, Damaris, Paul M, Joelle, Matt W, Asli, Karl and Annie for supporting me from the start, helping me to settle in and enduring the bad days whilst celebrating the good. Thanks also to the newer members of the lab for providing entertaining (though drunken) nights out and life-saving tea breaks to lighten the dark hours of writing up. Also thanks to my project student Pip for synthesising a fantastic pink PNP ligand. I am indebted to Asli, Ruth, Debbie and Karl for carrying out the unenviable task of proof reading without any complaints.

Finally thank you to my Mum for the long afternoon chats when I was feeling down (and occasionally annoyed) and Dads for not minding the rather large phone bills incurred! Also thank you to Graham for giving me a desk to put my computer on, living with my grumpy moods over the past few months and making me happy.

Memorandum

The work described in this thesis was carried out at the University of Bristol between October 2001 and August 2004. Unless otherwise acknowledged in this text, it is the original work of the author and has not been previously submitted for a degree. In addition, any views expressed in this thesis are those of the author, and not of the University.

Cassandra McCann
University of Bristol
September 2004

Contents

Table of contents

Abbreviations

General

Ar	Aryl group
anisyl	*o*-methoxyphenyl
t-Bu	*t*-butyl
COD	1,5-cyclooctadiene
CHT	Cycloheptatriene
CH_2Cl_2	Dichloromethane
p-cym	4-isopropyltoluene
dba	Dibenzylideneacetone
dppp	Bis(diphenylphosphino)propane
ee.	Enantiomeric excess
Et	Ethyl
g	Gram (s)
GC	Gas chromatography
h	Hour (s)
L	Ligand
M	Metal
MAO	Methyl aluminiunoxane
MMAO	Modified methyl aluminiunoxane
Me	Methyl
MeCN	Acetonitrile

NMR Data

NMR	Nuclear Magnetic Resonance
δ	Chemical Shift (in ppm)
ppm	Parts per million
J	Coupling constant
Hz	Hertz
s	Singlet
d	Doublet
dd	Doublet of doublets
t	Triplet
q	Quartet
qt	Quartet of triplets
m	Multiplet
sept	Septet
br	Broad
$\{^1H\}$	Proton decoupled

MeOH	Methanol
min	Minute (s)
mol	Mole (s)
mmol	Millimole (s)
nbd	norbornadiene
o	Ortho
Ph	Phenyl
i-Pr	*i*-propyl
n-Pr	*n*-propyl
TEAL	Triethylaluminuim
THF	Tetrahydrofuran
o-tol	*Ortho*-tolyl
THI	[1,2-Bis(2-tetrahydroindenyl)ethane]$ZrCl_2$
TOF	Turnover frequency
TON	Turnover number

Mass Spectrometry Data

m/z	Mass/charge
CI	Chemical ionisation
EI	Electron impact
ESI	Electron spray ionisation
FAB	Fast atom bombardment

Chapter 1:

Introduction to the chemistry of PNP compounds

Introduction to the chemistry of PNP compounds

1.1 Scope of PNP compounds

The use of bidentate phosphines in co-ordination chemistry and catalysis is widespread and the great majority of those studied contain a hydrocarbon linkage between the phosphine moieties.[1] However, diphosphinoamines containing a nitrogen atom linking the two phosphorus atoms (**1.1**) are attracting considerable attention. They are versatile ligands[2] because the substituents can be varied on both the nitrogen and phosphorus atoms with subsequent changes in the PNP angle and conformation about the phosphorus centres.[3]

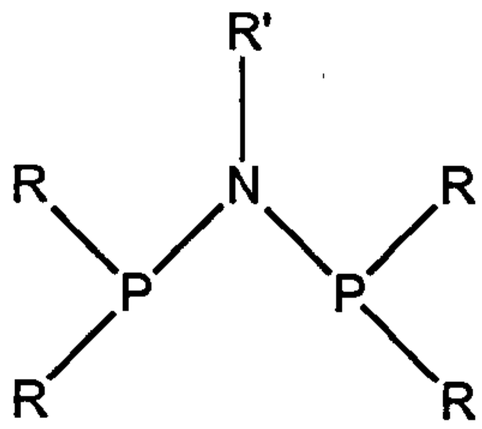

(1.1)

There are a variety of diphosphinoamines available with the substituents on the nitrogen (R′) being alkyl groups such as Me, Et, *n*-Pr, *i*-Pr or H, and the phosphorus substituents (R) being Cl, F, Ph.[4-6] Other PNP skeletons have been studied for example, iminodiphosphines (**1.2**) and bis(phosphine)hydrazines (**1.3**);[7, 8] iminodiphosphines have not been studied to the extent of diphosphinoamines due to their relative instability.[9]

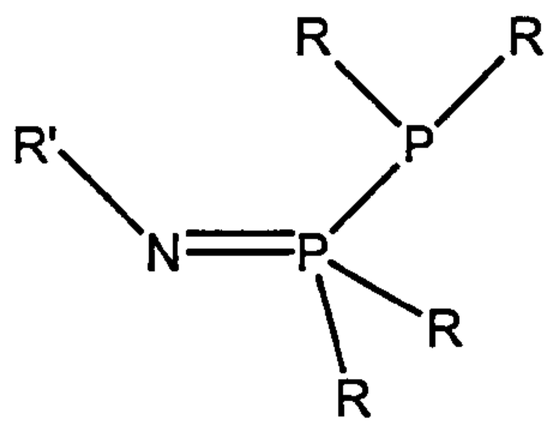

(1.2)

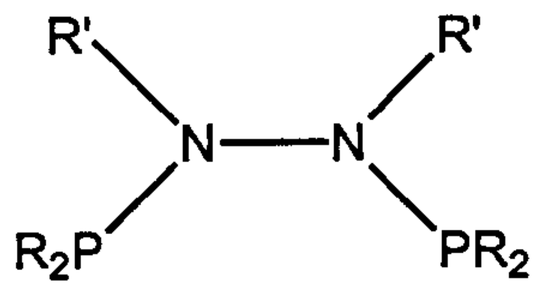

(1.3)

Another range of PNP ligands that have been synthesised contain a mixture of nitrogen and carbon links between the phosphorus atoms.

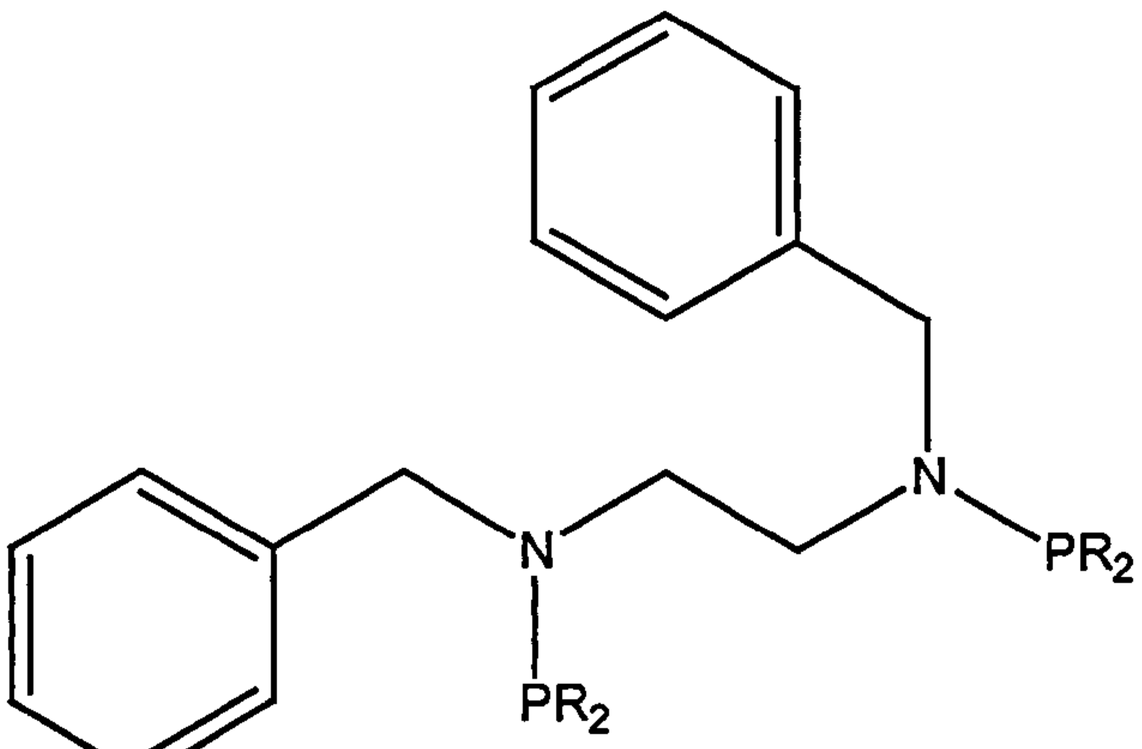

R = Ph, *i*-Pr

(1.4)

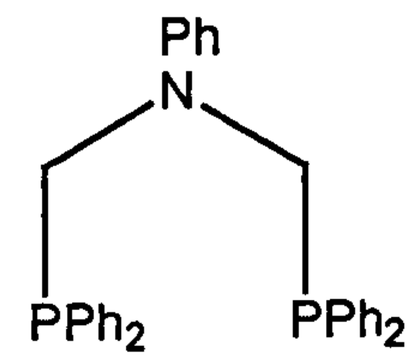

(1.5)

Compound **(1.4)** was tested for the Rh-catalysed hydroformylation of hex-1-ene, but poor linear to branched selectivity of 1.9:1 was observed.[10] Reetz and co-workers tested ligand **(1.5)** for the Rh-catalysed hydroformylation of 1-octene and high selectivity to the linear product 62:38 was observed.[11] A PNP ligand containing a bridging silyl group **(1.6)** has been synthesised by Woollins and co-workers.[12]

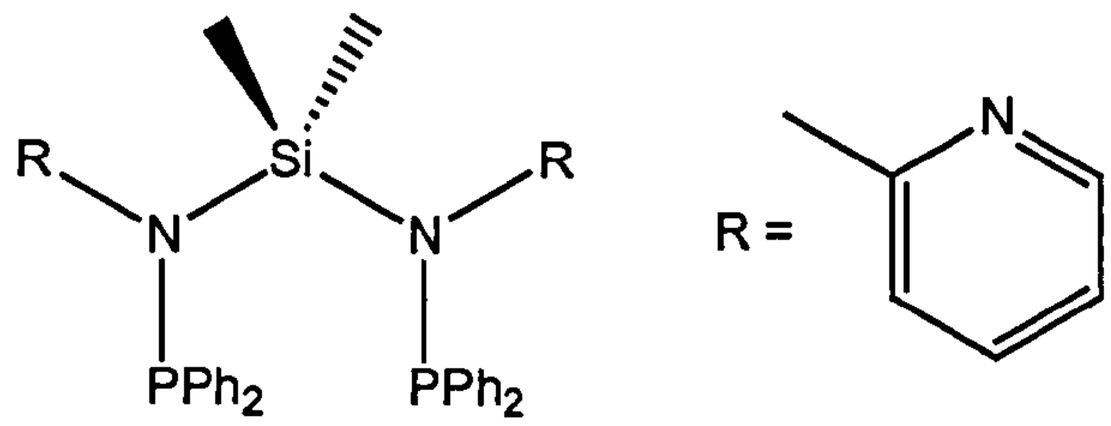

(1.6)

The diversity of PNP ligands is great and so this introduction will focus on derivatives of the basic PNP structure **(1.1)** but will also include phosphoramidites.

1.2 Chemistry of $Ph_2PNHPPh_2$

The synthesis of bis(diphenylphosphino)amine (dppa) $Ph_2PNHPPh_2$ was first reported in 1967 by Nöth and Meinel.[13] The preparation involves condensation of hexamethyldisilazane with chlorodiphenylphosphine, yielding dppa in 50% yield (Equation 1.1).

Equation 1.1

The chemistry of dppa has been investigated and compared to the isoelectronic bis(diphenylphosphino)methane (dppm). Dppa like dppm forms highly strained, though stable, 4-membered chelates, for example $[M(dppa)_2]^{n+}$ M = Rh^I **(1.7)**, Ir^I **(1.8)** (n = 1) and Pt^{II} (n = 2) **(1.9)**.[14, 15]

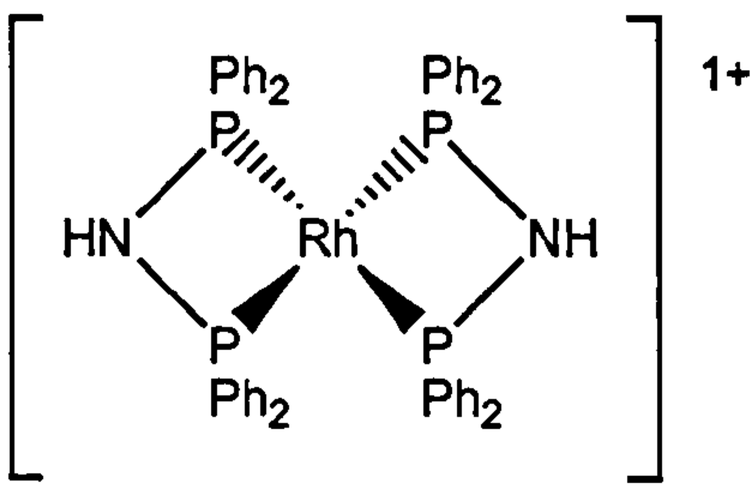

(1.7)

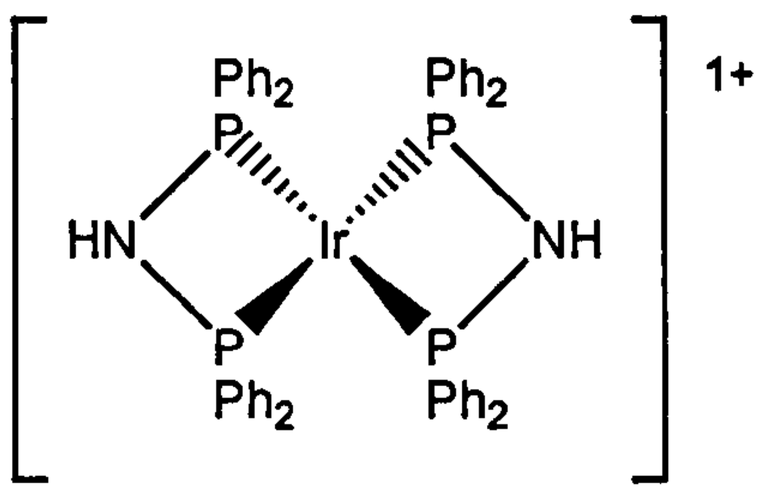

(1.8)

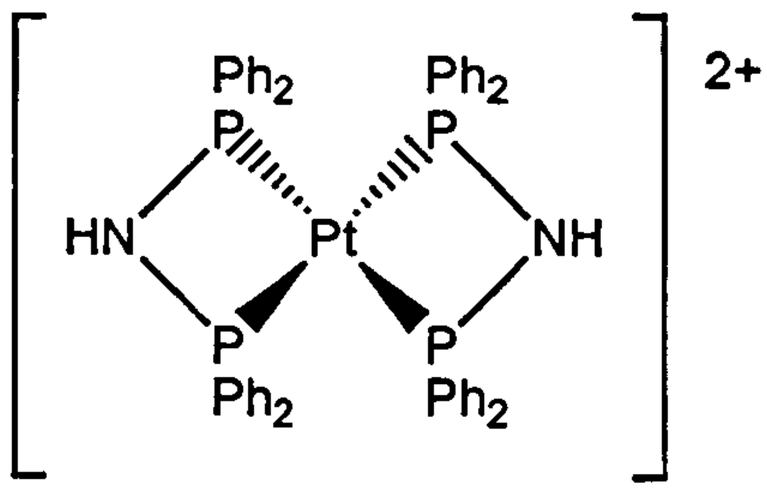

(1.9)

Dppa also readily forms bimetallic compounds with palladium which are isoelectronic with their dppm counterparts, for example the dipalladium(I) complex shown in Equation 1.2.[16]

$$[PdCl_2(NCPh)_2] + 0.5[Pd_2(dba)_3] + 2\ dppa \longrightarrow [Pd_2Cl_2(\mu\text{-}dppa)_2]$$

Equation 1.2

More recently, mixed-metal clusters of the type Co_2Pt, Co_2Pd and $MoPd_2$ have been reported containing bridging dppa. These triangular heterometallic clusters can be stabilized by one or two bridging dppa ligands, for example Equation 1.3.

Heterometallic triangular clusters containing mixed ligand sets dppm/dppa were synthesised by direct incorporation of the dppa ligand, see Equation 1.4.[17]

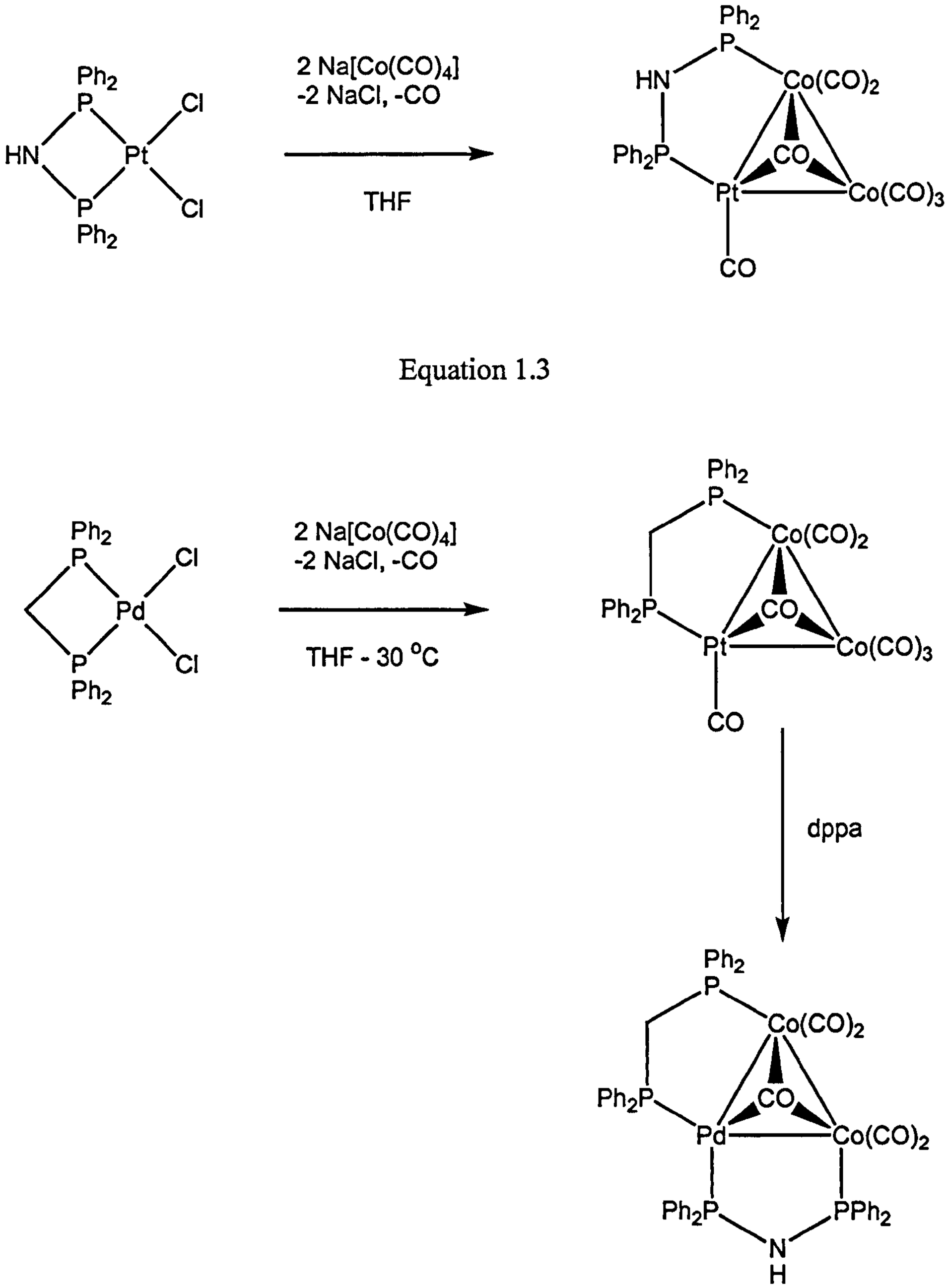

Equation 1.3

Equation 1.4

The $CoPd_2$ cluster stabilised by three bridging dppa ligands (**1.10**) has also been reported.[18]

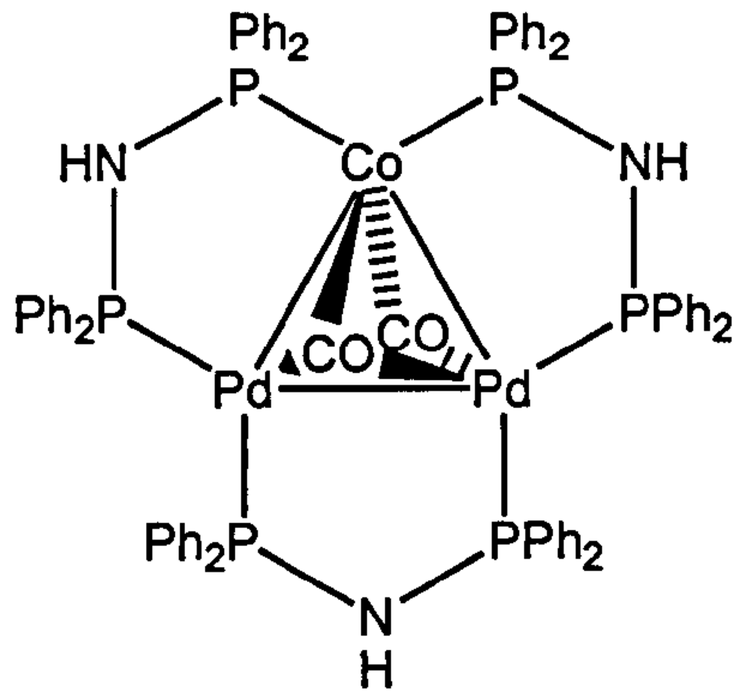

(1.10)

An important feature of the chemistry of dppa is its deprotonation to give $Li[Ph_2PNPPh_2]$[19] which can also form 4-membered chelates; this chemistry has been reviewed recently in detail by Bhattacharyya and Woollins,[20] and will not be discussed further here.

1.3 Chemistry of $R_2PN(R')PR_2$

1.3.1 Chemistry of $Cl_2PN(R')PCl_2$

The first $R_2PN(R')PR_2$ compounds to be synthesised were the halo derivatives where R = Cl, F, I. These were synthesised with a variety of alkyl groups on the nitrogen, R′ = Me, Et, Pr. The synthesis involves prolonged heating of an excess of phosphorus

trichloride under reflux with the appropriate amine hydrochloride in 1,1,2,2-tetrachloroethane or octane (Equation 1.5).[4, 21, 22, 23]

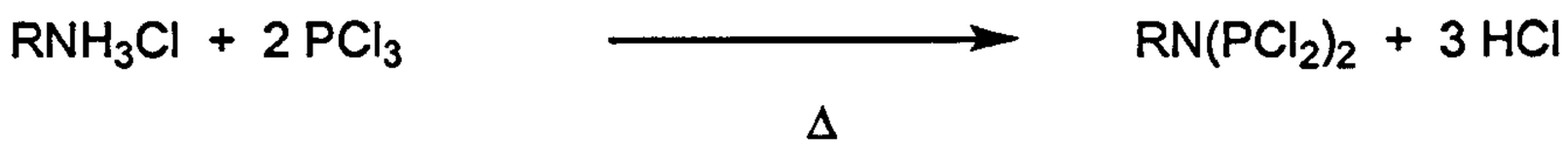

Equation 1.5

The moisture sensitive oils produced react readily with antimony trifluoride under mild conditions to give $RN(PF_2)_2$ where R = Me, Et in high yields (Equation 1.6).[4]

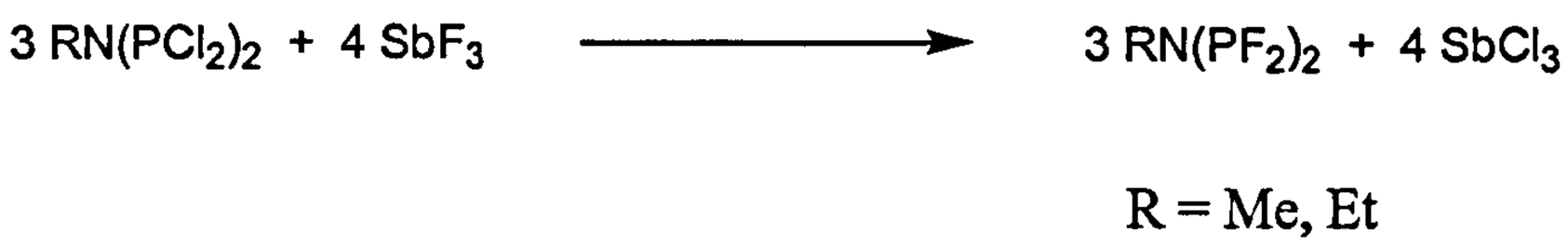

Equation 1.6

The fluoro derivatives are more thermally stable, more volatile and less moisture sensitive than their chloro analogues. The iodo derivatives are prepared by addition of sodium iodide to the corresponding chlorophosphine (Equation 1.7).

Equation 1.7

These compounds are moisture sensitive and decompose on standing (at 20 °C). They can be converted into the alkylaminobis(diphenoxyphosphine) upon reaction with sodium phenoxide (Equation 1.8).[23]

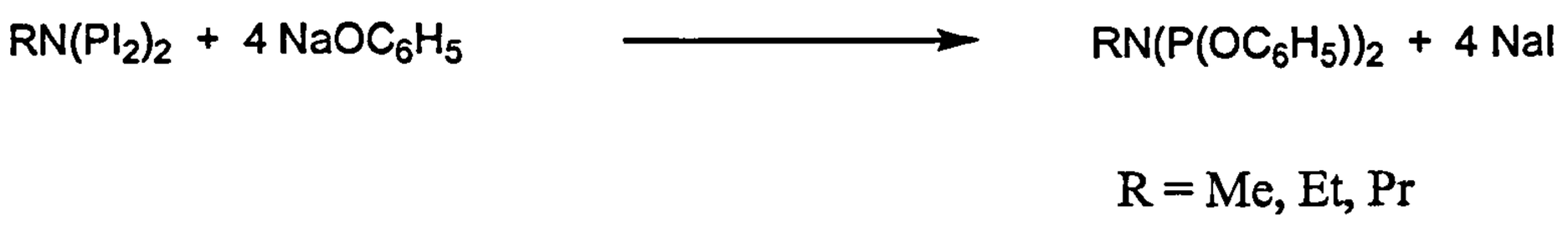

Equation 1.8

There is a wide co-ordination chemistry reported of the halophosphines $X_2PN(R')PX_2$. Studies by Johnson and Nixon[24] on the fluoro derivative $RN(PF_2)_2$ have shown the ability of this ligand to complex to Group 6 metal carbonyls. Further investigation by King *et al.*[2, 25] showed the ability of $X_2PN(R')PX_2$ to bind to transition metals in a monodentate or bidentate mode giving rise to mononuclear and binuclear complexes. These carbonyl compounds are synthesised *via* three different routes; co-condensation of metal vapours with ligands, photochemical reactions and thermal reactions (see Scheme 1.1).[26]

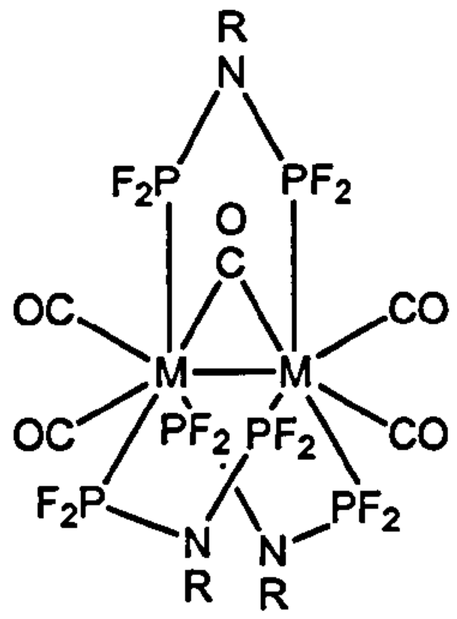

R = Ph; M = Mo
R = Me; M = Cr, Mo, W

pyrolysis in hydrocarbon solvents at 100 - 120 °C

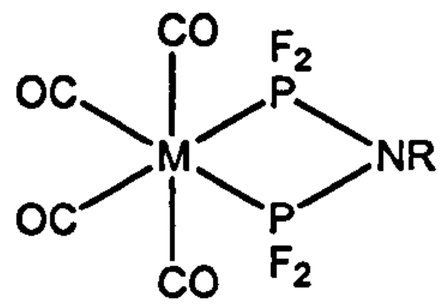

R = Me, Et, Ph; M = Cr, Mo, W

[M(CO)4nbd] 1:1 M/L ratio

[M(CO)4nbd] 1:4 M/L ratio

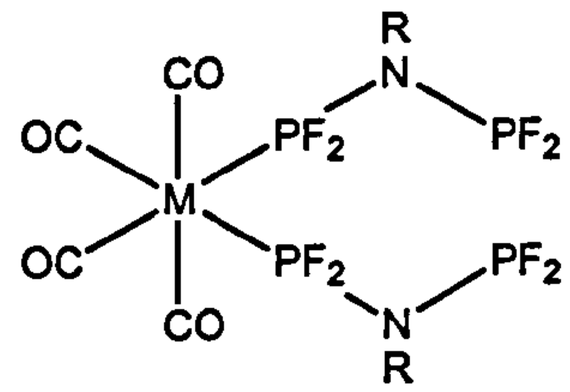

R = Me, Ph; M = Mo, W

[Cr(CO)4nbd] sealed tube

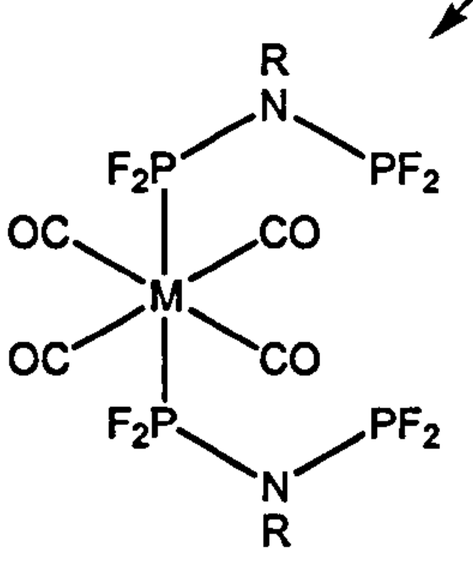

R = Me, Ph; M = Cr

[M(CO)3CHT] [W(CO)6] thermal

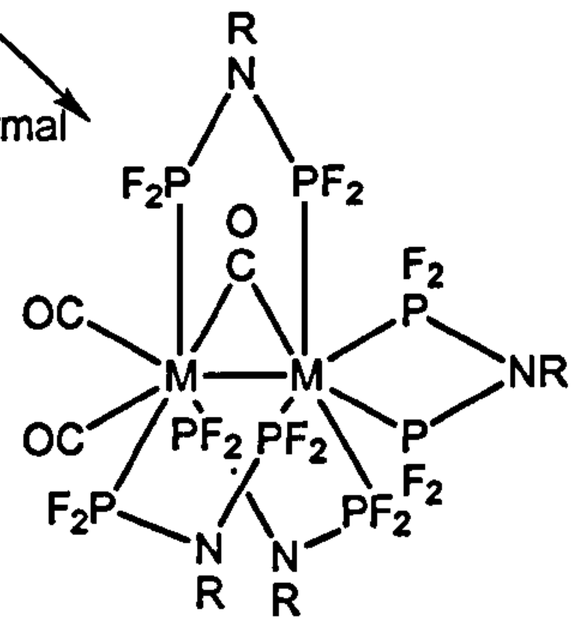

R = Me; M = Mo, W

Scheme 1.1

Studies by Hedberg *et al.*[27] on $MeN(PF_2)_2$ have shown the bonds between the phosphorus and nitrogen to have multiple-bond character, involving delocalisation of the nitrogen electron pair and utilisation of the phosphorus d orbitals. X-ray crystallographic studies and electron-diffraction investigations found the nitrogen atom and its three substituents to be co-planar and the PN bond to be shorter than expected for a single bond.

1.3.2 Chemistry of $Ph_2PN(R')PPh_2$

The compounds $Ph_2PN(R')PPh_2$ are synthesised by the reaction of chlorodiphenylphosphine with primary alkylamines (Equation 1.9) with R = Me, Et, *n*-Pr,[5, 6] CH_2Ph.[28] Addition of triethylamine to the reaction mixture improved the yield of the ligand where R = Ph,[29, 30] *p*-C_6H_4Me.[31]

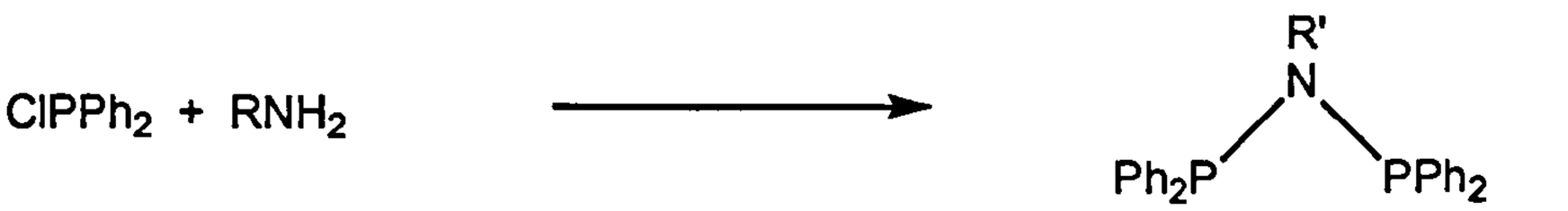

Equation 1.9

The chelation of nickel(II) and palladium(II) complexes by $EtN(PPh_2)_2$ have been confirmed by X-ray crystallography of the palladium complex.[5] However, complexation studies of $MeN(PPh_2)_2$ (dppma) with nickel have shown this PNP ligand is capable of chelating and bridging modes.[32, 33] Dppma reacts with $[Ni(CO)_4]$ to form a bimetallic bridged complex $[Ni_2(CO)_4(\mu\text{-(dppma)})_2]$ (**1.11**) which under vacuum converts to $[Ni_2(\mu\text{-CO})(CO)_2(\mu\text{-(dppma)})_2]$ (**1.12**). The oxidative addition of dihalogen gives the dihalo nickel(II) complex (**1.13**) (Scheme 1.2).

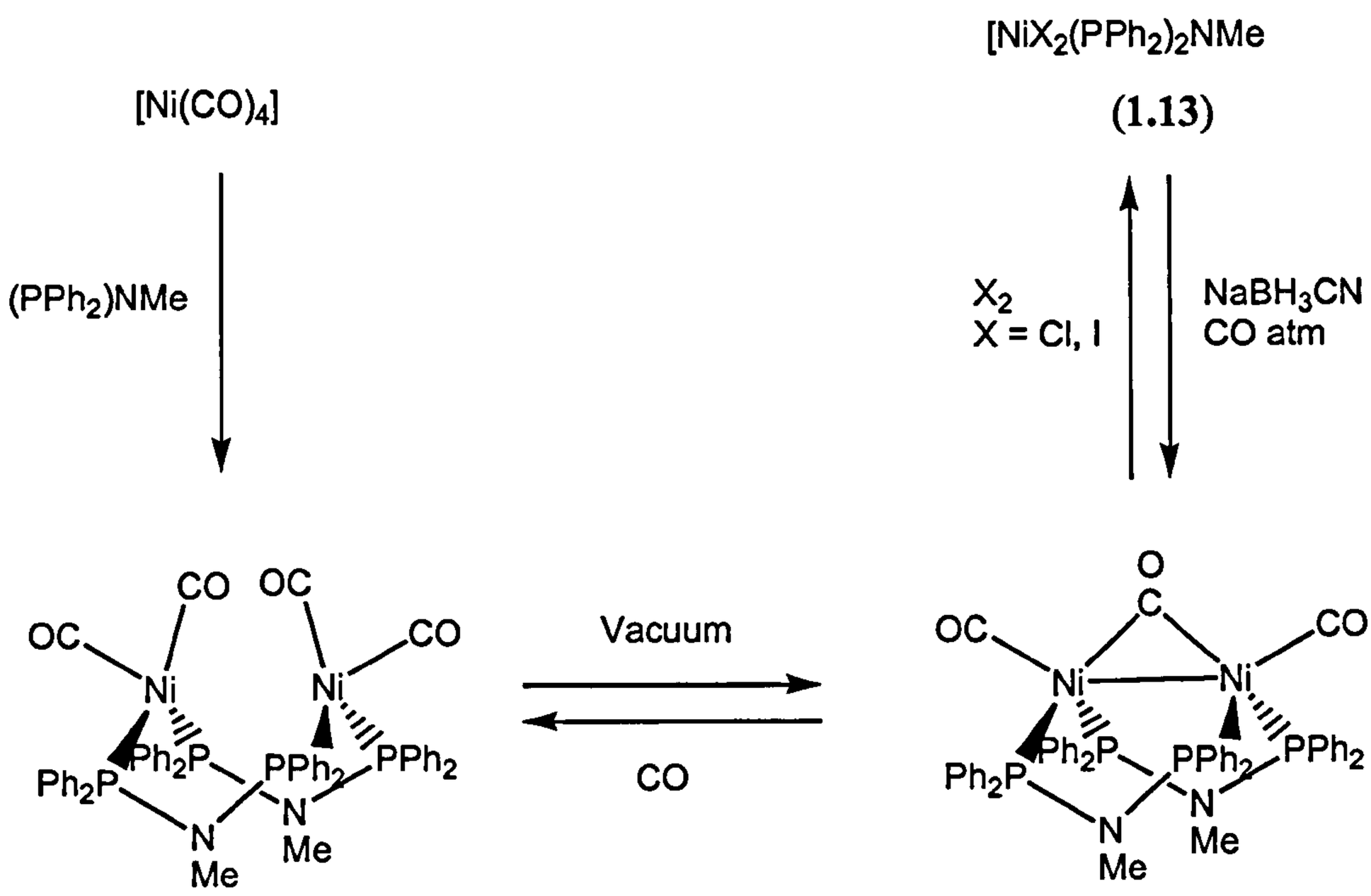

Scheme 1.2

The synthesis of a $Ph_2PN(R')PPh_2$ where R′ = *o*-anisyl **(1.14)** has been reported by Smith and co-workers.[34] The presence of a methoxy group increases the solubility of the ligand and its complexes and also upon coordination gives a hemilabile M – O interaction, which could be readily cleaved by substrates, for example in homogeneous catalytic reactions.[34] The ligand synthesis is shown in Equation 1.10.

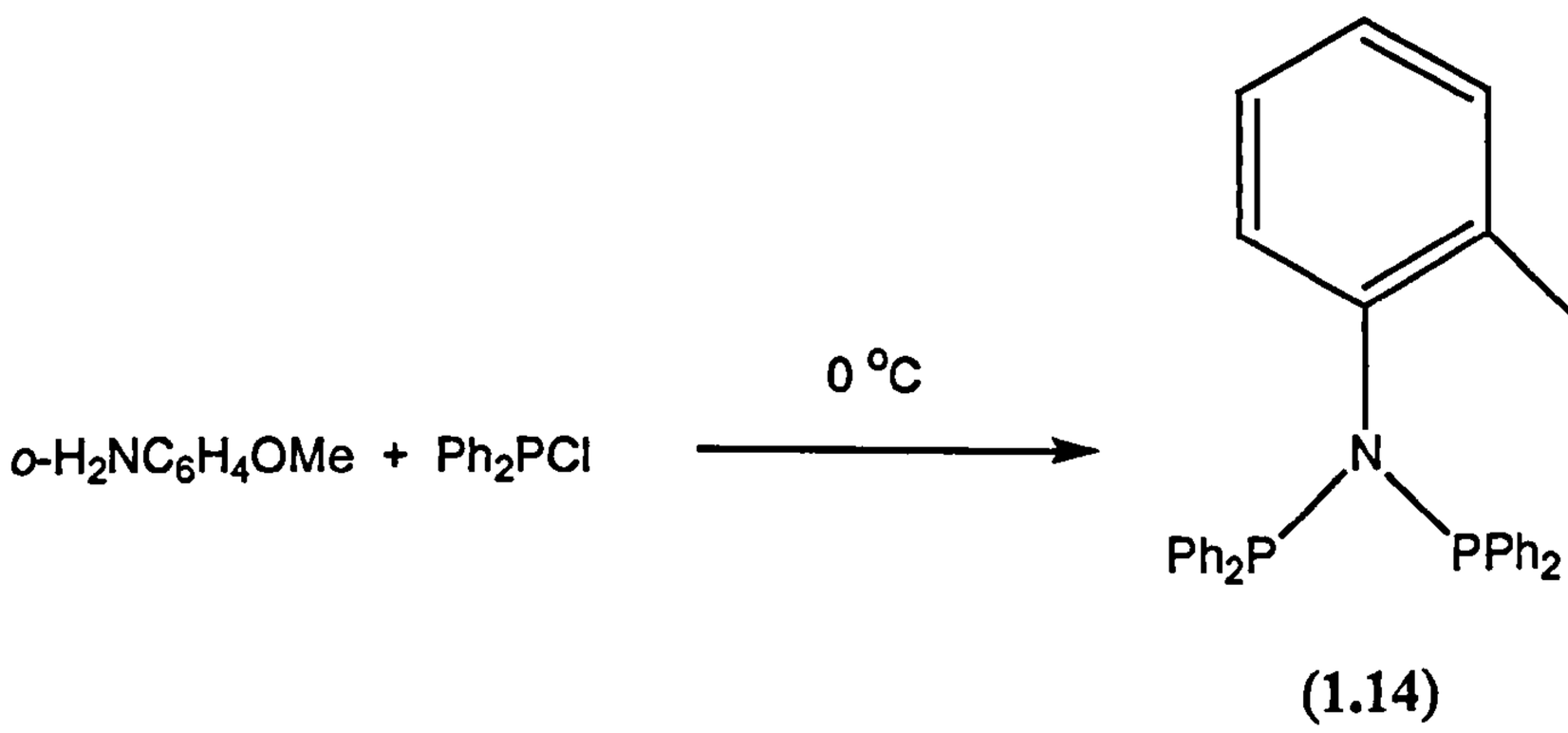

Equation 1.10

Complexation of ligand (**1.14**) to ruthenium(II), molybdenum(0), palladium(II) and platinum(II) has also been reported.[34] Reaction of (**1.14**) with $[MX_2(cod)]$ (M = Pd, Pt; X = Cl or CH_3), $[Mo(CO)_4(nbd)]$ and $[(Ru(p\text{-}cym)Cl_2)_2]$ affords the *cis* chelates (see Scheme 1.3).

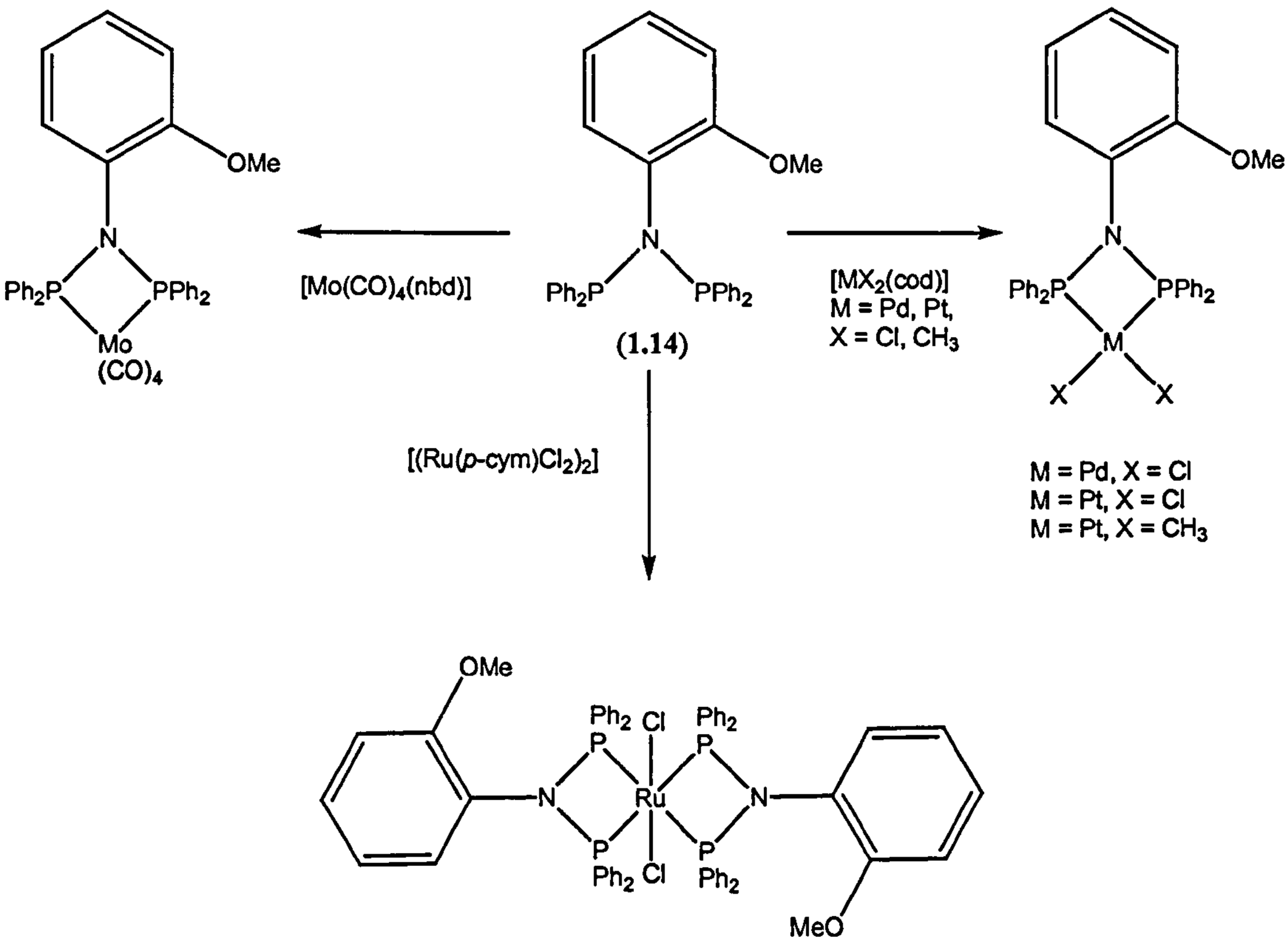

Scheme 1.3

1.3.3 Chemistry of $Ar_2PN(R')PAr_2$ where Ar = *ortho*-substituted phenyl

There is little literature on $Ar_2PN(R')PAr_2$ where Ar = *ortho*-substituted phenyl. In 2001, Pringle *et al.* published the polyketone catalytic results for four-membered palladium(II) diphosphine chelates.[35] It was discovered that palladium(II) complexes

of the type $Ar_2PCH_2PAr_2$ (Ar = *ortho*-substituted phenyl group) are efficient catalysts for the copolymerisation of CO and C_2H_4 (Equation 1.11).

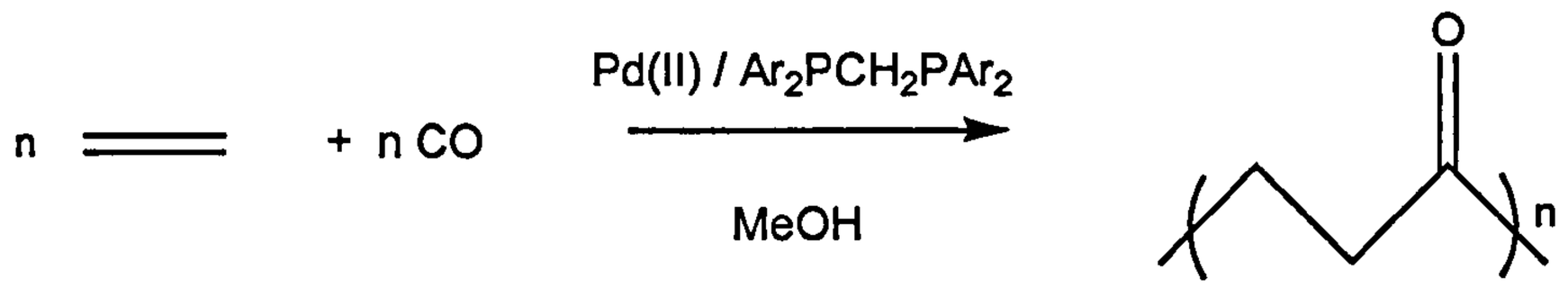

Equation 1.11

The success with bulky diarylphosphinomethane (PCP) ligands led to the investigation into other one-atom backbone diphosphines with similar steric properties. Thus the *ortho*-substituted phenyl aminodiphosphines (PNP) were synthesised according to Equation 1.12, and the palladium complexes tested for polymerisation activity.

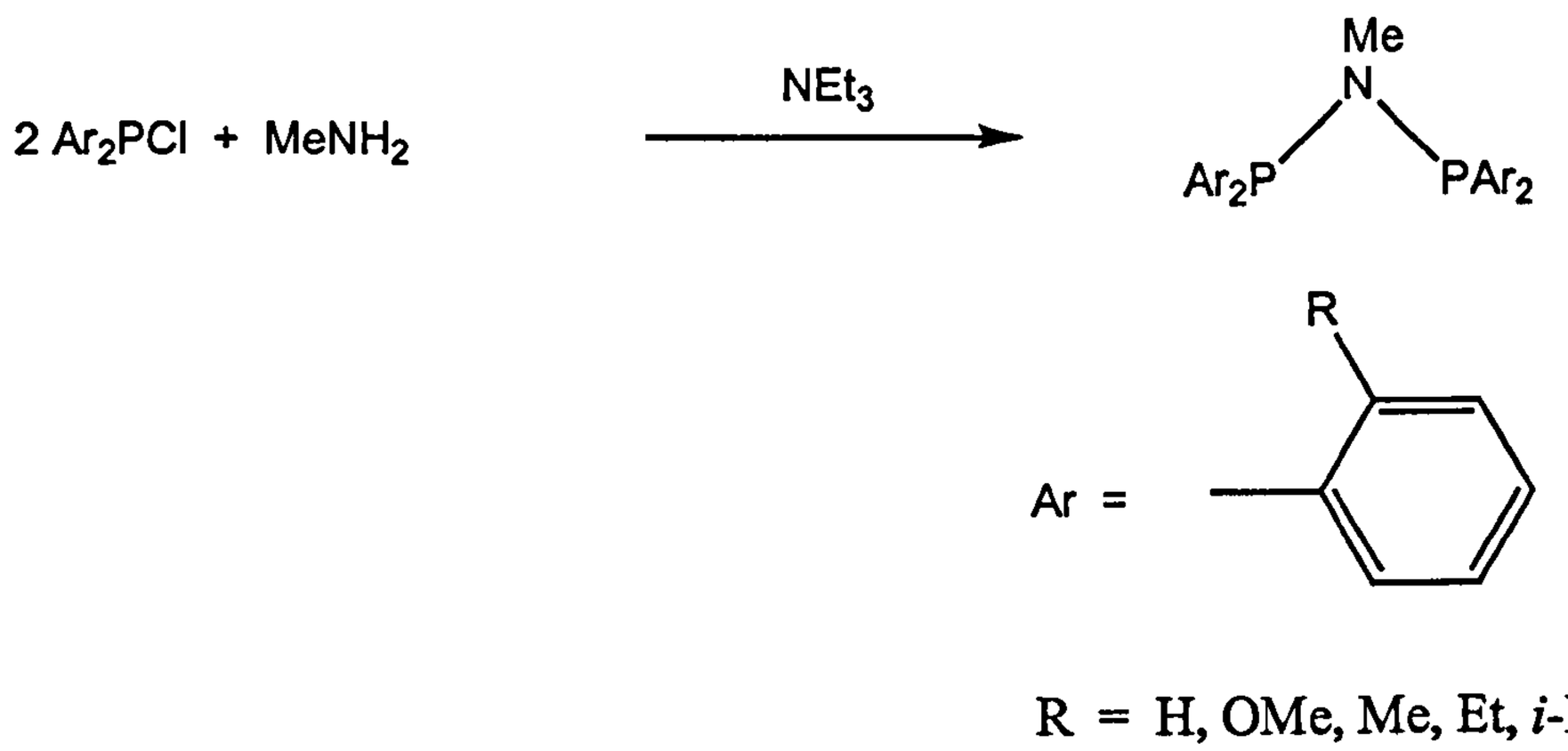

Equation 1.12

The catalytic results showed the PNP chelates to be consistently superior to their PCP counterparts. The polymerisation rate is greater and the polymer produced is of higher molecular weight. The results also indicated that the presence of bulky *ortho* substituents on the aryl group dramatically increased the rate of polymerisation for both the PCP and PNP ligands.[37 - 40]

The discovery that *ortho*- substituted PNP ligands on palladium were superior catalysts for polyketone polymerisation led to the screening of a number of catalytic processes. Wass and co-workers have shown nickel(II) complexes of ligands of the type $Ar_2PN(Me)PAr_2$ (Ar = *ortho*-substituted phenyl group) to be highly active and poison-tolerant catalysts for the polymerisation of ethylene.[41] Previous discoveries of active nickel and palladium polyolefin catalysts have been based almost exclusively on hard nitrogen or oxygen donors,[42, 43] with softer phosphorus donors being largely unsuccessful in this field,[44, 45] even though they have been shown to be active in many other late transition metal catalysed reactions.[36, 46] The ligand forming the most active polymerisation catalyst has an *ortho*-isopropyl substituted phenyl group present **(1.15)**. Upon activation with methyl alumoxane (MAO) a high molecular weight polymer was formed (Equation 1.13). The reactivity of the catalyst is dependent on the Me_3Al content of the MAO, with activity only observed when no detectable Me_3Al was present.[47] Decreasing the bulk of the *ortho*-substituent also decreased the activity of the catalyst, as previously observed for the polyketone catalysis.[35]

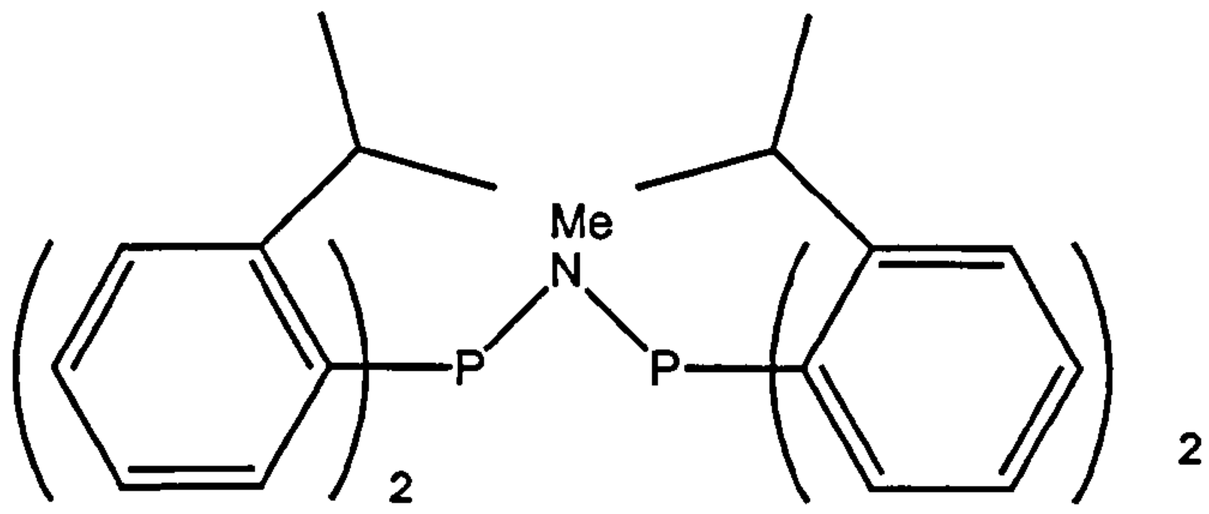

(1.15)

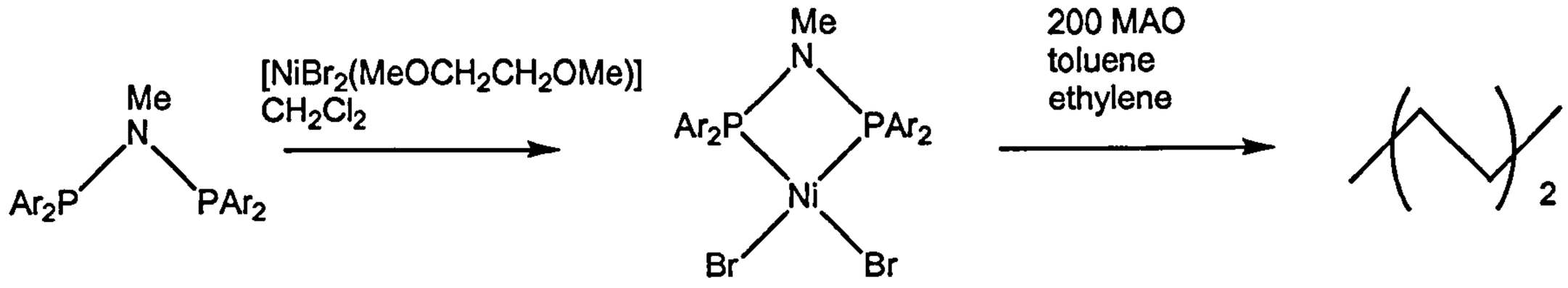

Ar = 2-(*i*-Pr)C_6H_4
2-(Et)C_6H_4
2-(Me)C_6H_4

Equation 1.13

In 2002, a significant further use for the *ortho*-substituted PNP ligand was discovered. Upon activation with MAO, the chromium complexes of $Ar_2PN(Me)PAr_2$ (Ar = *ortho*-methoxy substituted aryl group) **(1.16)** were shown to be highly active and selective systems for the trimerisation of ethylene.[48] One of the best known ethylene trimerisation catalysts is based on chromium with a 2,5-dimethylpyrrole ligand and an alkyl aluminium activator, developed by Phillips.[49]

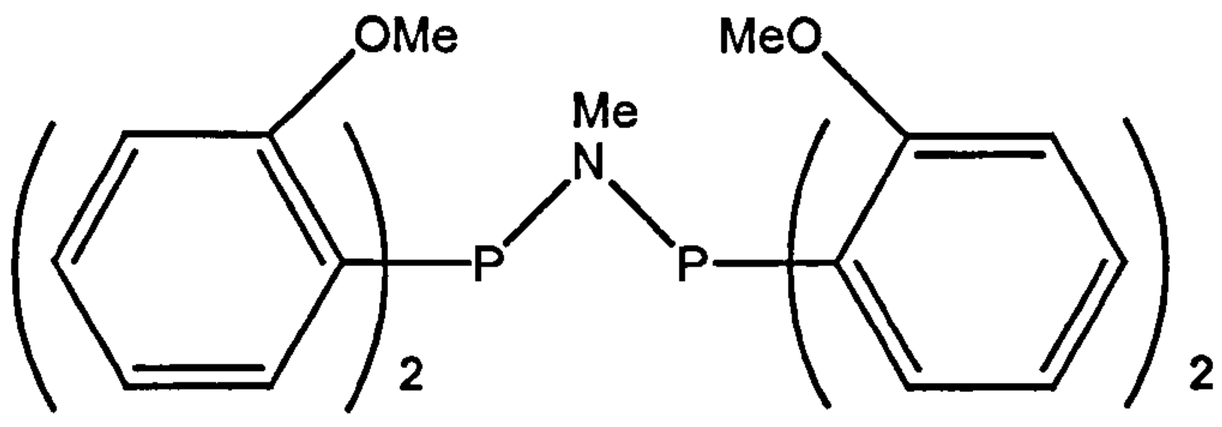

(1.16)

The new PNP catalyst for the trimerisation of ethylene shows the importance of the *ortho*-methoxy substituent. Similar ligands with a methoxy group in other positions on the phenyl ring showed no activity. The idea that the bulk of the *ortho*-methoxy group may be increasing the activity as in the polyethylene polymerisation[41] was postulated but other PNP ligands bearing *ortho*-substituents showed no activity. The *ortho*-

methoxy substituent is thought to act as a pendant donor and so increase the coordinative saturation of the chromium centre.[50]

1.4 The chemistry of phosphoramidites

Monodentate chiral phosphine ligands have been synthesised for enantioselective hydrogenation catalysis on rhodium.[51, 52] The first of these were synthesised by Knowles[53, 54] and Horner[55] for the asymmetric hydrogenation of olefins, but the enantioselectivities were poor (15% ee for preparation of hydratropic acid). Dang and Kagan reported the first chiral diphosphine ligand DIOP (**1.17**)[56, 57] giving remarkably high enantioselectivities, this led to an emphasis on research towards bidentate chiral phosphorus ligands.

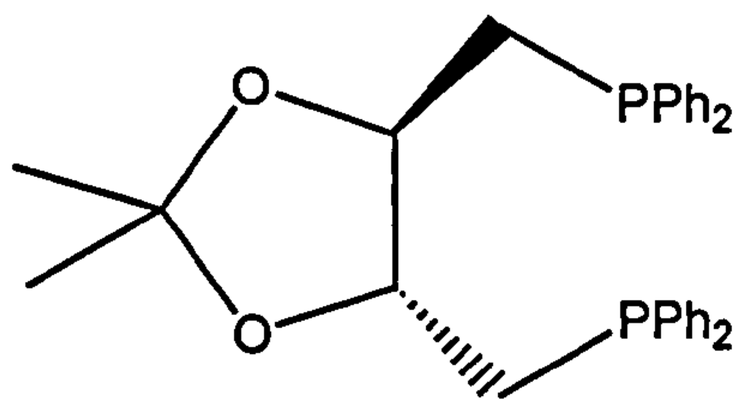

(1.17)

Recently highly enantioselective hydrogenation catalysts have been reported with monodentate chiral phosphorus ligands.[58 - 62] Phosphonite ligands have been synthesised by Pringle *et al.*[63] **(1.18)** and phosphites **(1.19)** by Reetz *et al.*.[64] The phosphonite ligands **(1.18)** on Rh(I) gave enantioselectivities (80% ee) higher than those found for the corresponding diphosphonite (19% ee) for the asymmetric hydrogenation of 2-acetoamido cinnamate (Equation 1.14).[63]

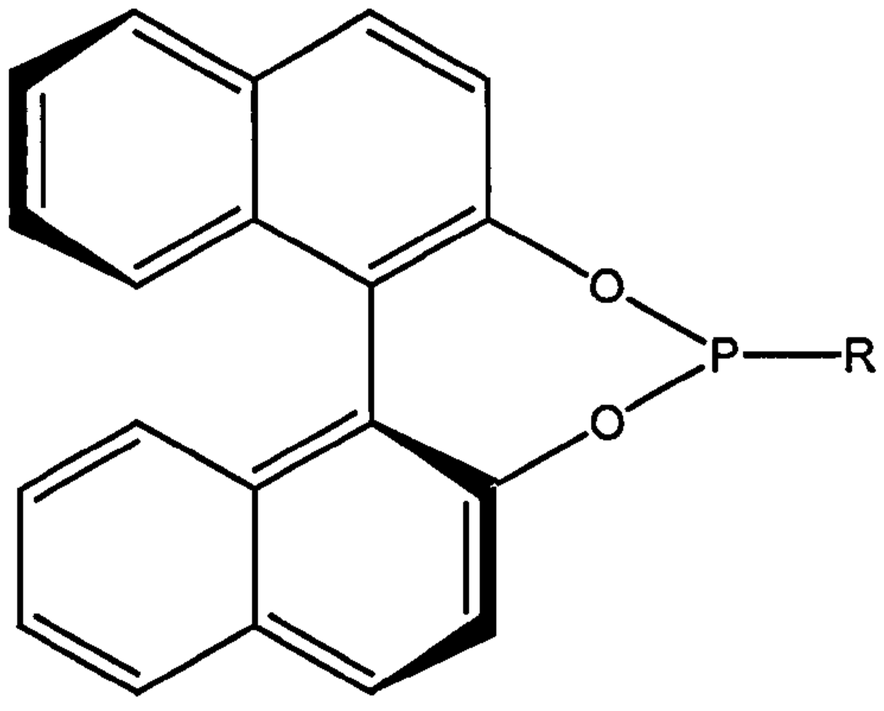

R = Me
R = Ph
R = *t*-Bu

(1.18)

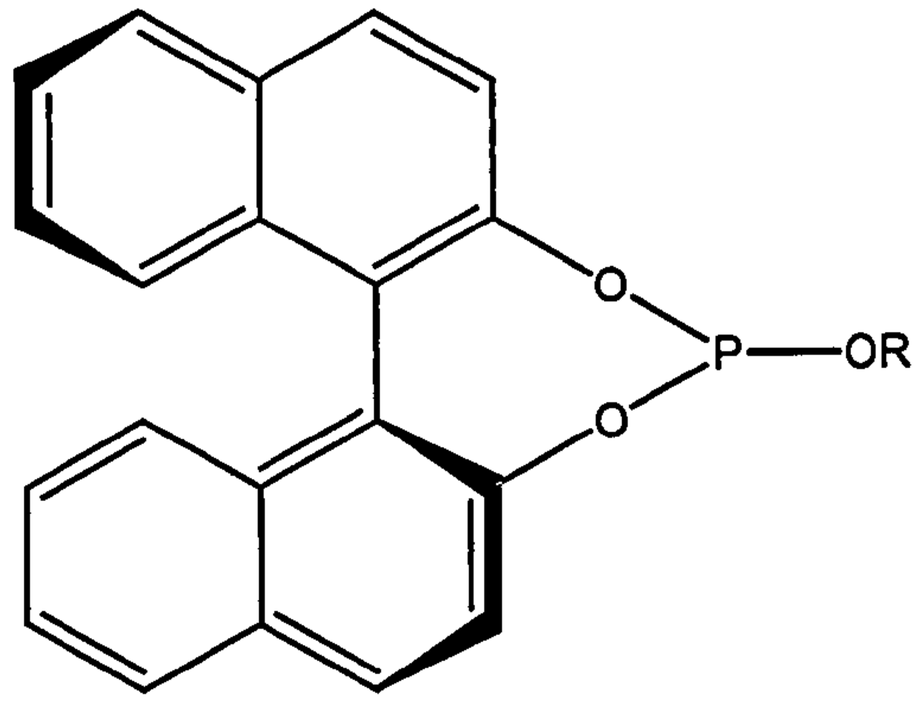

R = Me
R = Ph
R = *t*-Bu

(1.19)

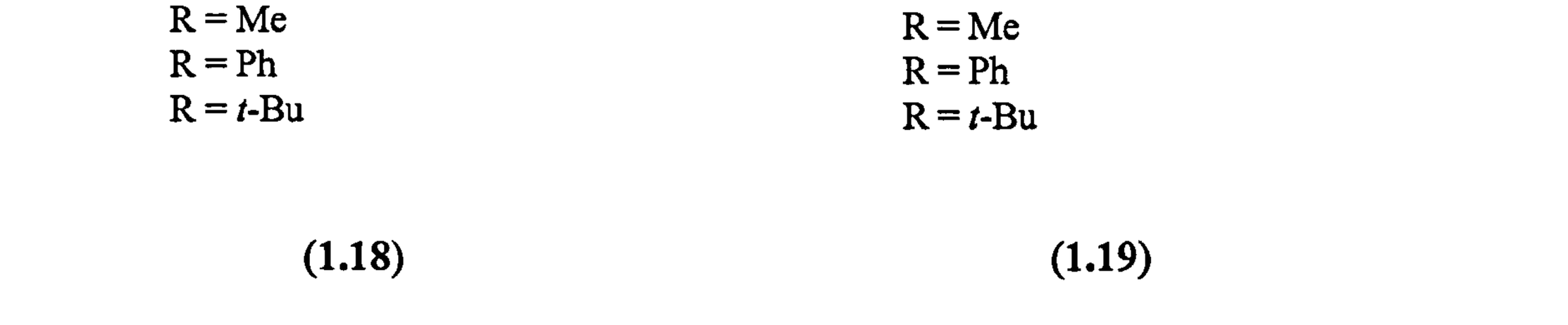

Equation 1.14

In the Rh-catalysed asymmetric hydrogenation reaction using chiral monophosphite ligands equivalent enantioselectivities to their diphosphite counterparts were observed. For the hydrogenation of itaconic acid dimethyl ester the monophosphite **(1.19)** gave 89.2% ee with the diphosphite achieving 88% ee (Equation 1.15).[64]

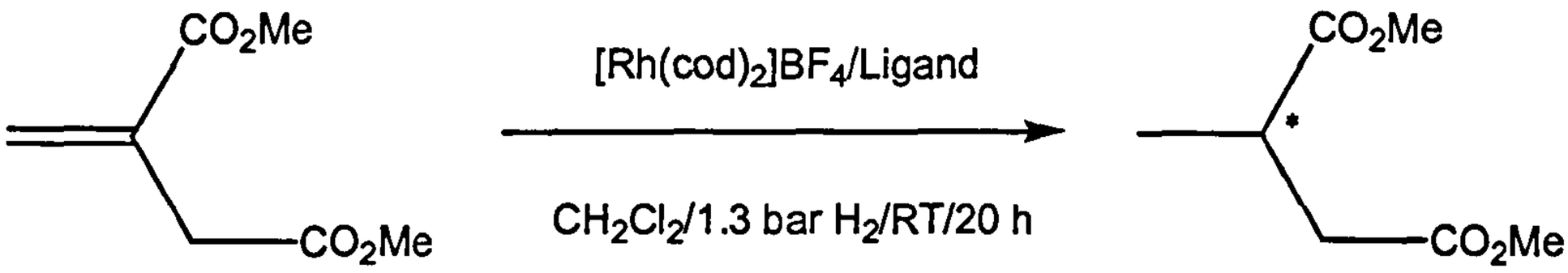

Equation 1.15

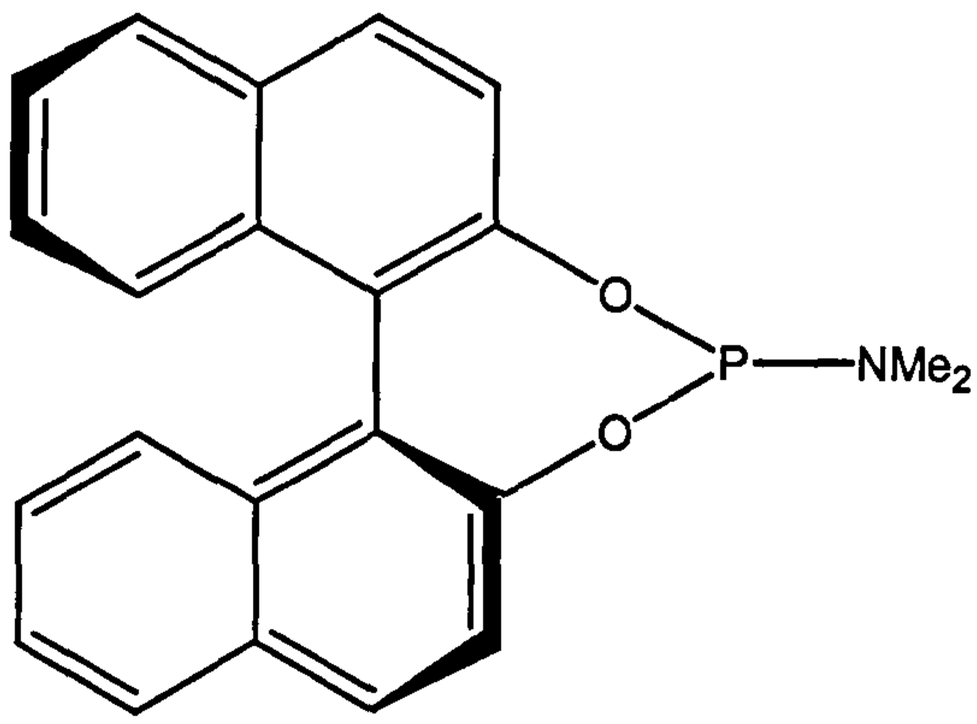

(1.20)

The ligand named MonoPhos (**1.20**) was first synthesised in 1994 by Feringa and co-workers *via* a one-pot reaction of (*S*)-2,2′-binaphthol and hexamethylphosphorus triamide (Equation 1.16)[65]

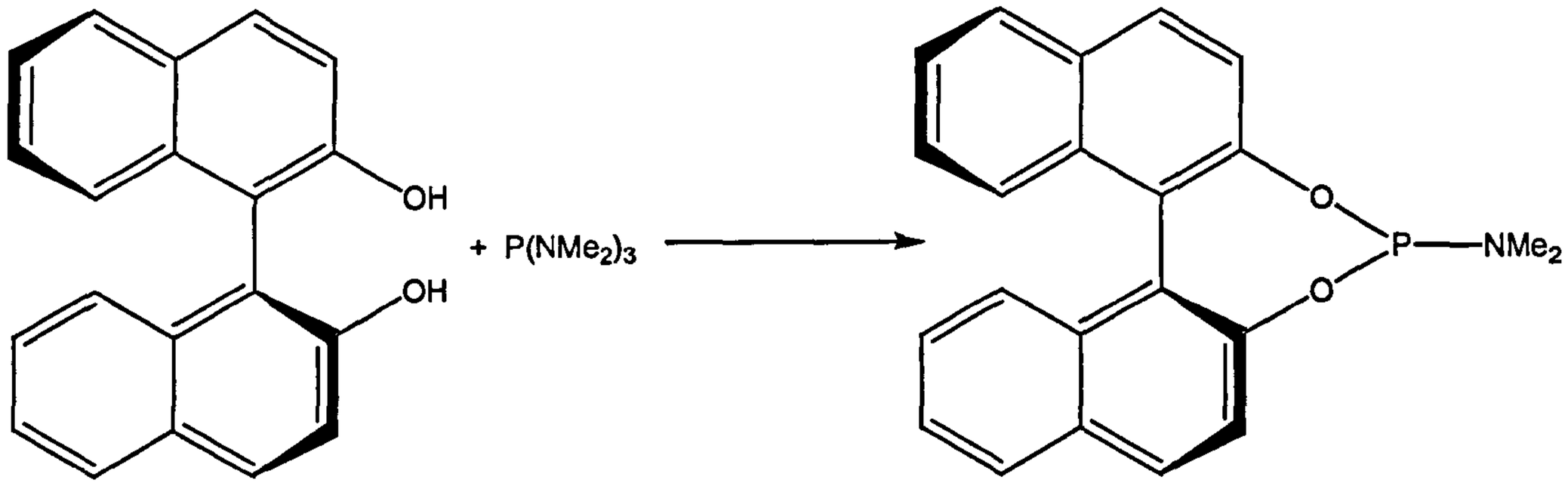

(1.20) Monophos

Equation 1.16

MonoPhos has been shown to form highly selective rhodium catalysts for asymmetric hydrogenation of olefins, with ee's up to 94%.[66, 67] Alternative methods for the synthesis of bulkier phosphoramidites use the reaction of phosphorus trichloride with a diol in the presence of triethylamine followed by reaction with a secondary amine or its lithiated amide, or the reaction of phosphorus trichloride with the secondary amine followed by the diol (Scheme 1.4).[68 - 70]

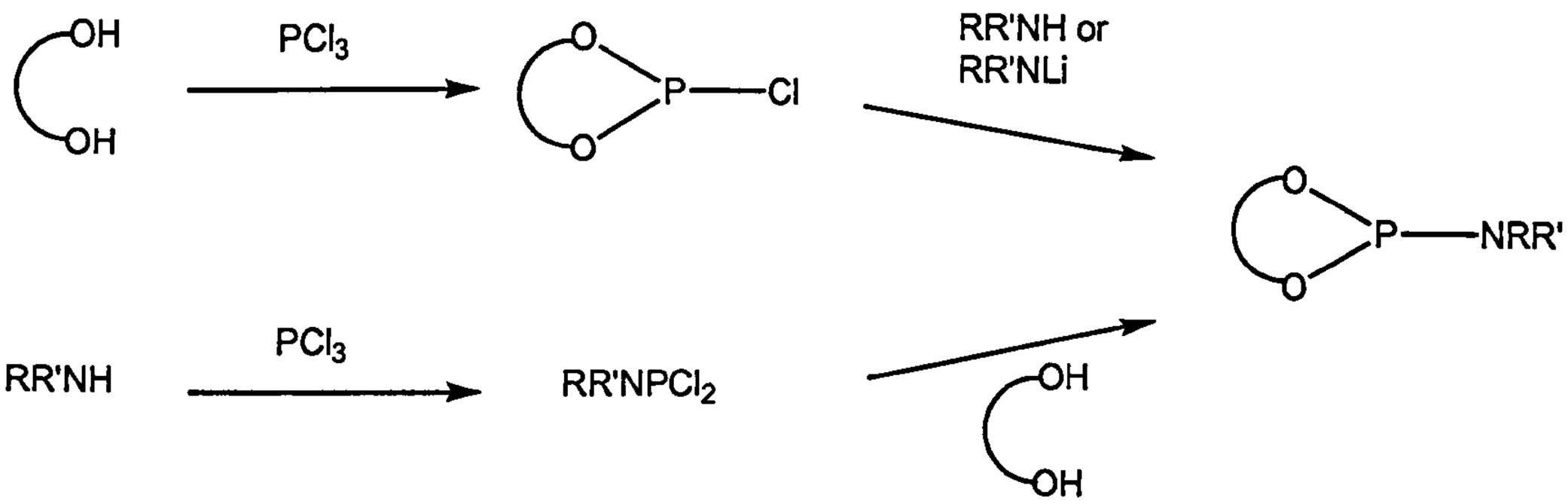

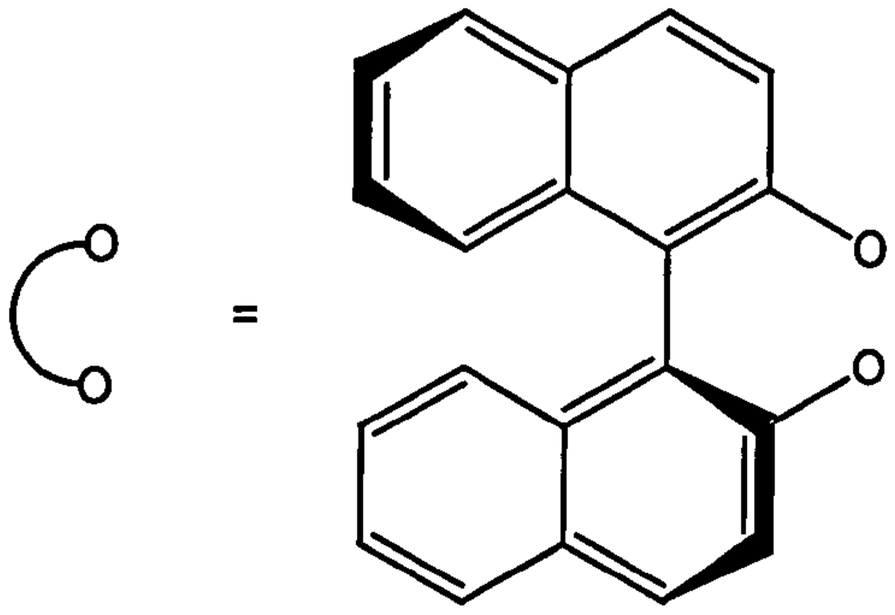

R, R' = Me
R, R' = (*S*)-Ph(CH_3)CH

Scheme 1.4

The MonoPhos ligand has also found uses in the asymmetric hydrogenation of α-arylenamides. The limited number of studies into the hydrogenation of this form of substrate indicates it is difficult to achieve with high enantioselectivity. However, recent results by Feringa *et al.*[71] and Chan *et al.*[72] have shown the monodentate phosphoramidite ligand MonoPhos **(1.20)** when complexed to rhodium gives high enantioselectivities of up to 94%.

One of the most recent discoveries has been the highly enantioselective copper catalysed allylic alkylation using phosphoramidite ligands.[73] Allylic alkylation is an important C-C bond forming reaction due to its versatility.[74] Control of the regio- and stereo-chemistry and the development of highly enantioselective catalysts has been a focal point for research.[75 – 77] Copper catalysts have been shown to be good catalysts for the allylic substitution reaction[78, 79] although little studied for allylic alkylation.[80] Feringa and co-workers have reported ee's of 77% for **(1.22)** for the copper catalysed asymmetric allylic alkylation with dialkyzinc reagents and phosphoramidite ligand **(1.21)**[73, 81] (Equation 1.17).

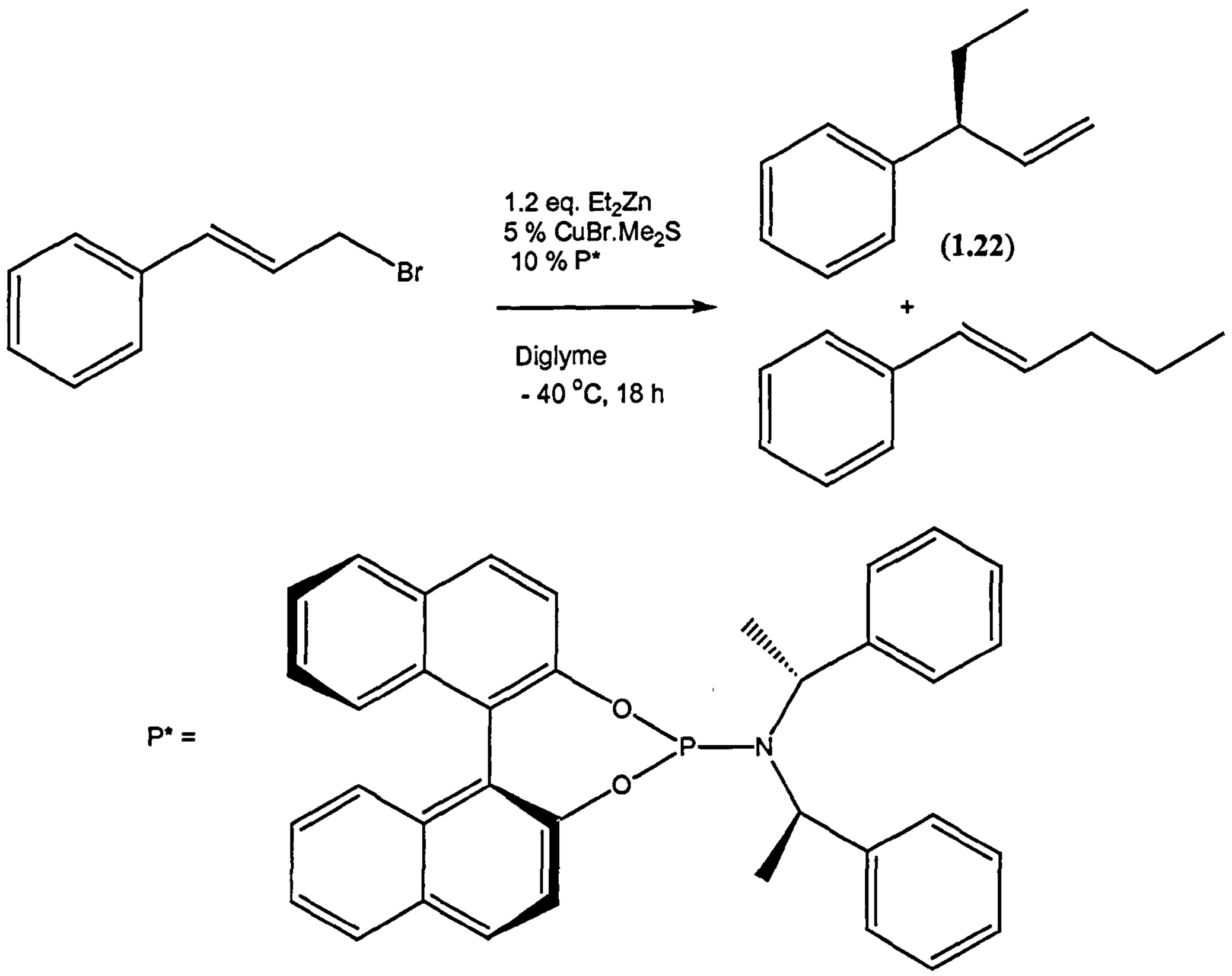

(1.21)

Equation 1.17

The diphosphoramidite **(1.23)** was screened for copper catalysed enantioselective conjugate addition of diethylzinc to cyclohexanone but gave lower ee's of 37% compared to the monodentate **(1.21)** with 75%.[73, 82]

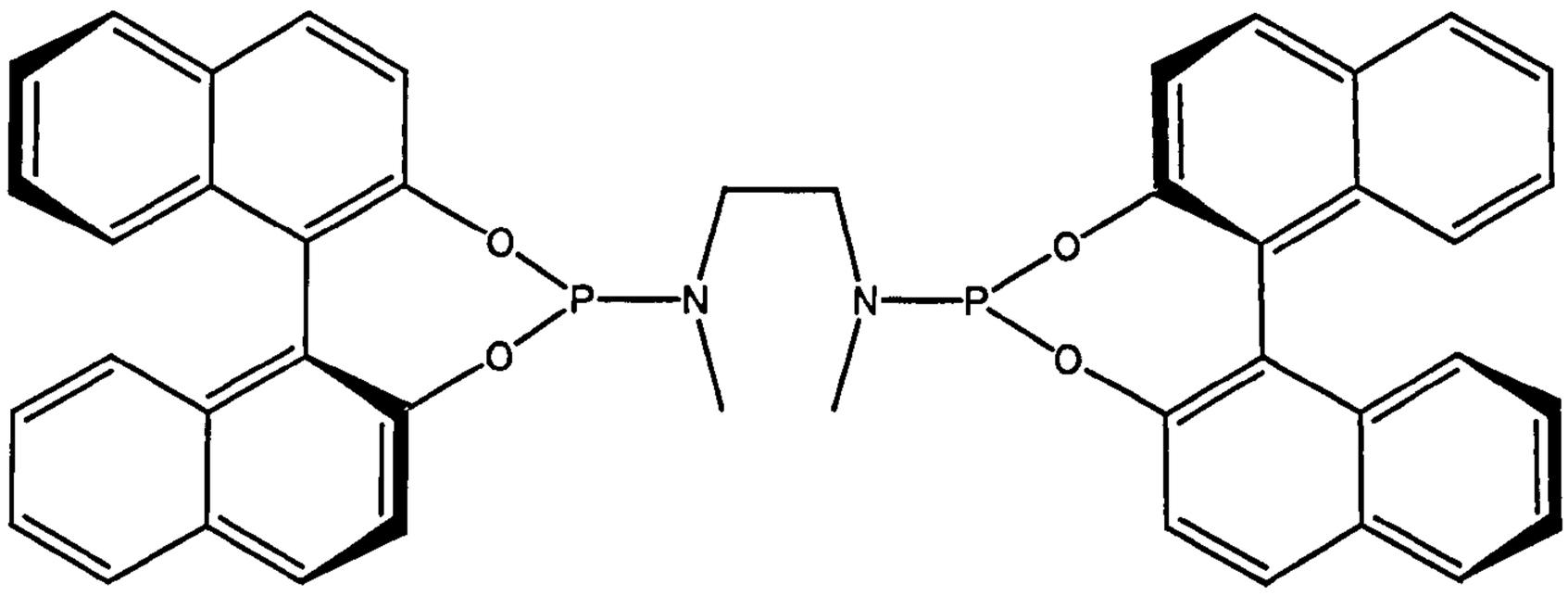

(1.23)

The diphosphoramidite **(1.23)** is readily obtained from N,N′-dimethylethylenediamine and chlorophosphite in the presence of triethylamine (Equation 1.18).[82]

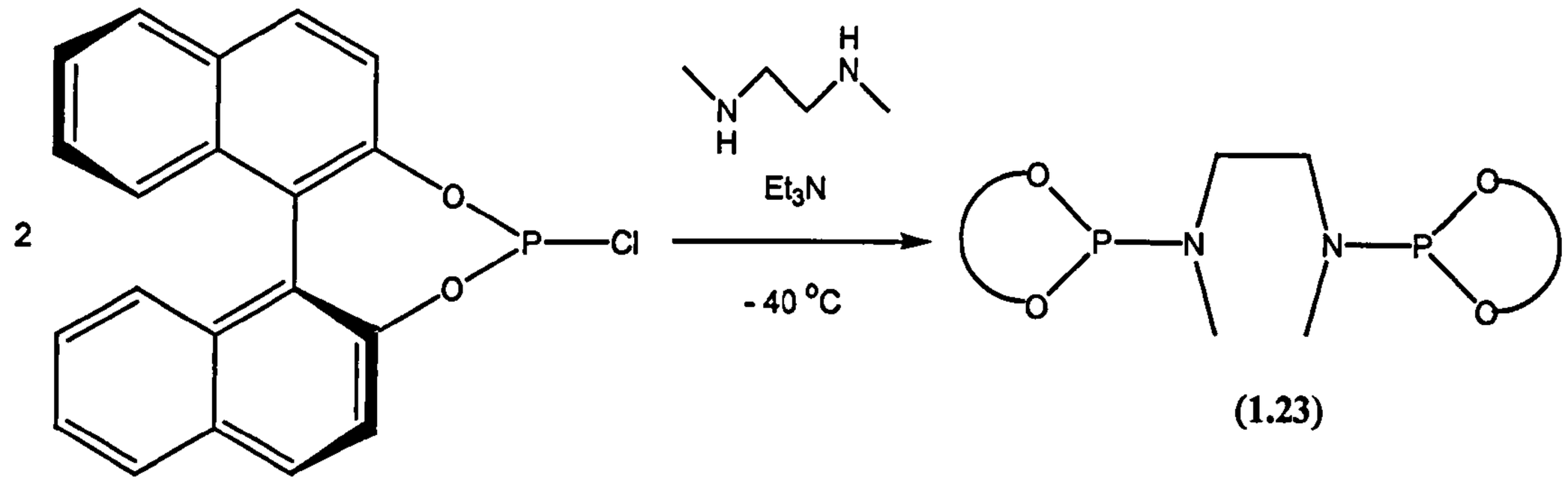

Equation 1.18

Another variation of the diphosphoramidite ligand is illustrated by the short bite angle PNP ligand **(1.24)**.

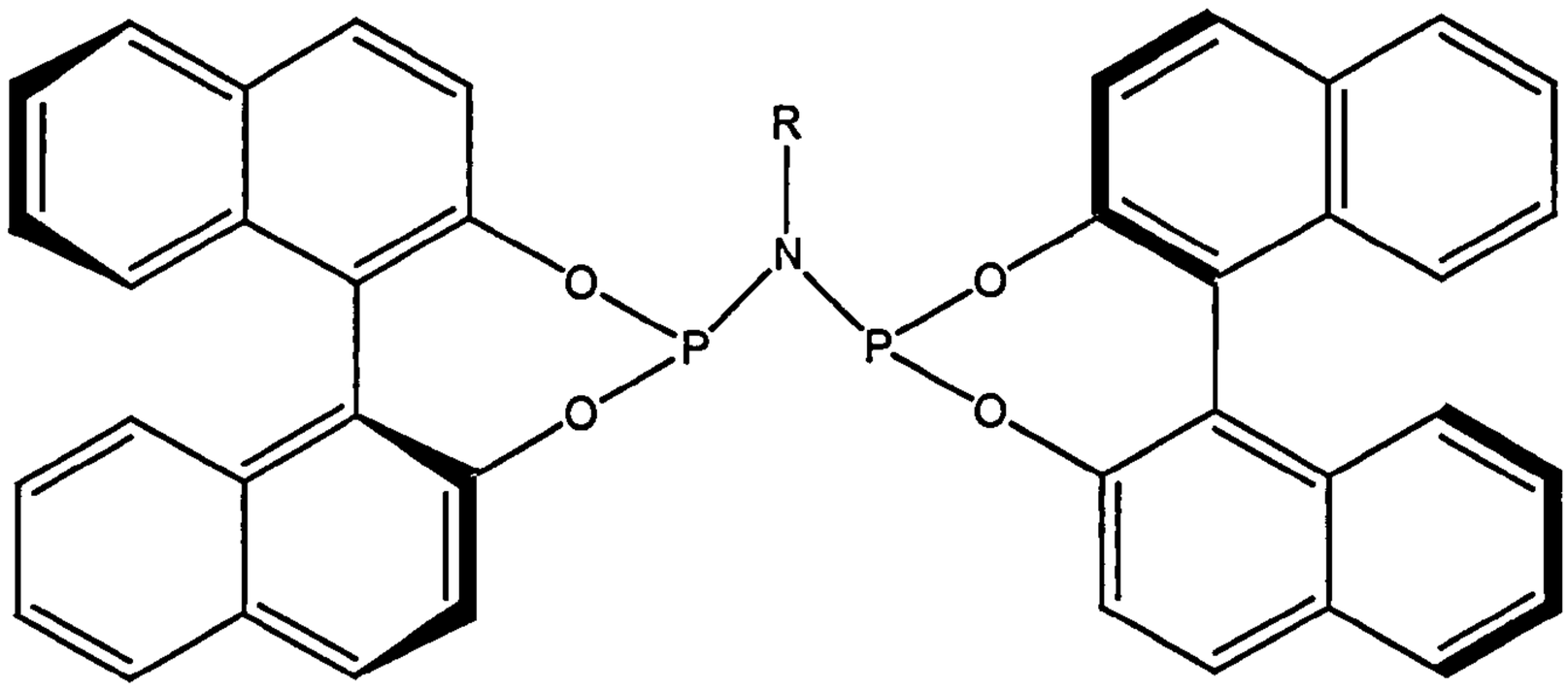

R = (*S*)-*sec*-butyl
Ph

(1.24)

The ligand **(1.24)** has been tested for activity in enantioselective palladium catalysed allylic substitution reactions of 1,3-diphenylallyl acetate with dimethylmalonate (Equation 1.19).

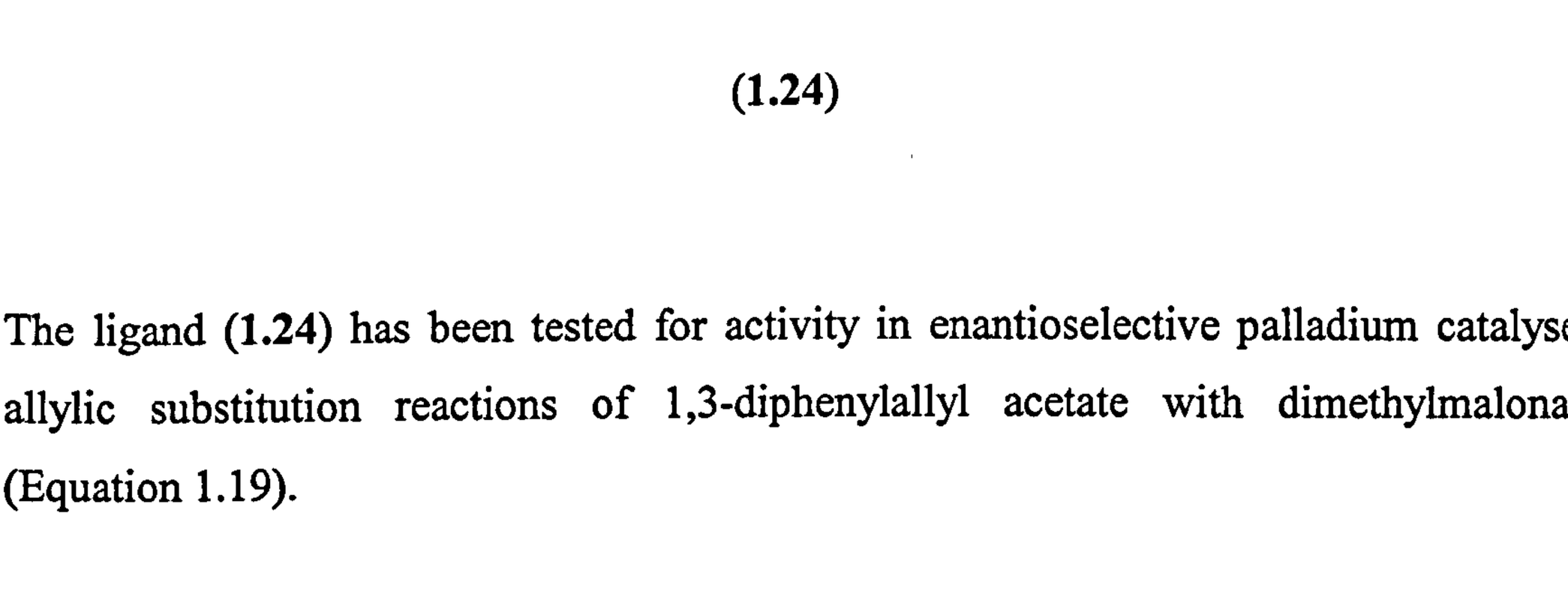

(1.24)

Equation 1.19

The ligand **(1.24)** is present in solution as a single highly symmetric conformer, therefore no induction of any significant ee is observed and the catalytic product 2-(1,3-

diphenylallyl)dimethylmalonate was obtained as a racemic mixture.[83] The ligand was prepared from the reaction of the chlorophosphite and the primary amine at 0 °C in the presence of triethylamine (Equation 1.20).

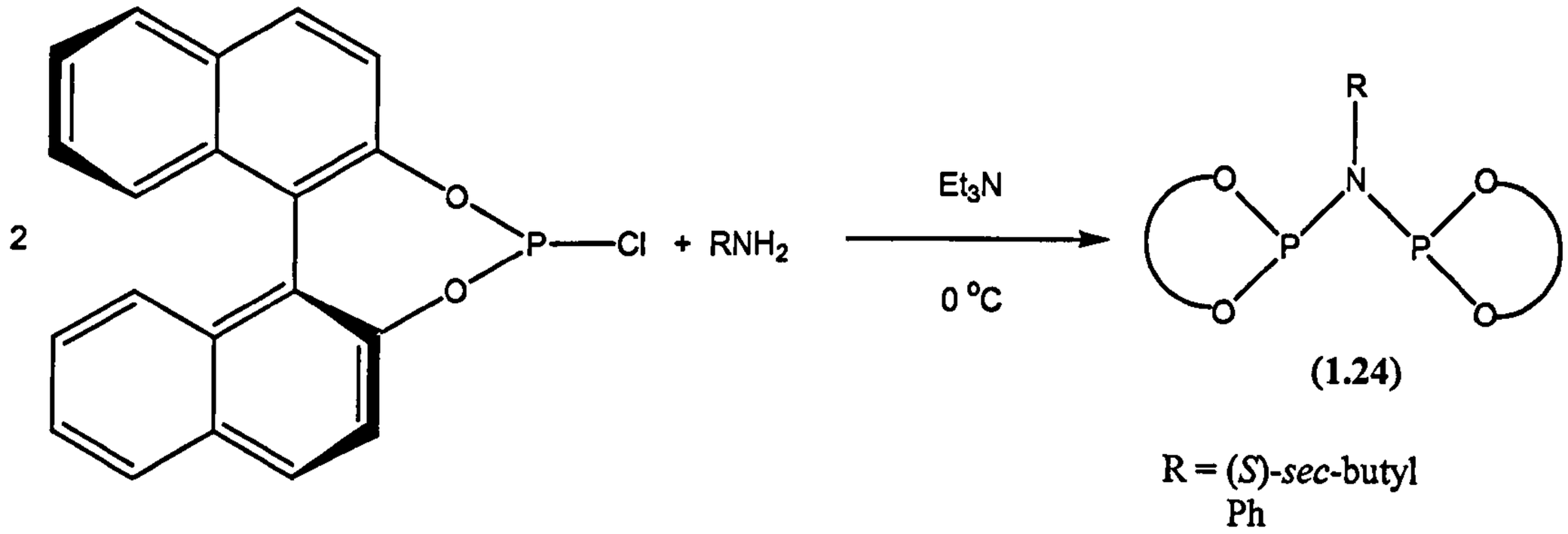

Equation 1.20

1.5 Aims of project

The main aim of this research project was to synthesise new PNP ligands for ethylene polymerisation and trimerisation catalysis. The ligands to be synthesised will be based on the simple PNP skeleton where groups on the nitrogen and *ortho*-substituents on the aryl group on phosphorus will be modified. A series of diphosphoramidites will also be prepared. These ligands will then be complexed to platinum and palladium compounds and their coordination chemistry and solid state structures investigated. The activity of the ligands in Ni-catalysed ethylene polymerisation and Cr-catalysed trimerisation will be studied.

Chapter 2:

Synthesis of PNP ligands

Synthesis of PNP ligands

2.1 Introduction

The synthesis of PNP ligands can be achieved *via* the general route shown in Equation 2.1.

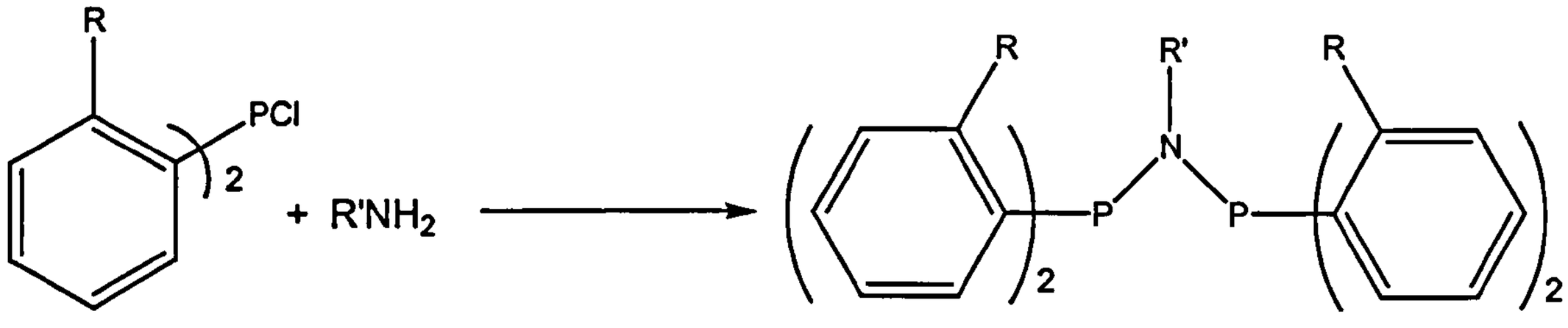

Equation 2.1

The reactions of alkylamines and Ph_2PCl and the synthesis of $RN(PCl_2)_2$ have been reviewed in detail by Balakrishna *et al.*,[26] Ewart[5] and Keat.[6] The synthesis of PNP ligands of the type $Ar_2PN(Me)PAr_2$ where Ar = *ortho* substituted phenyl, has been described by Dossett, Wass and co workers[35, 37 – 39, 41, 48, 84] using methylamine and Ar_2PCl (Equation 2.2).

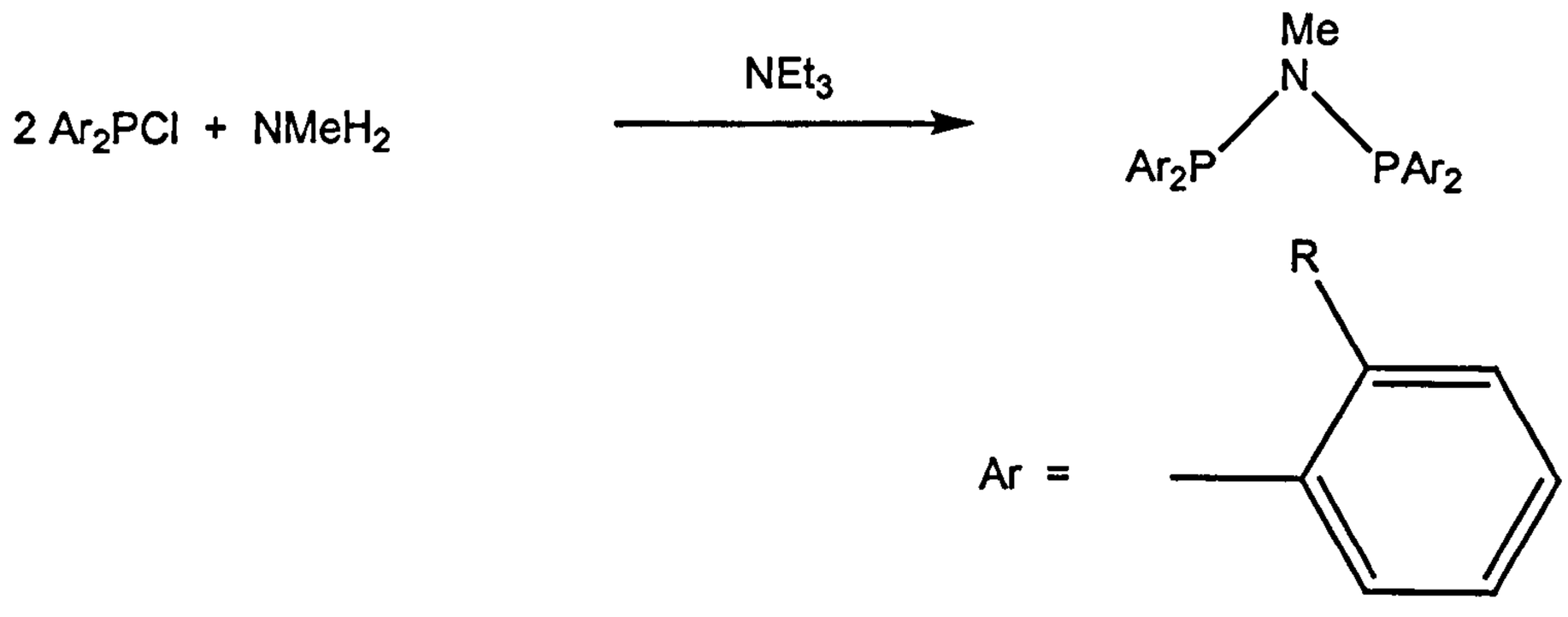

Equation 2.2

The synthesis of bisphosphoramidites has been achieved by Faraone and co-workers,[83] from the reaction of chlorophosphite with the primary amine at 0 °C in the presence of triethylamine (Equation 2.3). This synthesis produced bisphosphoramidites with bulky groups on the nitrogen.

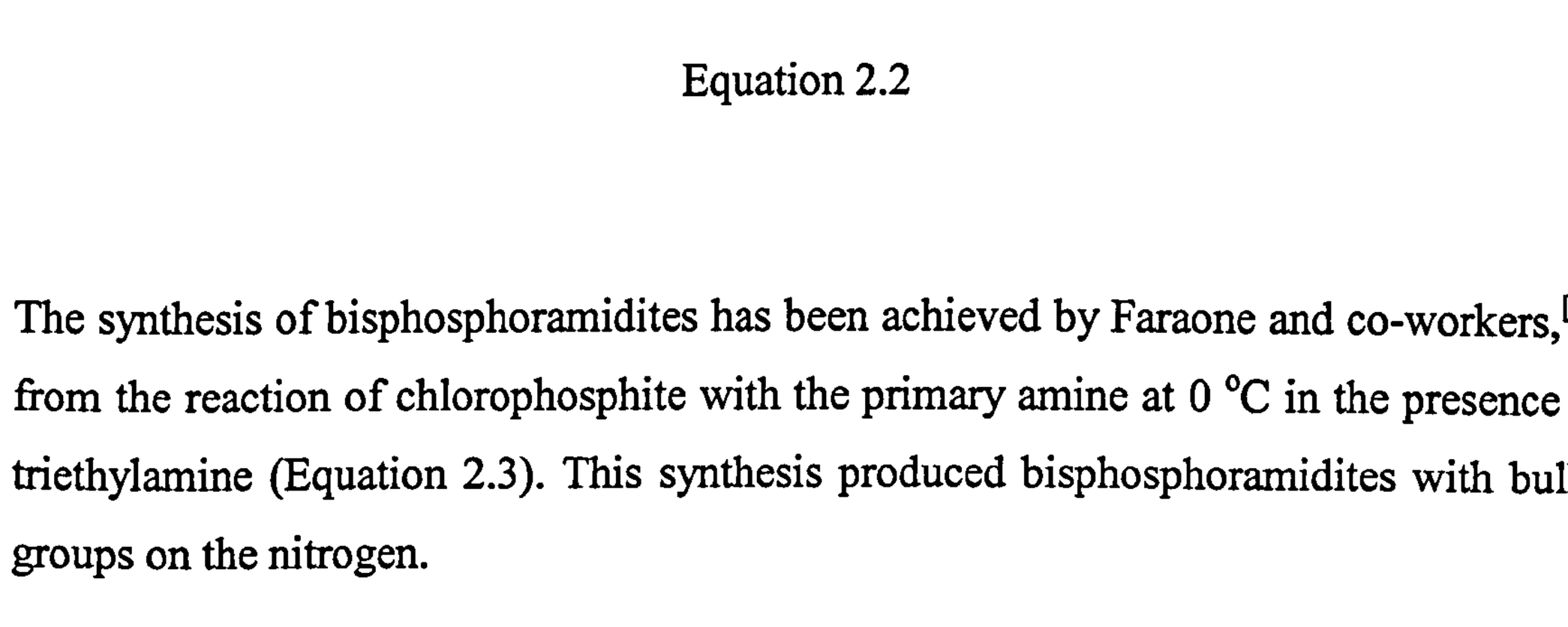

Equation 2.3

An alternative route to PNP ligands with no literature precedent has been developed, see Equation 2.4. This novel route will be used extensively throughout this Chapter.

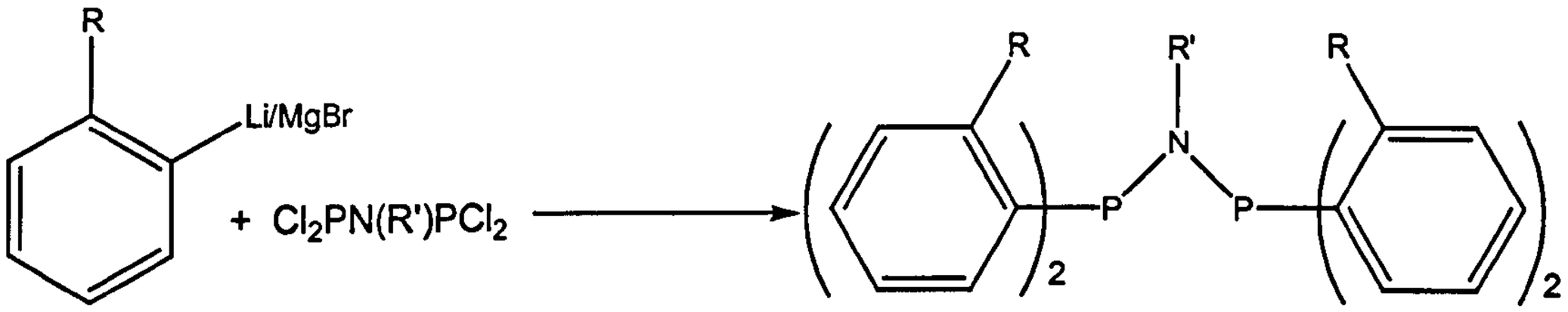

R' = alkyl group
R = H, alkyl group, halide

Equation 2.4

2.2 Synthesis of $Cl_2PN(R)PCl_2$

The compounds $RN(PCl_2)_2$ where R is methyl (**2.1**) and ethyl (**2.2**), were made according to the route of Nixon.[85, 4] The alkylaminehydrochloride was refluxed with PCl_3 in 1,1,2,2-tetrachloroethane for a period of 7 to 14 days to give the desired product after distillation. This route was then extended to the synthesis of the *n*-propyl (**2.3**) and *i*-propyl (**2.4**) analogues (Equation 2.5). See Table 2.1 for $^{31}P\{^1H\}$ NMR data.

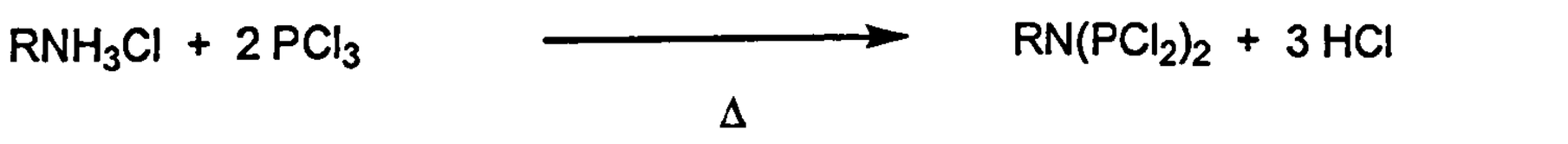

R = Me (**2.1**), Et (**2.2**),
n-Pr (**2.3**), *i*-Pr (**2.4**)

Equation 2.5

Table 2.1 $^{31}P\{^{1}H\}$ NMR data for ligands **(2.1 – 2.4)**

No.	Ligand	δ ppm
(2.1)	$Cl_2PN(Me)PCl_2$	160.8 (s)[a]
(2.2)	$Cl_2PN(Et)PCl_2$	164.8 (s)[a]
(2.3)	$Cl_2PN(n\text{-}Pr)PCl_2$	165.1 (s)[a]
(2.4)	$Cl_2PN(i\text{-}Pr)PCl_2$	170.5 (s)[a]

[a] Spectra recorded at 121 MHz in $CDCl_3$ at 22 °C. Chemical shifts (δ) in ppm (± 0.1) to high frequency of H_3PO_4.

2.3 Synthesis of $Ph_2PN(R)PPh_2$ R = Me (2.5), Et (2.6), *n*-Pr (2.7), *i*-Pr (2.8)

The ligand $Ph_2PN(Me)PPh_2$ ligand **(2.5)** was prepared by literature methods, described by Dossett and co-workers.[35] The compounds $RN(PCl_2)_2$ were used to prepare the analogues **(2.6 – 2.8)** according to Equation 2.6. The reagents were added at – 78 °C and stirred for 3 h and upon work up with deoxygenated water, white solid products of high purity were obtained (Equation 2.6) and characterised by $^{31}P\{^{1}H\}$ NMR data (Table 2.2), mass spectrometry, $^{13}C\{^{1}H\}$ and ^{1}H NMR and elemental analysis (see Experimental Section for data).

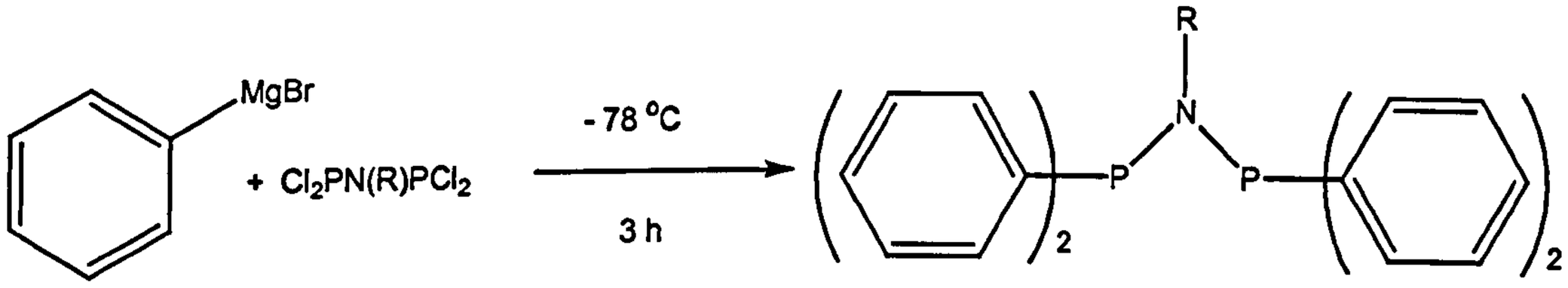

R = Et **(2.6)**, *n*-Pr**(2.7)**, *i*-Pr **(2.8)**

Equation 2.6

Table 2.2 $^{31}P\{^{1}H\}$ NMR data for ligands **(2.5 – 2.8)**

No.	Ligand	δ ppm
(2.5)	$(C_6H_5)_2PN(Me)P(C_6H_5)_2$[b]	73.6 (s)[a]
(2.6)	$(C_6H_5)_2PN(Et)P(C_6H_5)_2$	62.3 (s)[a]
(2.7)	$(C_6H_5)_2PN(n\text{-}Pr)P(C_6H_5)_2$	63.0 (s)[a]
(2.8)	$(C_6H_5)_2PN(i\text{-}Pr)P(C_6H_5)_2$	50.0 (br)[a]

[a] Spectra recorded at 162 MHz in $CDCl_3$ at 22 °C. Chemical shifts (δ) in ppm (± 0.1) to high frequency of H_3PO_4.

[b] Prepared by Dossett.[5]

2.4 Synthesis of $Ph_2PN(R)PPh_2$ R = $CH_2CH_2OCH_3$ (2.9), $CH_2CH_2CH_2OCH_3$ (2.10), $CH_2(2\text{-}OCH_3)C_6H_4$ (2.11)

The success of the *ortho*-methoxy PNP ligand $(2\text{-}OCH_3C_6H_4)_2PN(Me)P(2\text{-}OCH_3C_6H_4)_2$ in Cr-catalysed ethylene trimerisation[48, 84] prompted the synthesis of the above mentioned series of ligands. Studies of the Cr complexation of the *ortho*-methoxy PNP ligand showed the methoxy group to act as a pendant donor increasing the coordinative saturation of the chromium centre.[48, 50] It was postulated that having the methoxy group appended to the nitrogen could also yield hemilabile ligands.

2.4.1 Synthesis of $Ph_2PN(R)PPh_2$ R = $CH_2CH_2OCH_3$ (2.9)

The ligand $Ph_2PN(CH_2CH_2OCH_3)PPh_2$ **(2.9)** was synthesised according to Equation 2.7. Triethylamine and diphenylchlorophosphine in dichloromethane was stirred for 1 h and 2-methoxyethylamine was then added dropwise to the orange solution to form a

precipitate. Upon filtration and concentration of the solution, a yellow residue was formed which was then triturated with acetonitrile to yield a white solid of 90% purity.

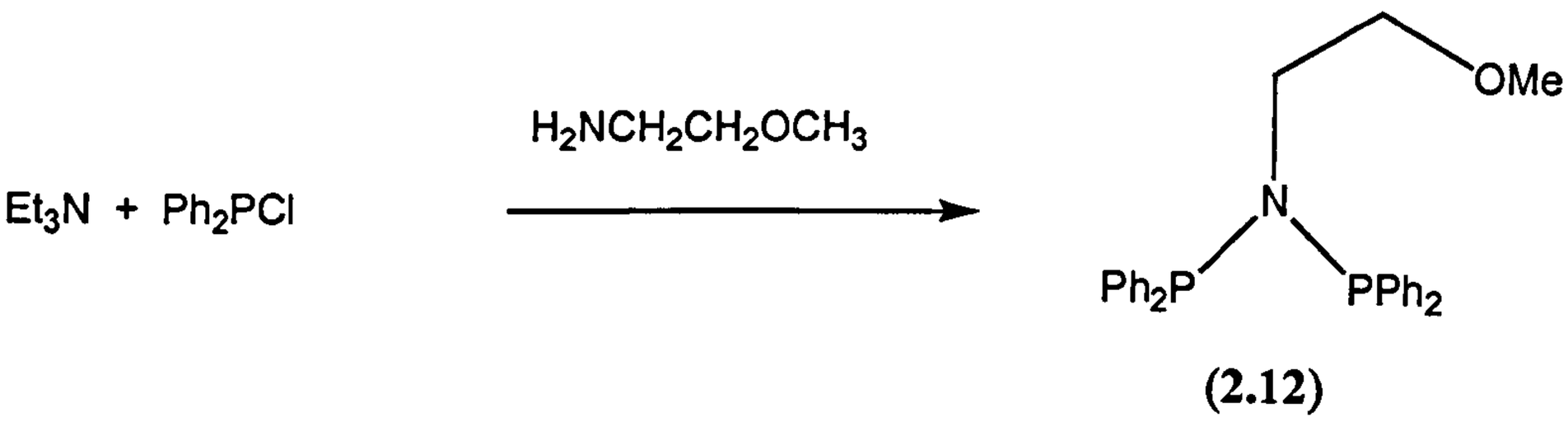

(2.12)

Equation 2.7

The acetonitrile solution was left to crystallise at 0 °C, giving block crystals which were analysed by $^{31}P\{^{1}H\}$ (see Table 2.5), $^{13}C\{^{1}H\}$, ^{1}H NMR spectroscopy, mass spectrometry and elemental analysis (see Experimental section for data). The structure was determined by X–ray crystallography (Figure 2.1) and selected bond lengths and angles are given in Table 2.3. The crystals were shown to be monoclinic with 4 molecules per unit cell; the solid state structure for the ligand shows the two phosphorus atoms to be in different environments. The P(1) - N(1) bond length is 1.716(14) Å, P(2) – N(1) 1.721(14) Å with the P(1) – N(1) – P(2) angle 122.7(7)° and the lone pairs on the phosphorus are in an *anti* comformation.

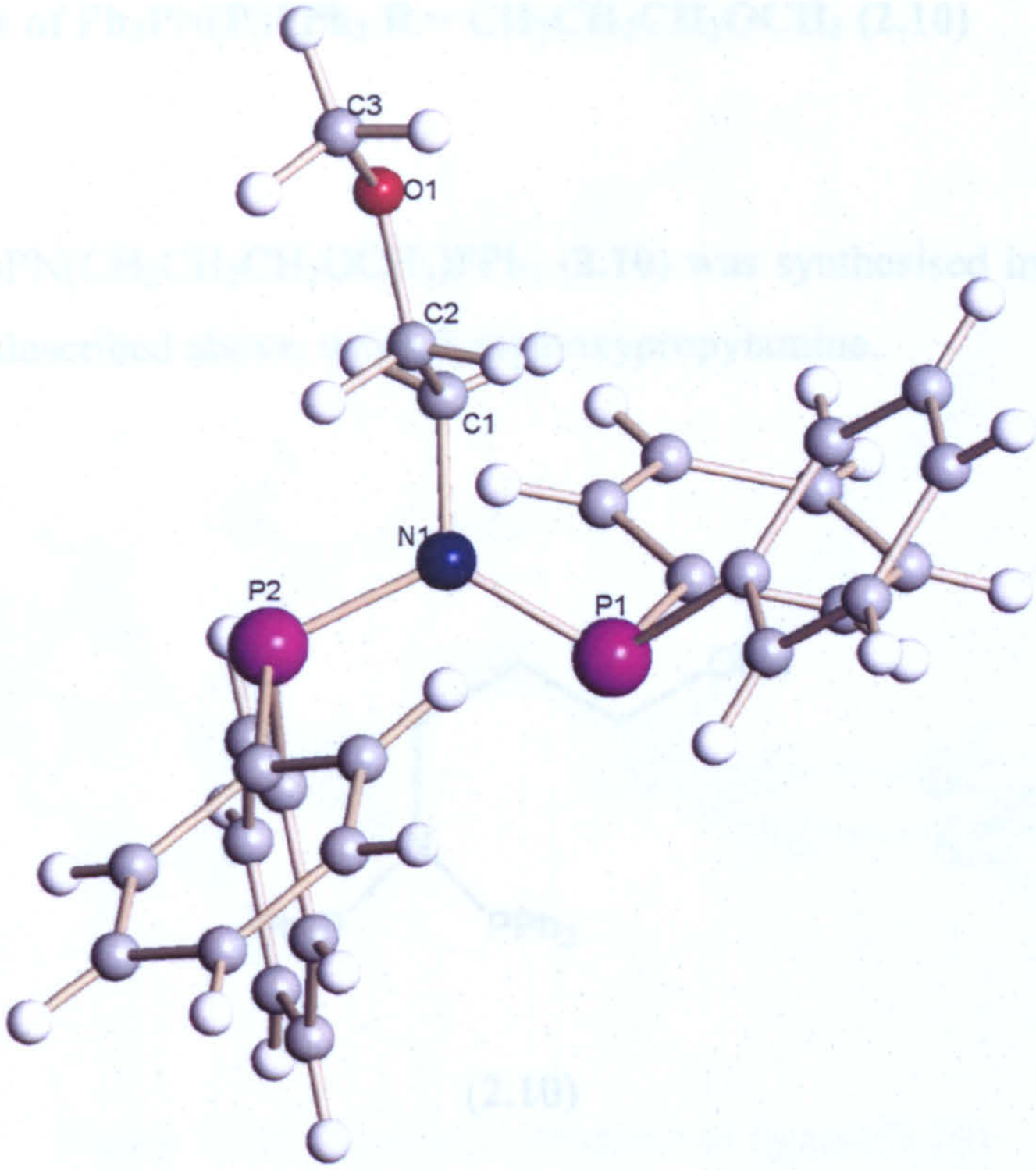

Figure 2.1 X–ray crystal structure of ligand (**2.9**)

Table 2.3 Selected bond angles and lengths for ligand (**2.9**)

Bond Length	Å	Bond Angle	Degrees °
P(1) – N(1)	1.716(14)	N(1) – P(1) – C(10)	103.8(7)
P(2) – N(1)	1.721(14)	N(1) – P(1) – C(4)	103.8(7)
C(1) – N(1)	1.484(19)	C(10) – P(1) – C(4)	99.9(8)
C(4) – P(1)	1.845(17)	N(1) – P(2) – C(16)	104.4(7)
C(10) – P(1)	1.838(18)	N(1) – P(2) – C(16)	106.0(7)
C(16) – P(2)	1.834(17)	C(16) – P(2) – C(22)	100.6(7)
C(22) – P(2)	1.834(17)	C(1) – N(1) – P(1)	122.9(11)
		C(1) – N(1) – P(2)	114.1(11)
		P(1) – N(1) – P(2)	122.7(7)

2.4.2 Synthesis of $Ph_2PN(R)PPh_2$ R = $CH_2CH_2CH_2OCH_3$ (2.10)

The ligand $Ph_2PN(CH_2CH_2CH_2OCH_3)PPh_2$ (**2.10**) was synthesised in a similar fashion to ligand (**2.9**) described above, using 3-methoxypropylamine.

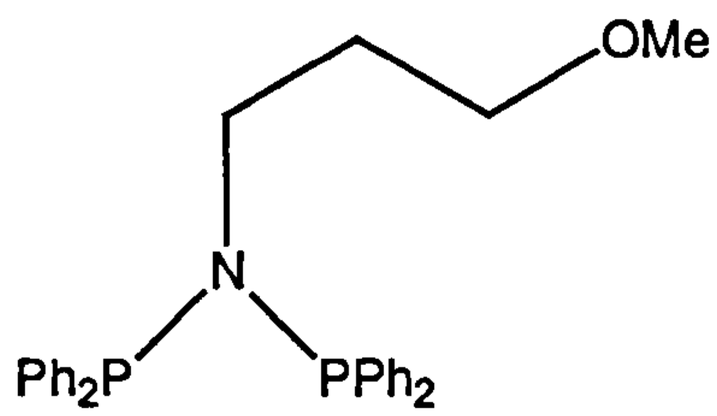

(2.10)

Single crystals were formed from the acetonitrile solution at 0 °C, and these were analysed by $^{31}P\{^1H\}$ (see Table 2.5), $^{13}C\{^1H\}$, ^1H NMR spectroscopy, mass spectrometry and elemental analysis (see Experimental section for data). The structure was determined by X–ray crystallography (Figure 2.2) and selected bond lengths and angles are given in Table 2.4. The crystals are orthorhombic with 4 molecules per unit cell; in the solid state the phosphorus atoms appear to be in the same environment unlike ligand (**2.9**). The P(1) - N(1) bond length is 1.702(3) Å, P(2) – N(1) 1.715(3) Å with the P(1) – N(1) – P(2) angle 110.8(16)°. The PNP angles are similar for (**2.10**) 110.8(16)° and for the analogous ligand (**2.9**), 122.7(7)°. The lone pairs in (**2.10**) are *syn* to each other unlike in (**2.9**) where an *anti* conformation is adopted.

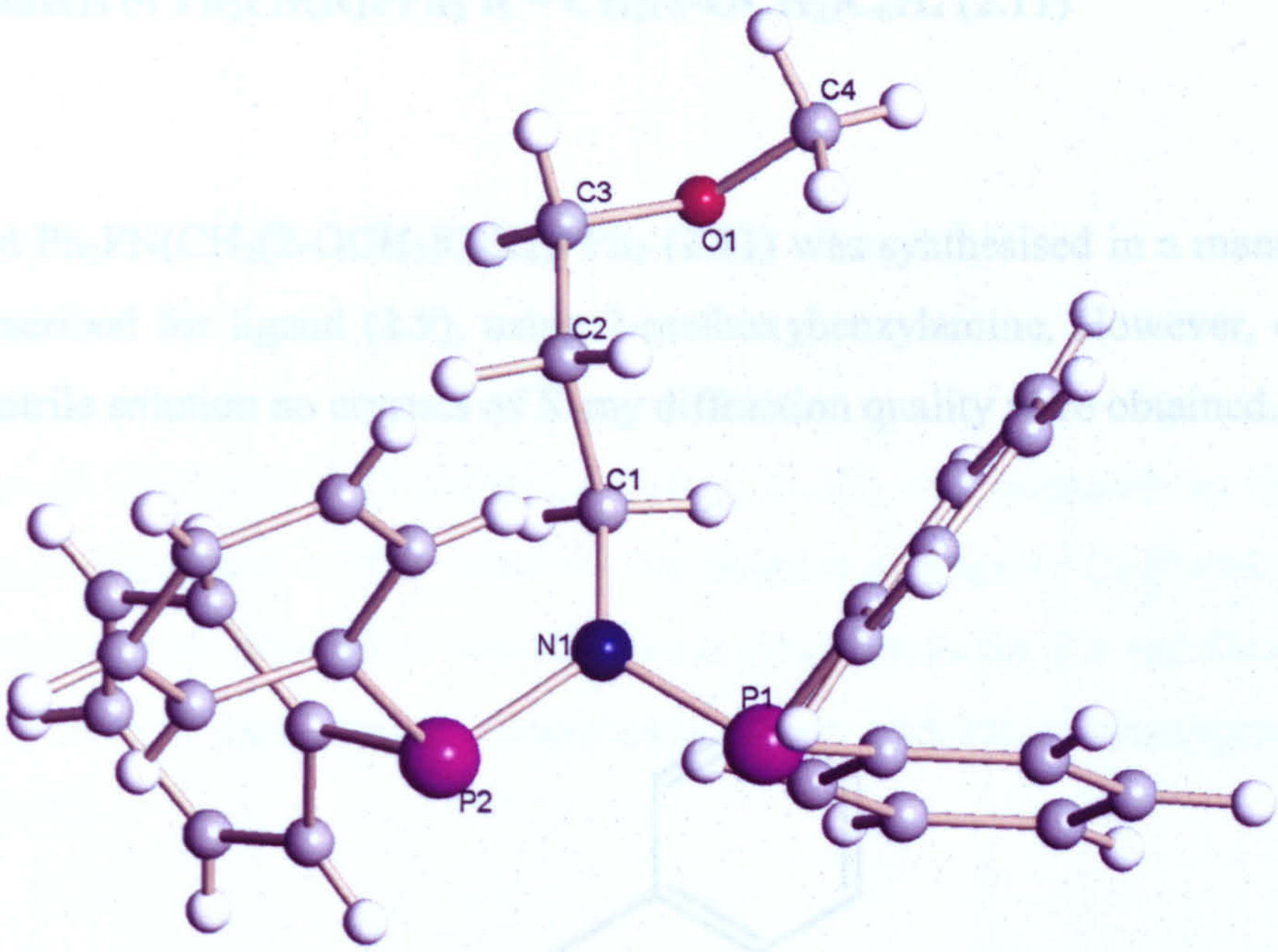

Figure 2.2 X–ray crystal structure of ligand (**2.10**)

Table 2.4 Selected bond angles and lengths for ligand (**2.10**)

Bond Length	Å	Bond Angle	Degrees °
P(1) – N(1)	1.702(3)	N(1) – P(1) – C(17)	103 2(17)
P(2) – N(1)	1.715(3)	N(1) – P(1) – C(23)	106.4(16)
C(1) – N(1)	1.470(5)	C(17) – P(1) – C(23)	103.3(17)
C(17) – P(1)	1.834(4)	N(1) – P(2) – C(5)	106.3(16)
C(23) – P(1)	1.834(4)	N(1) – P(2) – C(11)	105.1(17)
C(5) – P(2)	1.829(4)	C(5) – P(2) – C(11)	102.2(17)
C(11) – P(2)	1.827(4)	C(1) – N(1) – P(1)	124.0(2)
		C(1) – N(1) – P(2)	124.6(3)
		P(1) – N(1) – P(2)	110.8(16)

2.4.3 Synthesis of $Ph_2PN(R)PPh_2$ R = $CH_2(2\text{-}OCH_3)C_6H_4$ (2.11)

The ligand $Ph_2PN(CH_2(2\text{-}OCH_3)C_6H_4)PPh_2$ (**2.11**) was synthesised in a manner similar to that described for ligand (**2.9**), using 2-methoxybenzylamine. However, on cooling the acetonitrile solution no crystals of X-ray diffraction quality were obtained.

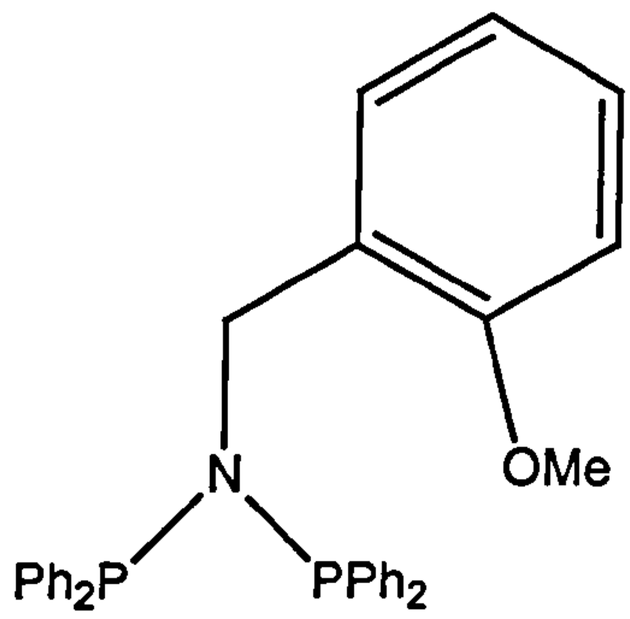

(2.11)

The ligand (**2.11**) was analysed by $^{31}P\{^1H\}$ (see Table 2.5), $^{13}C\{^1H\}$, ^1H NMR spectroscopy, mass spectrometry and elemental analysis (see Experimental section for data).

Table 2.5 $^{31}P\{^1H\}$ NMR data for ligands (**2.9 – 2.11**)

No.	Ligand	δ ppm
(2.9)	$(C_6H_5)_2PN(CH_2CH_2OCH_3)P(C_6H_5)_2$	64.9 (s)[a]
(2.10)	$(C_6H_5)_2PN(CH_2CH_2CH_2OCH_3)P(C_6H_5)_2$	63.4 (s)[b]
(2.11)	$(C_6H_5)_2PN(CH_2(2\text{-}OCH_3)C_6H_4)P(C_6H_5)_2$	58.8 (s)[a]

[a] Spectra recorded at 162 MHz in $CDCl_3$ at 22 °C. Chemical shifts (δ) in ppm (± 0.1) to high frequency of H_3PO_4.

[b] Spectra recorded at 162 MHz in CD_2Cl_2 at 22 °C. Chemical shifts (δ) in ppm (± 0.1) to high frequency of H_3PO_4.

2.5 Synthesis of $Ar_2PNMePAr_2$

2.5.1 Synthesis of $(2\text{-}CF_3C_6H_4)_2PN(Me)P(2\text{-}CF_3C_6H_4)_2$ (2.12)

The ligand $(2\text{-}CF_3C_6H_4)_2PN(Me)P(2\text{-}CF_3C_6H_4)_2$ **(2.12)** was prepared by lithiating 2-bromobenzotrifluoride at – 78 °C followed by the slow addition of $Cl_2PN(Me)PCl_2$. The reaction mixture was allowed to warm to room temperature for 2 h and then quenched using dilute HCl; a pure product precipitated out on addition of deoxygenated water (Equation 2.8).

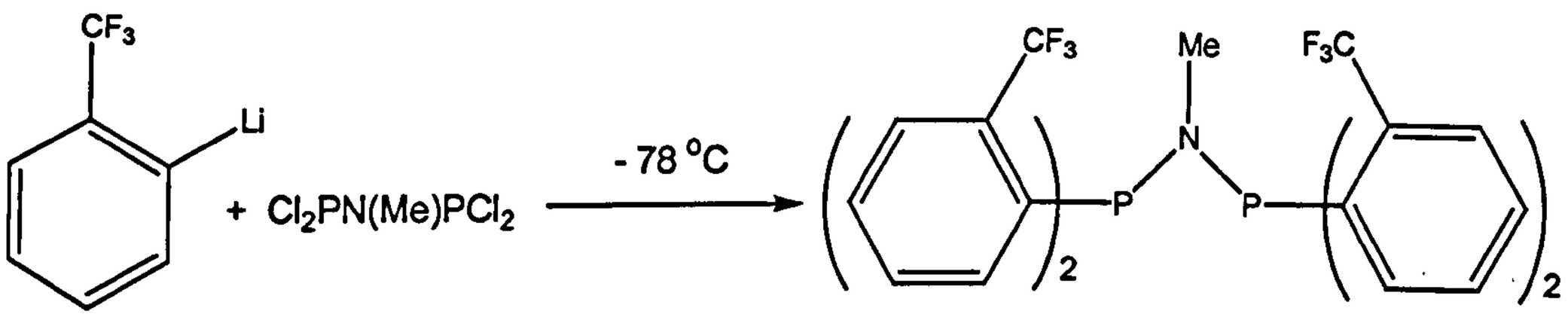

(2.12)

Equation 2.8

The $^{31}P\{^1H\}$ NMR spectrum is shown in Figure 2.3; the complex multiplet at δ 63.8 ppm is due to the $AX_6A'X'_6$ spin system (see Experimental for $^{19}F\{^1H\}$, $^{13}C\{^1H\}$, ^1H NMR spectroscopy and elemental analysis data).

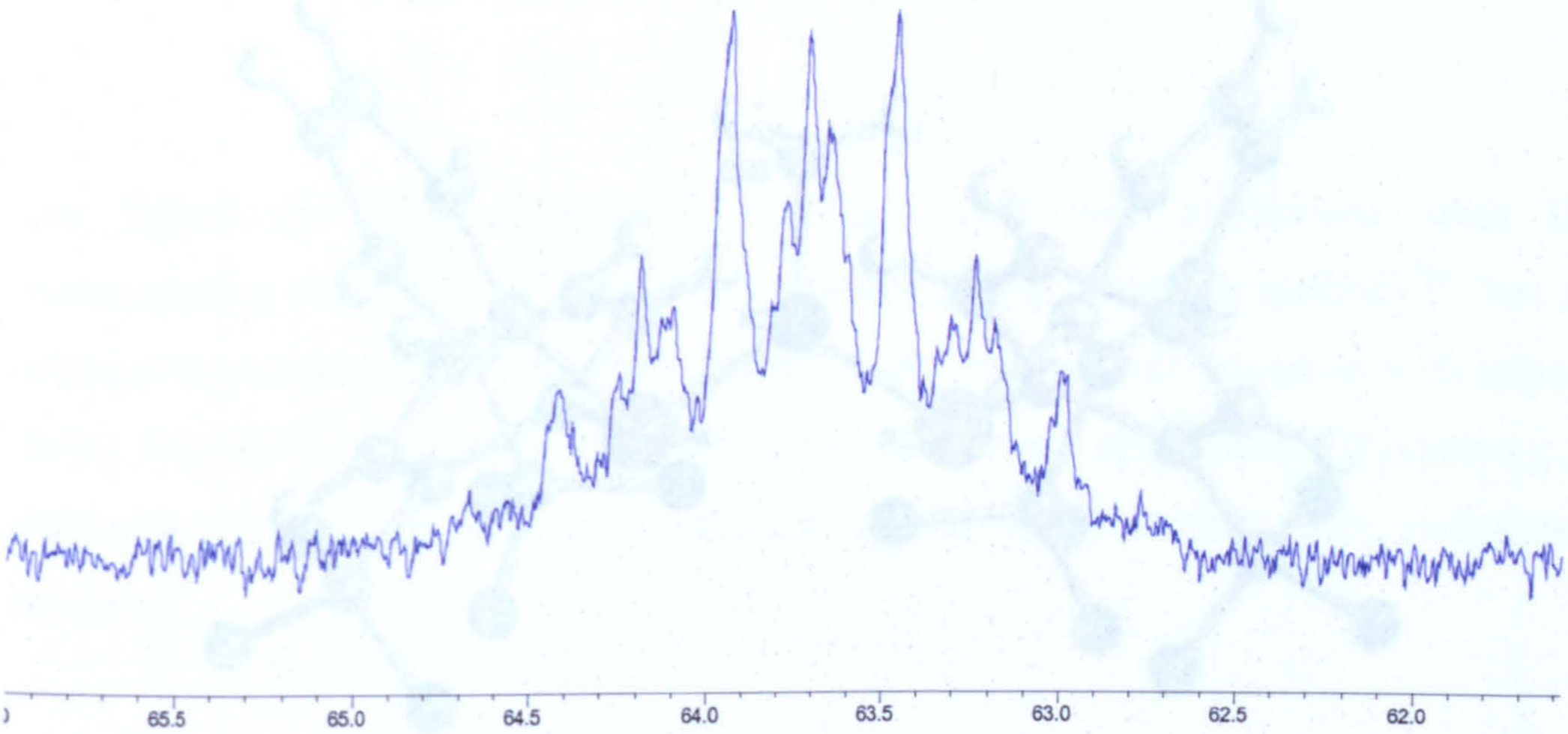

Figure 2.3 $^{31}P\{^{1}H\}$ NMR spectrum for (**2.12**)

The mass spectrum of (**2.12**) showed an M^+ at $m/z = 671$. Single crystals of (**2.12**) were grown from dichloromethane and the structure was determined by X–ray crystallography (Figure 2.4). Selected bond lengths and angles are given in Table 2.6. The crystal is orthorhombic with 8 molecules per unit cell. The P(3) - N(2) bond length is 1.703(6) Å, P(4) – N(2) 1.723(6) Å with the P(1) – N(1) – P(2) angle 112.2(3)° and the lone pairs on the phosphorus are *syn* to each other. The PN bond lengths are comparable to those for ligands (**2.9**) and (**2.10**) with the PNP angle of 112.2(3)° for (**2.12**) of a similar magnitude to (**2.10**) 110.8(16)°.

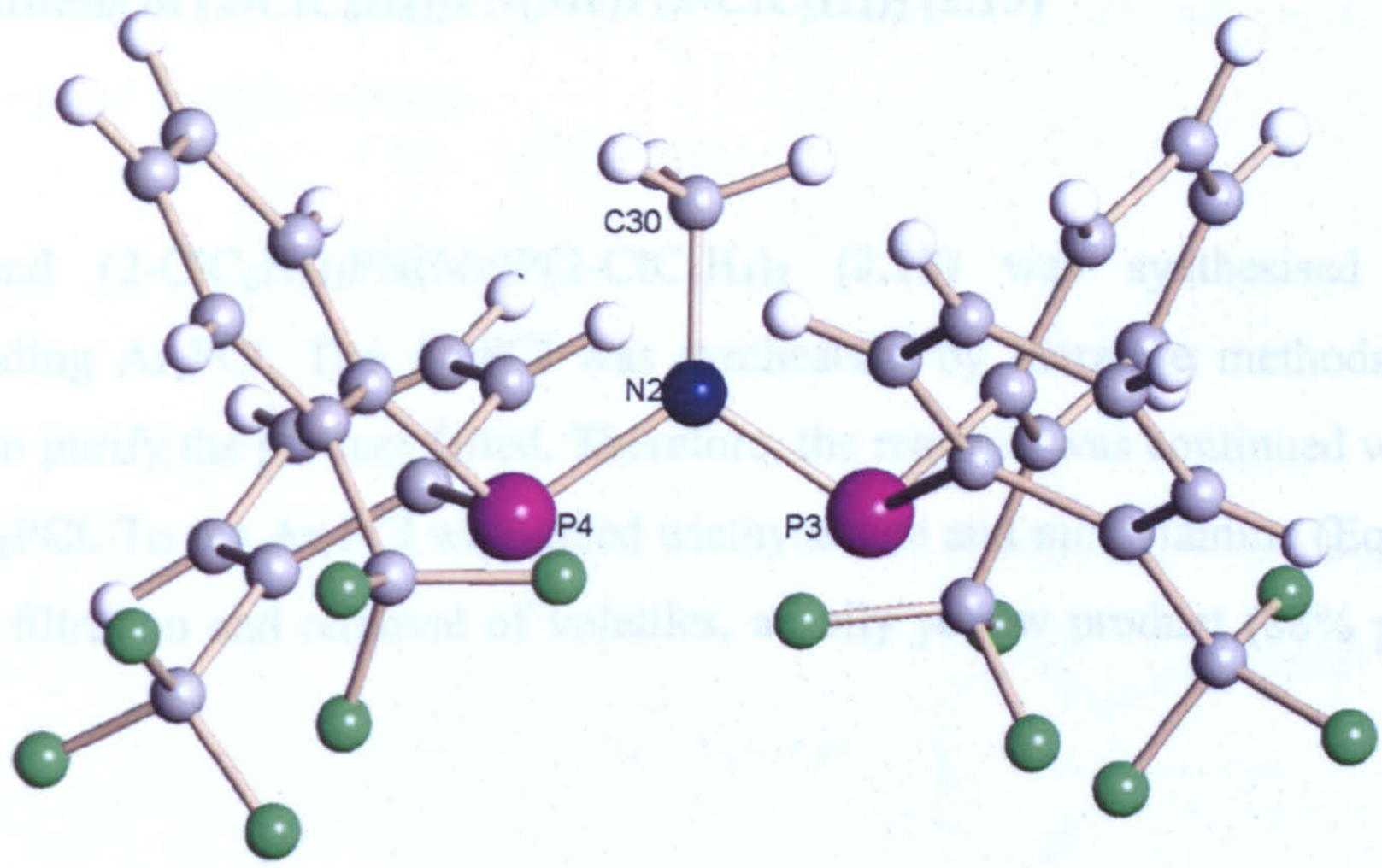

Figure 2.4 X–ray crystal structure of ligand (**2.12**)

Table 2.6 Selected bond angles and lengths for ligand (**2.12**)

Bond Length	Å	Bond Angle	Degrees °
P(3) – N(2)	1.703(6)	N(2) – P(3) – C(38)	100.7(3)
P(4) – N(2)	1.725(6)	N(2) – P(3) – C(31)	105.2(3)
N(2) – C(30)	1.495(8)	C(38) – P(3) – C(31)	99.4(4)
P(3) – C(38)	1.846(9)	N(2) – P(4) – C(52)	104.9(3)
P(3) – C(31)	1.852(8)	N(2) – P(4) – C(45)	101.9(3)
P(4) – C(45)	1.845(8)	C(30) – N(2) – P(3)	123.8(5)
P(4) – C(52)	1.844(8)	C(30) – N(2) – P(4)	123.9(5)
		P(3) – N(2) – P(4)	112.2(3)

2.5.2 Synthesis of $(2\text{-}ClC_6H_4)_2PN(Me)P(2\text{-}ClC_6H_4)_2$ (2.13)

The ligand $(2\text{-}ClC_6H_4)_2PN(Me)P(2\text{-}ClC_6H_4)_2$ (**2.13**) was synthesised from the corresponding Ar_2PCl. The Ar_2PCl was synthesised by literature methods[86] but all attempts to purify the product failed. Therefore, the reaction was continued with impure (80%) Ar_2PCl. To the Ar_2PCl was added triethylamine and methylamine (Equation 2.9) and upon filtration and removal of volatiles, an oily yellow product (88% purity) was obtained.

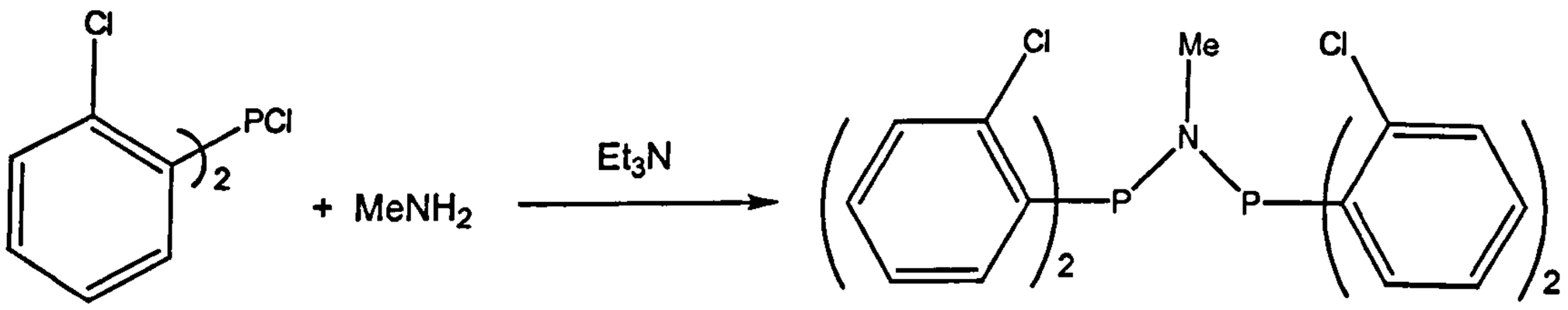

(2.13)

Equation 2.9

Mass spectrometry confirmed the product to be (**2.13**) with the M^+ at m/z = 538 displaying the correct isotope pattern expected with the presence of 4 chlorine atoms (see Table 2.7 for $^{31}P\{^1H\}$ NMR data).

2.5.3 Synthesis of $(o\text{-}OCH_3C_6H_4)(C_6H_5)PN(Me)P(C_6H_5)(o\text{-}OCH_3C_6H_4)$ (2.14)

The ligand (**2.14**) was synthesised by Philip Winder according to Scheme 2.1. The $PhPCl(NEt_2)$ was reacted with lithiated anisole and this was followed by removal of the diethylamine with HCl to give the substituted chlorophosphine. This compound was then reacted with methylamine yielding the *rac* and *meso* diastereoisomers of the

desired product. On washing the residue with MeOH, the *rac* isomer was left undissolved and thereby isolated.

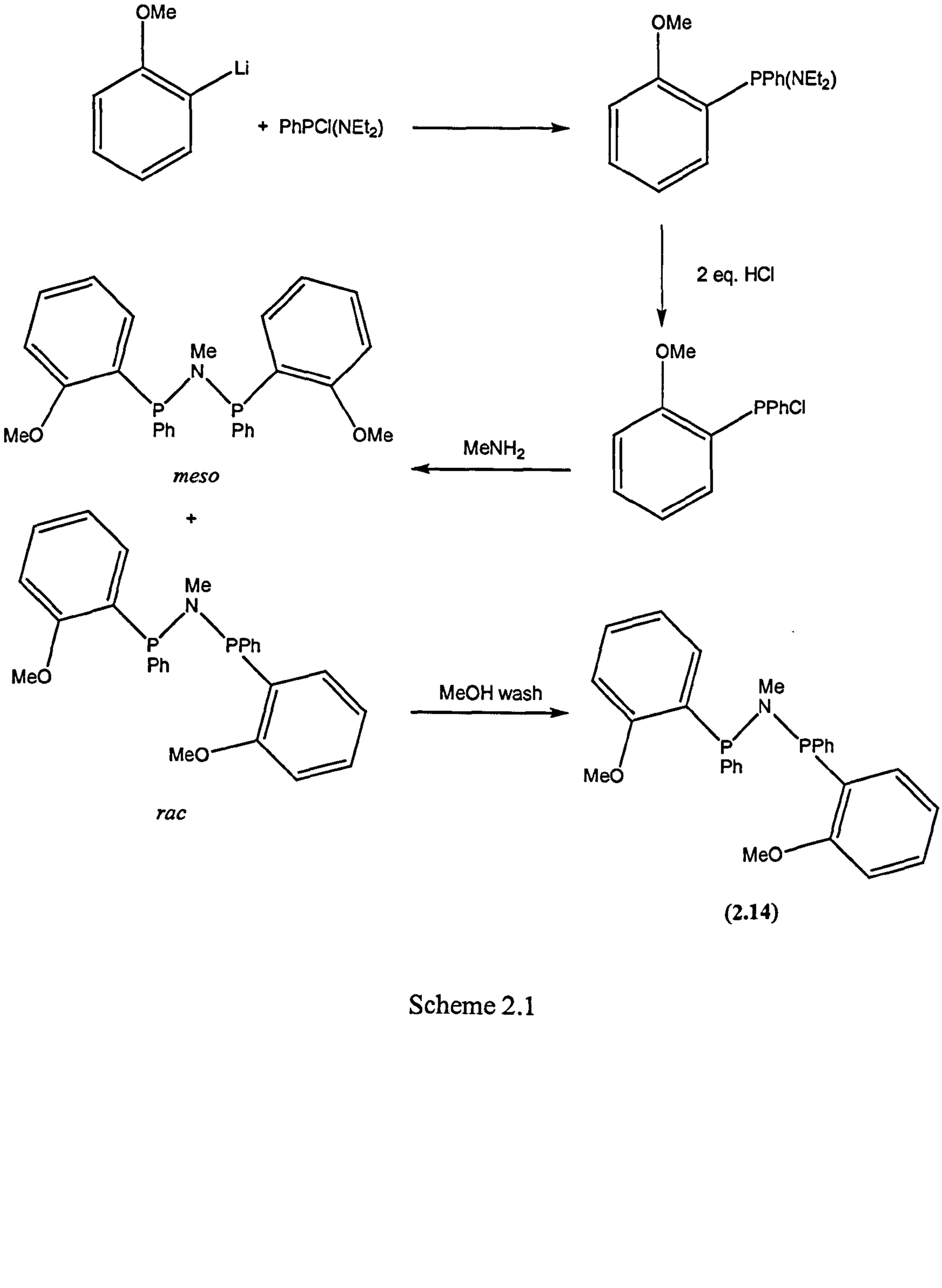

(2.14)

Scheme 2.1

Table 2.7 $^{31}P\{^{1}H\}$ NMR data for ligands (**2.12 – 2.14**)

No.	Ligand	δ ppm
(2.12)	$(2\text{-}CF_3C_6H_4)_2PN(Me)P(2\text{-}CF_3C_6H_4)_2$	63.8 (dsep, J_{PF} 27.3 Hz)[b]
(2.13)	$(2\text{-}ClC_6H_4)_2PN(Me)P(2\text{-}ClC_6H_4)_2$	36.3 (s)[a]
(2.14)	(*o*-$OCH_3C_6H_4$)(C_6H_5)PN(Me)P(C_6H_5)(*o*-$OCH_3C_6H_4$)[c]	64.5 (s, major *rac* isomer), 62.9 (s, minor *meso* isomer)[b]

[a] Spectra recorded at 121 MHz in $CDCl_3$ at 22 °C. Chemical shifts (δ) in ppm (± 0.1) to high frequency of H_3PO_4.

[b] Spectra recorded at 162 MHz in $CDCl_3$ at 22 °C. Chemical shifts (δ) in ppm (± 0.1) to high frequency of H_3PO_4. Coupling constants (*J*) in Hz (± 0.1).

[c] Synthesised by Philip Winder

2.6 Synthesis of diphosphoramidites

2.6.1 Synthesis of ((*R*)-1,1′-bi-2-naphthoxo)PN(Me)P((*R*)-1,1′-bi-2-naphthoxo) (2.15)

Initially the synthesis of ((*R*)-1,1′-bi-2-naphthoxo)PN(Me)P((*R*)-1,1′-bi-2-naphthoxo) (**2.15**) was attempted *via* the method described by Faraone[83] and co-workers, by reacting the chlorophosphite and primary amine at 0 °C in the presence of triethylamine (Equation 2.10). Unfortunately this gave rise to inseparable impurities.

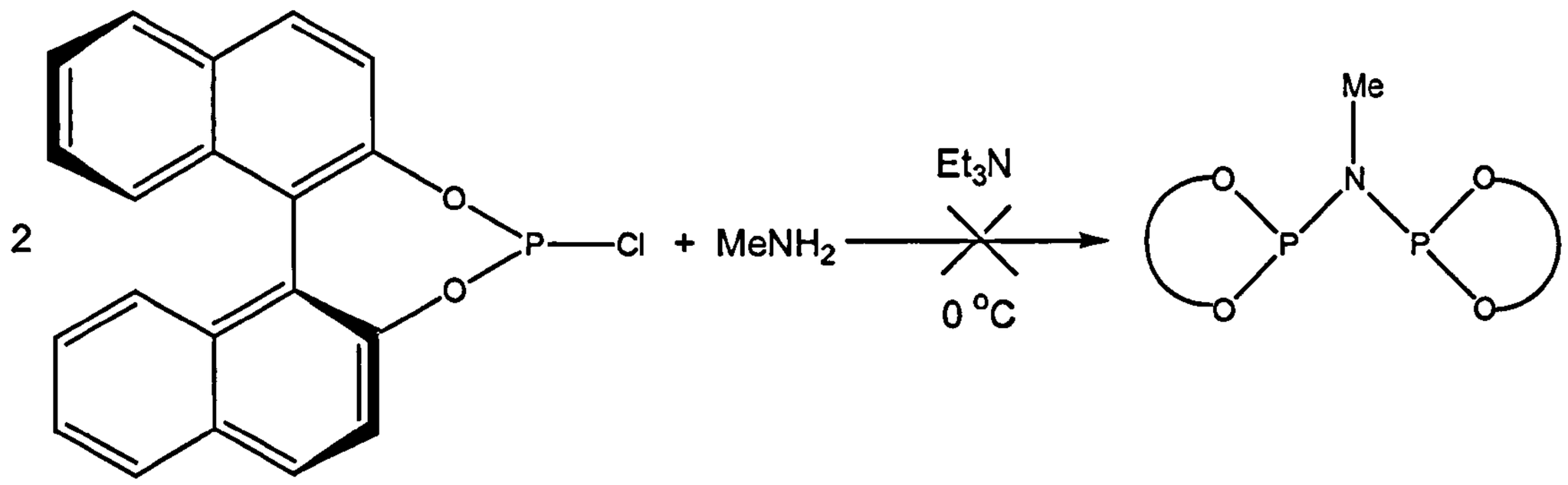

Equation 2.10

However, using anhydrous (*R*)-1,1′-bi-2-naphthol and reacting with $Cl_2PN(Me)PCl_2$ in toluene at room temperature in the presence of triethylamine (Equation 2.11), followed by subsequent filtration and removal of volatiles gave (**2.15**) as a white solid. While this work was in progress, this method was used by Krishnamurthy *et al.*[87] to produce (**2.15**) for the synthesis of ruthenium carbonyl clusters.

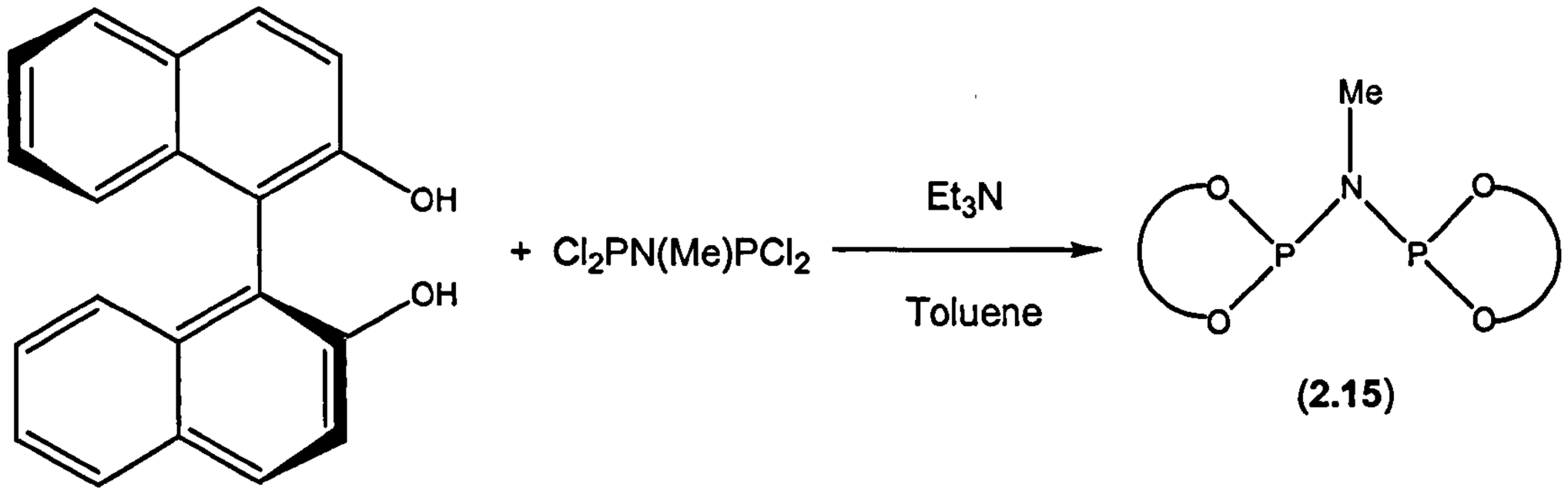

(2.15)

Equation 2.11

The product was analysed by $^{31}P\{^1H\}$ (see Table 2.10), $^{13}C\{^1H\}$, ^1H NMR spectroscopy mass spectrometry and elemental analysis (see Experimental section for data).

2.6.2 Synthesis of ((*S*)-9,9′-biphenanthryl-10,10′-dioxo)PN(Me)P((*S*)-9,9′-biphenanthryl-10,10′-dioxo) (2.16)

The ligand (**2.16**) was synthesised by the addition of $Cl_2PN(Me)PCl_2$ to anhydrous (*S*)-9,9′-biphenanthryl-10,10′-diol with triethylamine[88] in toluene (Equation 2.12).

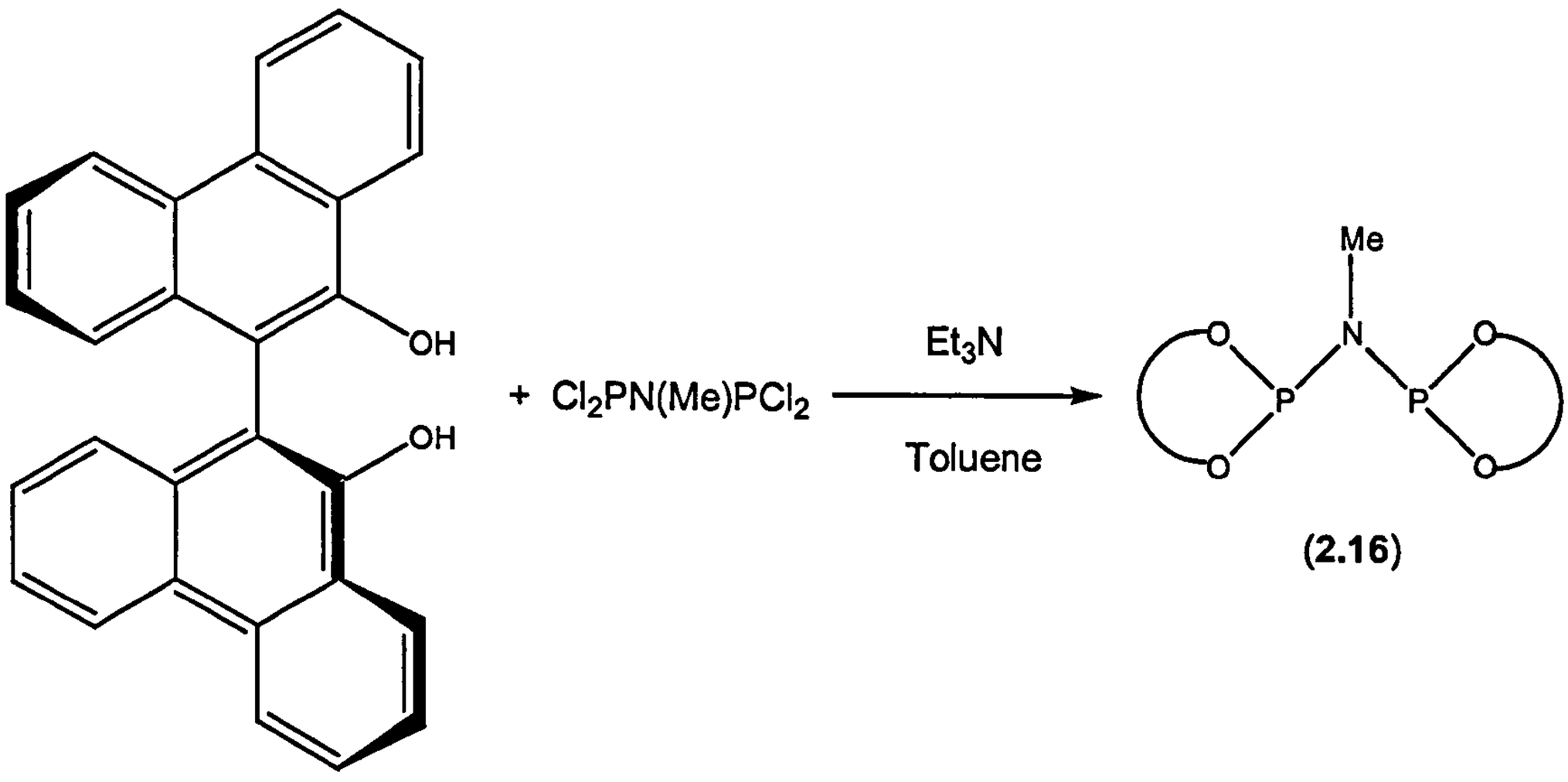

(2.16)

Equation 2.12

The reaction mixture was stirred overnight, filtered and upon removal of solvents *in vacuo*, (**2.16**) was formed as a yellow solid in 79% yield. This yellow solid was analysed by $^{31}P\{^1H\}$ (see Table 2.10), $^{13}C\{^1H\}$, ^1H NMR spectroscopy and elemental analysis (see Experimental section for data). Mass spectrometry is consistent with the product being (**2.16**), M^+ at $m/z = 860$.

2.6.3 Synthesis of a mixture of *rac* and *meso* (9,9′-biphenanthryl-10,10′-dioxo)PN(Me)P(9,9′-biphenanthryl-10,10′-dioxo) (2.17)

The mixture (**2.17**) was synthesised by the method described above for ligand (**2.16**) (Equation 2.12), using racemic-9,9′-biphenanthryl-10,10′-diol. A yellow solid was produced in 82% yield and the product was analysed by $^{31}P\{^{1}H\}$ (see Table 2.10) (Figure 2.6), ^{1}H NMR spectroscopy, mass spectrometry and elemental analysis (see Experimental section for data). Crystallisation from chloroform yielded single crystals and X–ray crystallography (Figure 2.8) revealed these to be the *meso* isomer of (**2.17**). The unit cell of the crystal structure for the *meso* product is triclinic, it shows the ligand to adopt two different conformations in the solid state (Figure 2.8). These have been labelled rotamer 1 (Figure 2.9) and rotamer 2 (Figure 2.10). Selected bond lengths and angles are given in Tables 2.8, 2.9.

The $^{31}P\{^{1}H\}$ NMR spectrum indicated a 5:1 mixture of diastereoisomers. The minor peak at δ 147.4 ppm corresponds to the *rac* diastereoisomer, confirmed by the $^{31}P\{^{1}H\}$ NMR of the optically pure (**2.16**). The major peak at δ 156.1 ppm was therefore assigned to the *meso* diastereoisomer and was broad at room temperature (Figure 2.6). At – 55 °C this peak splits into two peaks at δ 169.5 ppm and 151.0 ppm (Figure 2.7).

syn rotamer 1 *anti* rotamer 2

Figure 2.5

At low temperature the preferred geometry of (**2.17**) is tentatively assigned to rotamer 2 (Figure 2.10). Figure 2.5 shows the two phosphorus atoms in rotamer 2, a and b are in different environments and thus would be expected to give two peaks in $^{31}P\{^{1}H\}$ NMR spectrum of equal intensity. The ratio of the two peaks in (Figure 2.7) is approximately 1.1:2, which could indicate inaccurate integrals or could be due to a small quantity of rotamer 1 present where the singlet resonance is under the signal at δ 151.1 ppm. As the temperature increases the energetically less favourable rotamer 1 would become more accessible and then the ratio of the rotamers would change. This would explain the room temperature $^{31}P\{^{1}H\}$ NMR (Figure 2.6) showing coalescence, at δ 156.1 ppm instead of the mean value of 160 ppm.

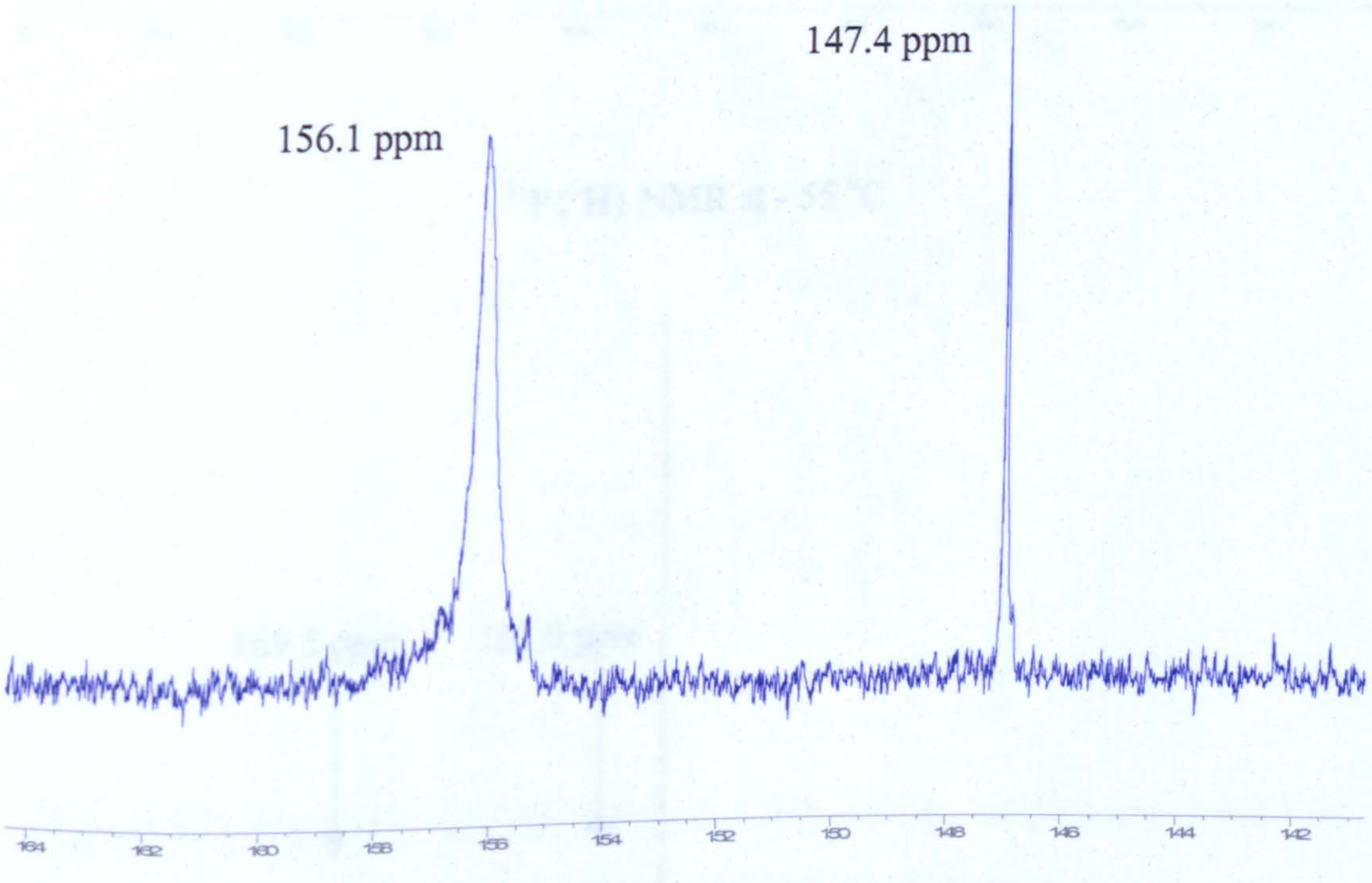

Figure 2.6 $^{31}P\{^{1}H\}$ NMR at room temperature (23 °C) for ligand (**2.17**)

$^{31}P\{H\}$ NMR at – 15 °C

$^{31}P\{^{1}H\}$ NMR at - 55 °C

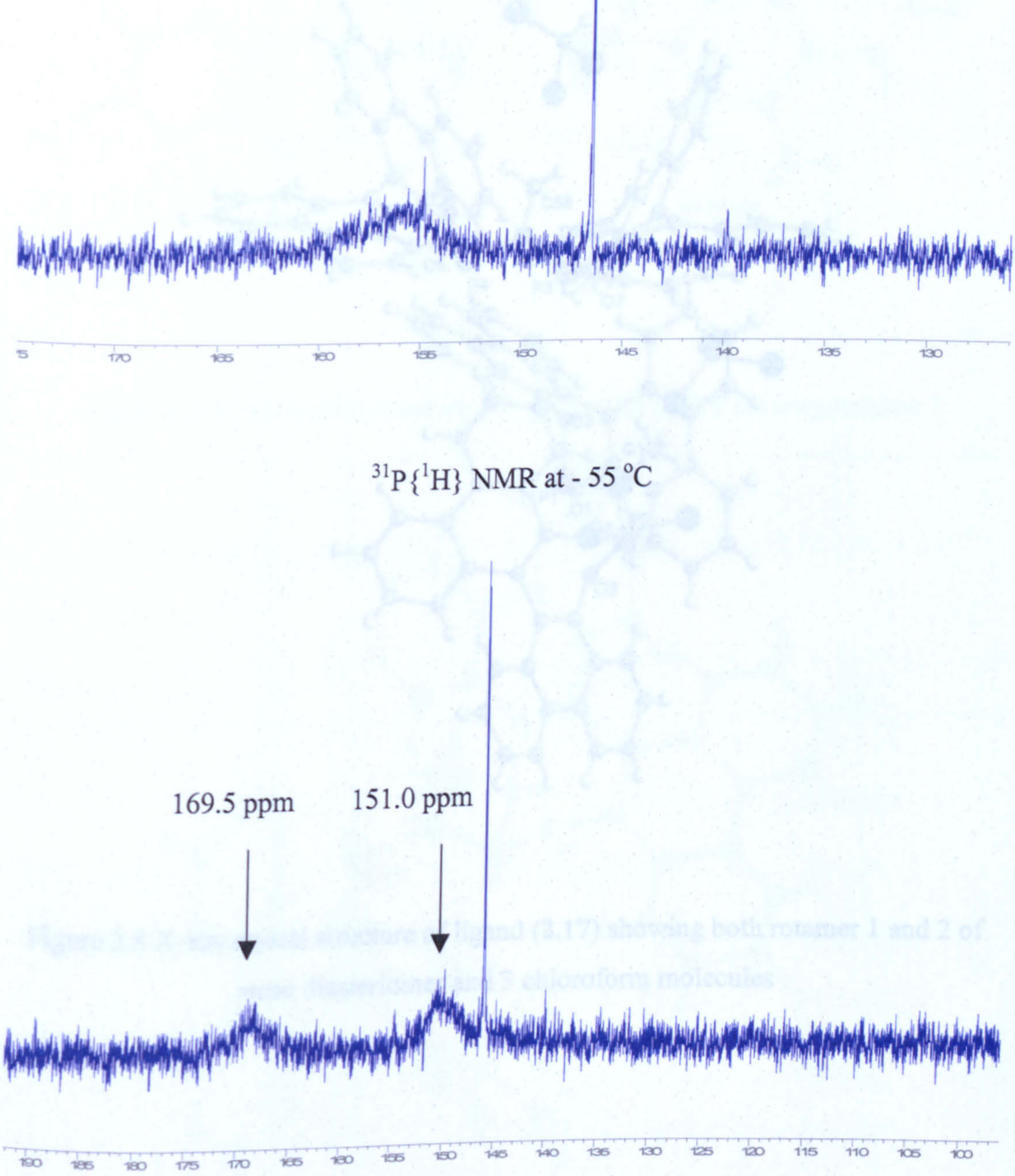

Figure 2.7 Low temperature $^{31}P\{^{1}H\}$ NMR for ligand (**2.17**)

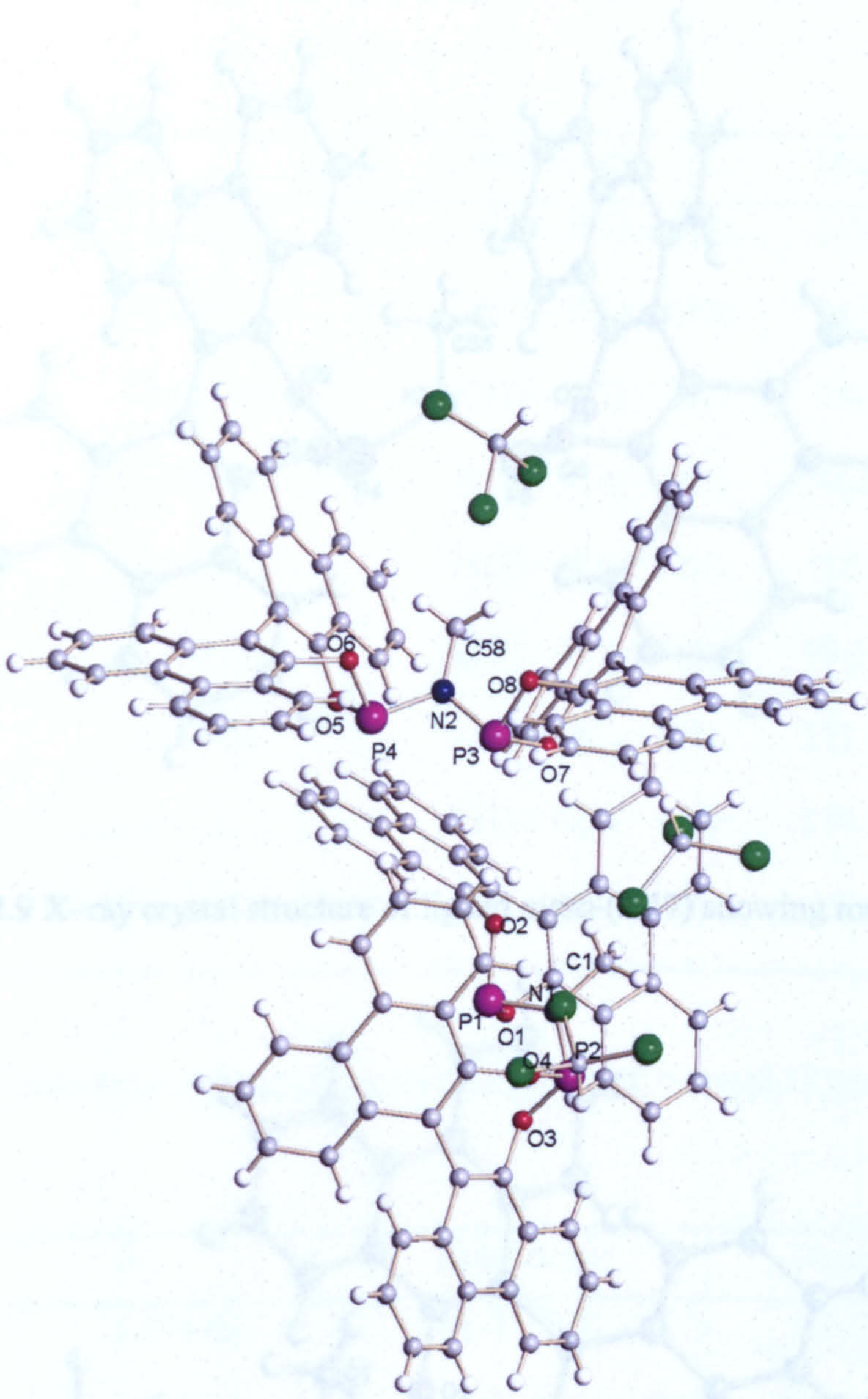

Figure 2.8 X–ray crystal structure of ligand (**2.17**) showing both rotamer 1 and 2 of *meso* diasteriomer and 3 chloroform molecules

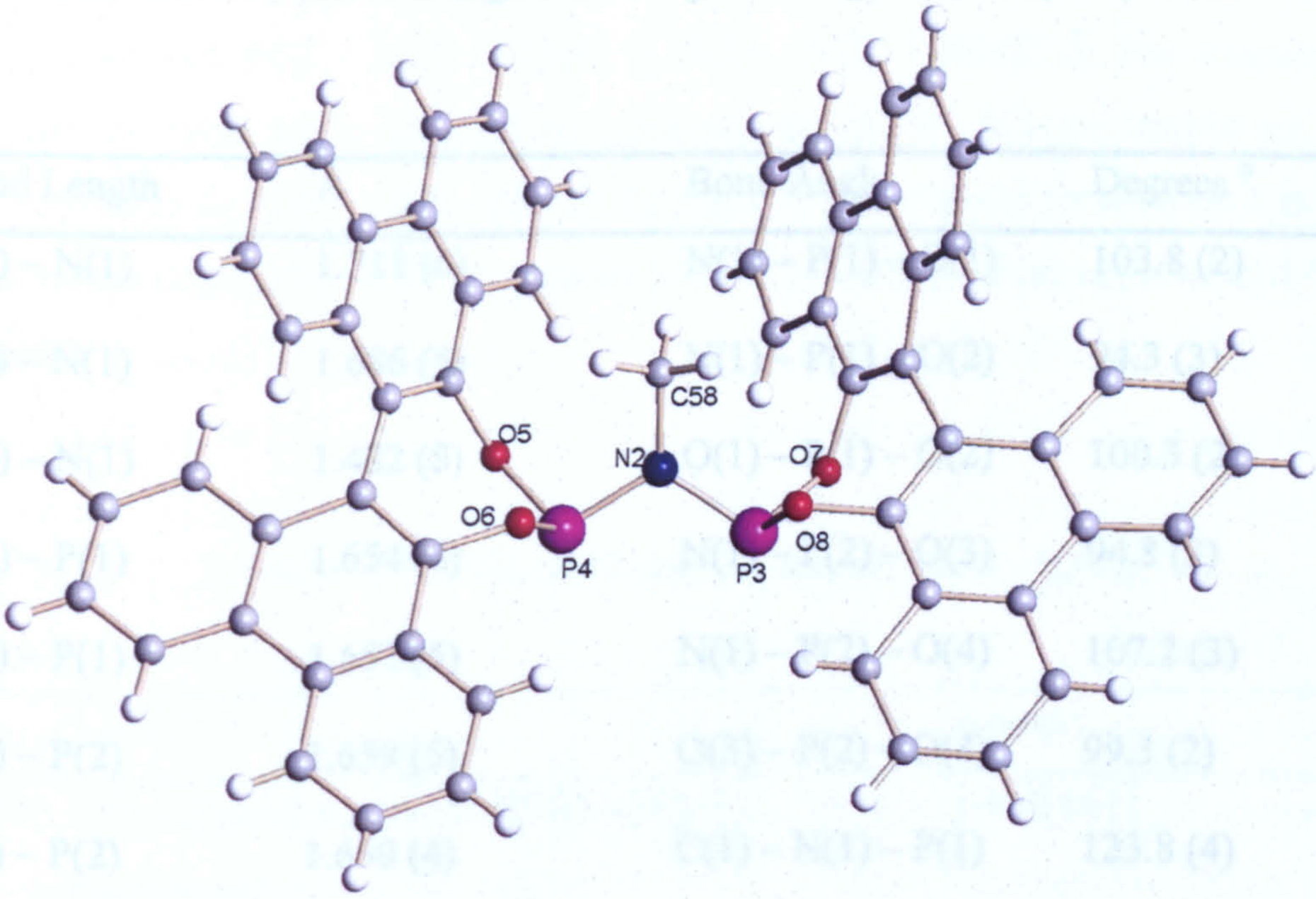

Figure 2.9 X–ray crystal structure of ligand *meso*-(**2.17**) showing rotamer 1

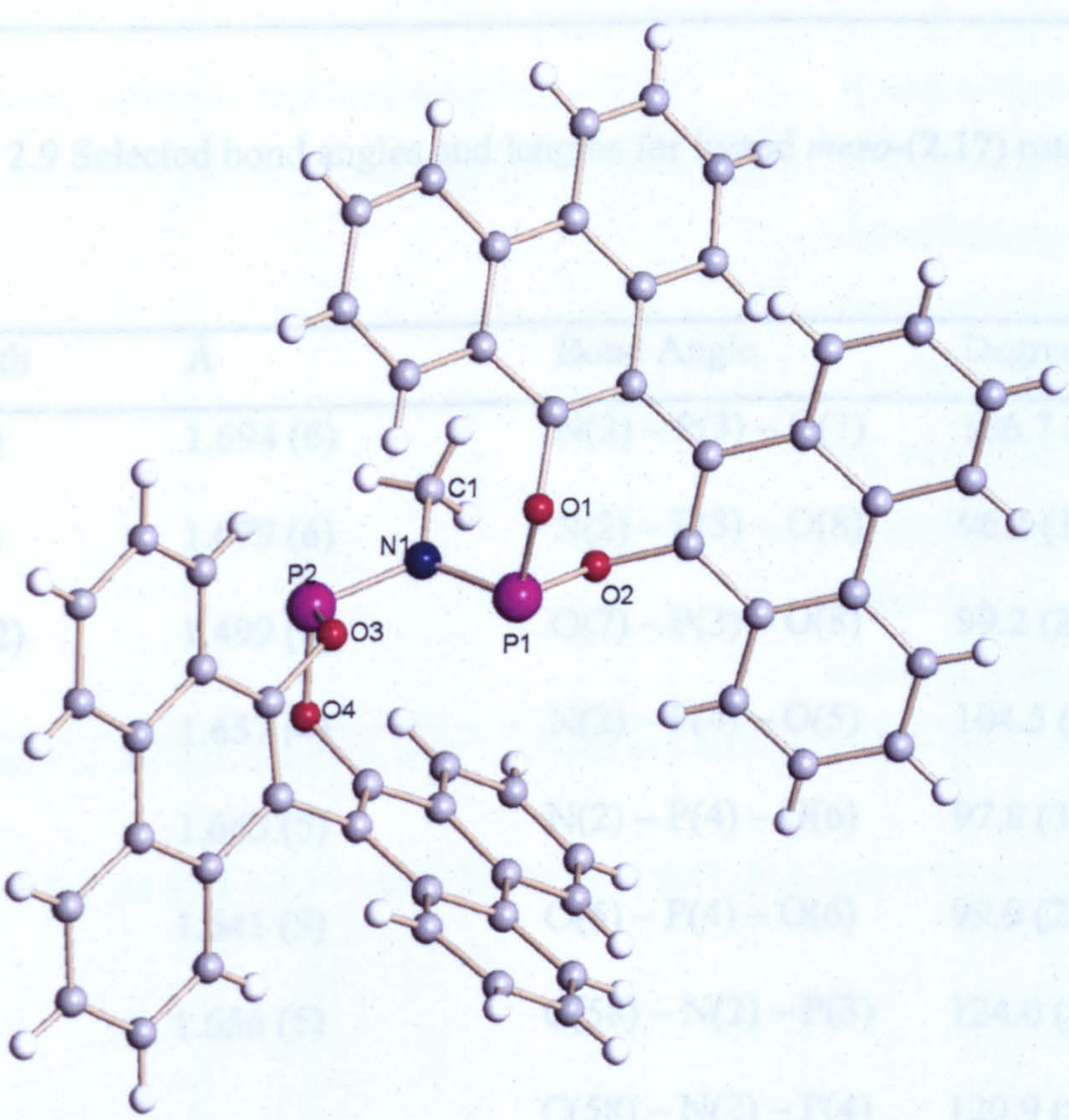

Figure 2.10 X–ray crystal structure of ligand *meso*-(**2.17**) showing rotamer 2

Table 2.8 Selected bond angles and lengths for ligand *meso*-(**2.17**) rotamer 1

Bond Length	Å	Bond Angle	Degrees °
P(1) – N(1)	1.711 (6)	N(1) – P(1) – O(1)	103.8 (2)
P(2) – N(1)	1.686 (5)	N(1) – P(1) – O(2)	94.3 (3)
C(1) – N(1)	1.482 (8)	O(1) – P(1) – O(2)	100.3 (2)
O(1) – P(1)	1.654 (4)	N(1) – P(2) – O(3)	94.8 (3)
O(2) – P(1)	1.653 (5)	N(1) – P(2) – O(4)	107.2 (3)
O(3) – P(2)	1.659 (5)	O(3) – P(2) – O(4)	99.3 (2)
O(4) – P(2)	1.650 (4)	C(1) – N(1) – P(1)	123.8 (4)
		C(1) – N(1) – P(2)	114.3 (4)
		P(1) – N(1) – P(2)	121.9 (3)

Table 2.9 Selected bond angles and lengths for ligand *meso*-(**2.17**) rotamer 2

Bond Length	Å	Bond Angle	Degrees °
P(3) – N(2)	1.694 (6)	N(2) – P(3) – O(7)	106.7 (3)
P(4) – N(2)	1.679 (6)	N(2) – P(3) – O(8)	96.3 (3)
C(58) – N(2)	1.499 (8)	O(7) – P(3) – O(8)	99.2 (2)
O(7) – P(3)	1.657 (4)	N(2) – P(4) – O(5)	104.5 (3)
O(8) – P(3)	1.643 (5)	N(2) – P(4) – O(6)	97.8 (3)
O(5) – P(4)	1.641 (5)	O(5) – P(4) – O(6)	99.9 (2)
O(6) – P(4)	1.656 (5)	C(58) – N(2) – P(3)	124.0 (5)
		C(58) – N(2) – P(4)	120.9 (5)
		P(3) – N(2) – P(4)	114.0 (3)

The P - N bond lengths for rotamer 1 with the phosphorus atoms in the same environment are P(1) – N(1) 1.711(6) Å, P(2) – N(1) 1.680(5) Å. For rotamer 2 the phosphorus atoms are in different environments and the P - N bond lengths are P(3) – N(2) 1.694(6) Å, P(4) – N(2) 1.679(6) Å. The PNP bond angle for rotamer 1 is P(1) – N(1) – P(2) angle 121.9(3)°, for rotamer 2 the P(3) – N(2) – P(4) angle of 114.0(3)° is smaller.

Table 2.10 $^{31}P\{^{1}H\}$ NMR data for ligands (**2.15 – 2.17**)

No.	Ligand	δ ppm
(2.15)	((*R*)-1,1′-bi-2-naphthoxo)PN(Me)P((*R*)-1,1′-bi-2-naphthoxo)	144.6 (s)[a]
(2.16)	((*S*)-9,9′-biphenanthryl-10,10′-dioxo)PN(Me)P((*S*)-9,9′-biphenanthryl-10,10′-dioxo)	147.0 (s)[a]
(2.17)	Mixed *rac/meso* (9,9′-biphenanthryl-10,10′-dioxo)PN(Me)P(9,9′-biphenanthryl-10,10′-dioxo)	Room temperature 23 °C: 156.1 (br, major *meso* diasteriomer) 147.4 (s, minor *rac* diastereoisomer) - 55 °C: 169.5 (br), 151.0 (br, major *meso* diasteriomer) 147.4 (s, minor *rac* diastereoisomer)[b]

[a] Spectra recorded at 162 MHz in CD_2Cl_2 at 22 °C. Chemical shifts (δ) in ppm (± 0.1) to high frequency of H_3PO_4.

[b] Spectra recorded at 162 MHz in $CDCl_3$ at 22 °C. Chemical shifts (δ) in ppm (± 0.1) to high frequency of H_3PO_4.

2.7 Conclusion

Three sets of ligands based on the basic PNP backbone have been successfully synthesised. Firstly, a series of ligands were prepared with varied R′ group on the nitrogen $Ph_2PN(R')PPh_2$ where R′ = CH_2CH_2OMe, $CH_2CH_2CH_2OMe$, $CH_2(2\text{-}OCH_3)C_6H_4$. A new route was developed for the synthesis of the ligands where R′ = Me, Et, *n*-Pr, *i*-Pr. The second series was based on varying the *ortho*-substituent on the aryl groups in $Ar_2PN(Me)PAr_2$ where Ar = $2\text{-}CF_3C_6H_4$, $2\text{-}ClC_6H_4$; an unsymmetrical ligand $PhArPN(Me)PPhAr$ Ar = $2\text{-}OCH_3C_6H_4$ has also been synthesised. Finally a series of diphosphoramidite ligands RPN(Me)PR where R = (*R*)-1,1′-bi-2-naphthoxo, (*S*)-9,9′-biphenanthryl-10,10′-dioxo and racemic-9,9′-biphenanthryl-10,10′-dioxo have been successfully prepared. In Chapter 3, the coordination chemistry of these ligands will be reported.

Chapter 3:

Coordination chemistry of PNP ligands

Coordination chemistry of PNP ligands

3.1 Introduction to the coordination chemistry of PNP ligands

In this chapter, the coordination chemistry of the PNP ligands reported in Chapter 2 and PC_nP ($n = 1 - 3$) ligands (Figure 3.1) will be discussed. The structures of complexes of PNP and PC_nP ligands will be compared with reference to the differences in catalytic performance.[41, 35] Complexation to platinum(II) and palladium(II) has been studied due to its ease of analysis and the formation of square planar complexes, mimicking the nickel compounds used in the polyethylene catalysis reported in Chapter 4.

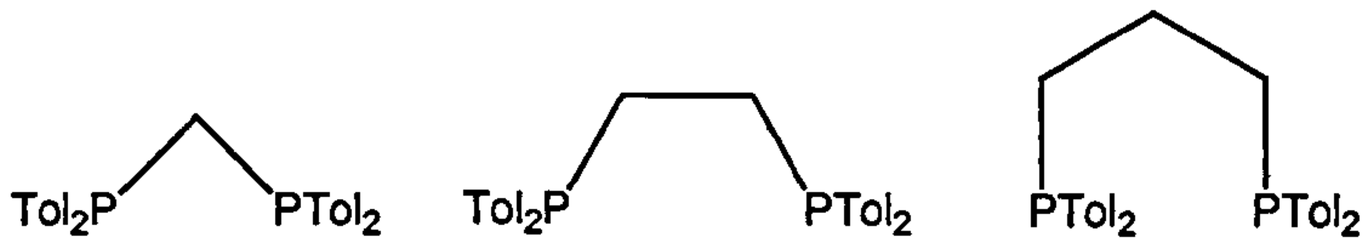

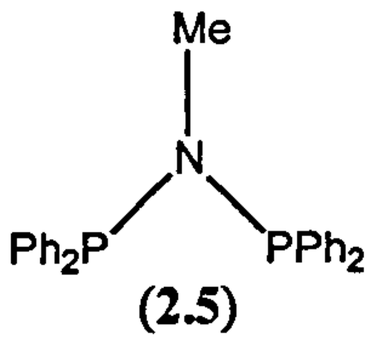

(2.5)

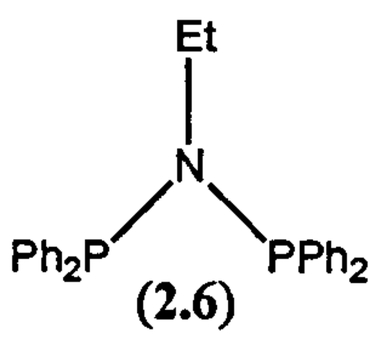

(2.6)

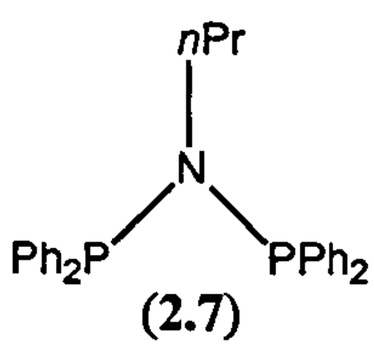

(2.7)

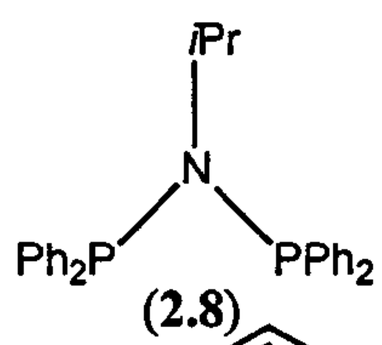

(2.8)

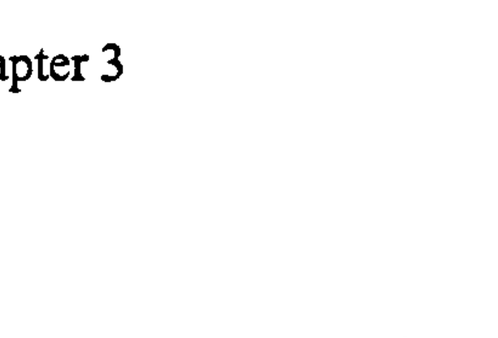

(2.9)

(2.10)

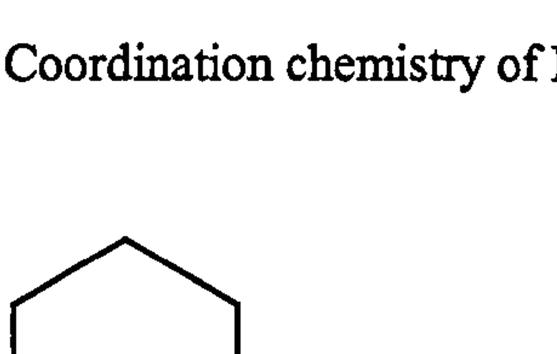

(2.11)

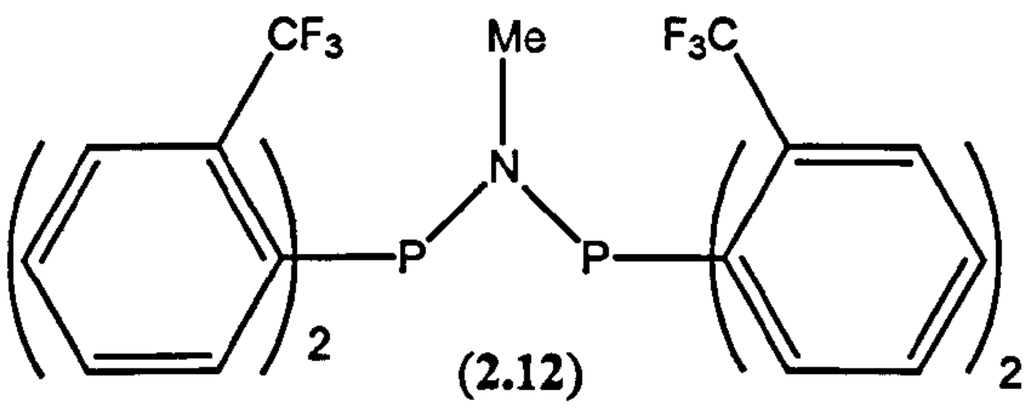

(2.12)

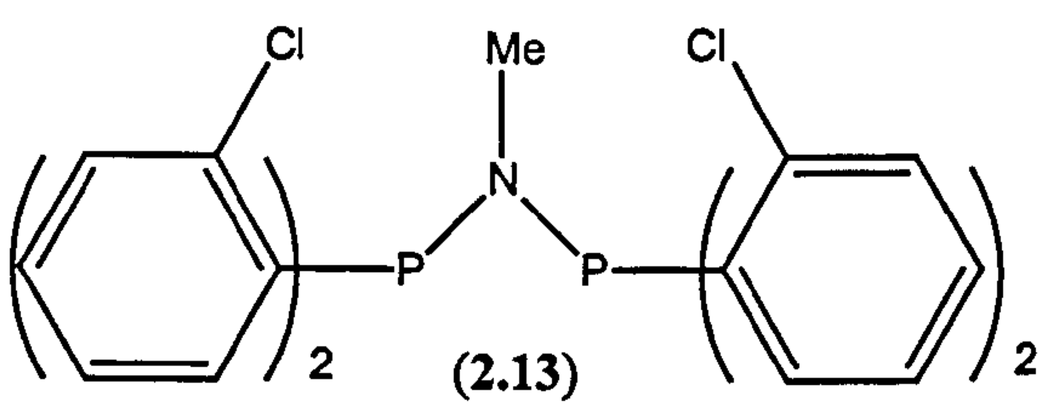

(2.13)

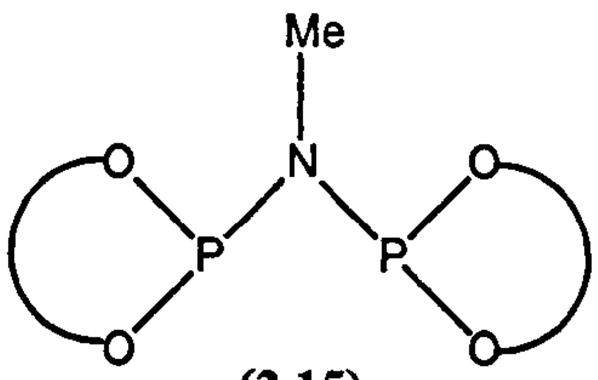

(2.15)

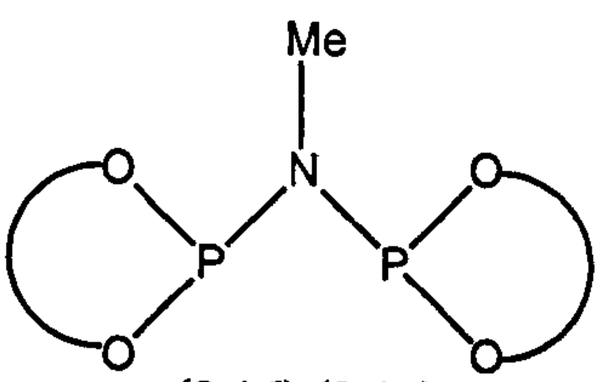

(2.16) (2.17)

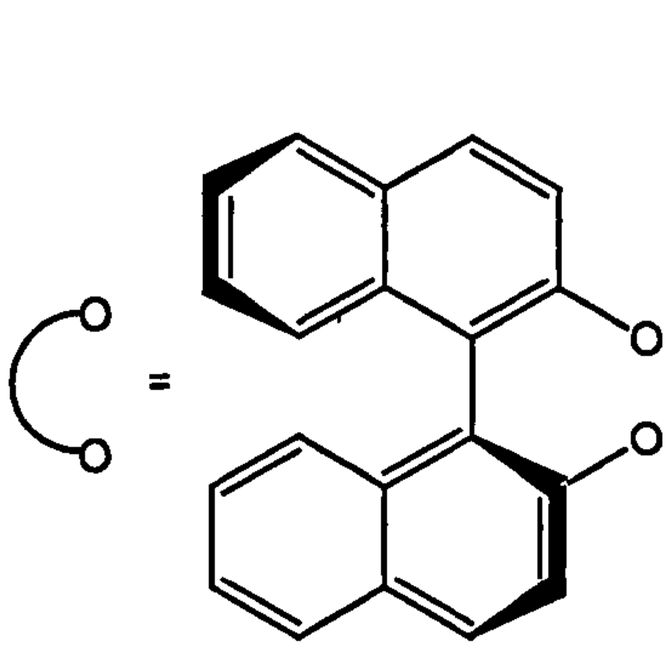

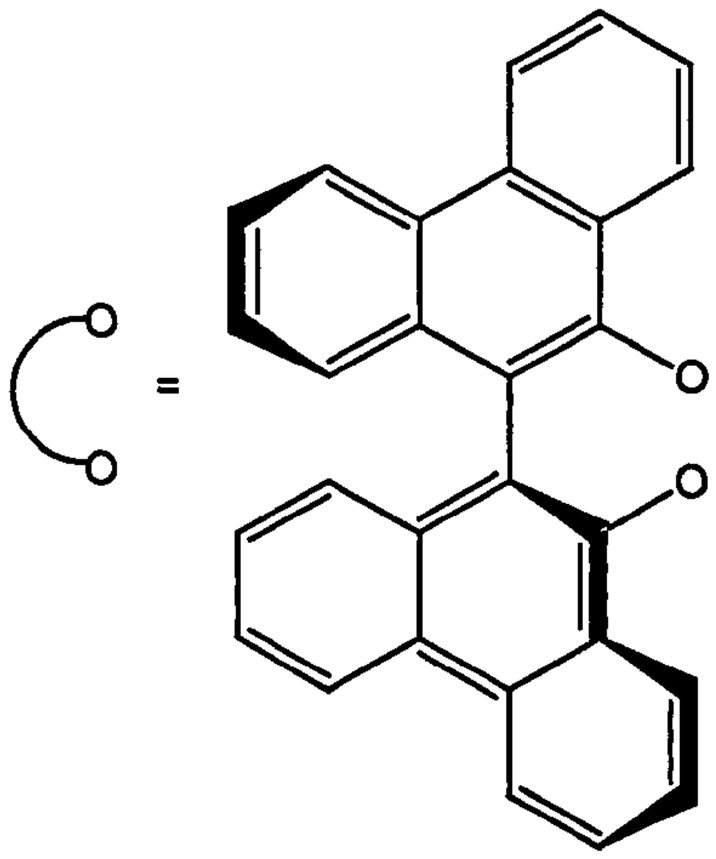

Figure 3.1

3.2 Complexation of *o*-tol$_2$P(CH$_2$)$_n$P*o*-tol$_2$ (n = 1 – 3)

The ligands *o*-tol$_2$P(CH$_2$)$_n$P*o*-tol$_2$ (n = 1 – 3) were reacted with [PtClMe(1,5-COD)] giving **(3.1 - 3.3)** (Equation 3.1).

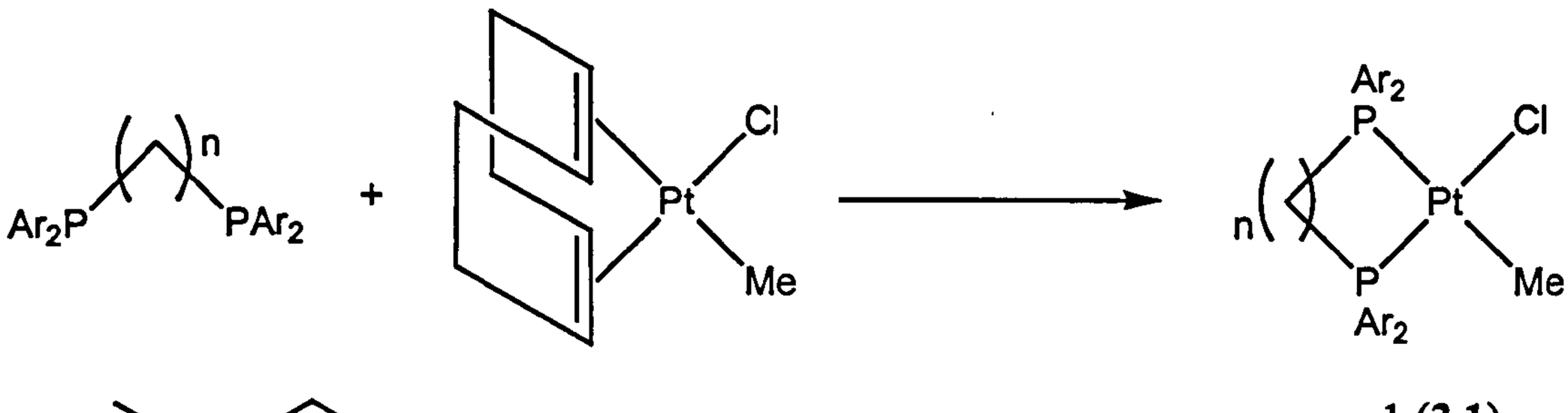

n = 1 **(3.1)**
n = 2 **(3.2)**
n = 3 **(3.3)**

Equation 3.1

The complexes were characterised by $^{31}P\{^1H\}$ NMR (Table 3.1) and ^1H NMR spectroscopy, mass spectrometry and elemental analysis (see Experimental section for the data). Crystals of complex **(3.3)** where n = 3 were obtained from dichloromethane and the structure determined by X-ray crystallography (see Section 3.7).

The $^{31}P\{^1H\}$ NMR spectrum of complex **(3.3)** is shown in Figure 3.1 At room temperature the spectrum is broad ($w_{1/2}$ = 278 Hz) indicating that the compound is fluxional. This may be associated with the presence of the *ortho*-substituents on the aryl ring causing restricted rotation about the C-P bond because the corresponding dppp complex containing unsubstituted phenyl rings shows a sharp spectrum at 25 °C. The smaller chelates **(3.1)** and **(3.2)** also have sharp peaks in their $^{31}P\{^1H\}$ NMR spectra and so the fluxionality in **(3.3)** could also be due to the conformationally more flexible larger chelate ring.

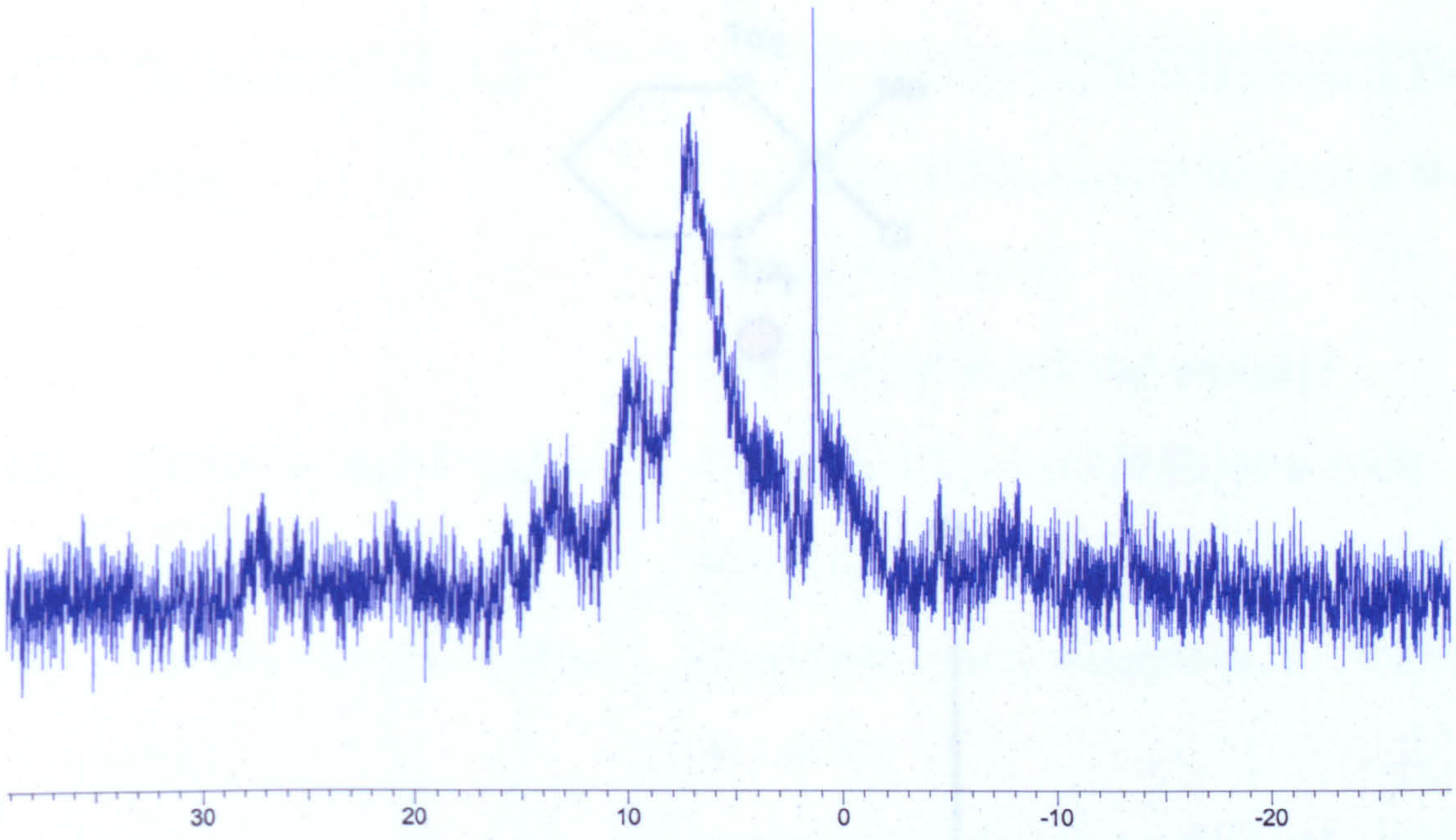

Figure 3.1 $^{31}P\{^{1}H\}$ NMR spectrum of complex (**3.3**) at 25 °C

Even at – 90 °C, the $^{31}P\{^{1}H\}$ NMR spectrum is still broad ($w_{1/2}$ = 53 Hz) (see Figure 3.2). This spectrum also shows there is a non-fluxional species present, which gives rise to a sharp singlet and is tentatively assigned to the dimer (**3.3b**) with *trans*-bridging diphosphines.

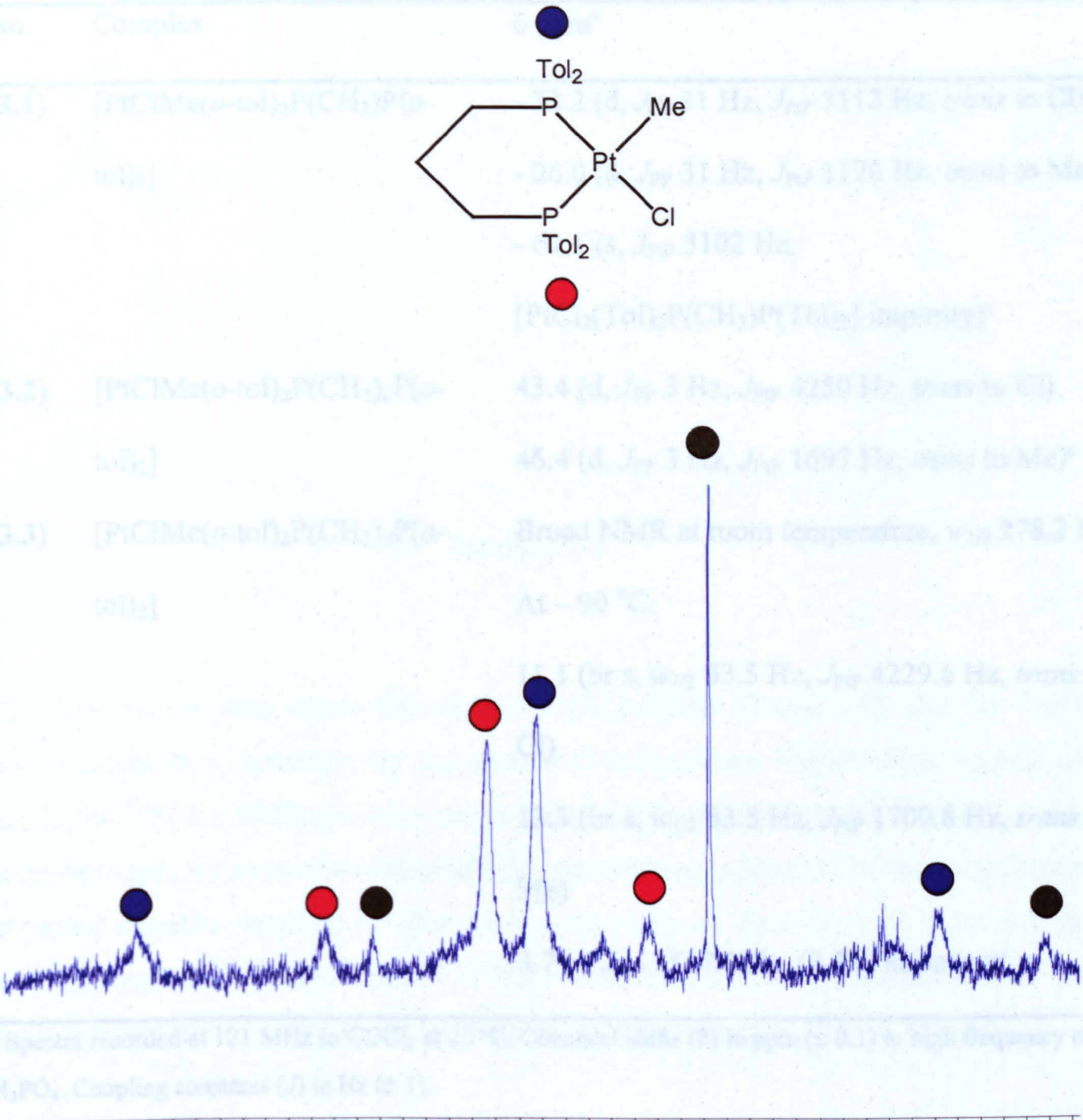

Figure 3.2 $^{31}P\{^{1}H\}$ NMR spectrum of complex (**3.3**) at - 90 °C

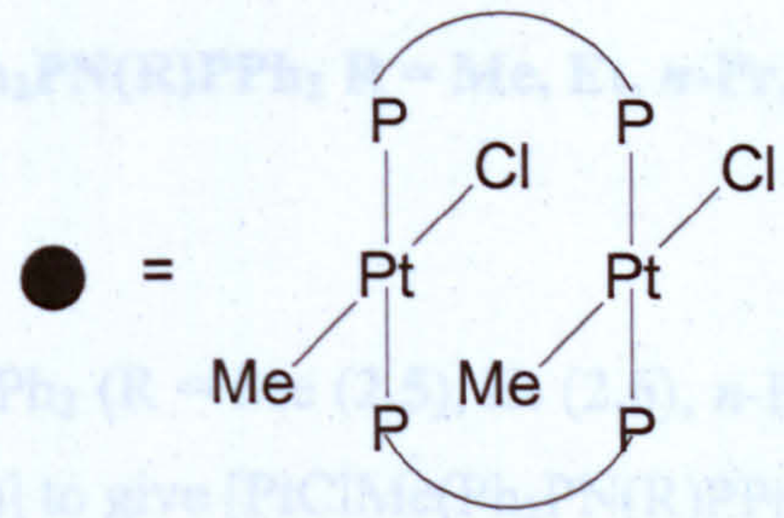

(3.3b)

Table 3.2 $^{31}P\{^{1}H\}$ NMR data for complexes (**3.1 – 3.3**)

No.	Complex	δ ppm[a]
(3.1)	[PtClMe(*o*-tol)$_2$P(CH$_2$)P(*o*-tol)$_2$]	- 33.2 (d, J_{PP} 31 Hz, J_{PtP} 3112 Hz, *trans* to Cl) - 26.0 (d, J_{PP} 31 Hz, J_{PtP} 1176 Hz, *trans* to Me) - 61.1 (s, J_{PtP} 3102 Hz, [PtCl$_2$(Tol)$_2$P(CH$_2$)P(Tol)$_2$] impurity)[a]
(3.2)	[PtClMe(*o*-tol)$_2$P(CH$_2$)$_2$P(*o*-tol)$_2$]	43.4 (d, J_{PP} 3 Hz, J_{PtP} 4250 Hz, *trans* to Cl) 46.4 (d, J_{PP} 3 Hz, J_{PtP} 1697 Hz, *trans* to Me)[a]
(3.3)	[PtClMe(*o*-tol)$_2$P(CH$_2$)$_3$P(*o*-tol)$_2$]	Broad NMR at room temperature, $w_{1/2}$ 278.2 Hz At – 90 °C: 11.1 (br s, $w_{1/2}$ 53.5 Hz, J_{PtP} 4229.6 Hz, *trans* to Cl) 13.3 (br s, $w_{1/2}$ 53.5 Hz, J_{PtP} 1700.8 Hz, *trans* to Me) 3.7 (s, J_{PtP} 3517.0 Hz, (**3.3b**) impurity)[a]

[a] Spectra recorded at 121 MHz in $CDCl_3$ at 22 °C. Chemical shifts (δ) in ppm (± 0.1) to high frequency of H_3PO_4. Coupling constants (*J*) in Hz (± 1).

3.3 Complexation of $Ph_2PN(R)PPh_2$ R = Me, Et, *n*-Pr, *i*-Pr

The ligands $Ph_2PN(R)PPh_2$ (R = Me (**2.5**), Et (**2.6**), *n*-Pr (**2.7**), *i*-Pr (**2.8**)) were reacted with [PtClMe(1,5-COD)] to give [PtClMe($Ph_2PN(R)PPh_2$)] (R = Me (**3.4**), Et (**3.5**), *n*-Pr (**3.6**), *i*-Pr (**3.7**)), (Equation 3.2).

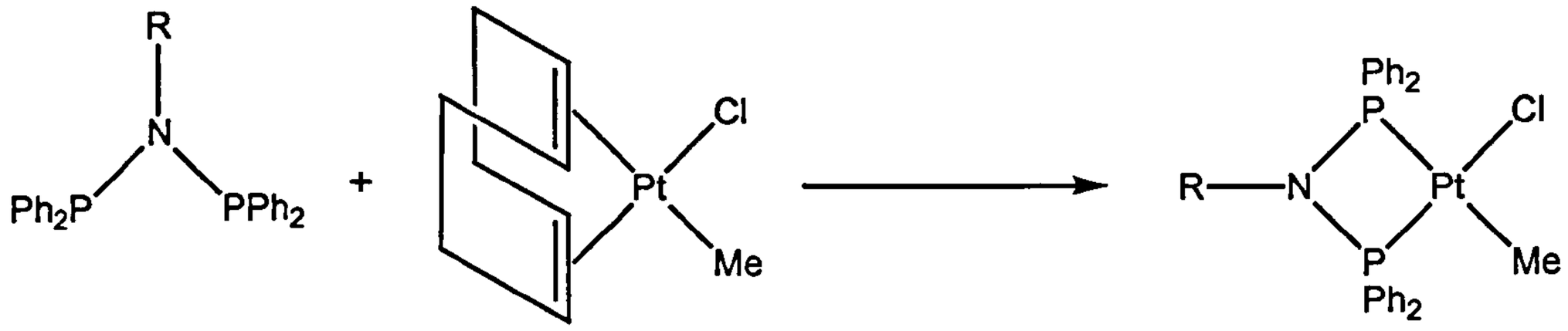

R = Me (**3.4**),
Et (**3.5**),
n-Pr (**3.6**),
i-Pr (**3.7**)

Equation 3.2

The compounds were characterised by $^{31}P\{^{1}H\}$ NMR (Table 3.9) and ^{1}H NMR spectroscopy, mass spectrometry and elemental analysis (see Experimental section for data). The $^{31}P\{^{1}H\}$ NMR spectra were all sharp, indicating rotation about the P-C bonds is unrestricted. All showed two doublets (Figure 3.3) corresponding to two inequivalent phosphorus nuclei coupling to each other with platinum satellites (see Table 3.3 for coupling constants). Single crystals of (**3.5**) were obtained from dichloromethane and the structure determined by X-ray crystallography (see Section 3.7).

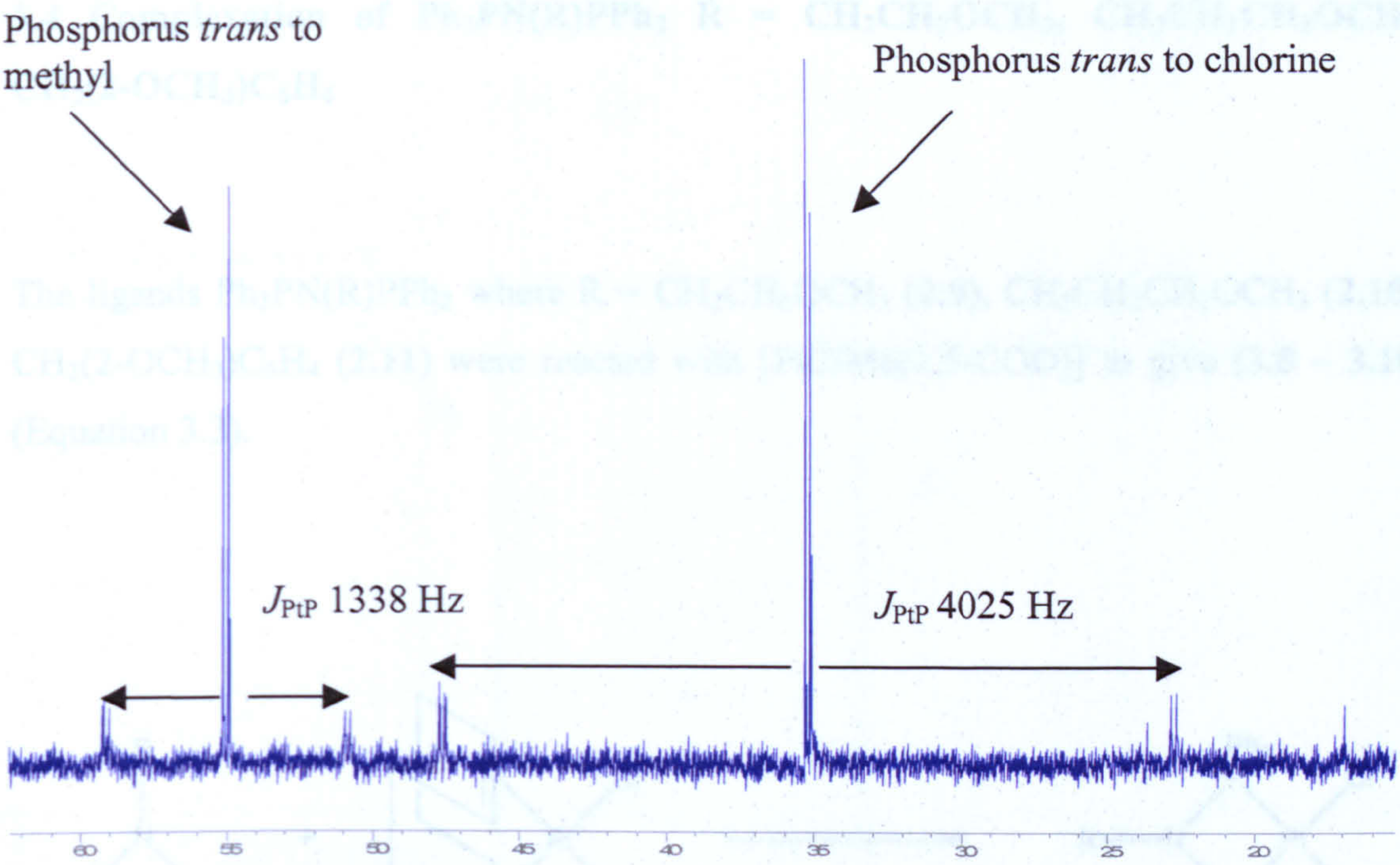

Figure 3.3 $^{31}P\{^{1}H\}$ NMR spectrum of complex (**3.4**)

Table 3.3 $^{31}P\{^{1}H\}$ NMR data for complexes (**3.4 - 3.7**)

No.	Complex	δ ppm[a]
(**3.4**)	[PtClMe(**2.5**)]	35.1 (d, J_{PP} 31 Hz, J_{PtP} 4025 Hz, *trans* to Cl)
		54.9 (d, J_{PP} 31 Hz, J_{PtP} 1338 Hz, *trans* to Me)[a]
(**3.5**)	[PtClMe(**2.6**)]	35.2 (d, J_{PP} 34 Hz, J_{PtP} 4015 Hz, *trans* to Cl)
		54.9 (d, J_{PP} 34 Hz, J_{PtP} 1358 Hz, *trans* to Me)[a]
(**3.6**)	[PtClMe(**2.7**)]	35.5 (d, J_{PP} 34 Hz, J_{PtP} 4015 Hz, *trans* to Cl)
		55.1 (d, J_{PP} 34 Hz, J_{PtP} 1360 Hz, *trans* to Me)[a]
(**3.7**)	[PtClMe(**2.8**)]	35.3 (d, J_{PP} 34 Hz, J_{PtP} 4017 Hz, *trans* to Cl)
		55.0 (d, J_{PP} 34 Hz, J_{PtP} 1357 Hz, *trans* to Me)[a]

[a] Spectra recorded at 121 MHz in $CDCl_3$ at 22 °C. Chemical shifts (δ) in ppm (± 0.1) to high frequency of H_3PO_4. Coupling constants (*J*) in Hz (± 1).

3.4 Complexation of $Ph_2PN(R)PPh_2$ R = $CH_2CH_2OCH_3$, $CH_2CH_2CH_2OCH_3$, $CH_2(2\text{-}OCH_3)C_6H_4$

The ligands $Ph_2PN(R)PPh_2$ where R = $CH_2CH_2OCH_3$ (**2.9**), $CH_2CH_2CH_2OCH_3$ (**2.10**), $CH_2(2\text{-}OCH_3)C_6H_4$ (**2.11**) were reacted with [PtClMe(1,5-COD)] to give (**3.8** – **3.10**) (Equation 3.3).

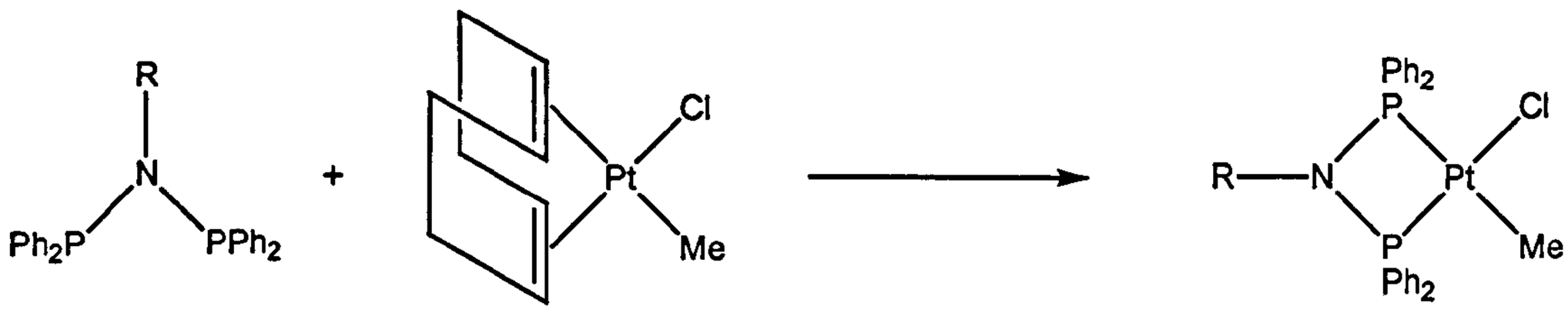

R = $CH_2CH_2OCH_3$ (**3.8**)
$CH_2CH_2CH_2OCH_3$ (**3.9**)
$CH_2(2\text{-}OCH_3)C_6H_4$ (**3.10**)

Equation 3.3

The $^{31}P\{^1H\}$ NMR spectra of complexes (**3.8**), (**3.9**), (**3.10**) (Table 3.14) showed two doublets indicating two different environments for the phosphorus atoms, one *trans* to chlorine and one *trans* to methyl, with corresponding platinum satellites (see Table 3.4 for coupling constants). The $^{31}P\{^1H\}$ spectrum of (**3.8**) is shown in Figure 3.4. The ^1H NMR spectroscopy, mass spectrometry and elemental analysis data are given in the Experimental Section.

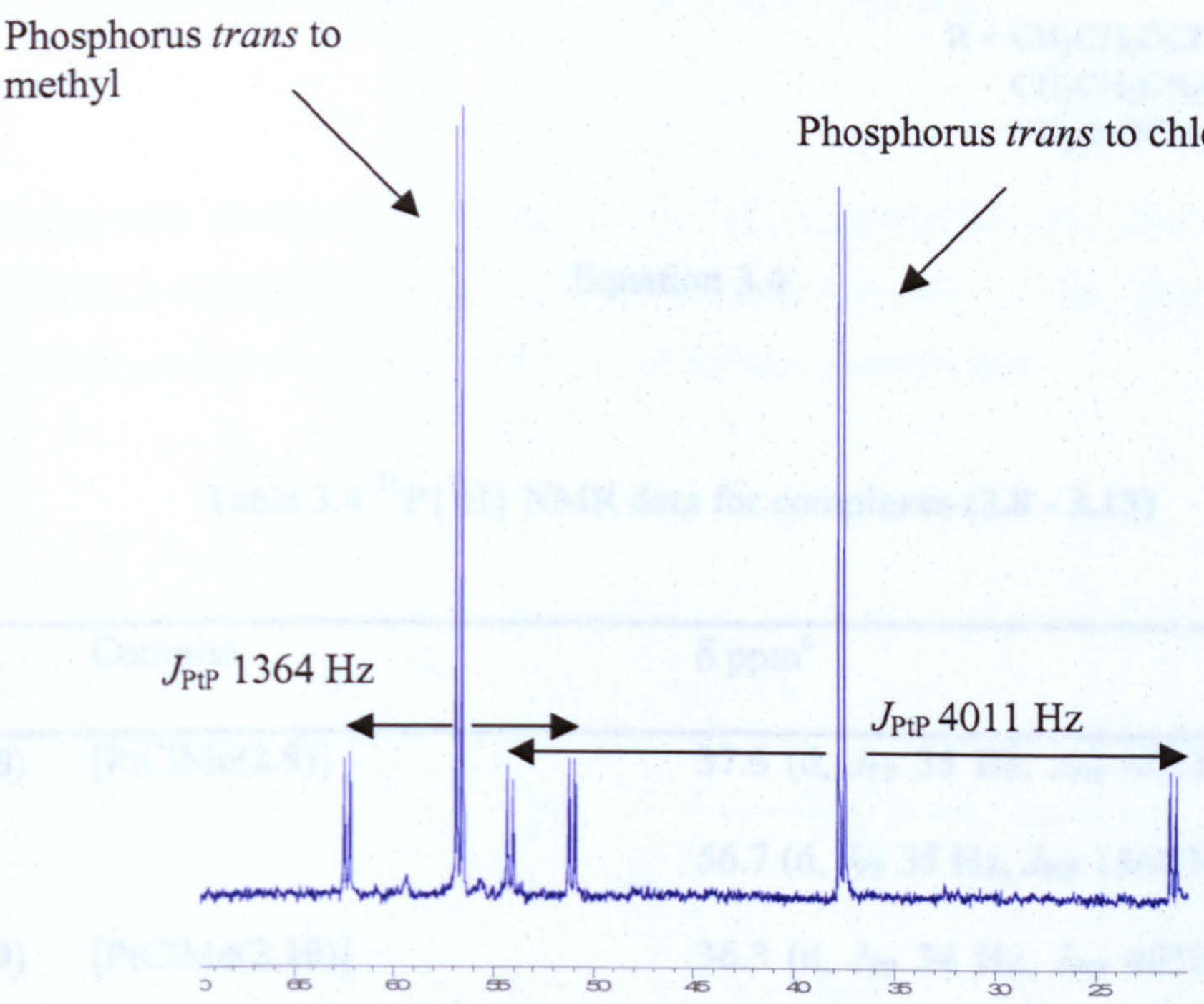

Figure 3.4 $^{31}P\{^{1}H\}$ NMR spectrum of complex (**3.8**)

The ligands $Ph_2PN(R)PPh_2$ where R = $CH_2CH_2OCH_3$ (**2.11**), $CH_2CH_2CH_2OCH_3$ (**2.12**), $CH_2(2\text{-}OCH_3)C_6H_4$ (**2.13**) were reacted with $[PdCl_2(NCPh)_2]$ in dichloromethane to give (**3.11** – **3.13**) (Equation 3.4). The $^{31}P\{^{1}H\}$ NMR spectra for all the compounds showed simply a singlet resonance (see Table 3.4 for data). The complexes were further analysed by ^{1}H NMR spectroscopy, mass spectrometry and elemental analysis (see Experimental section for data). Single crystals of compounds (**3.11**), (**3.12**) and (**3.13**) were grown from dichloromethane and diethylether and the structures determined by X-ray crystallography confirming the analysis (see section 3.7).

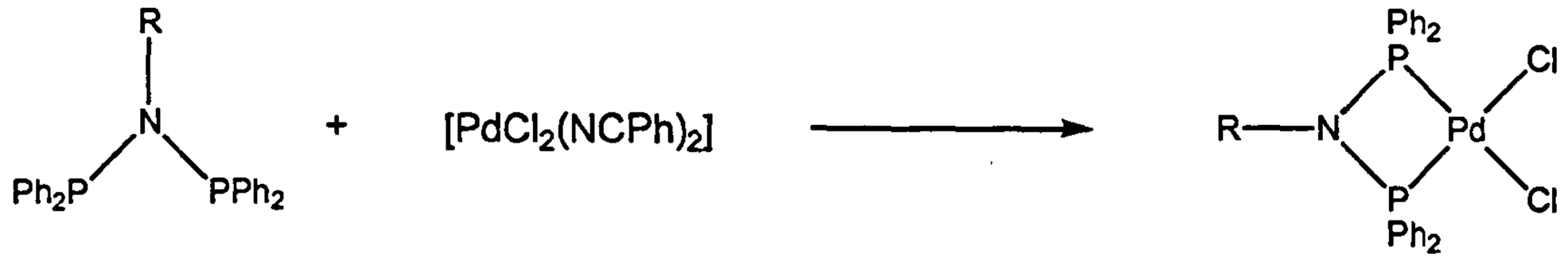

R = $CH_2CH_2OCH_3$ **(3.11)**
$CH_2CH_2CH_2OCH_3$ **(3.12)**
$CH_2(2\text{-}OCH_3)C_6H_4$ **(3.13)**

Equation 3.4

Table 3.4 $^{31}P\{^1H\}$ NMR data for complexes **(3.8 - 3.13)**

No.	Complex	δ ppm[a]
(3.8)	[PtClMe(**2.9**)]	37.6 (d, J_{PP} 35 Hz, J_{PtP} 4011 Hz, *trans* to Cl), 56.7 (d, J_{PP} 35 Hz, J_{PtP} 1364 Hz, *trans* to Me)[a]
(3.9)	[PtClMe(**2.10**)]	36.3 (d, J_{PP} 34 Hz, J_{PtP} 4018 Hz, *trans* to Cl), 55.9 (d, J_{PP} 34 Hz, J_{PtP} 1361 Hz, *trans* to Me)[b]
(3.10)	[PtClMe(**2.11**)]	37.4 (d, J_{PP} 35 Hz, J_{PtP} 4004 Hz, *trans* to Cl), 57.0 (d, J_{PP} 35 Hz, J_{PtP} 1378 Hz, *trans* to Me)[a]
(3.11)	[$PdCl_2$(**2.9**)]	32.6 (s)[b]
(3.12)	[$PdCl_2$(**2.10**)]	31.2 (s)[b]
(3.13)	[$PtCl_2$(**2.11**)]	33.3 (s)[b]

[a] Spectra recorded at 121 MHz in $CDCl_3$ at 22 °C. Chemical shifts (δ) in ppm (± 0.1) to high frequency of H_3PO_4. Coupling constants (*J*) in Hz (± 1).

[b] Spectra recorded at 121 MHz in CD_2Cl_2 at 22 °C. Chemical shifts (δ) in ppm (± 0.1) to high frequency of H_3PO_4. Coupling constants (*J*) in Hz (± 1).

3.5 Complexation of *ortho*-substituted phenyl PNP ligands

3.5.1 Complexation of $(2\text{-}CF_3C_6H_4)_2PN(Me)P(2\text{-}CF_3C_6H_4)_2$

Attempts were made to react the ligand $(2\text{-}CF_3C_6H_4)_2PN(Me)P(2\text{-}CF_3C_6H_4)_2$ (**2.12**) with [PtClMe(1,5-COD)] (Equation 3.5) but an insoluble white solid, suspected to be a polymeric species was formed and was not further characterised.

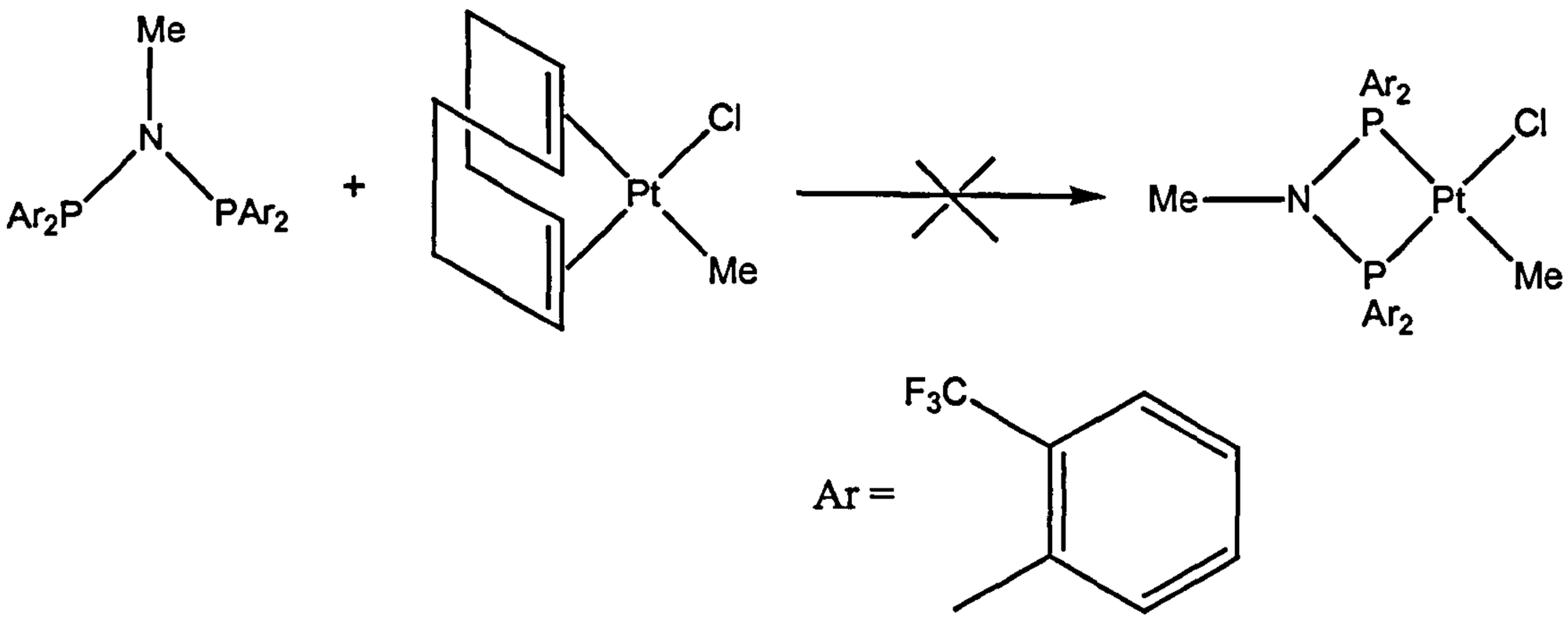

Equation 3.5

The reaction of (**2.12**) with $[PdCl_2(NCPh)_2]$ gave (**3.14**) (Equation 3.6) as a sparingly soluble solid. The product was analysed by $^{31}P\{^1H\}$ NMR spectroscopy (Table 3.5) giving a complex multiplet due to second order coupling between the phosphorus atoms (for ^1H NMR spectroscopy, mass spectrometry and elemental analysis see Experimental section).

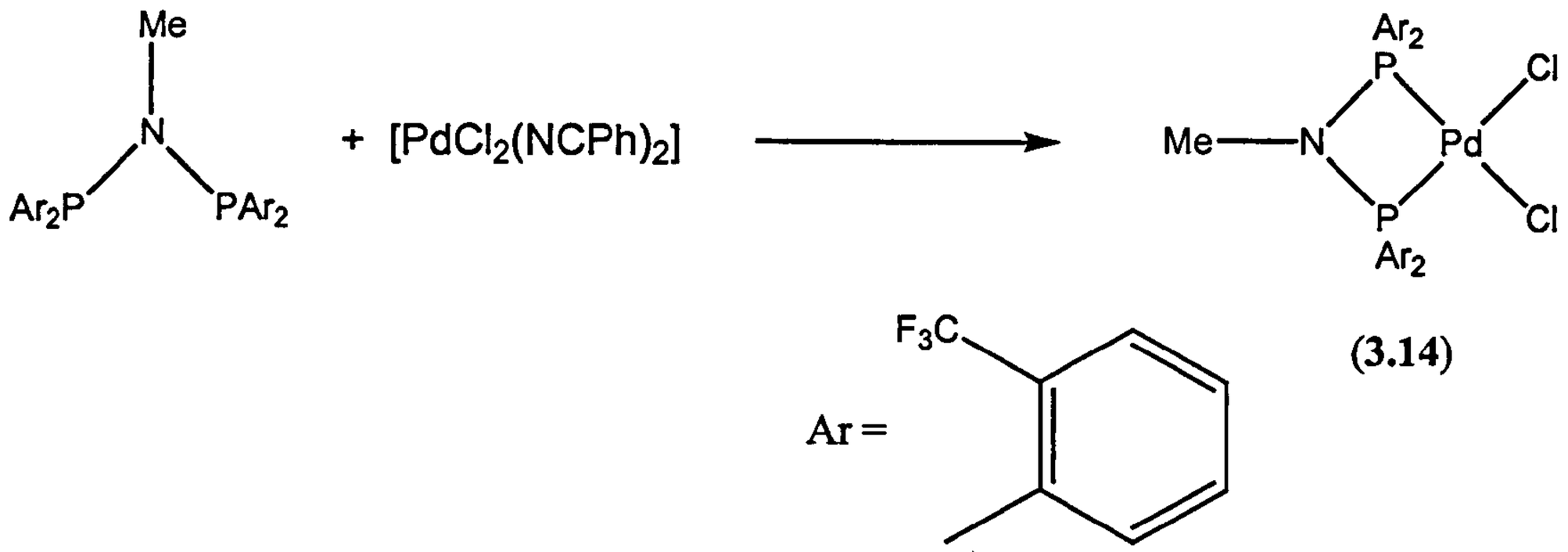

(3.14)

Equation 3.6

3.5.2 Complexation of $(2\text{-}ClC_6H_4)_2PN(Me)P(2\text{-}ClC_6H_4)_2$

The reaction of **(2.13)** with $[PtCl_2(1,5\text{-}COD)]$ or $[PtMe_2(1,5\text{-}COD)]$ gave **(3.15)** and **(3.16)** respectively (Equation 3.7).

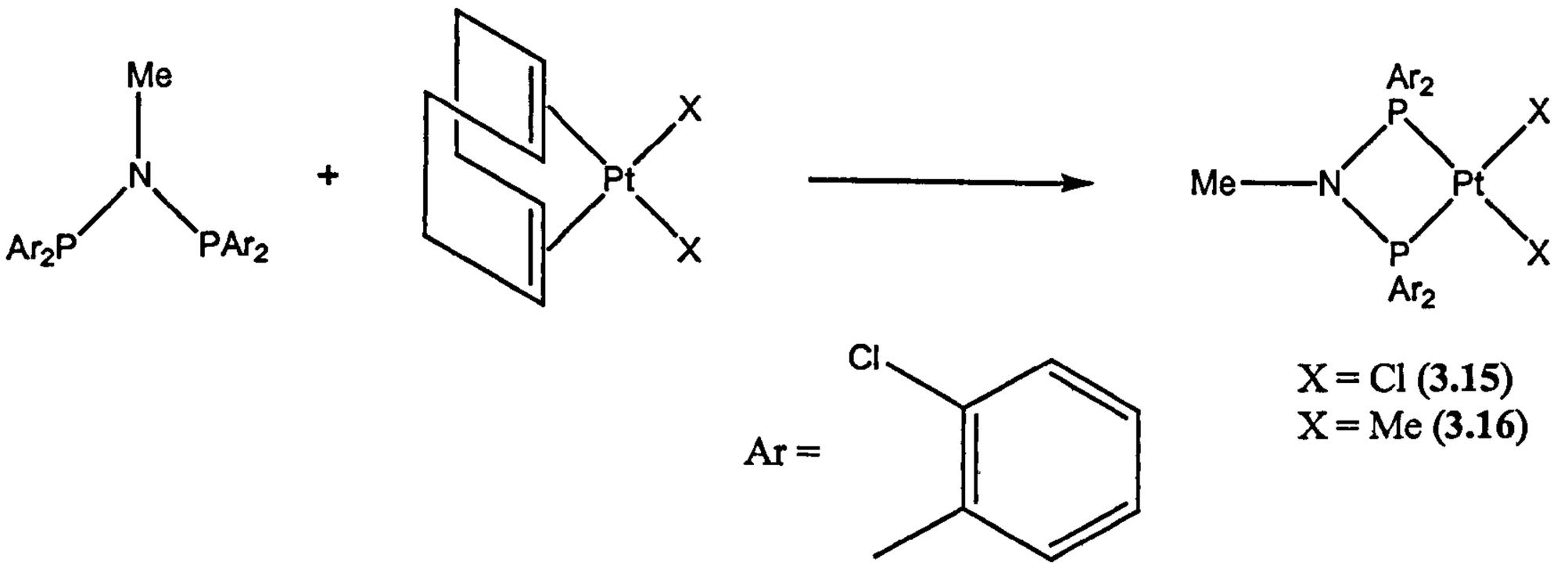

X = Cl **(3.15)**
X = Me **(3.16)**

Equation 3.7

The complexes were analysed by $^{31}P\{^{1}H\}$ NMR spectroscopy and the spectra showed single peaks at δ 42.8 ppm with platinum satellites J_{PtP} 4100 Hz for the dichloride compound (**3.15**) and at δ 65.7 ppm with J_{PtP} 2124 Hz for the dimethyl (**3.16**) (Table 3.5) (see Experimental section for ^{1}H NMR spectroscopy, mass spectrometry and elemental analysis)

Table 3.5 $^{31}P\{^{1}H\}$ NMR data for complexes (**3.8 – 3.10**)

No.	Complex	δ ppm[a]
(3.14)	$[PdCl_2(\mathbf{2.12})]$	45.3 (m)[a]
(3.15)	$[PtCl_2(\mathbf{2.13})]$	42.8 (s, J_{PtP} 4100 Hz)[b]
(3.16)	$[PtMe_2(\mathbf{2.13})]$	65.8 (s, J_{PtP} 2124 Hz)[b]

[a] Spectra recorded at 121 MHz in $CDCl_3$ at 22 °C. Chemical shifts (δ) in ppm (± 0.1) to high frequency of H_3PO_4. Coupling constants (*J*) in Hz (± 1).

[b] Spectra recorded at 121 MHz in CD_2Cl_2 at 22 °C. Chemical shifts (δ) in ppm (± 0.1) to high frequency of H_3PO_4. Coupling constants (*J*) in Hz (± 1).

3.6 Complexation of diphosphoramidites

3.6.1 Complexation of ((*R*)-1,1′-bi-2-naphthoxo)PN(Me)P((*R*)-1,1′-bi-2-naphthoxo)

Reaction of (**2.15**) with [$PtCl_2$(1,5-COD)] gave (**3.17**) (Equation 3.8).

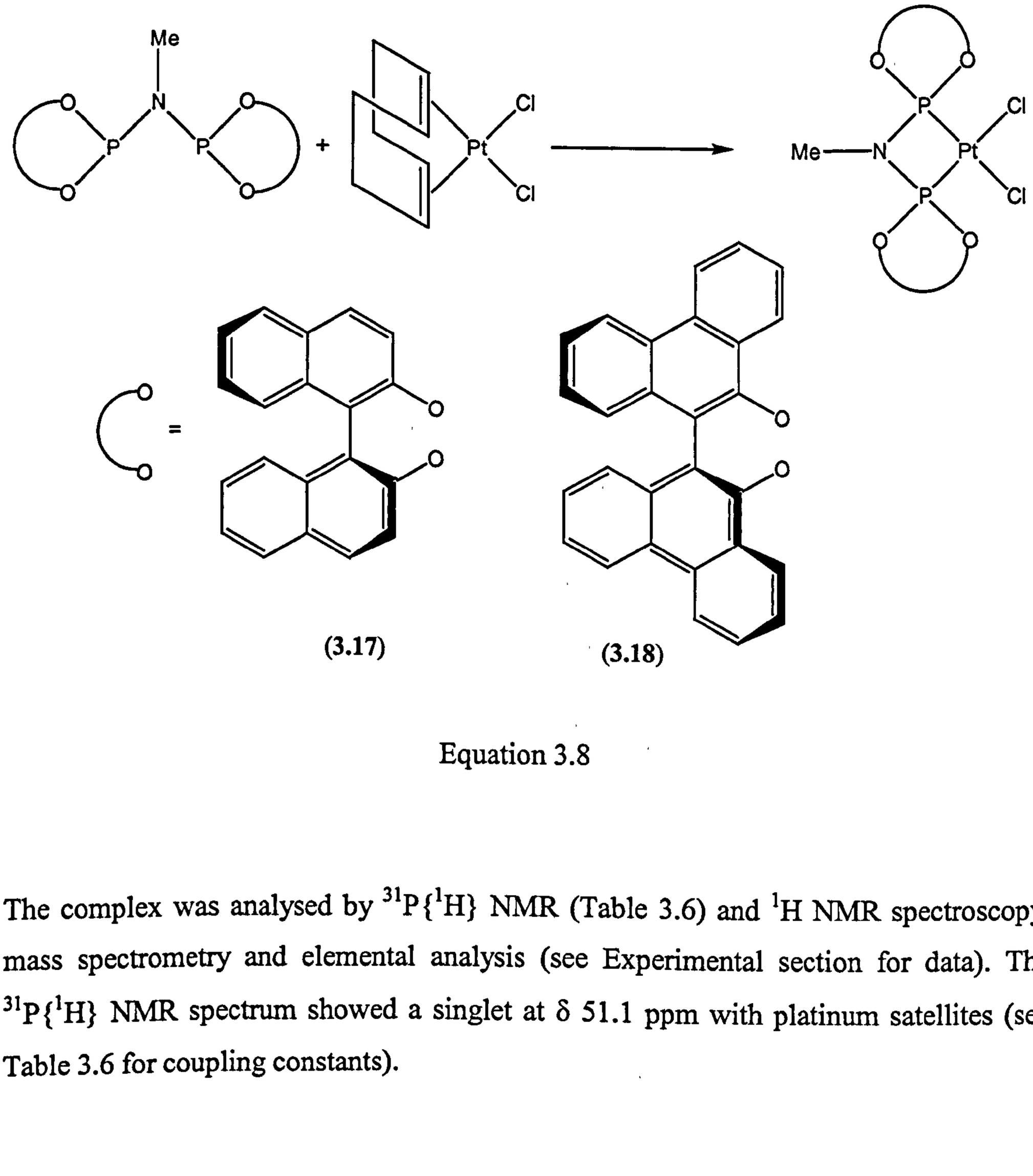

(3.17) **(3.18)**

Equation 3.8

The complex was analysed by $^{31}P\{^1H\}$ NMR (Table 3.6) and ^1H NMR spectroscopy, mass spectrometry and elemental analysis (see Experimental section for data). The $^{31}P\{^1H\}$ NMR spectrum showed a singlet at δ 51.1 ppm with platinum satellites (see Table 3.6 for coupling constants).

3.6.2 Complexation of ((*S*)-9,9′-biphenanthryl-10,10′-dioxo)PN(Me)P((*S*)-9,9′-biphenanthryl-10,10′-dioxo)

Reaction of (**2.16**) with [$PtCl_2$(1,5-COD)] produced the square planar complex (**3.18**) (see Equation 3.8). The product obtained was a sparingly soluble cream powder which was analysed by $^{31}P\{^1H\}$ NMR spectroscopy (Table 3.6) showing a single peak at δ 54.6 ppm with J_{PtP} 5042 Hz (see Experimental section for data).

3.6.3 Complexation of the mixed *rac* and *meso* ligand (9,9′-biphenanthryl-10,10′-dioxo)PN(Me)P(9,9′-biphenanthryl-10,10′-dioxo)

Several attempts were made to react the *rac*/*meso* mixture of ligands (**2.17**) with [$PdCl_2$(NCPh)$_2$] and [$PtCl_2$(1,5-COD)] (Scheme 3.1). However in each case no spectroscopic evidence of the desired product was observed. In the case of palladium, no reaction occurred. An insoluble species assumed to be a polymer resulted from reaction with platinum and was not characterised further.

This may be understood from the crystal structures for the *meso* isomer see Figures 2.7 and 2.8 in Chapter 2, which shows the ligand to adopt two different conformers labelled rotamer 1 and rotamer 2. The energetically most favorable rotamer is rotamer 2 (Figure 2.8) with the two phosphorus atoms in different environments. In rotamer 2, the lone pairs on the phosphorus are pointing in different directions. Therefore, in the reaction with platinum, the lone pairs as shown by the crystal structure are pointing in the wrong direction, making mononuclear complexation difficult to achieve resulting in a polymeric product. In the reaction with palladium, the bulk of the ligand could be hindering complexation.

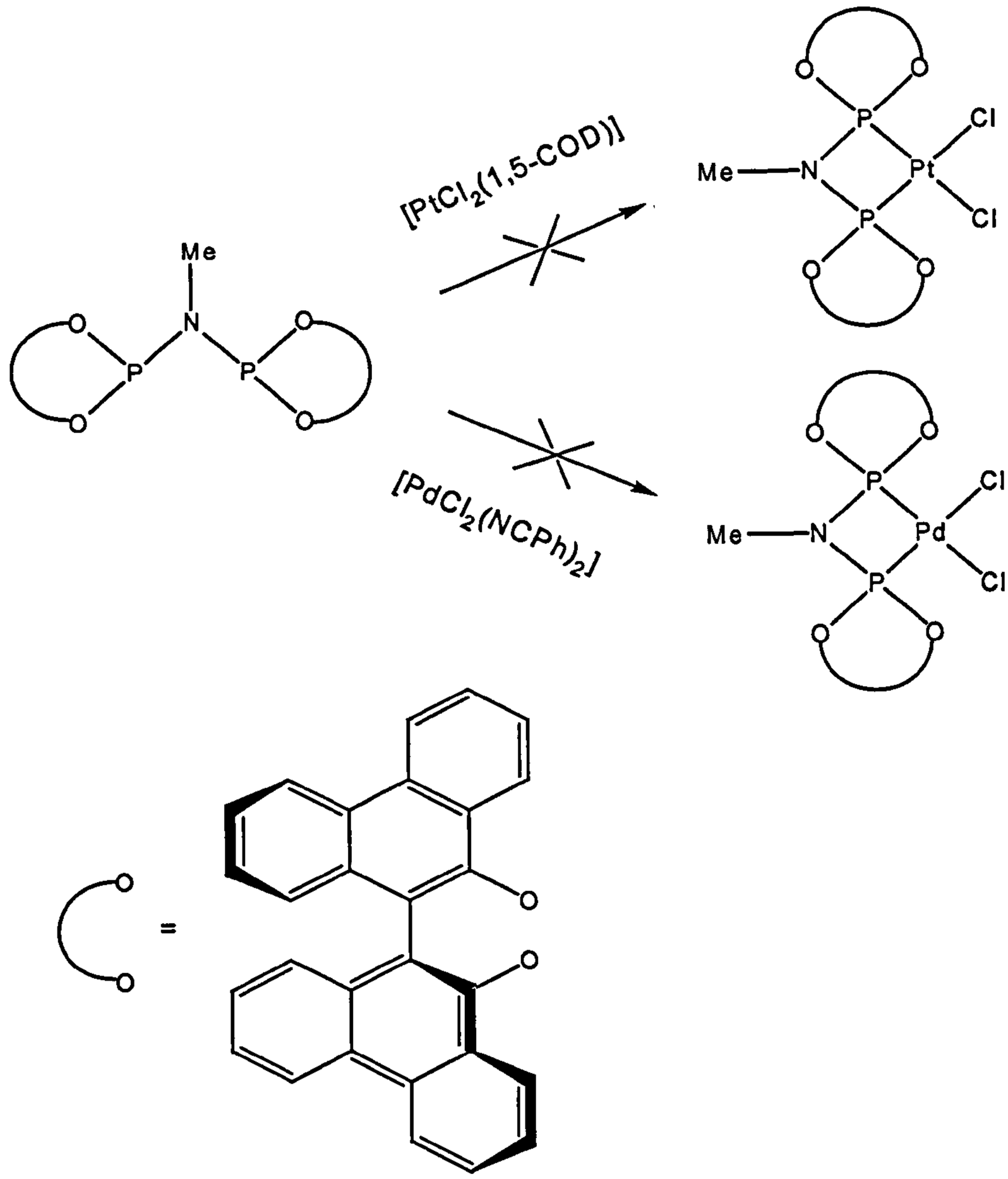

Scheme 3.1

Table 3.6 $^{31}P\{^{1}H\}$ NMR data for complexes **(3.17, 3.18)**

No.	Complex	δ ppm[a]
(3.17)	[$PtCl_2$(**2.15**)]	51.1 (s, J_{PtP} 5125 Hz)[a]
(3.18)	[$PtCl_2$(**2.16**)]	54.6 (s, J_{PtP} 5042 Hz)[a]

[a] Spectra recorded at 121 MHz in CD_2Cl_2 at 22 °C. Chemical shifts (δ) in ppm (± 0.1) to high frequency of H_3PO_4. Coupling constants (*J*) in Hz (± 1).

3.7 Comparison of crystal structures

Single crystals of some of the metal complexes synthesised in this Chapter have been grown, their structures have been determined by X-ray crystallography and will be discussed here.

Metal complexes with monodentate ligands can be investigated by comparing their cone angles, as described by Tolman.[89] This is a quantitative steric parameter which has been extended to diphosphines and is defined as the average cone angle as measured for the two substituents and the angle between the M-P bond and the bisector of the P-M-P angle. Another useful way of comparing complexes with bidentate ligands is in terms of their bite angles (Figure 3.5).

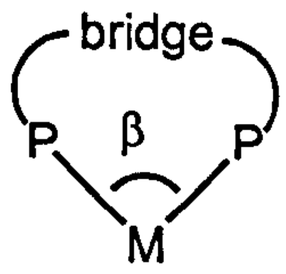

M = metal, P = phosphorus substituents, β = bite angle

Figure 3.5

The bite angle is determined by the angle between the two phosphorus substituents and the metal. The effect of ligand bite angle on metal catalysed C-C bond forming reactions has been studied in detail by van Leeuwen *et al.*[90, 46]

This section is a discussion of the ligand bite angles, cone angles and various bond lengths from the crystal structures described. Differences in the ligand bite angles, cone angles and bond lengths may explain the catalytic results described in Chapter 4. A molecular modelling study has also been carried out and the results discussed here.

3.7.1 Crystal structures of dichloropalladium complexes (3.11 – 3.13)

X-ray crystal structures of the dichloropalladium complexes (**3.11 – 3.13**) are shown in Figures 3.6 – 3.8. Selected bond lengths and angles are given in Tables 3.7 – 3.9. For comparison, the bite angles, cone angles and P – N bond lengths are given in Table 3.10. For the complexes (**3.11**) and (**3.12**), these P – N bond lengths will be compared with those of the free ligands (**2.9**) and (**2.10**) (crystal structures shown in Chapter 2).

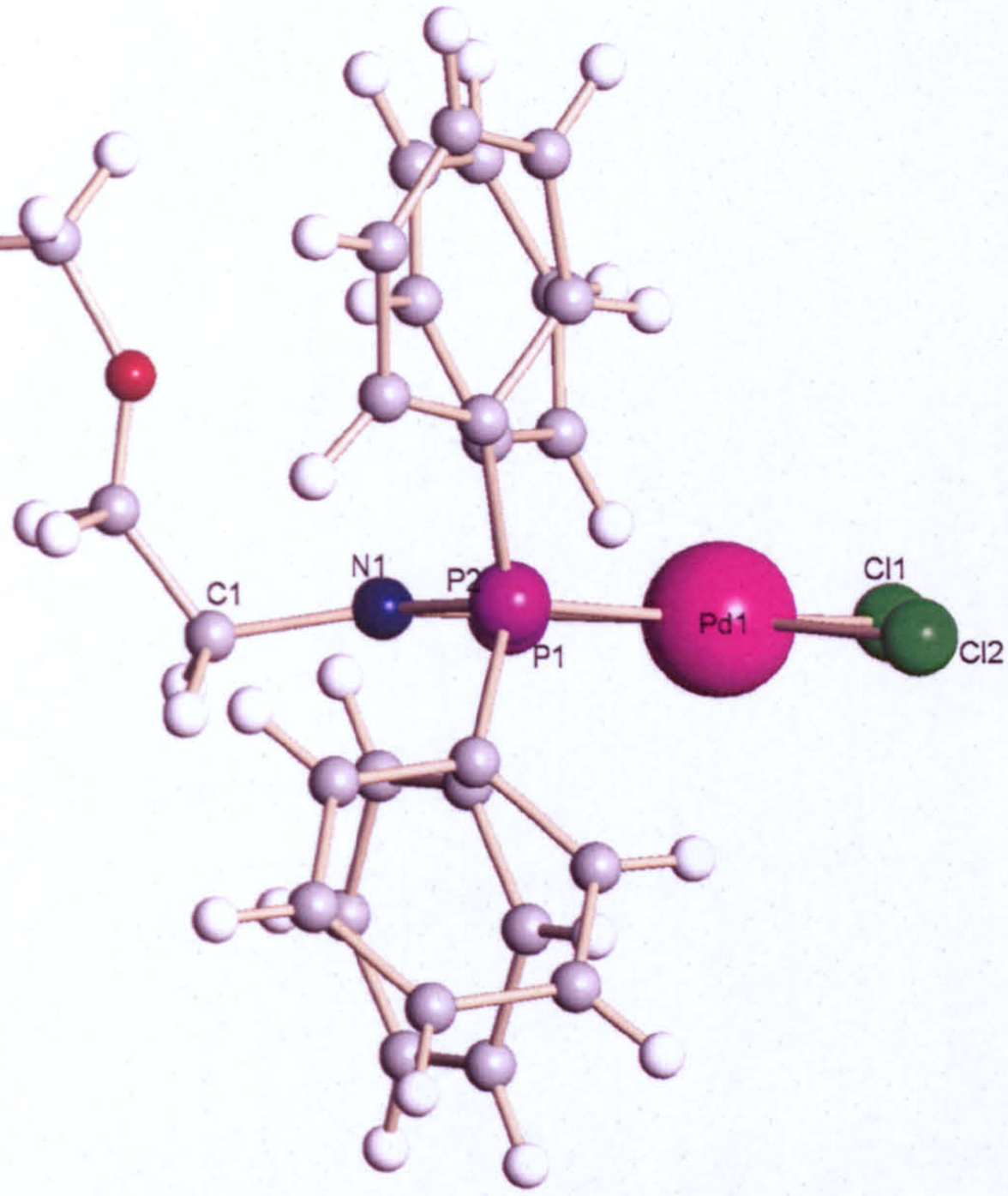

Figure 3.6 X–ray crystal structure of complex (**3.11**)

Table 3.7 Selected bond angles and lengths for complex (**3.11**)

Bond Length	Å	Bond Angle	Degrees °
Pd(1) – Cl(1)	2.353(4)	Cl(1) – Pd(1) – P(1)	93.2(13)
Pd(1) – Cl(2)	2.350(4)	Cl(1) – Pd(1) – P(2)	164.9(11)
Pd(1) – P(1)	2.192(4)	P(1) – Pd(1) – P(2)	71.9(11)
Pd(1) – P(2)	2.222(4)	Cl(1) – Pd(1) – Cl(2)	95.5(12)
		P(1) – Pd(1) – Cl(2)	171.0(10)
		P(2) – Pd(1) – Cl(2)	99.5(11)
		P(1) – N(1) – P(2)	100.6(5)

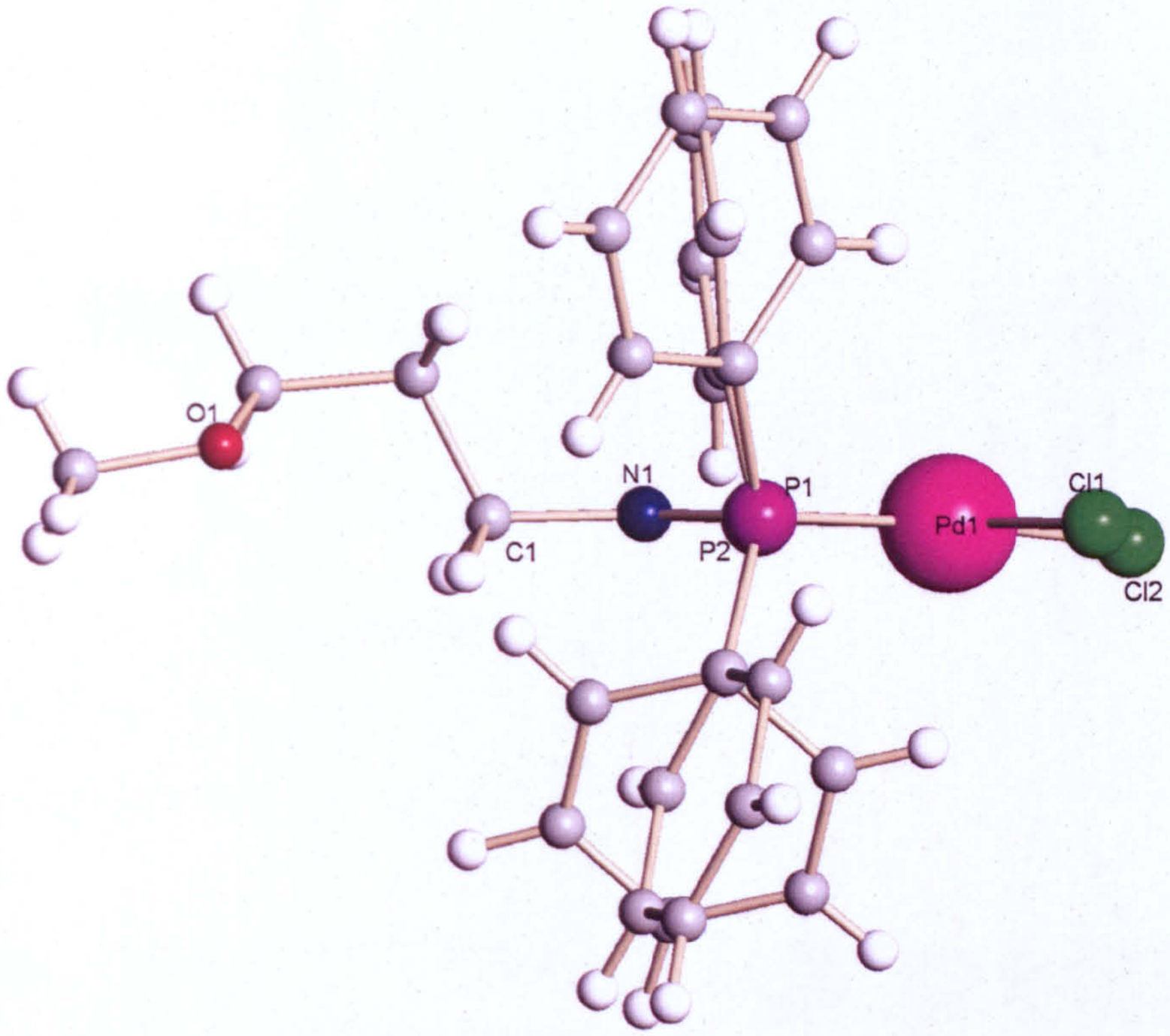

Figure 3.7 X–ray crystal structure of complex (**3.12**)

Table 3.8 Selected bond angles and lengths for complex (**3.12**)

Bond Length	Å	Bond Angle	Degrees ^{o}
Pd(1) – Cl(1)	2.360(8)	Cl(1) – Pd(1) – P(1)	90.5(3)
Pd(1) – P(2)	2.233(8)	Cl(1) – Pd(1) – P(2)	162.5(3)
Pd(1) – Cl(2)	2.360(9)	P(1) – Pd(1) – P(2)	71.9(3)
Pd(1) – P(1)	2.196(9)	Cl(1) – Pd(1) – Cl(2)	97.1(3)
		P(1) – Pd(1) – Cl(2)	171.7(3)
		P(2) – Pd(1) – Cl(2)	100.4(3)
		P(1) – N(1) – P(2)	100.1(13)

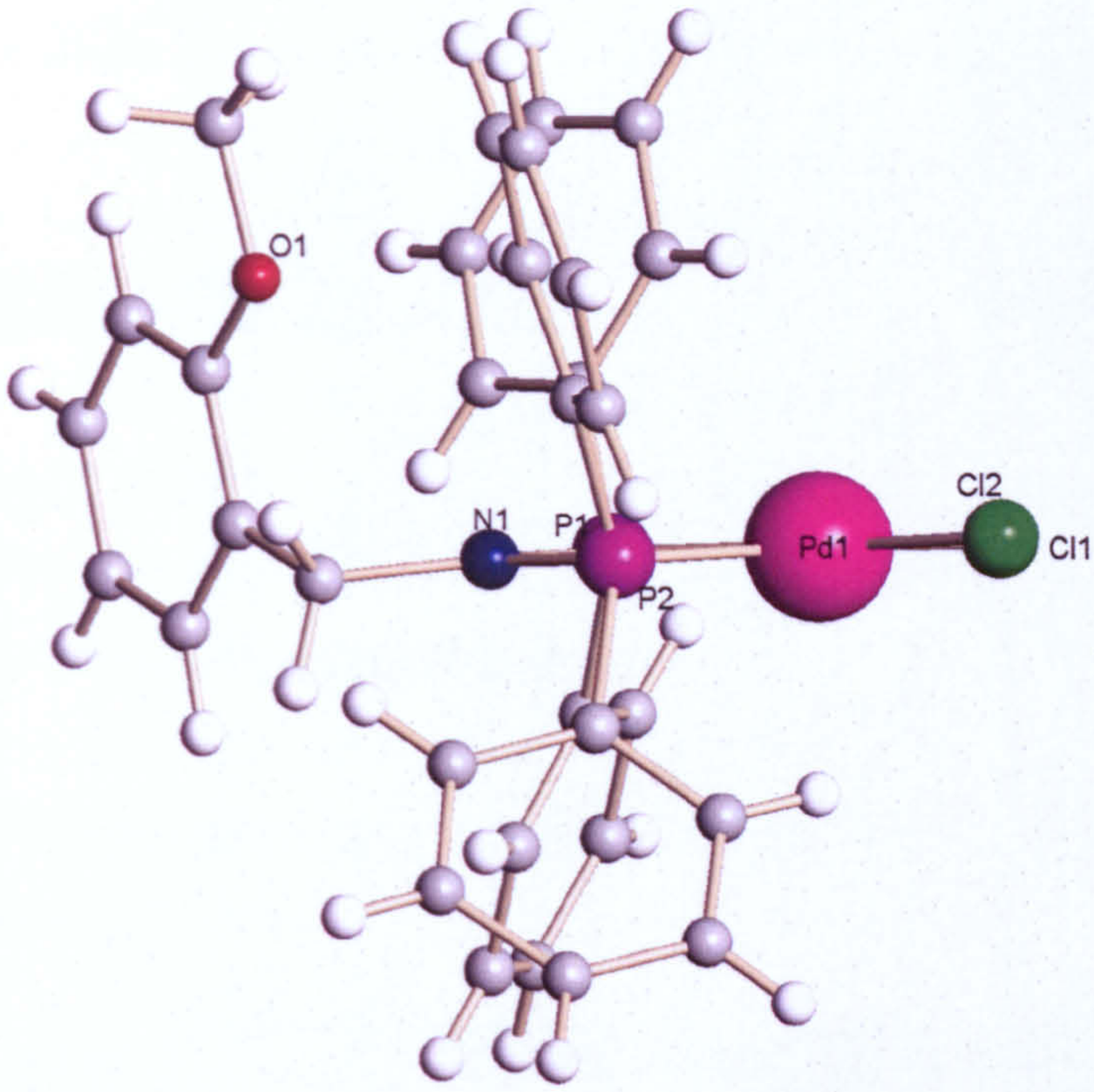

Figure 3.8 X–ray crystal structure of complex (**3.13**)

Table 3.9 Selected bond angles and lengths for complex (**3.13**)

Bond Length	Å	Bond Angle	Degrees °
Pd(1) – Cl(1)	2.360(8)	Cl(1) – Pd(1) – P(1)	96.9(3)
Pd(1) – P(2)	2.203(9)	Cl(1) – Pd(1) – P(2)	168.2(3)
Pd(1) – Cl(2)	2.370(8)	P(1) – Pd(1) – P(2)	71.4(3)
Pd(1) – P(1)	2.226(8)	Cl(1) – Pd(1) – Cl(2)	95.2(3)
		P(1) – Pd(1) – Cl(2)	167.8(3)
		P(2) – Pd(1) – Cl(2)	96.5(4)
		P(1) – N(1) – P(2)	99.7(11)

The crystal structures for the three complexes **(3.11)**, **(3.12)** and **(3.13)** are very similar, all forming monoclinic species with four molecules per unit cell. As expected, the ligand bite angles are very similar for **(3.11)**, **(3.12)** and **(3.13)**. The cone angles show small differences due to the orientation of the ether group on the nitrogen.

The P – N bond lengths for the complexes are not significantly different from each other. The average P – N bond distances in the complexes **(3.11)** and **(3.12)** are possibly shorter than in the free ligands **(2.9)** and **(2.10)**, but these small differences are still within 3σ thus no firm conclusion can be drawn.

The Pd – Cl bond lengths in the complexes **(3.11)**, **(3.12)** and **(3.13)** are not significantly different (see Tables 3.7 – 3.9).

Table 3.10 Bite angles, cone angles and P – N bond lengths for complexes

(3.11 – 3.13)

Complex	Ligand bite angle °	Cone angle °[a]	P – N bond length Å	
			N(1)– P(1)	N(1) – P(2)
(3.11)	71.9(11)	226.5	1.685(9)	1.685(9)
Ligand **(2.9)**			1.716(14)	1.721(14)
(3.12)	71.9(3)	219.9	1.689(2)	1.704(3)
Ligand **(2.10)**			1.702(3)	1.715(3)
(3.13)	71.4(3)	216.0	1.693(2)	1.688(2)

[a] Cone angle measured using three angles

The X-ray crystal structure for the complex **(3.11)** (Figure 3.6) shows that the planar N makes the ether chain too short for the methoxy group to act as a pendant donor to the metal centre. The longer chain on the nitrogen in **(3.12)** (Figure 3.7) shows the methoxy group to be rotated away from the metal. In **(3.13)** (Figure 3.8) the methoxy substituent on the benzyl group is also remote from the metal. It would thus appear that assuming

the N remains planar in solution, coordination of the ether groups in **(3.11 – 3.13)** is precluded.

3.7.2 Crystal structures of platinum methyl chloride complexes (3.3) and (3.5)

X-ray crystal structures of the platinum methyl chloride complexes **(3.3)** and **(3.5)** are shown in Figures 3.9 and 3.10. Selected bond lengths and angles are given in Tables 3.11 and 3.12. For comparison the bite angles and cone angles are given in Table 3.13.

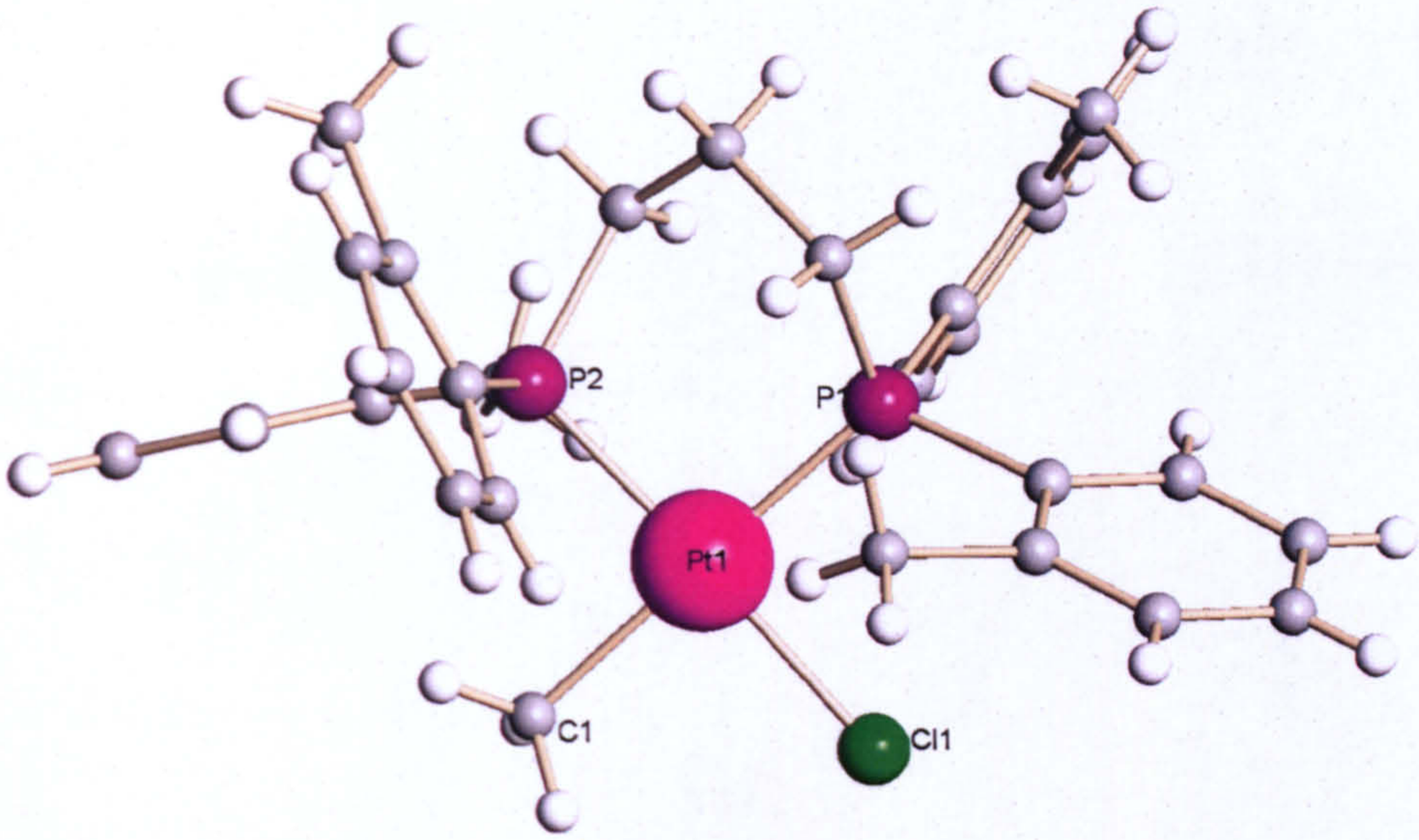

Figure 3.9 X–ray crystal structure of complex (**3.3**)

Table 3.11 Selected bond angles and lengths for complex (**3.3**)

Bond Length	Å	Bond Angle	Degrees °
Pt(1) – C(1)	2.170(2)	C(1) – Pt(1) – P(1)	179.1(7)
Pt(1) – Cl(1)	2.361(7)	C(1) – Pt(1) – P(2)	89.4(7)
Pt(1) – P(1)	2.237(7)	P(1) – Pt(1) – P(2)	91.3(8)
Pt(1) – P(2)	2.299(6)	C(1) – Pt(1) – Cl(1)	88.0(5)
		P(2) – Pt(1) – Cl(1)	176.3(3)
		P(1) – Pt(1) – Cl(1)	91.3(3)

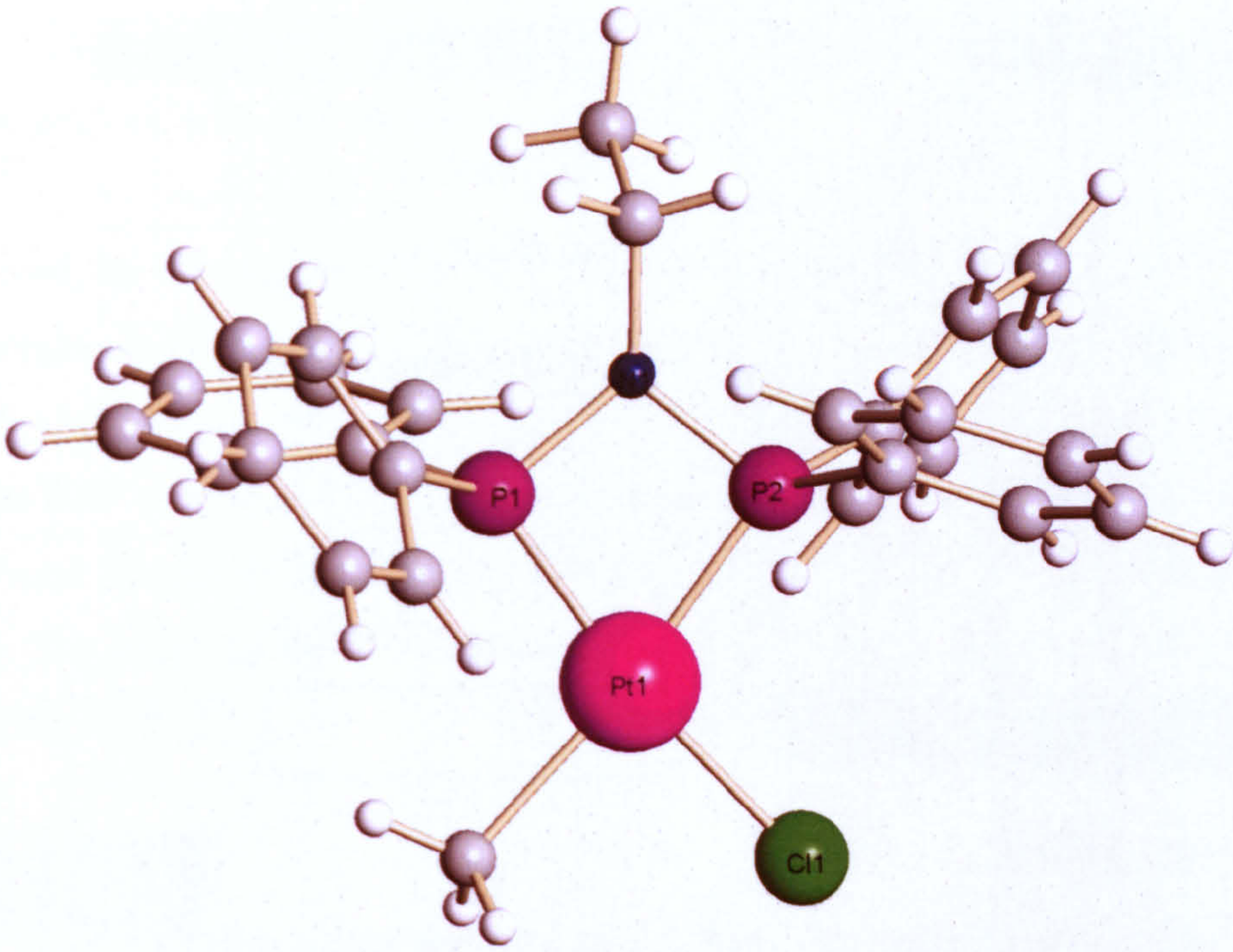

Figure 3.10 X–ray crystal structure of complex (**3.5**)

Table 3.12 Selected bond angles and lengths for complex (**3.5**)

Bond Length	Å	Bond Angle	Degrees °
Pt(1) – C(1)	2.227(13)	C(1) – Pt(1) – P(1)	100.8(4)
Pt(1) – Cl(1)	2.350(4)	C(1) – Pt(1) – P(2)	171.9(4)
Pt(1) – P(1)	2.195(4)	P(1) – Pt(1) – P(2)	72.1(14)
Pt(1) – P(2)	2.239(4)	C(1) – Pt(1) – Cl(1)	87.7(4)
		P(2) – Pt(1) – Cl(1)	99.7(17)
		P(1) – Pt(1) – Cl(1)	170.9(18)
		P(1) – N(1) – P(2)	100.5(6)

In complex **(3.3)** the structure is monoclinic with 2 molecules per unit cell. The methyl groups on the phenyl rings block the top and bottom faces of the platinum and the carbon backbone on the PC_3P ligand is twisted. The crystal structure for complex **(3.5)** is also monoclinic with four molecules per unit cell.

As expected, the bite angles and cone angles are different for **(3.3)** and **(3.5)**. This is due to the increase in the size of the ligand which forms a six-membered chelate in complex **(3.3)** and a four-membered chelate in **(3.5)**. The bite angle of **(3.5)** is of a similar size to that of the PNP chelate **(3.11)**. The Tables of selected bond lengths and angles show the Pt – Cl bond lengths to be of comparable sizes of 2.361(7) Å for **(3.3)** and 2.350(4) Å for **(3.5)**. The length of the Pt – C bond is shorter for **(3.3)** at 2.170(2) Å with the **(3.5)** at 2.227(13) Å.

Table 3.13 Bite angles and cone angles for complexes **(3.3)** and **(3.5)**

Complex	Ligand bite angle ^{o}	Cone angle ^{oa}
(3.3)	91.3(8)	256.2
(3.5)	72.1(14)	207.3

[a] Cone angle measured using three angles

3.7.3 Crystal structures of dichloroplatinum complexes

Attempts to grow single crystals of the complexes **(3.2, 3.4, 3.6, 3.7)** from dichloromethane gave the dichloroplatinum species **(3.2x, 3.4x, 3.6x, 3.7x)** due to reaction with the chlorinated solvent. However, the crystals produced are disordered with one of the chlorine atoms having a fractional site occupancy with methyl. This leads to structures with one of the Pt – Cl bond lengths being shorter than expected. For this reason, the interpretation of the data from these structures must be treated with caution. The structures are shown in Figures 3.11 – 3.14, with selected bond lengths and

angles given in Tables 3.14 – 3.17. For comparison, the bite angles and cone angles and P – N bond lengths are given in Table 3.18.

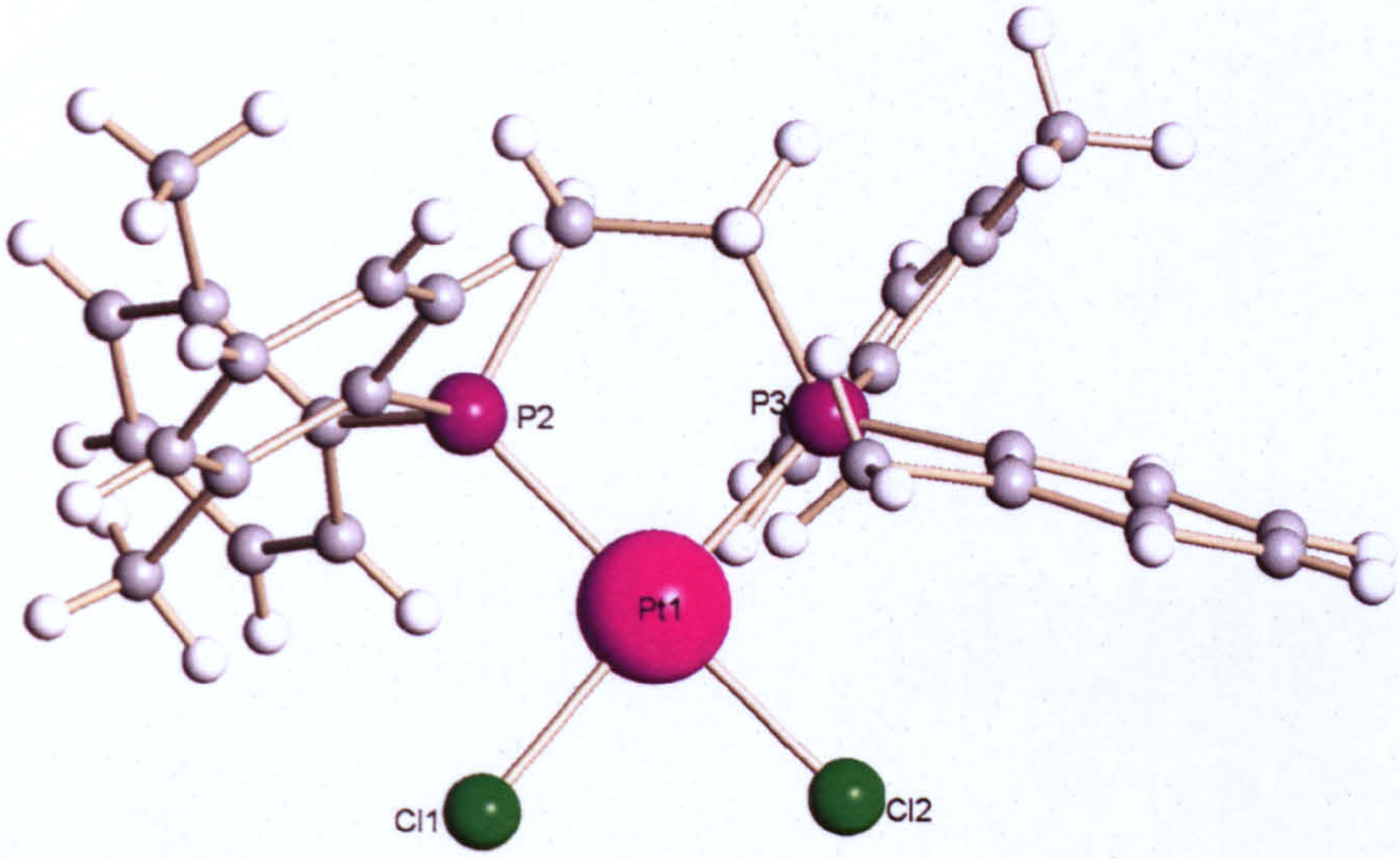

Figure 3.11 X–ray crystal structure of (**3.2x**)

Table 3.14 Selected bond angles and lengths for (**3.2x**)

Bond Length	Å	Bond Angle	Degrees °
Pt(1) – Cl(1)	2.335 (4)	Cl(1) – Pt(1) – P(2)	95.1 (15)
Pt(1) – Cl(2)	2.307 (3)	Cl(1) – Pt(1) – P(3)	176.2 (16)
Pt(1) – P(2)	2.294 (4)	P(2) – Pt(1) – P(3)	87.1 (14)
Pt(1) – P(3)	2.224 (3)	Cl(1) – Pt(1) – Cl(2)	86.1 (3)
		P(2) – Pt(1) – Cl(2)	177.5 (3)
		P(3) – Pt(1) – Cl(2)	91.8 (3)

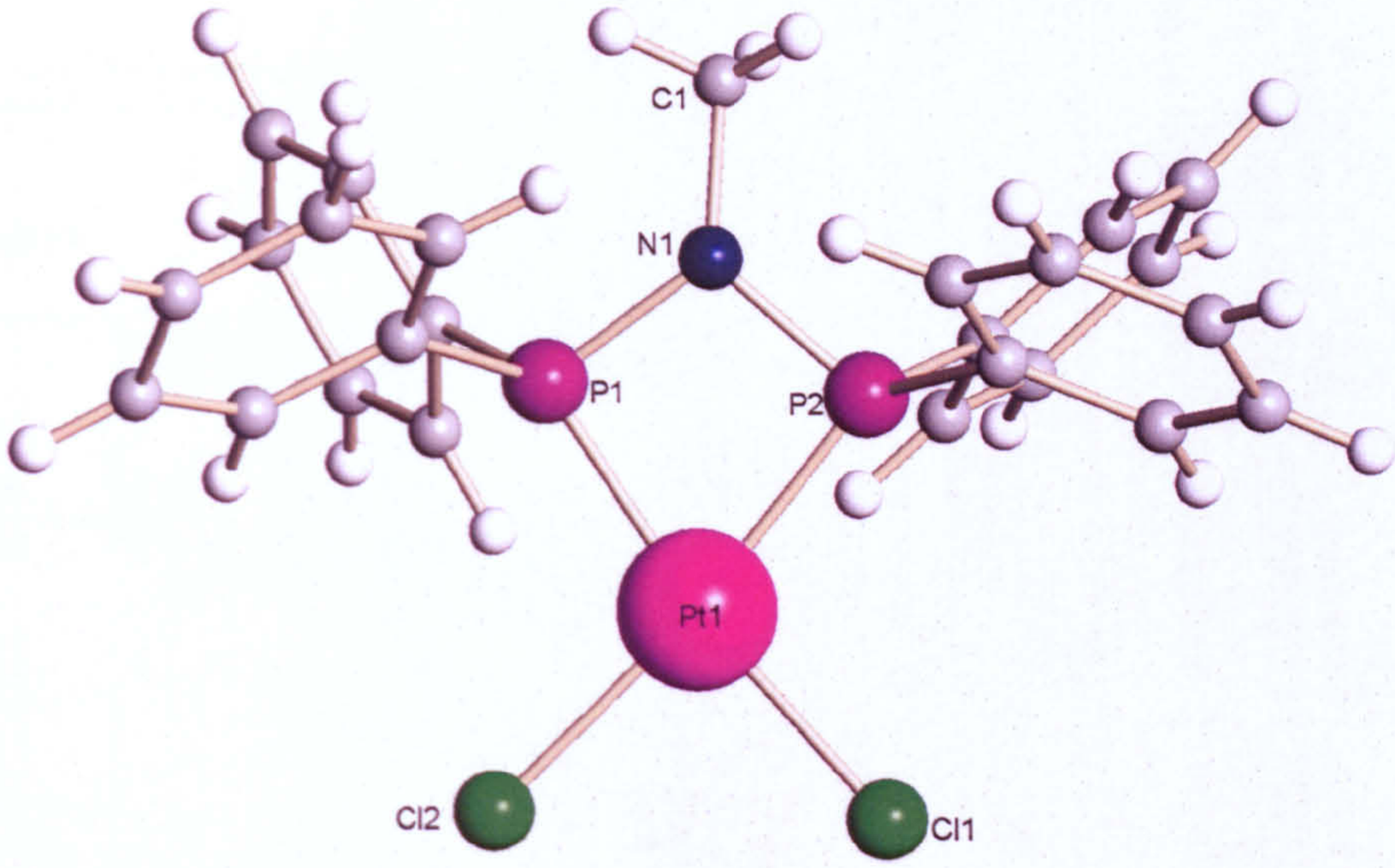

Figure 3.12 X–ray crystal structure of (**3.4x**)

Table 3.15 Selected bond angles and lengths for (**3.4x**)

Bond Length	Å	Bond Angle	Degrees °
Pt(1) – Cl(1)	2.303(2)	Cl(1) – Pt(1) – P(1)	171.4(7)
Pt(1) – Cl(2)	2.334(2)	Cl(1) – Pt(1) – P(2)	99.7(7)
Pt(1) – P(1)	2.240(13)	P(1) – Pt(1) – P(2)	71.8(5)
Pt(1) – P(2)	2.236(13)	Cl(1) – Pt(1) – Cl(2)	87.5(9)
		P(1) – Pt(1) – Cl(2)	101.0(7)
		P(2) – Pt(1) – Cl(2)	172.7(7)
		P(1) – N(1) – P(2)	101.0(2)

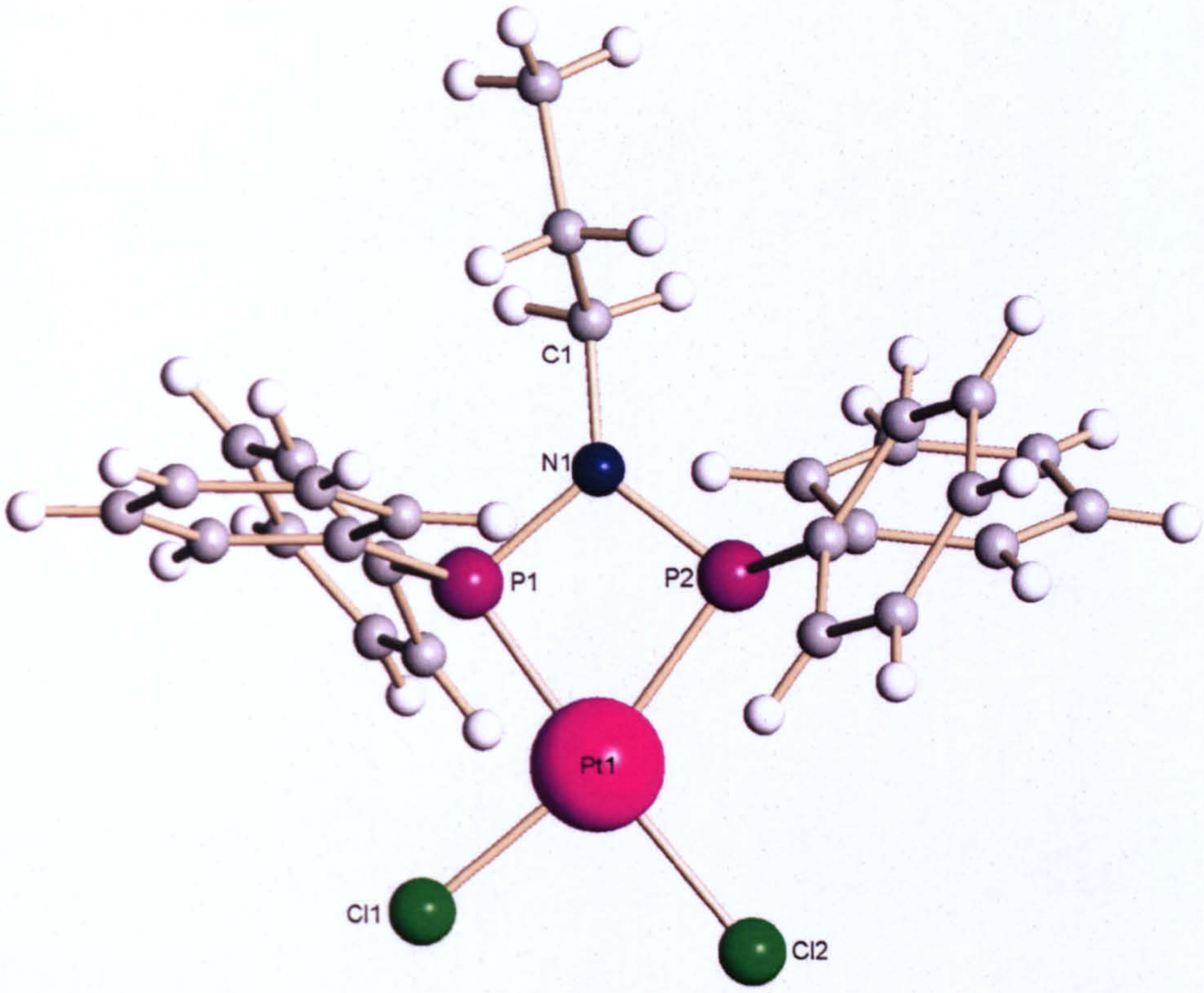

Figure 3.13 X–ray crystal structure of (**3.6x**)

Table 3.16 Selected bond angles and lengths for (**3.6x**)

Bond Length	Å	Bond Angle	Degrees °
Pt(1) – Cl(1)	2.237(7)	Cl(2) – Pt(1) – P(1)	174.3(9)
Pt(1) – P(2)	2.263(4)	Cl(2) – Pt(1) – P(2)	104.4(19)
Pt(1) – Cl(2)	2.360(6)	P(1) – Pt(1) – P(2)	71.9(19)
Pt(1) – P(1)	2.179(5)	Cl(2) – Pt(1) – Cl(1)	89.8(2)
		P(1) – Pt(1) – Cl(1)	94.0(2)
		Cl(1) – Pt(1) – P(2)	165.7(16)
		P(1) – N(1) – P(2)	101.0(4)

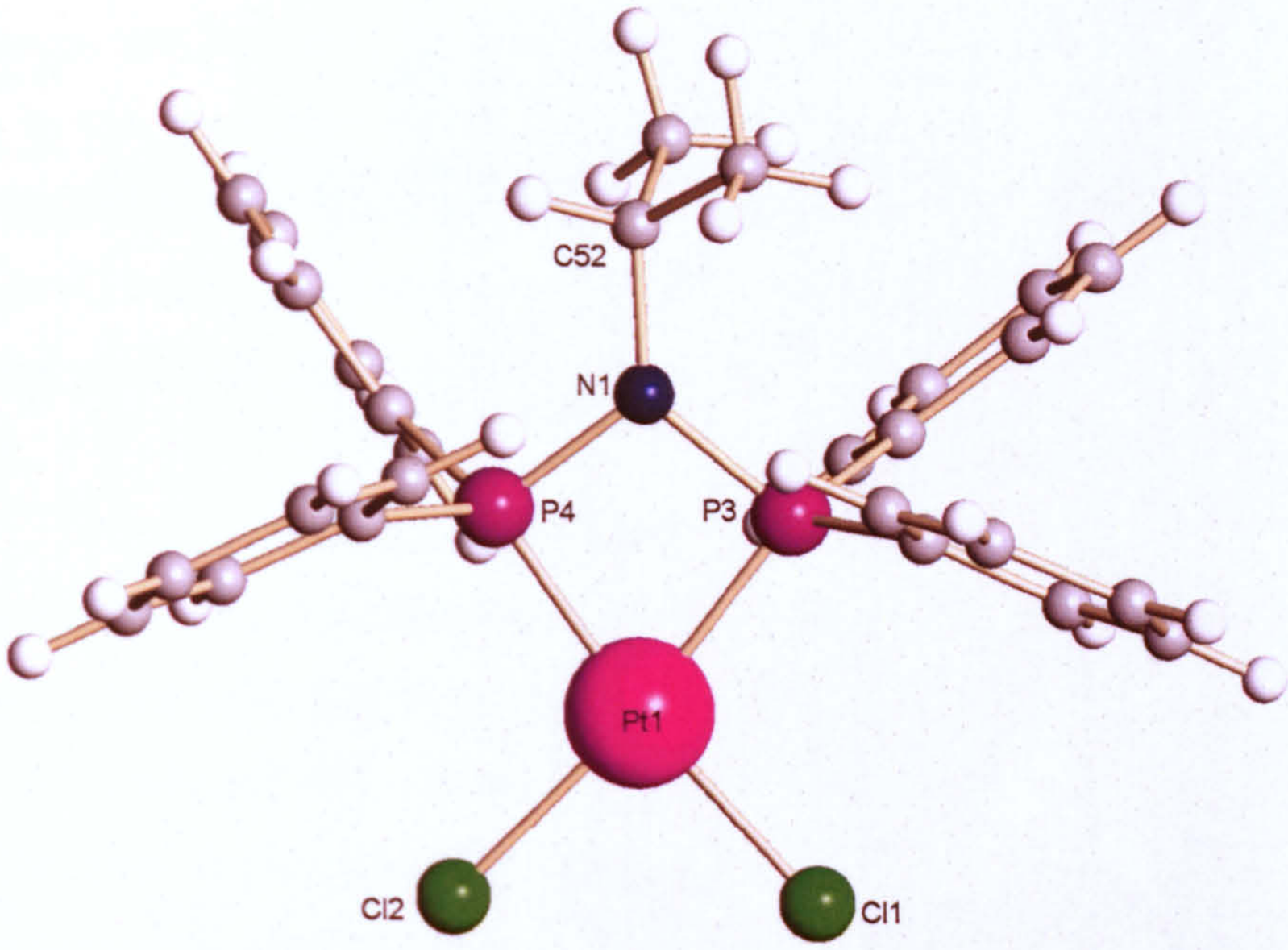

Figure 3.14 X–ray crystal structure of (**3.7x**)

Table 3.17 Selected bond angles and lengths for (**3.7x**)

Bond Length	Å	Bond Angle	Degrees °
Pt(1) – Cl(1)	2.281(2)	Cl(1) – Pt(1) – P(4)	168.9(8)
Pt(1) – Cl(2)	2.334(18)	Cl(1) – Pt(1) – P(3)	99.3(9)
Pt(1) – P(3)	2.213(15)	P(4) – Pt(1) – P(3)	71.8(6)
Pt(1) – P(4)	2.231(15)	Cl(1) – Pt(1) – Cl(2)	88.1(10)
		P(4) – Pt(1) – Cl(2)	101.0(7)
		P(3) – Pt(1) – Cl(2)	172.6(7)
		P(3) – N(1) – P(4)	99.4(2)

The crystal structure of **(3.2x)** is triclinic with 24 molecules per unit cell, the tolyl-methyl groups are shown to be orientated to block the axial sites of the platinum. However, in this case only one of the axial faces is blocked. No broadening of the $^{31}P\{^{1}H\}$ NMR spectrum was observed, indicating that there is no restricted rotation about the P - C bonds. The bite angle 87.1(14)° and cone angle 248.9° are larger for this five-membered chelate **(3.2x)** than for the smaller four-membered chelates shown in Table 3.18.

The crystal structures for complexes **(3.4x)**, **(3.6x)** and **(3.7x)** indicate very few differences in their solid-state structures. All complexes crystallise in a monoclinic state with four molecules per unit cell. As expected the bite angles of **(3.4x – 3.7x)** are very similar. The cone angles gradually increase in size for **(3.4x)** < **(3.6x)** reflecting the increase in size of the alkyl group on the nitrogen.

Comparison of the Pt – Cl bond lengths (from Tables of selected bond lengths) which showed no disorder, leads to the conclusion that there are no significant differences between the structures. The P – N bond lengths for complexes **(3.4)**, **(3.6)** and **(3.7)**, given in Table 3.18, are all of similar values. This shows that increasing the electron density on the nitrogen has no detectable effect on the solid-state structure of the compounds.

Table 3.18 Bite angles, cone angles and P – N bond lengths for complexes **(3.2x)**, **(3.4x)**, **(3.6x)** and **(3.7x)**

Complex	Ligand bite angle °	Cone angle °[a]	P – N bond length Å	
			N(1)– P(1)	N(1) – P(2)
(3.2)	87.1(14)	248.9		
(3.4)	71.8(5)	203.8	1.702(4)	1.701(4)
(3.6)	71.9(19)	213.2	1.697(8)	1.683(8)
(3.7)	71.8(6)	211.1	1.704(5)	1.704(5)

[a] Cone angle measured using three angles

3.7.4 Discussion of molecular modelling

The nickel hydride complex $[NiH(Ph_2PN(Me)PPh_2)]^+$ **(3.19)** and the corresponding compound $[NiH(Ph_2PCH_2PPh_2)]^+$ **(3.20)** were modelled using DFT B3LYP methods, in order to determine any differences between the structures.

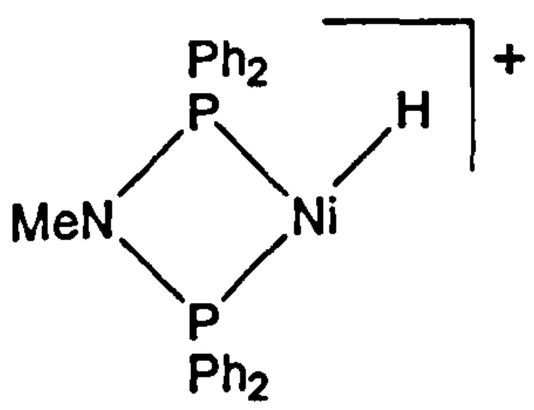

(3.19)

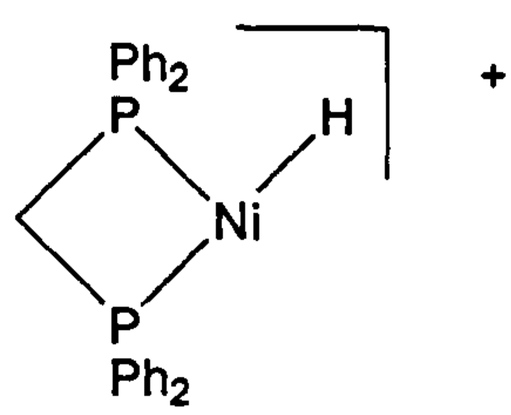

(3.20)

Geometry optimisation on **(3.19)** and **(3.20)** revealed only very minor differences in the structures. The LUMO energies of the orbital concentrated at the vacant site on nickel of – 563.3 $KJmol^{-1}$ **(3.19)** and – 565.5 $KJmol^{-1}$ **(3.20)** are also of similar values; this can

be seen pictorially in Figures 3.15 and 3.16. The LUMO is primarily the antibonding combination between a 4d - 5s hybrid on the metal and the lone pair on the phosphorus which lies *trans* to the vacant site.

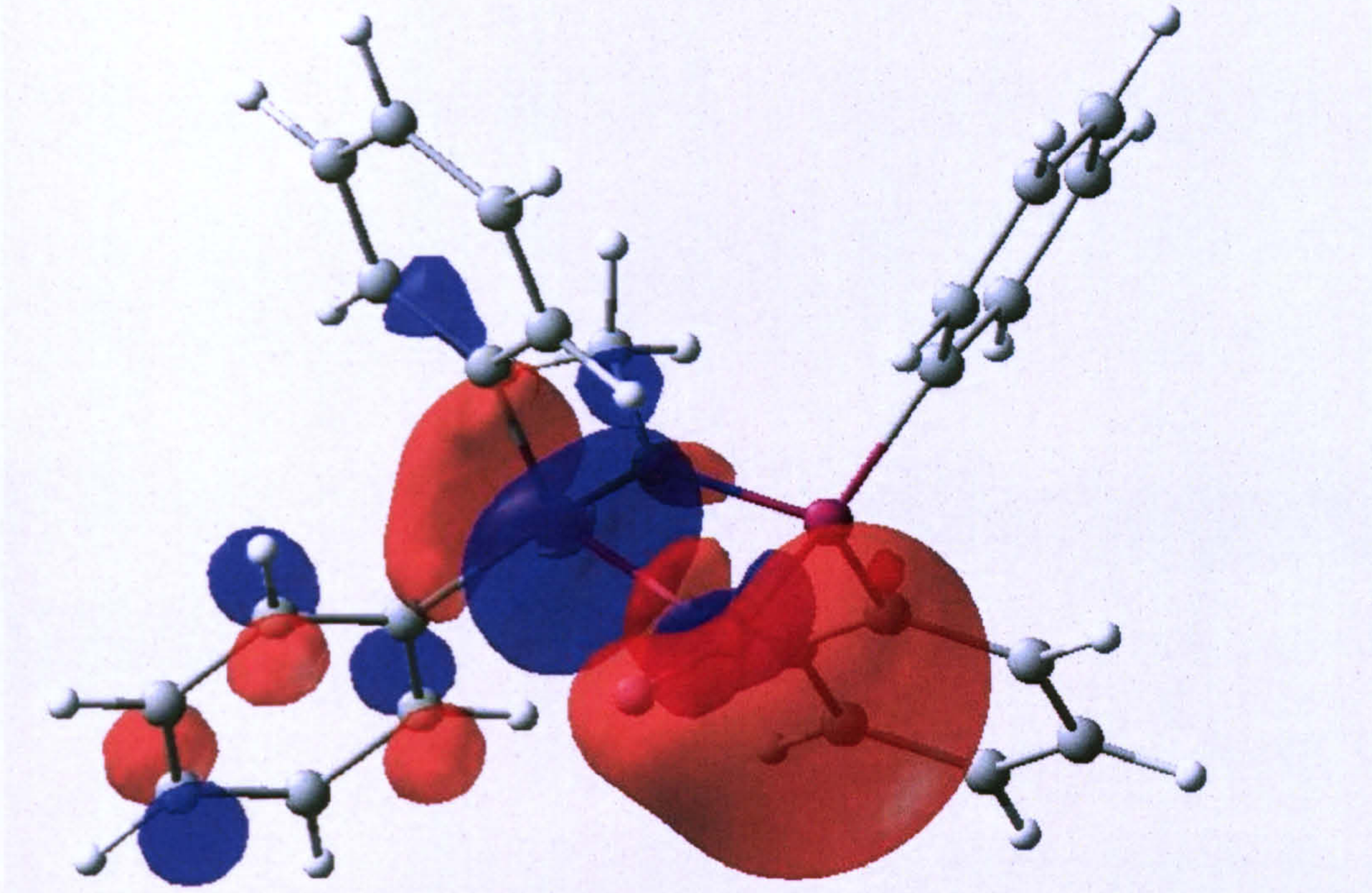

Figure 3.15 LUMO of $[NiH(Ph_2PN(Me)PPh_2)]^+$ (**3.19**) showing vacant site

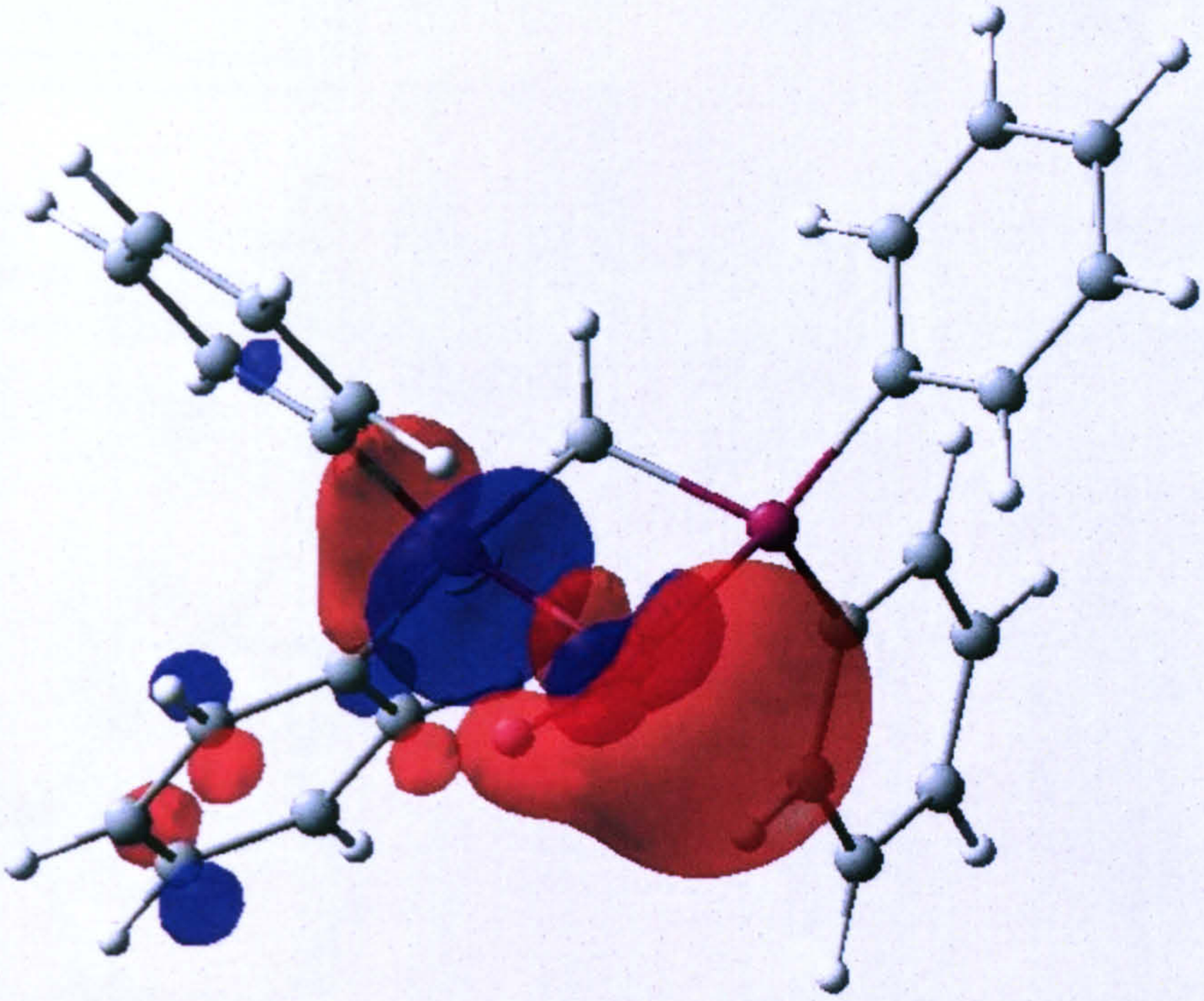

Figure 3.16 LUMO of $NiH(Ph_2PCH_2PPh_2)]^+$ (**3.20**) showing vacant site

However, the geometry optimisation did give some clear evidence of electronic communication between the PNP bridge on (**3.19**) and the metal centre, shown in Figure 3.17, in contrast to the PCP backbone where no interaction is seen. This interaction could help to explain the difference in behaviour between the two ligands in Ni-catalysed ethylene polymerisation.

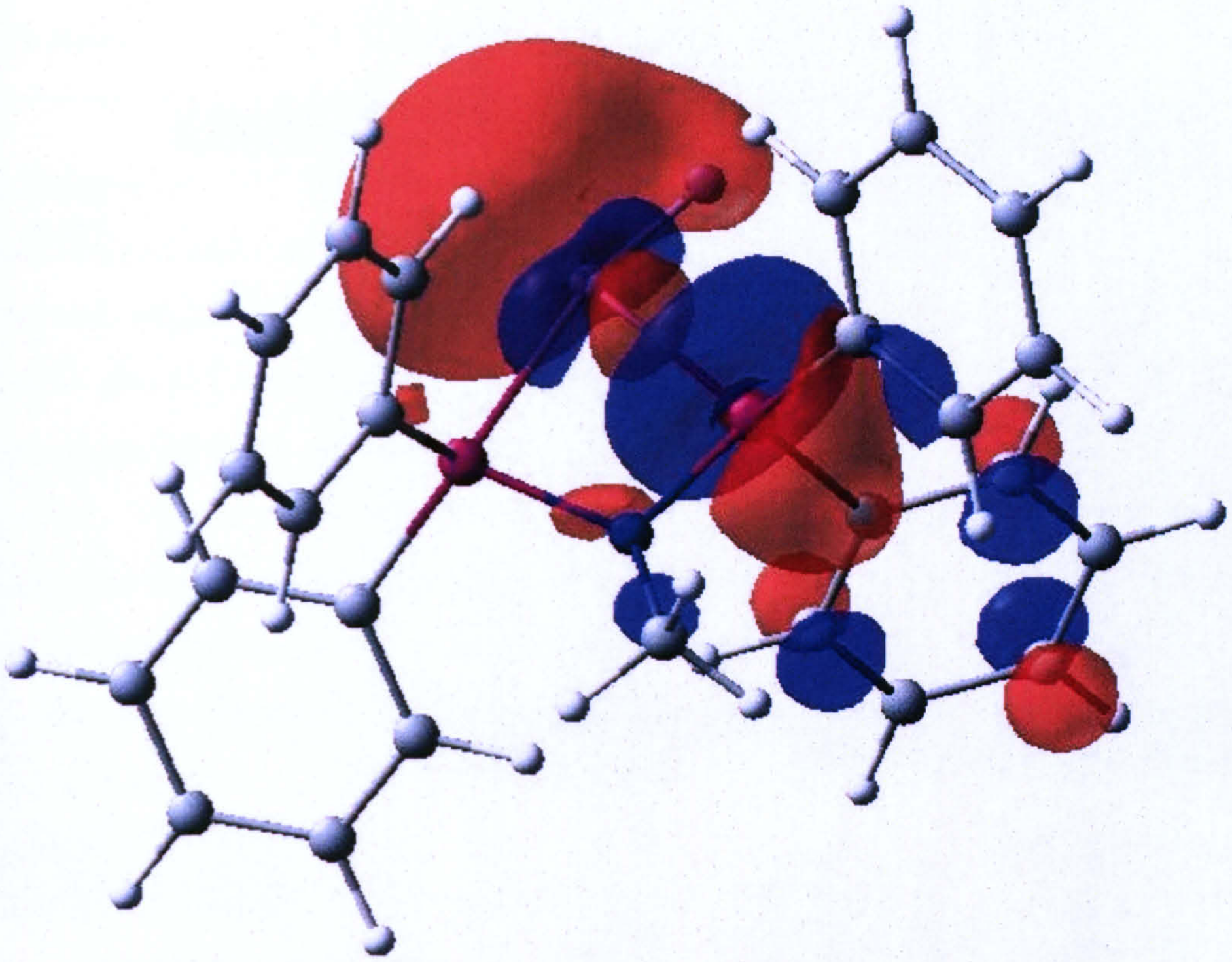

Figure 3.17 LUMO of $[NiH(Ph_2PN(Me)PPh_2)]^+$ (**3.19**) showing PNP bridge

Although very little difference between the geometry optimised species (**3.19**) and (**3.20**) has been detected using the modelling carried out here, subtle variations must exist in order to explain the differences in behaviour of PNP and PCP ligands in Ni-catalysed ethylene polymerisation.[41] In order to gain a further insight into this area more in-depth DFT calculations would be required. Studies of this type have been carried out by Ziegler *et al.* on Ni-catalysed ethylene polymerisation using diimine ligands.[91, 92]

3.8 Conclusion

Complexes of the ligands discussed in Chapter 2 have been synthesised and characterised and a preference for PNP ligands to bind in a chelating manner has been observed. Molecular modelling has shown there is little difference in the energy of the LUMO for the vacant site on the nickel hydride compound modelled. However, interactions between the phosphorus and nitrogen on the ligand backbone have been detected. The analysis of the crystal structures indicated there to be negligible differences between the compounds. This concurs with the $^{31}P\{^{1}H\}$ NMR spectroscopy data, which showed the J_{PtP} to be similar. The following Chapter will discuss the activity of the ligands in Cr-catalysed ethylene trimerisation and Ni-catalysed ethylene polymerisation.

Chapter 4:

Olefin oligomerisation with catalysts derived from PNP ligands

Olefin oligomerisation with catalysts derived from PNP ligands

4.1 Introduction

In this chapter a brief introduction to ethylene polymerisation, oligomerisation and trimerisation catalysis will be given, including the use of PNP ligands in these systems. This will be followed by results with nickel and chromium catalysts for ethylene oligomerisation using the ligands shown in Figure 4.1.

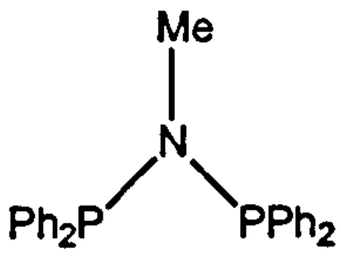

(2.5)

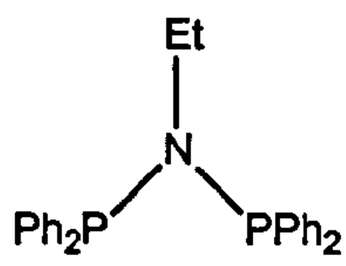

(2.6)

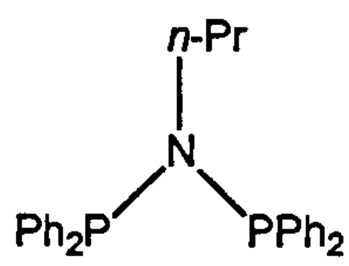

(2.7)

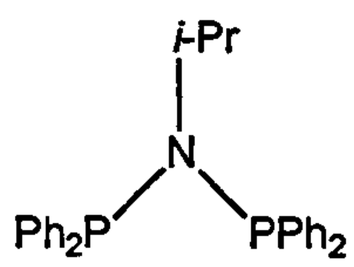

(2.8)

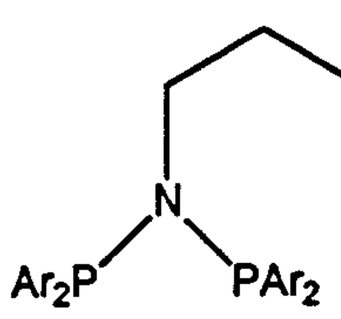

(2.9)

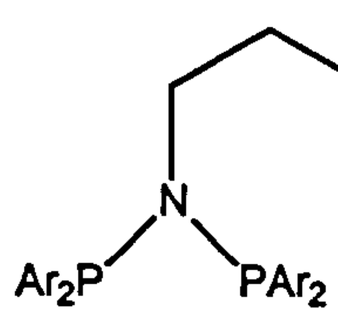

(2.10)

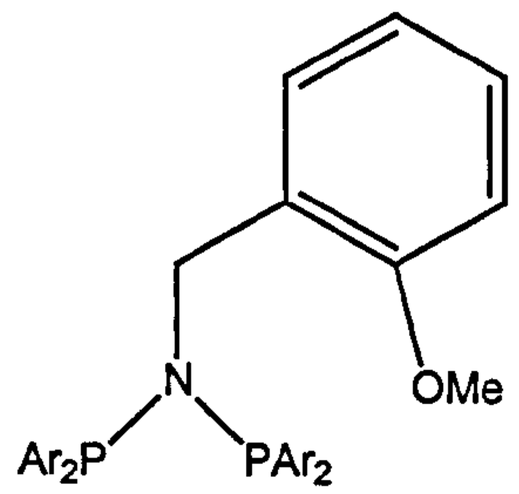

(2.11)

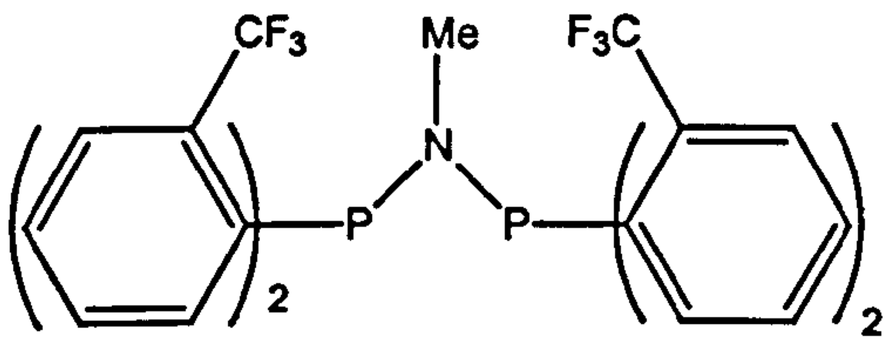

(2.12)

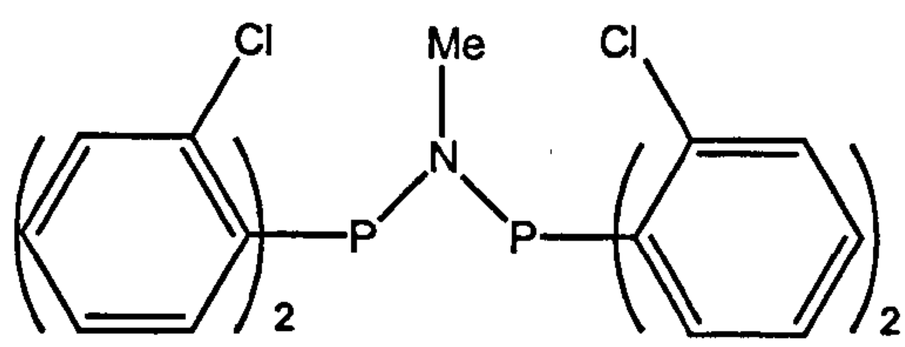

(2.13)

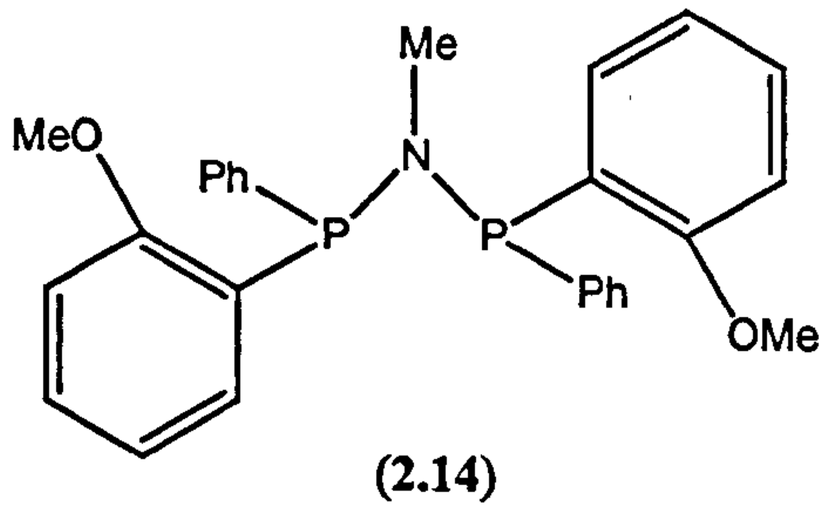

(2.14)

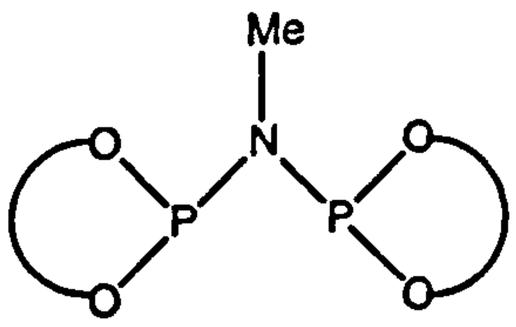

(2.15)

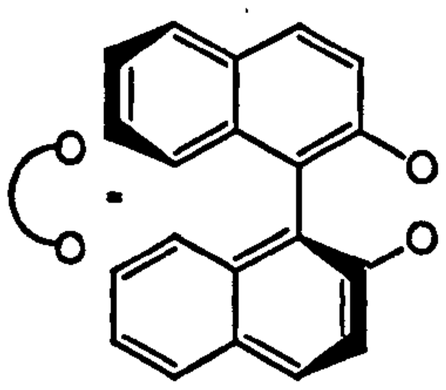

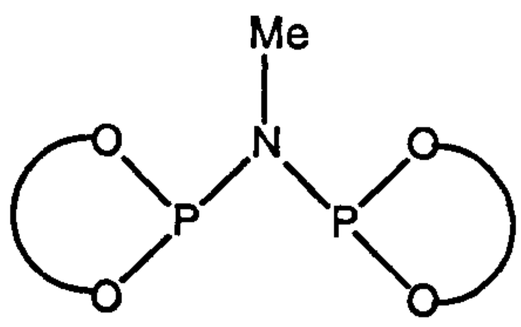

(2.16) (2.17)

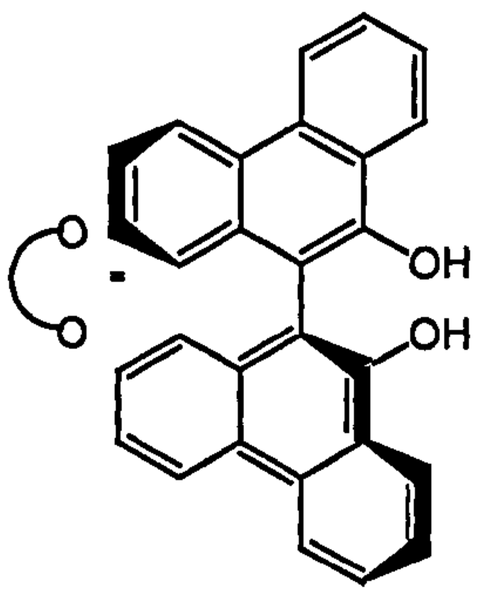

Figure 4.1

4.1.1 Ethylene polymerisation catalysis

The first catalysts for the production of polyethylene were discovered by Ziegler *et al.*[93] nearly 50 years ago, using $TiCl_4$-$AlClEt_2$. This was shortly followed by the discovery of the stereoselective polymerisation of propene by Natta.[94] Since then the polymerisation of α-olefins has developed into a major industry. Classical Ziegler catalysts are heterogeneous early transition metal complexes. Newer Ziegler-type catalysts are metallocenes of Group 4, and related half sandwich amide or constrained geometry catalysts[95] such as **(4.1)**. Ziegler catalysts, fifty years after their discovery have been reviewed by Böhm.[96]

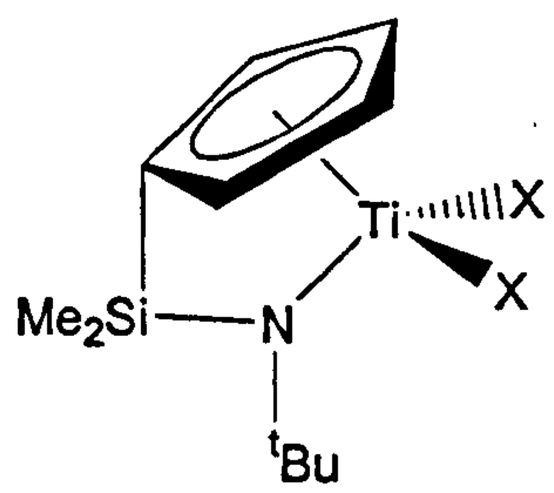

(4.1)

Industry's desire to obtain greater control over the properties of polymers has led to research into a wide variety of selective catalysts. There are now a large number of highly active non-metallocene polymerisation catalysts across the transition series.[42, 97, 98] Over the past decade, late-transition metal catalysts for olefin polymerisation have received increasing attention. The main advantage over early transition metal catalysts is the lower oxophillicity and therefore tolerance of polar functional groups and increased ease of handling. These catalysts may therefore be capable of incorporating functionalised co-monomers, (for example vinyl acetate) into the polyethylene. Developments into polyethylene catalysts using late transition metals,[43] for example nickel and palladium have been made. The nickel(II) and palladium(II) systems reported

by Brookhart and co-workers[99] based on square planar cationic alkyl compounds supported by bulky diimine [N,N] ligands **(4.2)**, were the first examples of late transition metal catalysts capable of polymerising higher olefins as well as ethylene to high molecular weight polymers. For example, propylene is polymerised to produce amorphous polypropylene (126 kg of PP mol^{-1} Ni h^{-1}, 3000 TO/h), while 1-hexene produces amorphous poly-1-hexene (176 kg mol^{-1} of Ni h^{-1}, 2000 TO/h).[99]

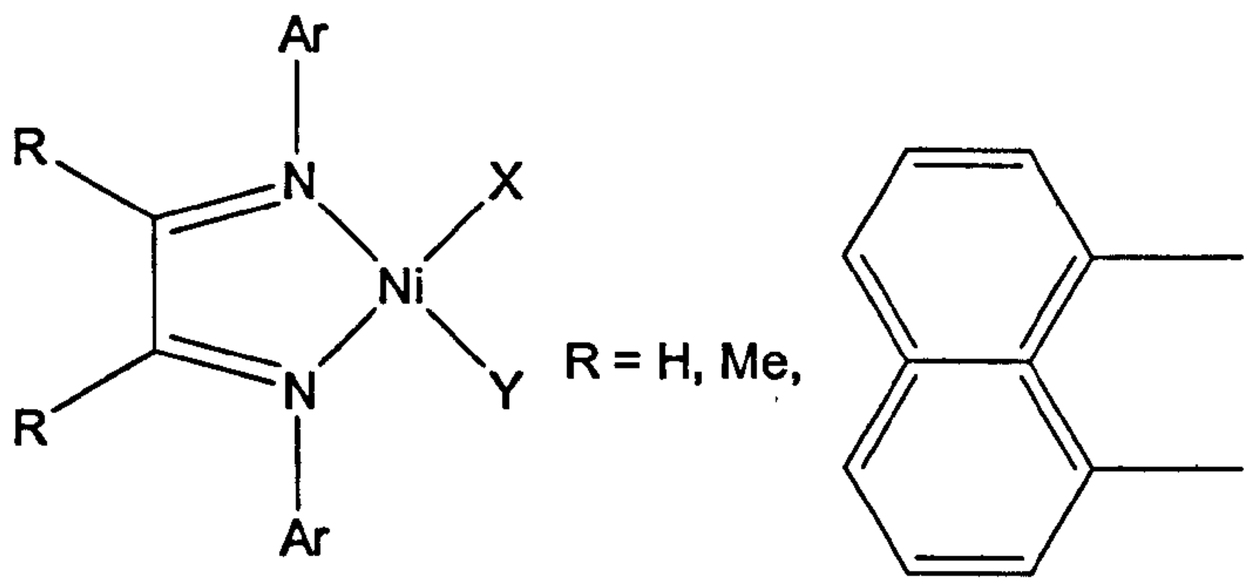

X = Y = Br

X = B[3,5-$(CF_3)_2C_6H_3]_4.Et_2O$, Y = Me

Ar = 2,6-*i*-$Pr_2C_6H_3$, 2,6-$Me_2C_6H_3$, 2-*t*-BuC_6H_4

[N,N]

(4.2)

α-Diimine ligands on copper have also been discovered to be active catalysts for ethylene polymerisation. A copper α-diimine complex containing 2,6-diphenylphenylimino substituents were found to give good activities for polyethylene catalysis upon activation with MAO, (300 g $mmol^{-1}$ $h^{-1}$with 500 eq MAO at 30 bar ethylene pressure). The high activity is thought to be a result of the special stabilising effect of the *ortho*-phenyl groups.[100]

There is only one example in the literature of the use of PNP ligands in ethylene polymerisation catalysis. Wass *et al.* reported nickel(II) complexes of ligands of the type $Ar_2PN(Me)PAr_2$ (Ar = *ortho*-substituted phenyl group) to be highly active and poison tolerant catalysts for the polymerisation of ethylene (Equation 4.1).[41, 101]

Activities of up to 2200 g $mmol^{-1}$ h^{-1} are observed at 50 °C, 8 bar ethylene pressure and 200 eq MAO. The catalyst performance is described as approaching that of the best existing nickel-based systems.[99, 102] When the ligand contains isopropyl groups in the *ortho* position (**4.3**), the polymer produced is of high molecular weight with low levels of branching. Ligands with less sterically demanding *ortho* groups present, yield lower molecular weight polymer.

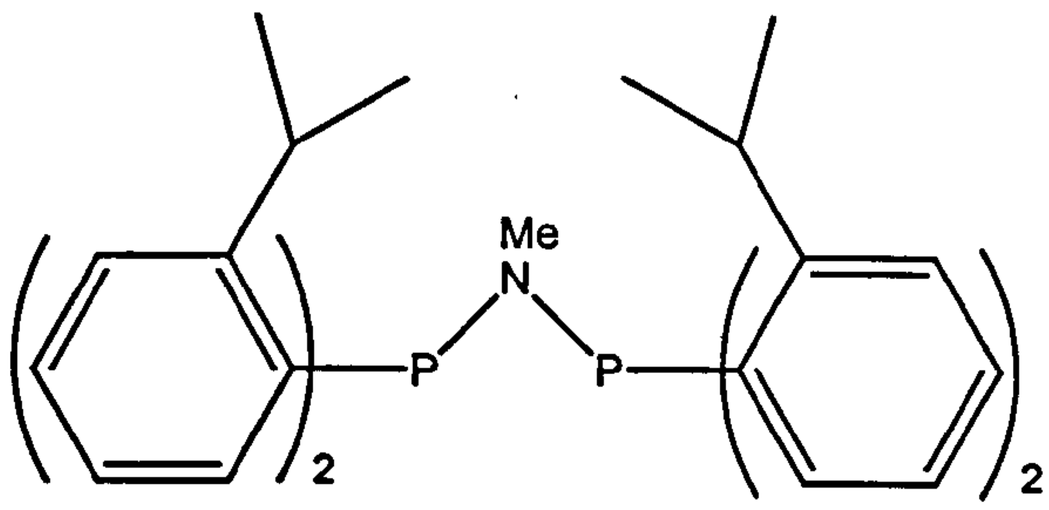

(4.3)

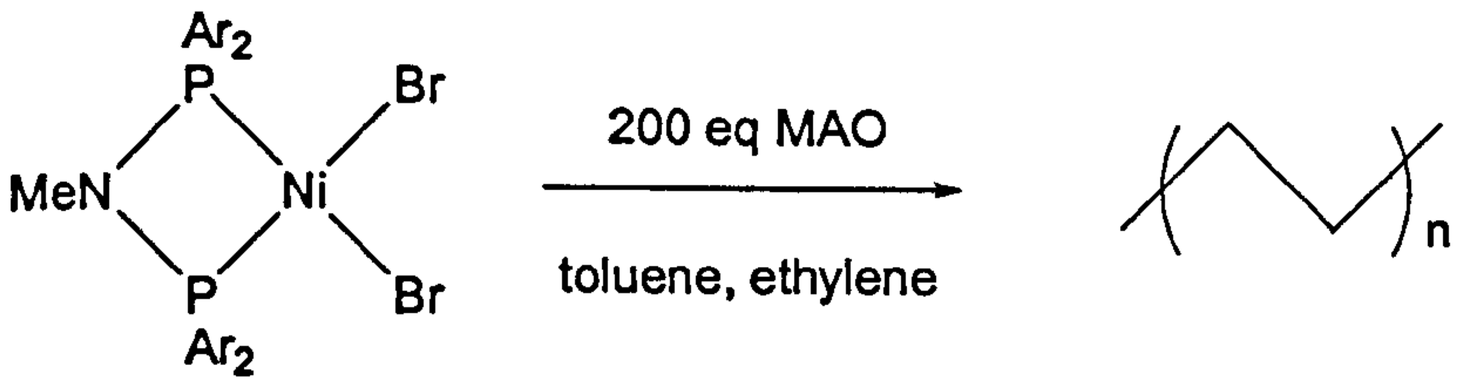

Ar = 2-C_6H_4(*i*-Pr)
2-C_6H_4(Et)
2-C_6H_4(Me)

Equation 4.1

4.1.2 Ethylene oligomerisation catalysis

Higher α-olefins are an important family of industrial chemicals which, through hydroformylation, copolymerisation and arylation become components of plasticisers, solvents, plastics and surfactants. Higher α-olefins can be obtained from ethylene through oligomerisation processes which usually gives a broad Schultz-Flory[103 - 106] distribution of ethylene oligomers, that are then separated by distillation. Oligomerisation of ethylene to higher α-olefins through the use of transition metal catalysis has been reviewed by Skupińska.[107]

One of the largest applications of homogeneous catalysis by transition metals, especially nickel, is the Shell Higher Olefin Process (SHOP).[108 - 110] The SHOP process converts ethylene into value added chemicals, α-olefins, using the nickel complex **(4.4)** as the catalyst. The complex **(4.4)** is prepared by the reaction shown in Equation 4.2.[111]

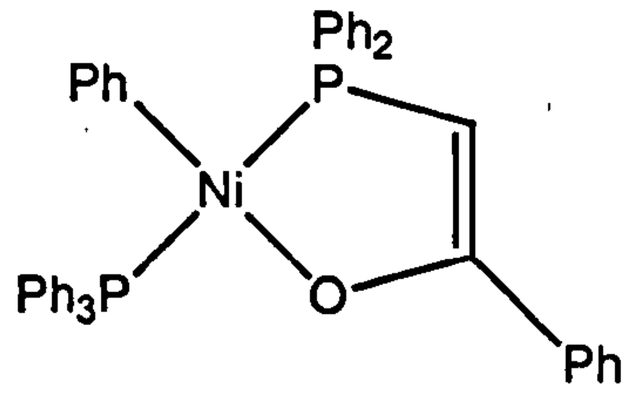

(4.4)

Reaction of a toluene solution of **(4.4)** with ethylene at 50 bar and 50 °C affords olefins which are up to 99% linear and up to 98% α-olefins. Activities of 6000 mol ethylene per mol of **(4.4)** are reported. However, when the reaction is carried out in *n*-hexene, high molecular weight polymer is formed.[111, 112]

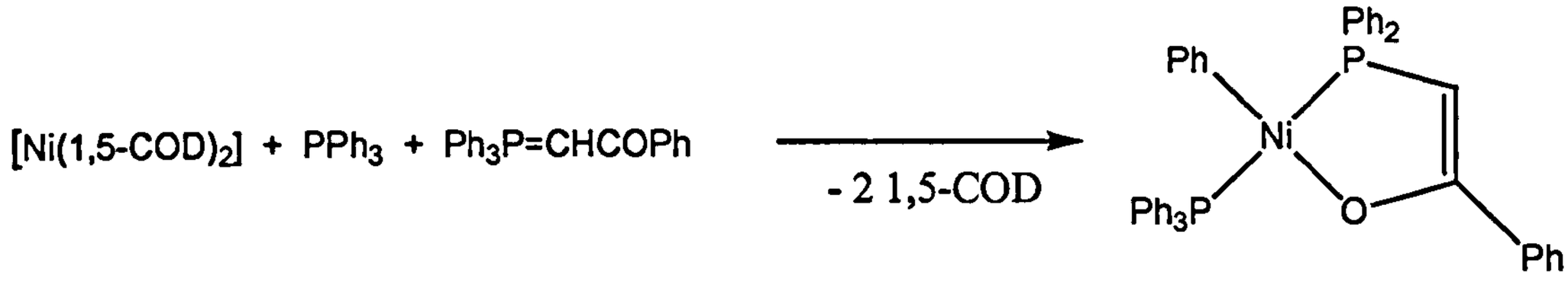

(4.4)

Equation 4.2

The analogous arsenic chelate (**4.5**) has been reported by Keim *et al.*[113] to be active for ethylene oligomerisation (see Equation 4.3).

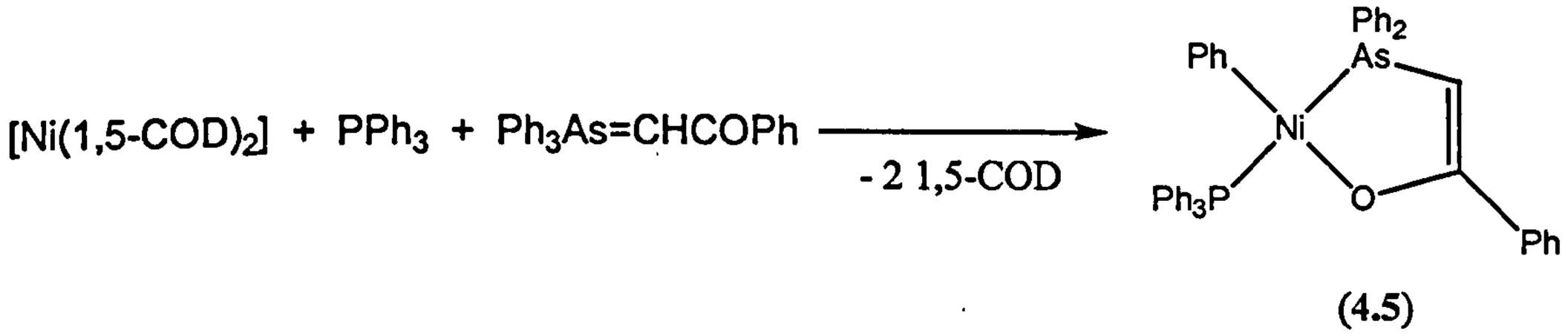

(4.5)

Equation 4.3

Complex (**4.5**) in toluene yields an *in-situ* catalyst which oligomerises ethylene under mild conditions (40 °C, 15 bar ethylene). Linear olefins are formed almost exclusively (> 95%) and the proportion of α-olefins exceeds 70% with activities of 1600 mol ethylene per mol nickel per hour.

More recently α-diimine ligands on nickel have been shown to generate α-olefins. Studies by Brookhart and co-workers have shown α-diimine nickel complexes to be highly active ethylene polymerisation catalysts.[99] However, decreasing the steric bulk in the *ortho* position of the aryl rings (for example see (**4.6**)), results in oligomerisation rather than polymerisation reactions. This is a consequence of a fast rate of chain

transfer relative to chain propagation. Chain transfer is inhibited by the axial bulk provided by the *ortho*-substituents.[114]

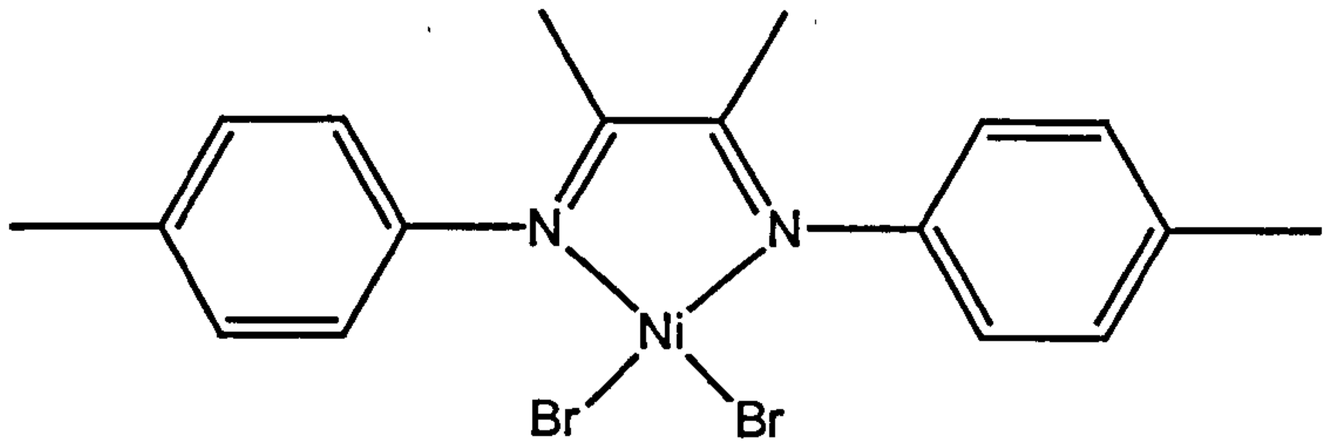

(4.6)

The complex **(4.6)** yields up to 94% α-olefins at 56 atm ethylene, 35 °C and 100 eq MMAO (TOF 57 x 10^{-3}/h).[115]

Ferrocene substituted nitrogen ligands when complexed to nickel have been reported by Gibson *et al.* to be active oligomerisation pre-catalysts.[116] The compound **(4.7)** has been shown to be selective for the formation of butene and gives trace amounts of higher oligomers (TON 19 x 10^3 mol ethylene per mol catalyst, 1 bar ethylene, 100 eq MAO).

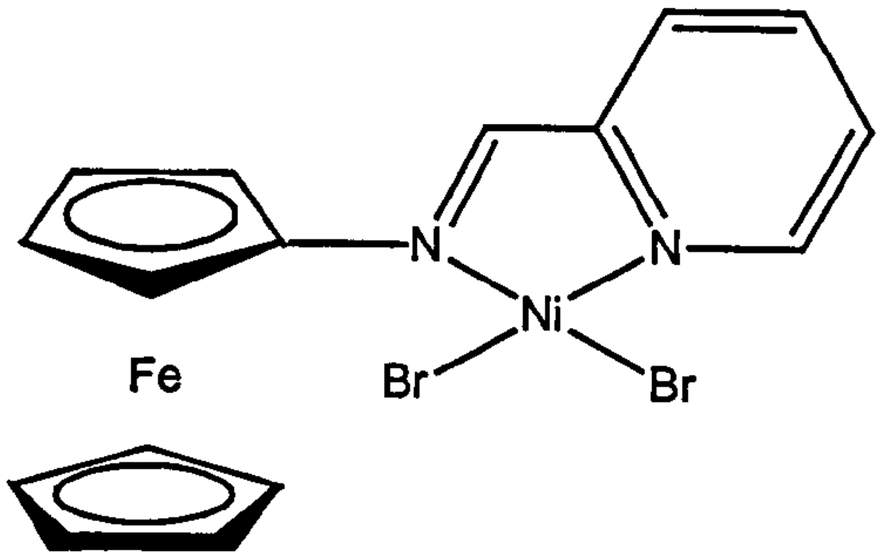

(4.7)

One of the only uses of PNP ligands in ethylene oligomerisation reported to date are the ligands $Ph_2PN(i\text{-}Pr)PPh_2$ **(4.8)** and $(p\text{-}CH_3OC_6H_4)_2PN(i\text{-}Pr)P(p\text{-}CH_3OC_6H_4)_2$ **(4.9)** which in 2004 were patented by Sasol for Cr-catalysed ethylene tetramerisation giving selective formation of 1-octene in yields of 69% and 72% respectively.[117]

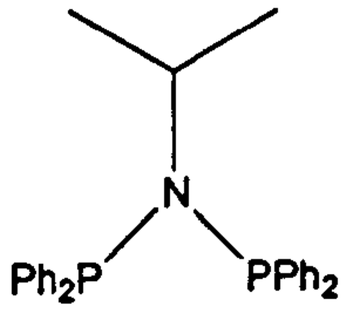

(4.8)

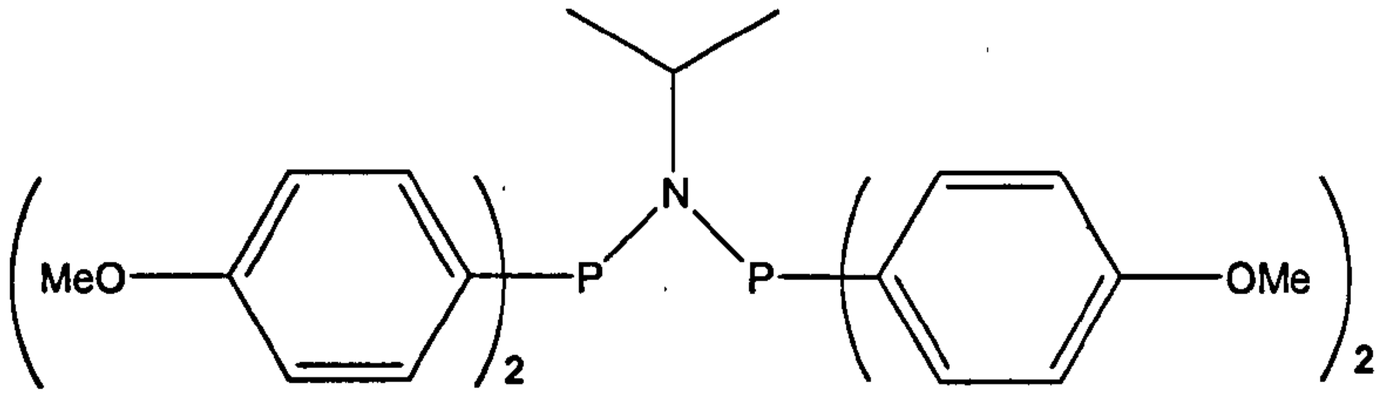

(4.9)

4.1.3 Ethylene trimerisation catalysis

One of the most useful products of ethylene oligomerisation is 1-hexene. 1-Hexene is a co-monomer for linear low-density polyethylene (LLDPE) and catalysts that are selective for 1-hexene are of great interest. In recent years, a remarkable family of catalysts has emerged capable of the selective trimerisation of ethylene to 1-hexene. One of the best known ethylene trimerisation catalysts is based on chromium with a 2,5-dimethylpyrrole ligand and an alkyl aluminium activator, developed by Phillips.[49] PNP ligands have been discovered which catalyse this reaction on chromium. Ligands with ethane bridges between the nitrogen and phosphorus moieties **(4.10)** have been shown to have average activities and good selectivity to 1-hexene, up to 99% where R = ethyl.[118] McGuinness and co-workers have also developed the SNS analogue of **(4.10)** see **(4.11)**[119] giving selectivities of up to 99.8% for 1-hexene when complexed to chromium.

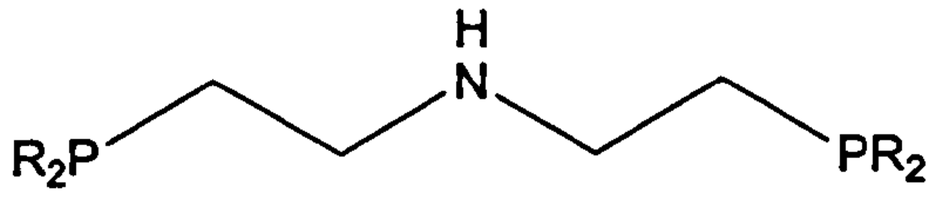

R = phenyl
cyclohexyl
ethyl

(4.10)

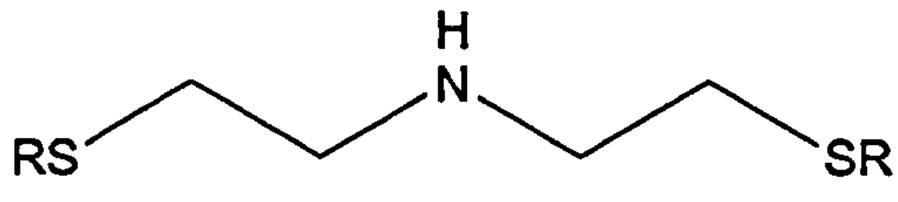

R = methyl
ethyl
n-butyl

(4.11)

Triazacyclohexane ligands on Chromium (see **4.12**) have been reported by Köhn *et al.*[120] to catalyse the trimerisation of ethylene to yield 1-hexene with > 90% conversion at 0 °C

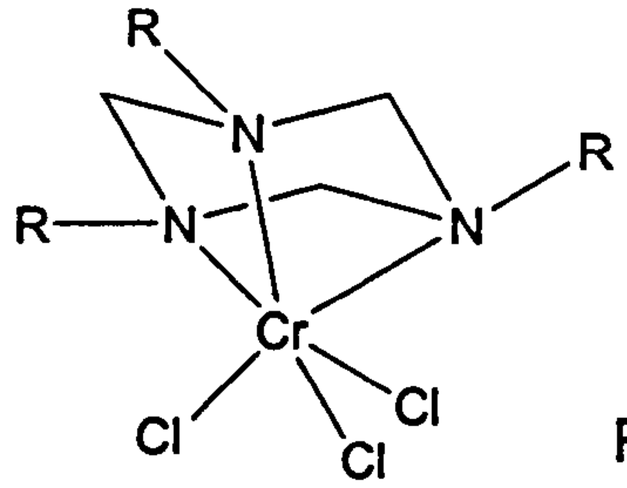

R = *n*-octyl

(4.12)

It has recently been reported that chromium complexes of ligands of the type $Ar_2PN(Me)PAr_2$ (Ar = *ortho*-methoxy-substituted aryl group) (**4.13**), on activation with MAO, are extremely active and selective catalysts for the trimerisation of ethylene, producing 1-hexene with a selectivity greater than 85%.[48]

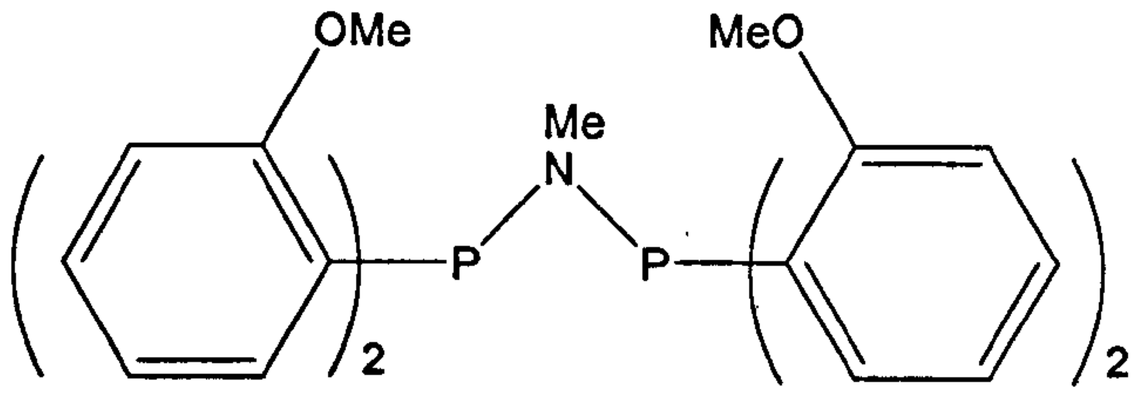

(4.13)

The *ortho*-methoxy substituent is thought to act as a pendant donor and so increase the coordinative saturation of the chromium centre. Mechanistic studies of the ethylene trimerisation reaction with chromium-diphosphine catalysts have been carried out by Bercaw *et al.*[50] Their results support a mechanism for the catalytic reaction involving a metallacycle intermediate, see Scheme 4.1.[121]

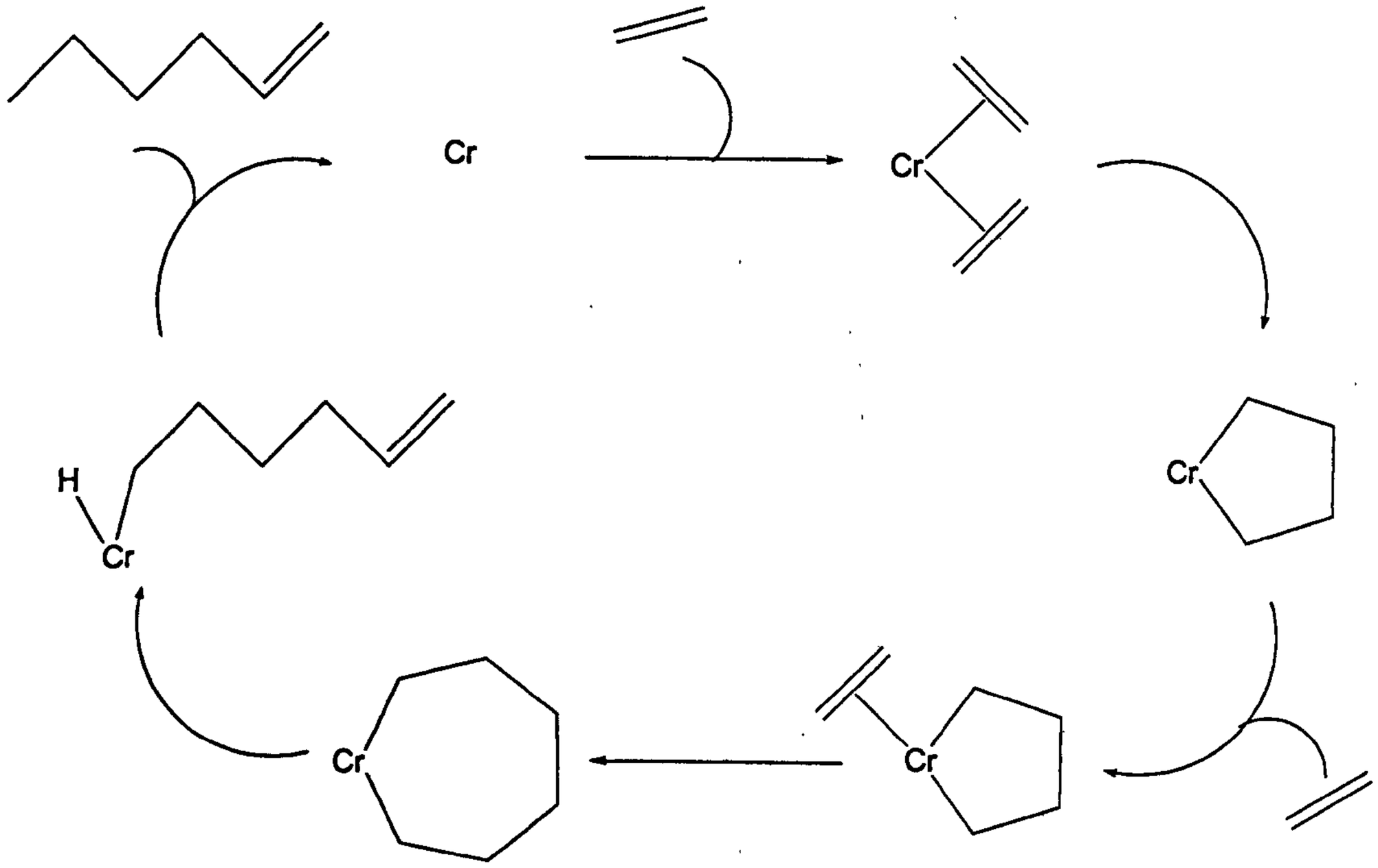

Scheme 4.1

4.2 Nickel catalysed ethylene oligomerisation

4.2.1 *GreenHouse* screening

All the ligands depicted in Figure 4.1 were tested for Ni-catalysed ethylene polymerisation using a *GreenHouse* parallel synthesis reactor. This allows large numbers of catalysts to be screened for activity in a single experiment. The reactor consists of 24 x 8 cm^3 sample vials which fit into a perspex walled container, through which ethylene can be added at atmospheric pressure. The *GreenHouse* reactor fits on to a stirrer hotplate allowing magnetic stirring and temperature control of the runs (see Experimental details). Upon completion of the catalytic runs the ethylene is replaced by nitrogen by pump-fill cycles, during this process solvent loss can occur. Therefore it is essential to have a blank sample vial containing only solvent in the reactor, as the activity of the catalyst is determined by the weight gain of the sample. In practice, a net weight loss due to solvent evaporation can be observed; the blank sample can be used to estimate the value of this. The increase in weight of the catalyst's solution is compared to known catalyst systems, in this case zirconocene (**THI**), (**Ni diimine**) and (***i*-PrPNP**) were used (see Figure 4.2). The results of the *GreenHouse* ethylene polymerisation run are shown in Figure 4.3 with details of the experimental procedure given in the Experimental section.

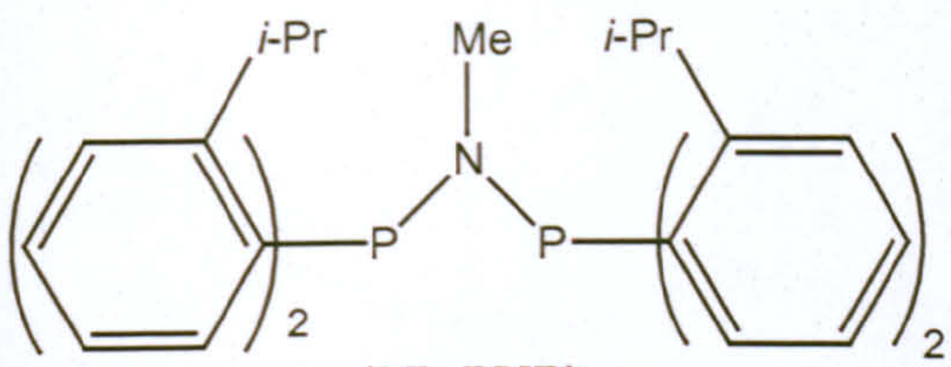

(*i*-PrPNP)

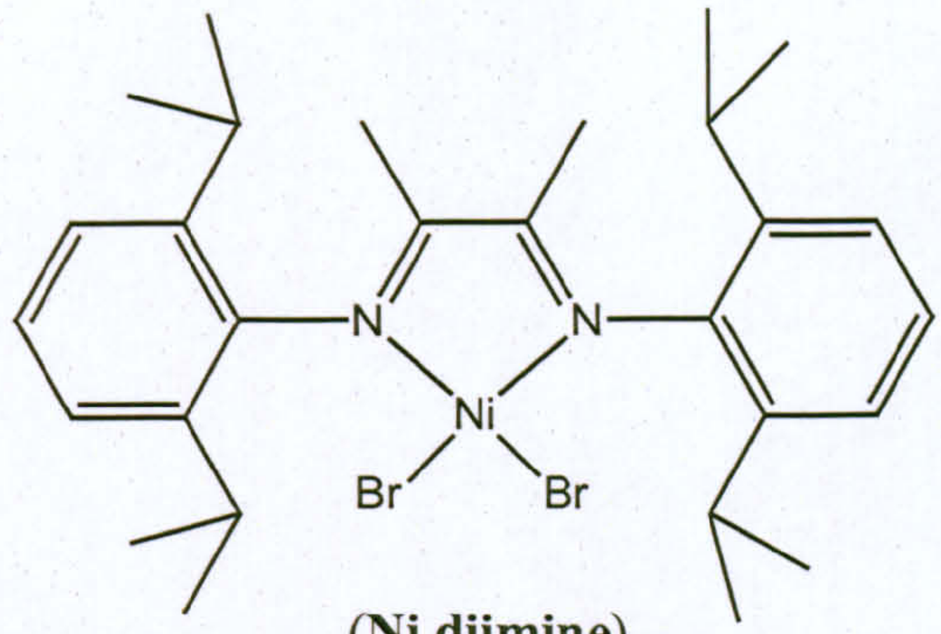

(Ni diimine)

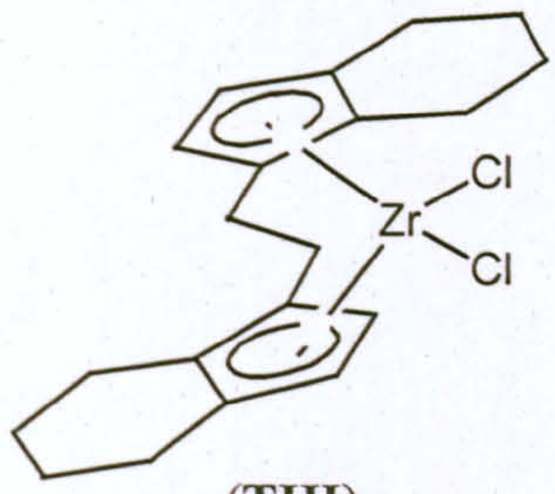

(THI)

Figure 4.2

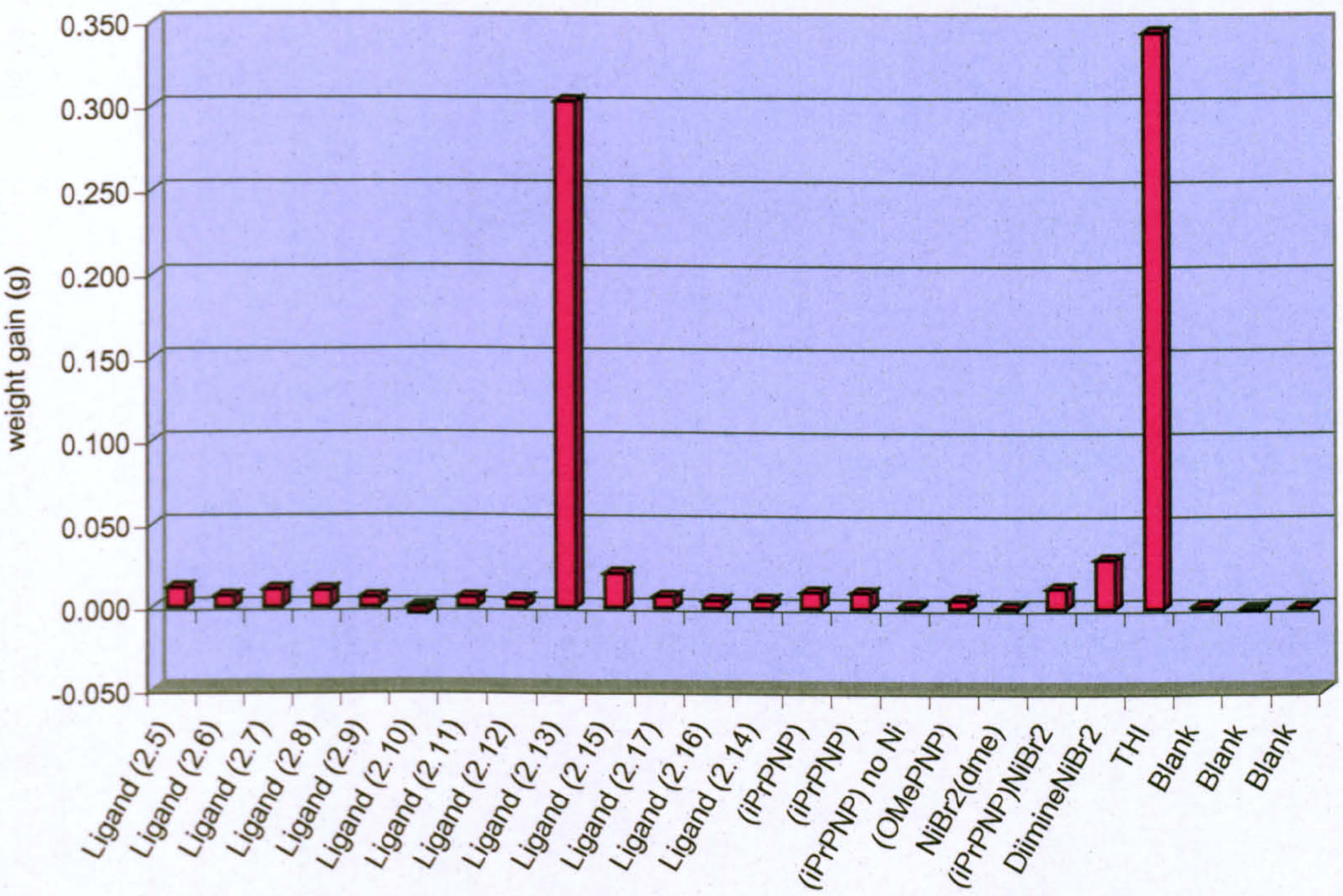

General conditions: 5 μmol catalyst, 200 eq MAO, 1 atmosphere C_2H_4, + 20 °C, 30 mins

Figure 4.3 Results of *GreenHouse* catalysis run

The catalyst screening using the *GreenHouse* reactor has shown two of the ligands synthesised in Chapter 2 to be active when complexed to nickel, indicated by the increase in mass. Colour changes were observed upon heating of the metal-ligand solutions suggesting complexation did occur prior to catalysis. The zirconocene (**THI**) a very active catalyst, shows a weight gain of 0.344 g and the results for (**2.13**) shows a similar increase in mass of 0.303 g. The nickel diimine (**Ni diimine**) compound has been reported by Brookhart *et al.*[99] to be a highly active catalyst for the polymerisation of ethylene. The Ni diimine shows a weight increase of 0.030 g in this screening run, a similar increase is shown by (**2.15**) of 0.021 g. As a result of the preliminary success of the ligands (**2.13**) and (**2.15**) in the *GreenHouse* Ni-catalysed ethylene polymerisation screen, more in depth studies were carried out using an *Endeavor* reactor.

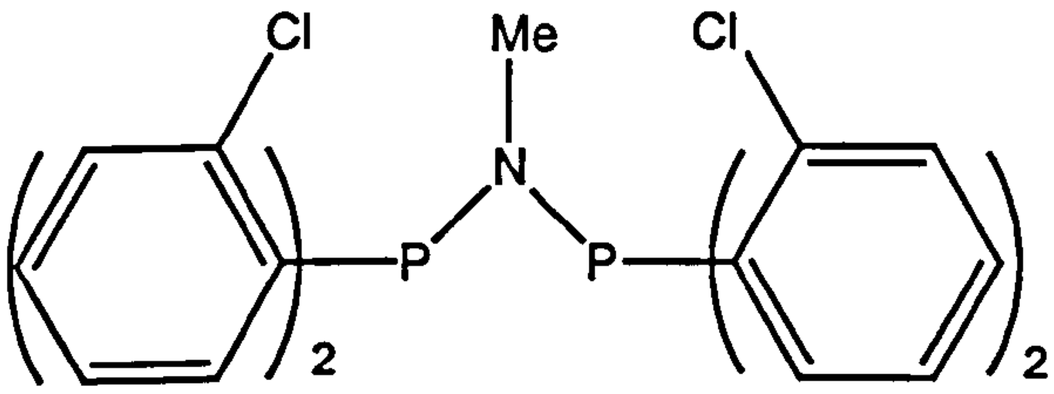

(2.13)

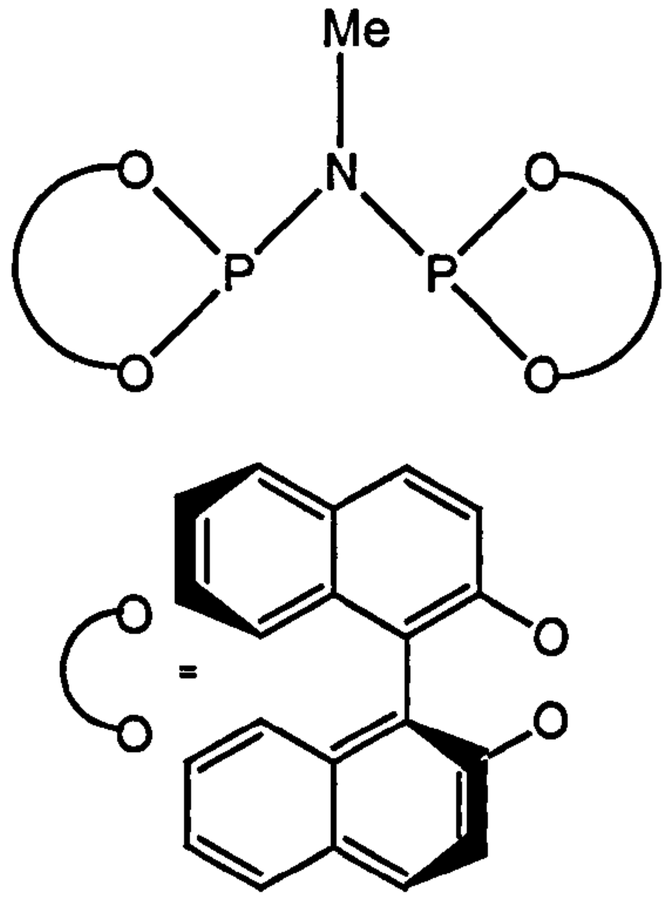

(2.15)

4.2.2 Detailed studies of Ni-catalysed ethylene oligomerisation with ligands (2.13) and (2.15)

The *Endeavor* reactor is a high pressure, parallel reactor containing 8 reaction chambers with a volume of 8 cm^3. They can be individually pressurised and temperature controlled, which allows a compound to be investigated at a range of pressures and temperatures in one run. The uptake of ethylene is calculated using the pressure difference between the ethylene inlet and the reaction chamber assuming ideal gas behaviour and plotted against time for the different runs. The catalyst solutions were prepared and stirred at 50 °C for 45 min prior to injection. Colour changes were observed indicating complexation had occurred; for details of the procedure, see the Experimental section.

Previous studies by Wass *et al.* [41, 101] on the activity of PNP ligands in Ni-catalysed ethylene polymerisation catalysis used temperatures of 50 °C. Thus the conditions used for catalytic runs were as shown in Table 4.1 with pressures of 5 and 10 bar and additional hydrogen (1 bar partial pressure), with the (***i*-PrPNP**) complex present as a standard. A graph of the uptake of ethylene in the 30 minute run is shown in Figure 4.4 and the results of the run from GC analysis are given in Table 4.1.

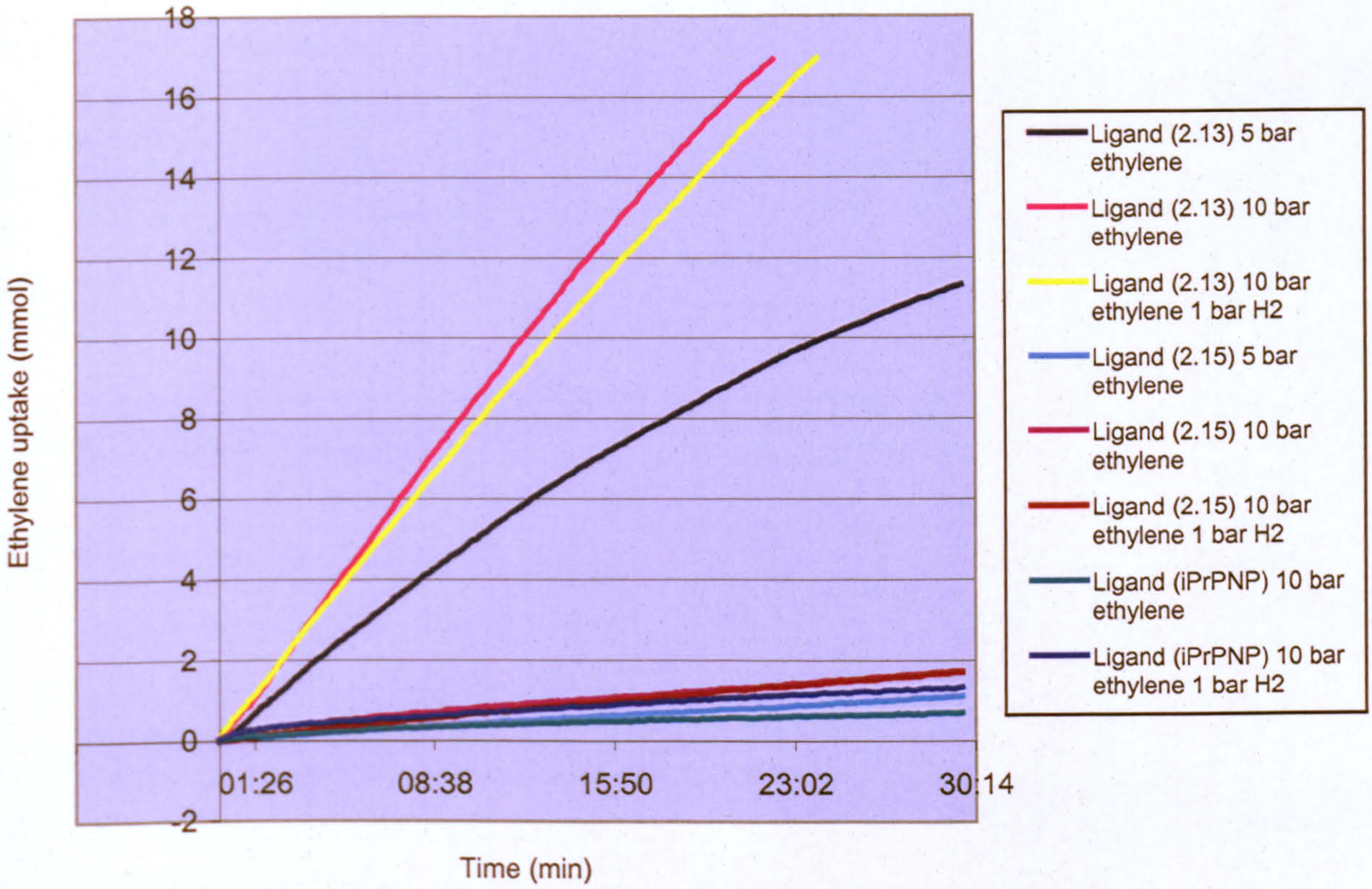

General conditions 200 eq MAO, 4 cm^3 toluene, 2 μmol catalyst solution, 30 min

Figure 4.4 Uptake of ethylene using the *Endeavor* reactor Ni-catalysed ethylene oligomerisation runs

Table 4.1 Results for Ni-catalysed ethylene oligomerisation runs on the *Endeavor* reactor

Ligand	Product and observations	Pressure C_2H_4 bar	Pressure H_2 bar	Activity g $mmol^{-1}$ h^{-1} bar^{-1}	k^a
(2.13)	C_4H_8 C_6H_{12} small quantity C_8H_{16}	5	0	58.9	0.04
(2.13)	C_4H_8 C_6H_{12} small quantity C_8H_{16}	10	0	57.9	0.05
(2.13)	C_4H_8 C_6H_{12} small quantity C_8H_{16}	10	1	54.3	0.04
(2.15)	C_4H_8 C_6H_{12} small quantity C_8H_{16}	5	0	5.4	0.12
(2.15)	C_4H_8 C_6H_{12} small quantity C_8H_{16}	10	0	4.1	0.11
(2.15)	C_4H_8 C_6H_{12} small quantity C_8H_{16}	10	1	4.5	0.10

[a] *k* value is derived from Schulz-Flory model see Section 4.3.1

General conditions 200 eq MAO, 4 cm^3 toluene, 2 μmol catalyst solution, 30 min

No solid was present in the solutions after the catalytic runs, indicating no production of high molecular weight polymer and GC analysis confirmed no high molecular weight oligomers were formed. For the catalysts derived from ligands **(2.13)** and **(2.15)**, the GC analysis of the solutions shows the presence of mainly butenes and hexenes as a result of ethylene dimerisation and trimerisation, respectively; small quantities of octene are also produced. The products formed are the same irrespective of ethylene pressure or presence of hydrogen. The relative quantities of butenes, hexenes and octene produced can be seen by Figure 4.5 (the values are set relative to **(2.13)** at 5 bar ethylene pressure equalling 1). The catalyst with ligand **(2.15)** yields significantly less than **(2.13)**; at 5 bar the relative values are 1.00 for **(2.13)** and 0.0974 for **(2.15)** for the production of butene. Increasing the pressure to 10 bar gives a 50% increase in productivity of butene to 1.46 for **(2.13)** and to 0.154 for **(2.15)**. Adding 1 bar hydrogen to the reactors has no effect when using **(2.13)** and quantities of oligomer produced are very similar see Figure 4.5. With **(2.15)** there is a 15% increase in the yields of butene.

It is interesting to note that ligand **(2.15)** makes more butenes relative to hexenes than **(2.13)**; at 5 bar ethylene pressure **(2.15)** gives almost 6 times as much butenes as hexenes and for **(2.13)** this value is less than 3. This is due to a greater rate of chain termination as indicated by the different *k* values (see Section 4.3.1) of 0.04 **(2.13)** and 0.12 **(2.15)** indicating different kinetics (see Table 4.1). There are 10 peaks for hexene in the GC, probably due to branched and linear C_6 isomers (see Figure 4.6).

The formation of internal, external, linear and branched olefins from ethylene is consistent with a chain-walking mechanism with nickel catalysts as described by Brookhart *et al.*[43, 122] The chain-walking mechanism occurs prior to insertion of ethylene, where the metal alkyl species undergoes a series of β-hydride eliminations and re-additions which result in the metal migrating (walking) along the polymer chain, see Scheme 4.2.[43] If the chain transfer rate is fast relative to chain propagation then linear as well as branched oligomers are produced, which is likely to account for the observed product distribution obtained with **(2.13)** and **(2.15)**.

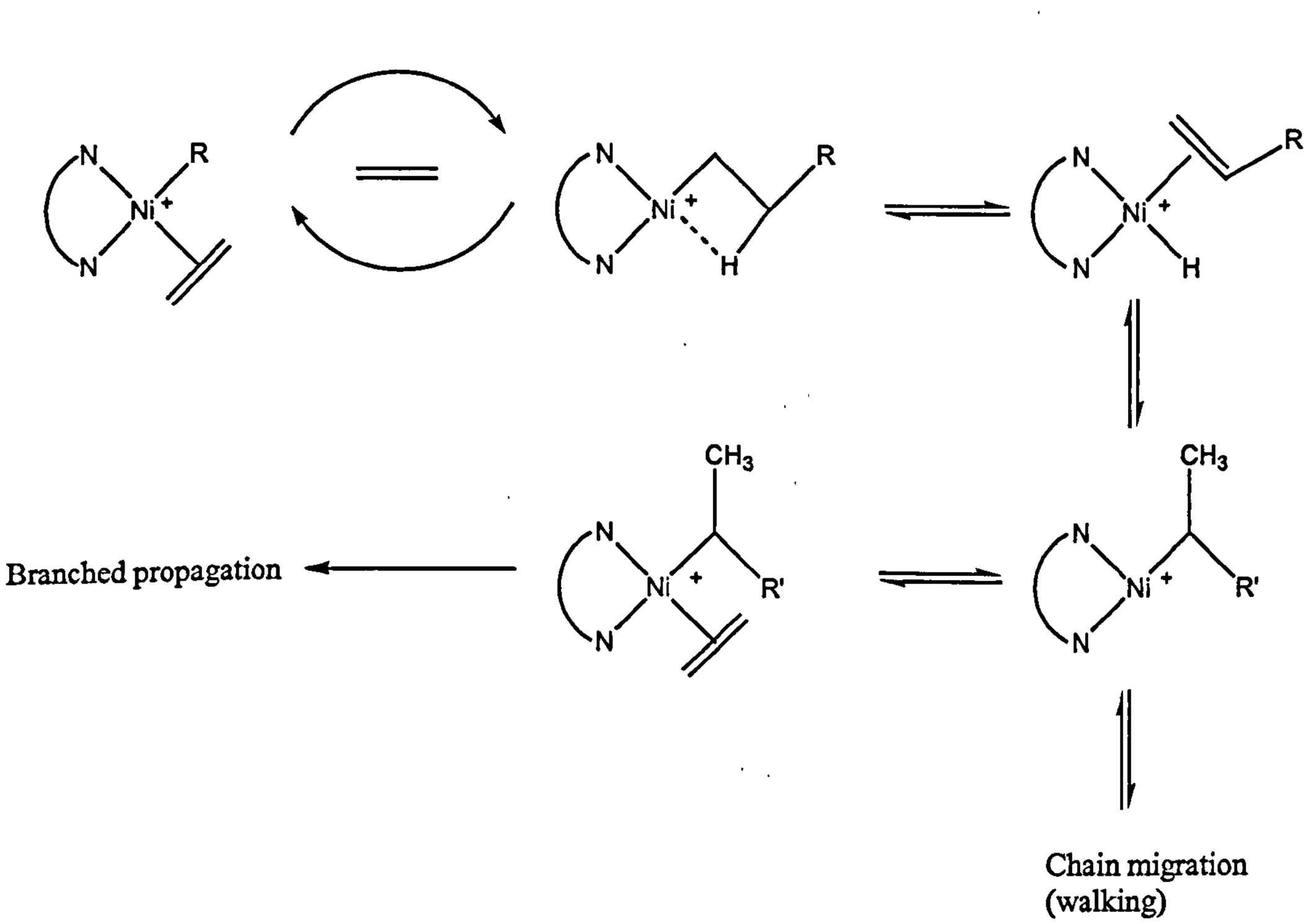

Scheme 4.2 Mechanism for ethylene polymerisation and polymer branch formation with Ni diimine complexes

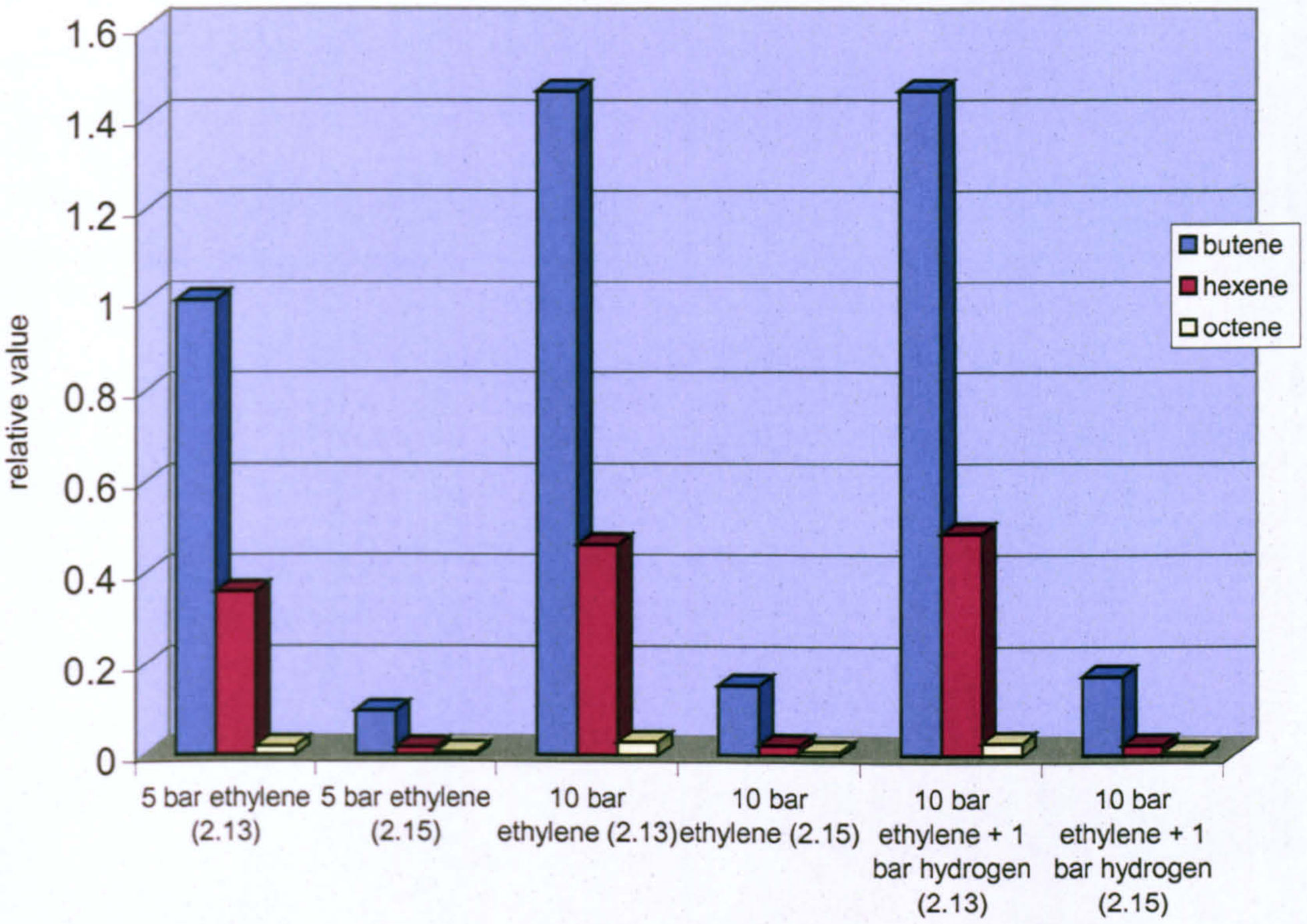

Figure 4.5 Graph showing relative values of oligomers produced at different pressures for (**2.13**) and (**2.15**) (relative to (**2.13**) at 5 bar ethylene pressure)

The activity of the catalyst with the *ortho*-chloro PNP ligand (**2.13**) is greater than 50 g $mmol^{-1}$ h^{-1} bar^{-1}, with activities of 58.9 g $mmol^{-1}$ h^{-1} bar^{-1} at 5 bar ethylene and 57.9 g $mmol^{-1}$ h^{-1} bar^{-1} at 10 bar ethylene. The similarities of these two values at different pressures indicates a first order dependence on ethylene. The presence of hydrogen has a negligible effect giving 54.3 g $mmol^{-1}$ h^{-1} bar^{-1}. In comparison the activity of the nickel complex with the diphosphoramidite ligand (**2.15**) has a much lower activity of 5.4 g $mmol^{-1}$ h^{-1} bar^{-1} at 5 bar and 4.5 g $mmol^{-1}$ h^{-1} bar^{-1} at 10 bar ethylene and the presence of hydrogen has a negligible effect at 4.5 g $mmol^{-1}$ h^{-1} bar^{-1} (see Table 4.1).

From the pressure dependence of the standard (***i*-PrPNP**) catalyst reported by Wass and co-workers, zero order dependence on ethylene was determined.[41] However, the catalyst with ligand (**2.13**) has a first order dependence on ethylene pressure, increasing the ethylene pressure from 5 to 10 bar doubles the ethylene uptake as well as the final productivity (295 and 427 g $mmol^{-1}$ h^{-1} at 5 and 10 bar respectively). This is interesting as it implies a change in the rate-determining step of the mechanism for the catalytic

cycle. With the nickel complexes of (***i*-PrPNP**) or (**2.15**), free ethylene is not involved in the rate-determining step. The ethylene binds to the metal, but the insertion step has a high energy barrier to overcome. With the complex of (**2.13**) where the dependence is first order in ethylene, the rate-determining step is the binding of the ethylene, with the insertion step occurring rapidly.

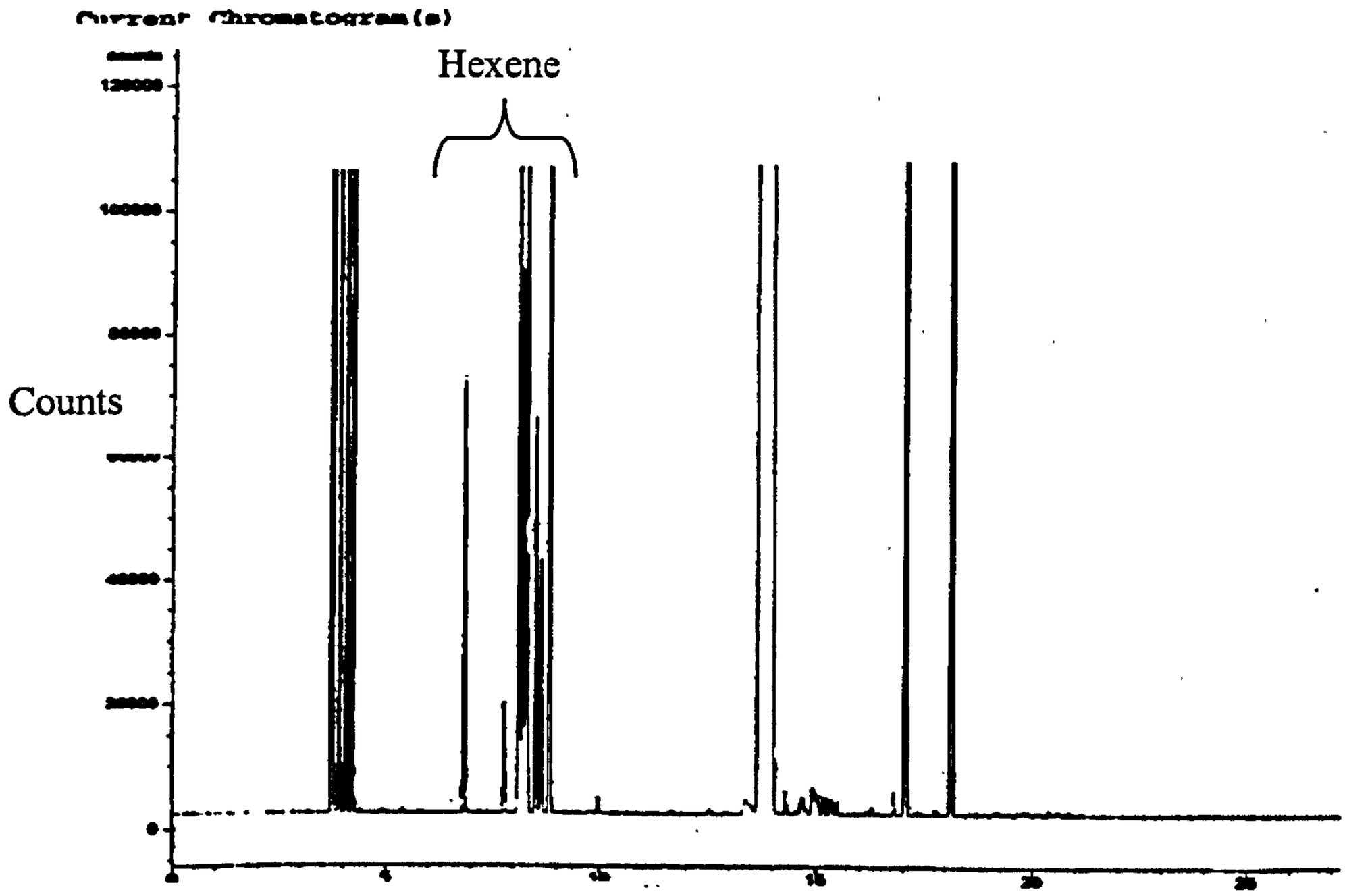

Figure 4.6 GC graph for catalytic run with (**2.13**)

4.2.3 Conclusion

Nickel complexes with the ligands (**2.13**) and (**2.15**) have been shown to be active oligomerisation catalysts, with (**2.13**) (the *ortho*-chloro PNP ligand) having the greatest activity of up to 58 g $mmol^{-1}$ h^{-1} bar^{-1}. Both systems give butenes and hexenes as major products. This has previously been shown to be common for nickel complexes of diimine ligands which do not contain sterically demanding *ortho*-substituents (**4.6**).[115]

The rate of chain transfer was shown to be greatly retarded by bulky diimine ligands. Chain transfer is proposed to occur by associative ethylene displacement (Equation 4.4) and is hindered by the axial bulk provided by the *ortho*-substituents on the aryl rings. The aryl rings on the diimine lie roughly perpendicular to the square plane, and bulky *ortho*-substituents block axial approach of ethylene.[43] This feature results in rates of chain propagation which are much greater than chain transfer rates and thus permits formation of higher molecular weight polymers.

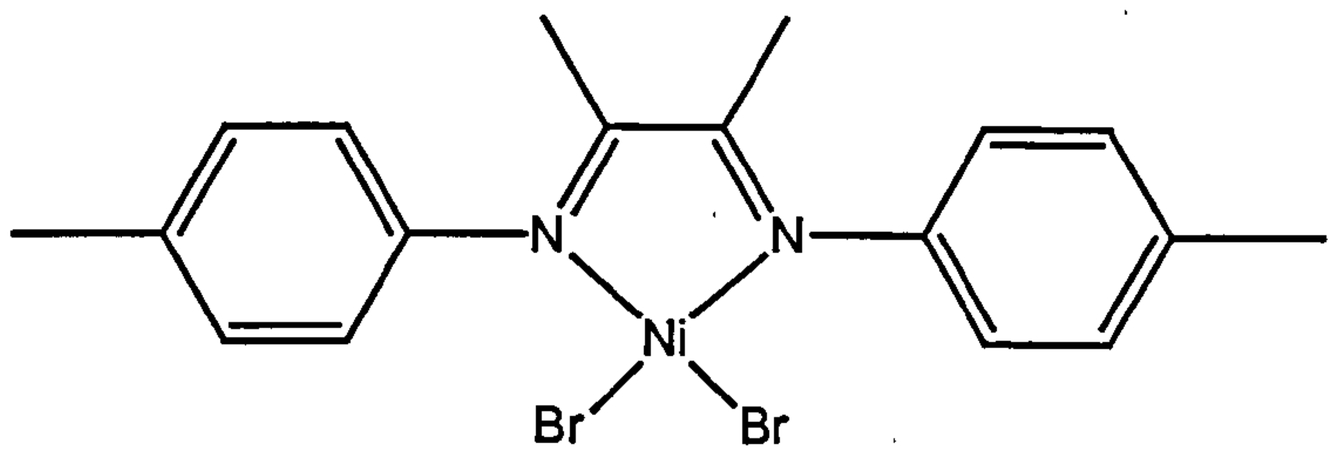

(4.6)

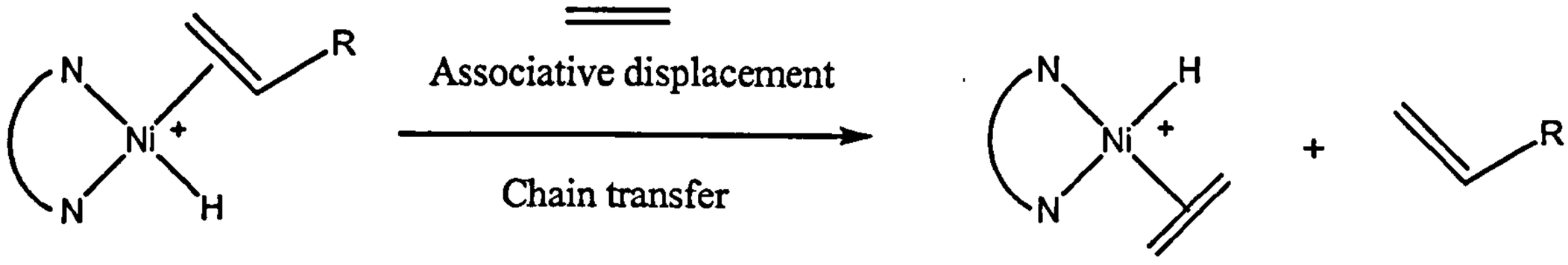

Equation 4.4 Chain transfer by associative ethylene displacement

Therefore this leads us to conclude that increasing the bulk of the ligands could help to switch the catalyst from oligomerisation to polymerisation. Consequently the most active ligand **(2.13)** could be modified to have a greater steric bulk but keeping the activity provided by the *ortho*-chloro substituent. Therefore ligand **(4.14)** would be of great interest to investigate.

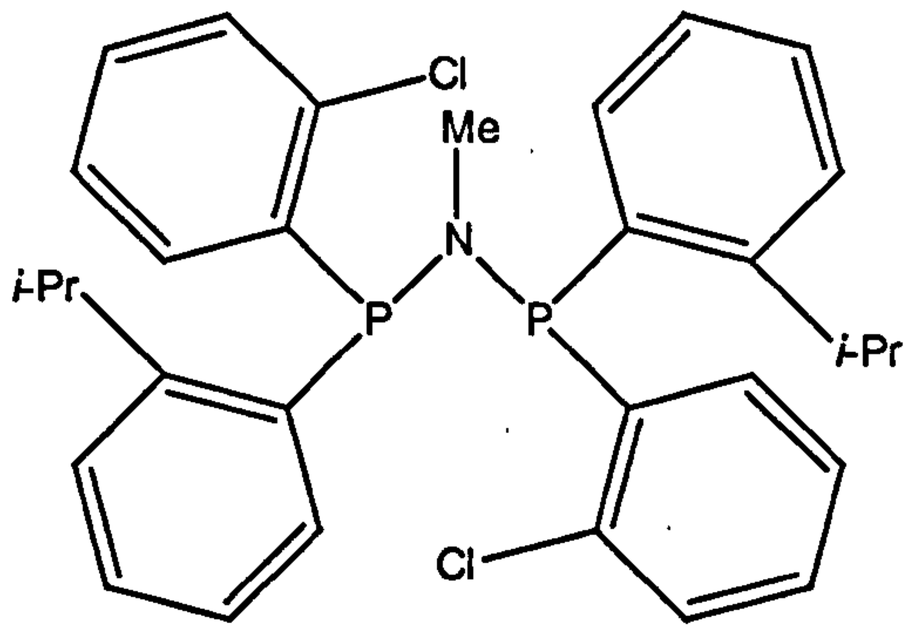

(4.14)

4.3 Cr-catalysed ethylene oligomerisation

The ligands **(2.9)**, **(2.10)**, **(2.11)**, **(2.12)**, **(2.14)** and **(2.15)** shown in Figure 4.1 were investigated in Cr-catalysed ethylene trimerisation using an *Endeavor* reactor as described in Section 4.2.2, see the Experimental Section for details. The ligand **(OMePNP)** described by Wass *et al.* to be highly active for ethylene trimerisation catalysis when complexed to chromium[48] was included as a standard. Previous catalytic studies were carried out at 80 °C. Based on this, the temperature for all the runs was kept at 80 °C and the pressure at 12 bar; additional hydrogen (1 bar partial pressure) was also added. Enhancement of productivity has been previously reported for ethylene trimerisation catalysis on addition of hydrogen although no explanation has been offered for this effect.[49] An increase in productivity was observed for the **(OMePNP)** Cr system, but little effect on selectivity.[48]

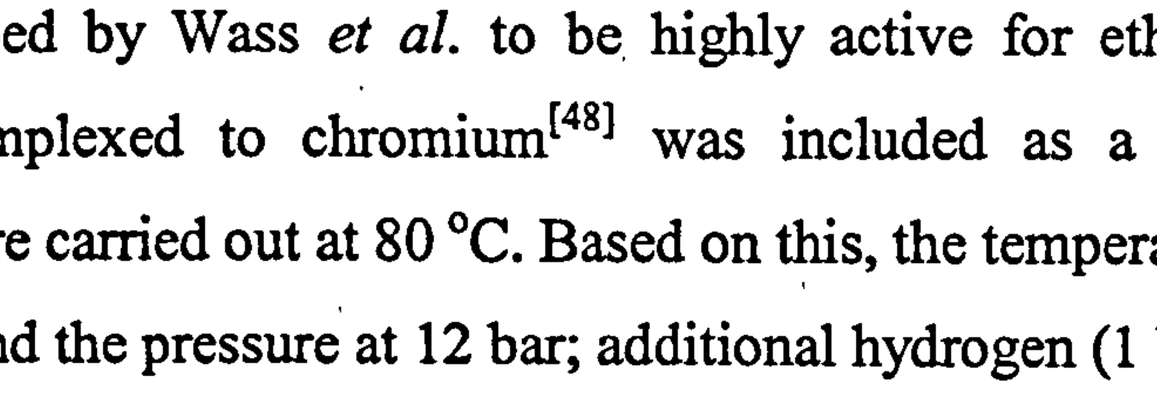

(OMePNP)

4.3.1 Schulz-Flory distribution of alkenes

It has been observed[103 – 106, 123, 124] that for ethylene oligomerisation catalysis shown in Scheme 4.3, the distribution of products can be described by the constant k in Equation 4.5. The derivation of the constant k is beyond the scope of this thesis and is given by the Schulz-Flory expression, Equation 4.6. The k value represents the probability of chain propagation and is experimentally determined by the mole ratio of two oligomer fractions.

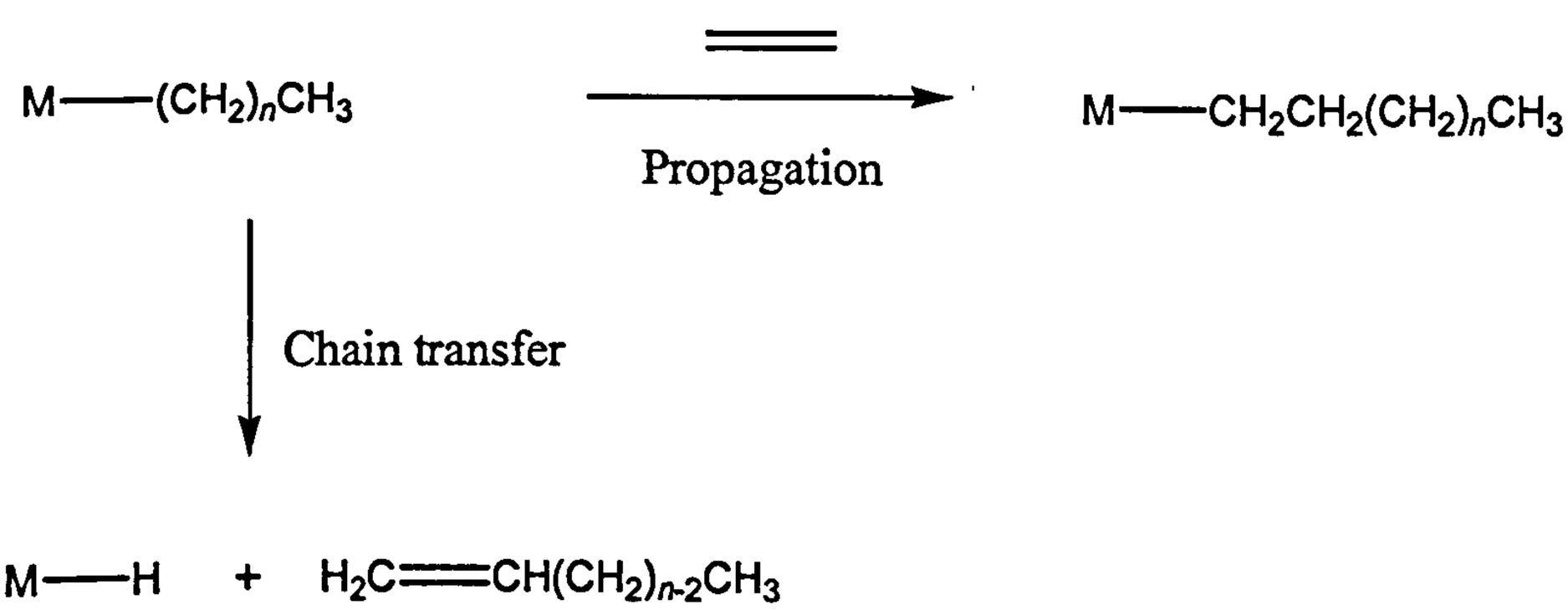

Scheme 4.3

$$k = \frac{\text{rate of propagation}}{\text{rate of propagation + rate of chain transfer}} = \frac{\text{Moles of } C_{n+2}}{\text{Moles } C_n}$$

Equation 4.5

The experimentally obtained oligomer distributions were analysed using a Solver add-in for Microsoft Excel,[125] which enabled a least-square fit of the experimentally obtained molar distributions to the following formula:

Schulz-Flory expression: $$C_p = c \cdot (1-k) \cdot k^{(p-1)}$$

Equation 4.6

Where k is the probability of chain propagation, c is the total amount of product (mol) and C_p is the amount of oligomer (mol) having p monomer units inserted into the metal-carbon bond of the metal alkyl. The parameters varied in the optimisation procedure are k and c.

When the k value is close to 1, a flat molecular weight distribution with large quantities of high molecular weight oligomers are produced, reflecting a low rate of chain transfer and thus the chains are allowed to grow prior to termination. If the k value is closer to 0 a narrow distribution of low molecular weight oligomers is produced, indicating the rate of chain transfer to be fast relative to propagation.

4.3.2 Comparison of Cr-catalysed ethylene oligomerisation with PNP ligands (2.9), (2.10), (2.11), (2.14) and (OMePNP)

The ligand (**2.14**) (Figure 4.1) was synthesised in order to probe structurally the highly active ethylene trimerisation catalyst that uses (**OMePNP**) ligand. Ligand (**2.14**) has only two *ortho*-methoxy groups present. The *ortho*-methoxy groups may act as pendant donors during the catalytic cycle, thereby increasing the activity of the catalyst by stabilising the metallacyclic intermediate[50] and we postulated that four methoxy groups may not be necessary. The ligands (**2.9**), (**2.10**) and (**2.11**) (Figure 4.1) were prepared to investigate whether having methoxy groups on the nitrogen backbone may also enhance catalysis. The results for the 30 min catalytic runs are shown in Figure 4.6 and Table 4.2.

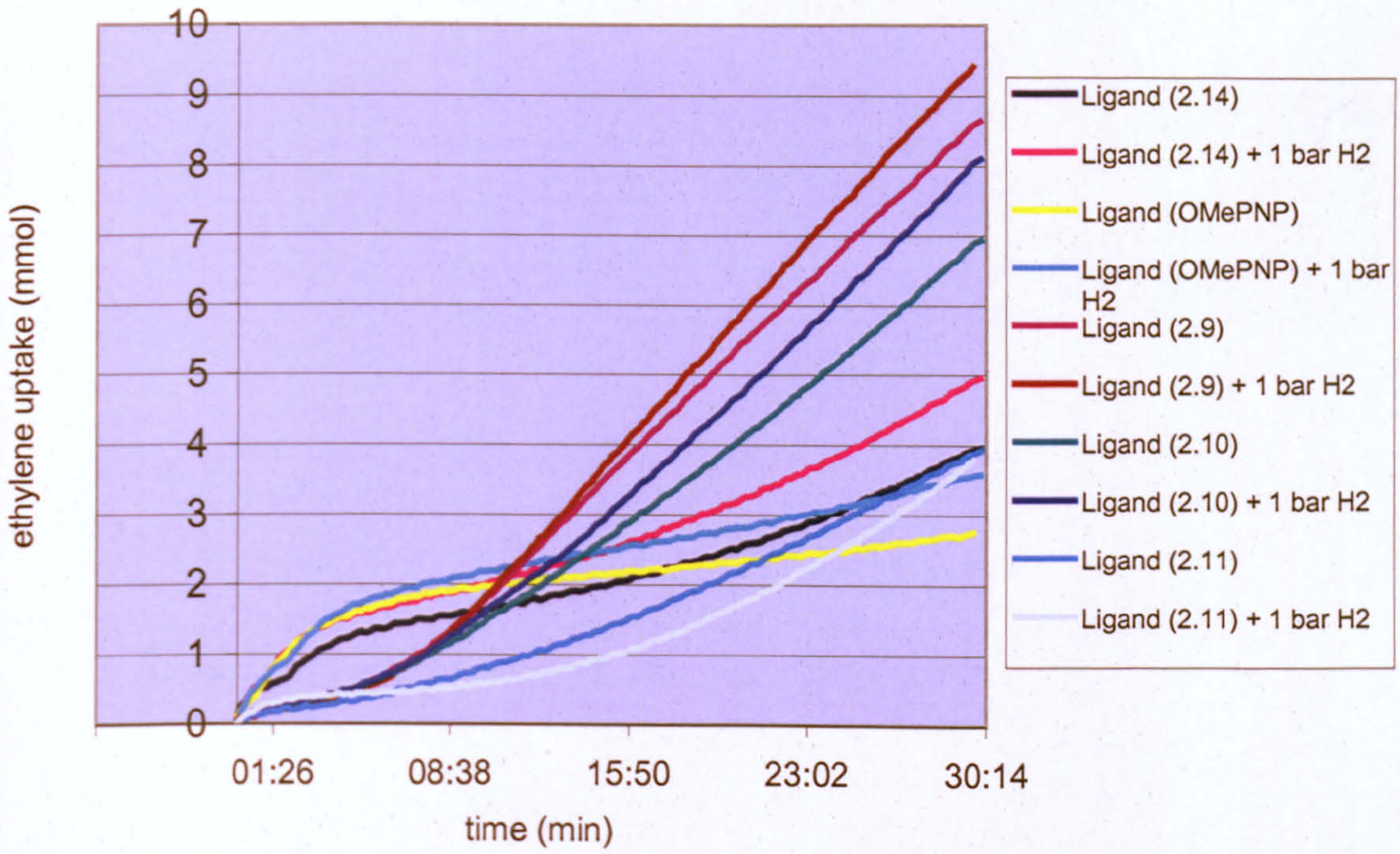

General conditions 300 eq MAO, 4 cm^3 toluene, 2 μmol catalyst solution, 30 min, 80 °C, 12 bar ethylene pressure

Figure 4.6 Uptake of ethylene for *Endeavor* Cr-catalysed oligomerisation runs

The graphs of the ethylene uptake for the two different sets of ligands show different profiles. It is unclear as to whether this is a true effect of the catalyst or due to the method of measuring the ethylene by pressure difference (see Figure 4.6). There seems to be two different behaviours, one with a fast induction period, (**2.14**) and (**OMePNP**), and one with a slower induction, (**2.9**), (**2.10**) and (**2.11**) which may be due to two different mechanisms operating.

Table 4.2 Ethylene oligomerisation results

Ligand	H_2 (bar)	Yield (g/kg)	Productivity (g $mmol^{-1}$ h^{-1})	Selectivity (wt%)[a]	Product analysis (wt%)			
					C_4	C_6	C_8	C_{10}
(2.14)	0	40.3	215	98.6	0.09	35.1	5.7	22.1
(2.14)	1	69.6	384	99.3	0.5	66.0	4.7	13.2
(OMePNP)	0	43.3	233	99.6	0.2	88.5	3.1	4.1
(OMePNP)	1	63.1	346	99.8	0.1	88.3	2.2	6.3
(2.9)	0	65.2	487	79.2	1.5	1.5	12.4	13.4
(2.9)	1	73.5	531	19.0	0.9	23.9	11.3	12.5
(2.10)	0	86.6	358	67.4	1.0	11.9	11.4	12.2
(2.10)	1	93.7	407	84.5	0.9	9.3	12.6	13.3
(2.11)	0	36.4	194	92.6	0.8	9.4	13.3	11.7
(2.11)	1	17.0	89	85.5	1.2	12.4	31.0	11.8

[a] Selectivity to 1-hexene within C_6 fraction.

General conditions 300 eq MAO, 4 cm^3 toluene, 2 μmol catalyst solution, 30 min, 80 °C, 12 bar ethylene pressure

The catalytic run using ligand **(2.14)** gave a product distribution similar to **(OMePNP)**, yielding mainly 1-hexene. The yield of C_6 products for **(2.14)** was lower at 66.0% compared to 88.3% for the standard **(OMePNP)** (12 bar ethylene 1 bar hydrogen pressure), but the selectivity to 1-hexene within this C_6 fraction was over 99% for both. However the total activity with **(2.14)** was greater, 384 g $mmol^{-1}$ h^{-1} compared to 346 g $mmol^{-1}$ h^{-1} at 12 bar ethylene pressure and 1 bar hydrogen. The presence of hydrogen had little effect on selectivity for the **(OMePNP)** catalyst,[48] but an increase from 35.1% to 66.0% in C_6 production was observed for **(2.14)** with the selectivity to 1-hexene within this fraction maintained above 98%. Without hydrogen, **(2.14)** appears to have an underlying Schulz-Flory distribution of oligomers, which is removed on addition of hydrogen, thereby increasing the C_6 selectivity. Figure 4.7 shows the distributions from the GC analysis for **(2.14)**. The increase in the C_6 fraction on addition of the hydrogen can be clearly seen as can the underlying Schulz-Flory distribution in

the absence of hydrogen. Increases in the activity were seen for both (**2.14**) and (**OMePNP**) on addition of 1 bar hydrogen pressure see Table 4.2, Figure 4.10.

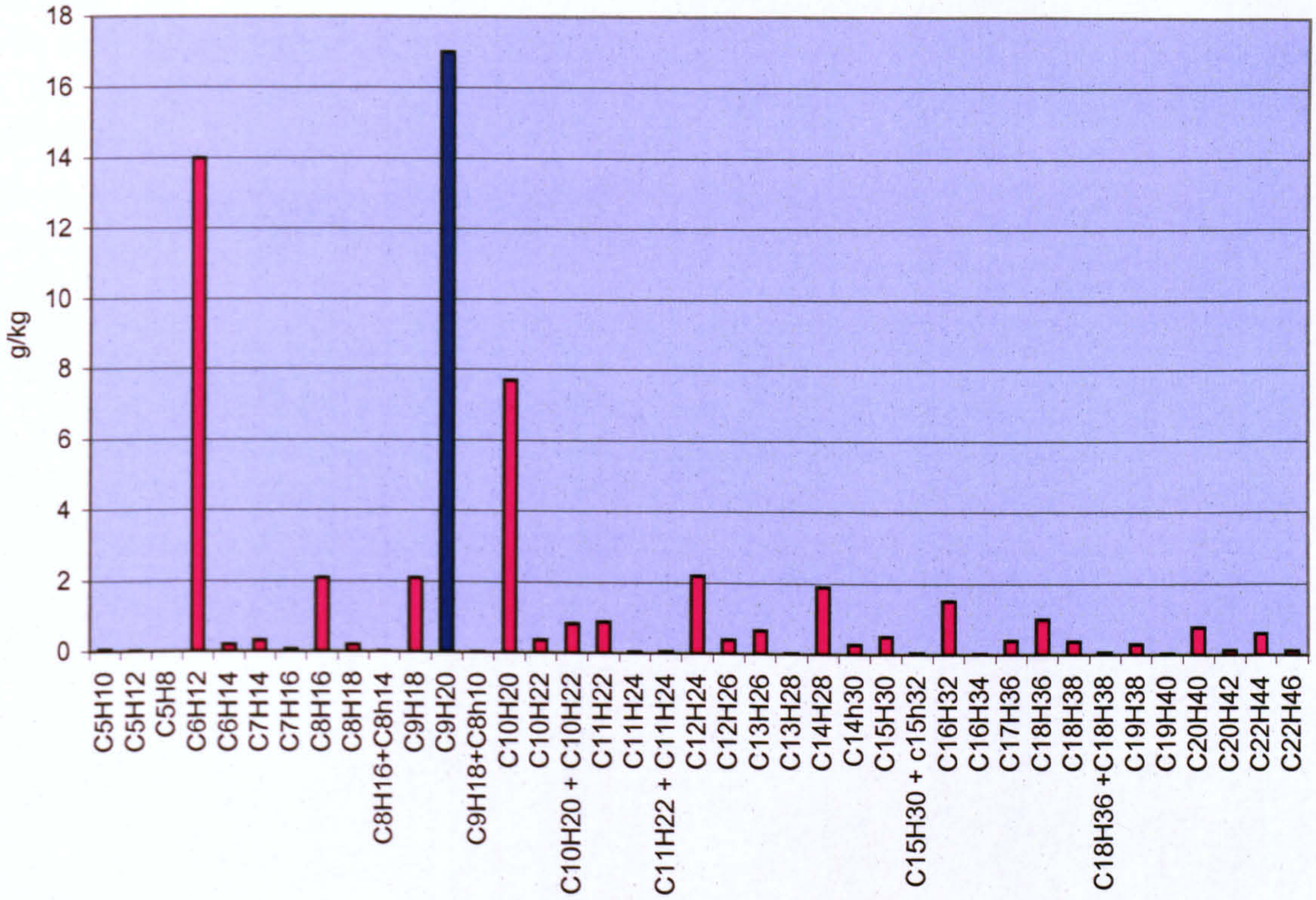

Addition of 1 bar hydrogen

Figure 4.7 Distributions from the GC analysis for (**2.14**) (C_9H_{20} present as reference for GC)

The catalytic runs using ligands (**2.9**), (**2.10**) and (**2.11**) with the methoxy groups on the nitrogen all show a Schulz-Flory distribution of oligomers (see Figure 4.8).

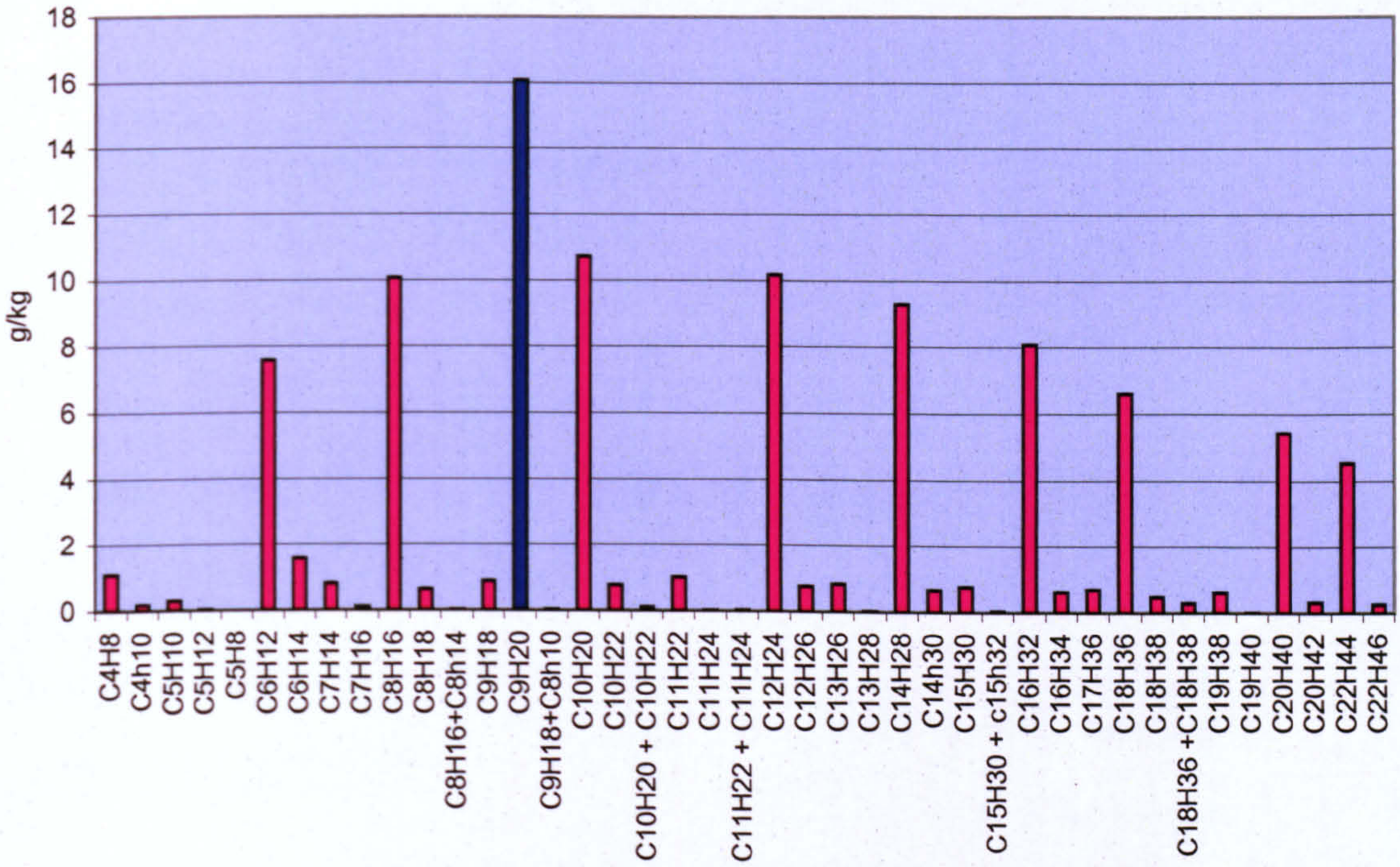

Figure 4.8 Distributions from the GC analysis for (**2.9**) (no H_2 present) (C_9H_{20} present as reference for GC)

The *k* values characteristic for the distribution of oligomers obtained when using the ligands (**2.9**), (**2.10**) and (**2.11**) with and without the presence of hydrogen are given in Table 4.3. A plot of the fit for the Schulz-Flory distribution for (**2.9**) is shown in Figure 4.9, the *R* value (goodness of fit) is 0.964 and the *k* value 0.77, indicating the weight fraction is at a maximum for C_{10}. The higher the *k* value, the greater the weight maximum due to a greater rate of propagation relative to chain transfer (see Section 4.3.1). The values for C_4 and C_6 oligomers are not included in the fitting due to their volatility and therefore loss during work up.

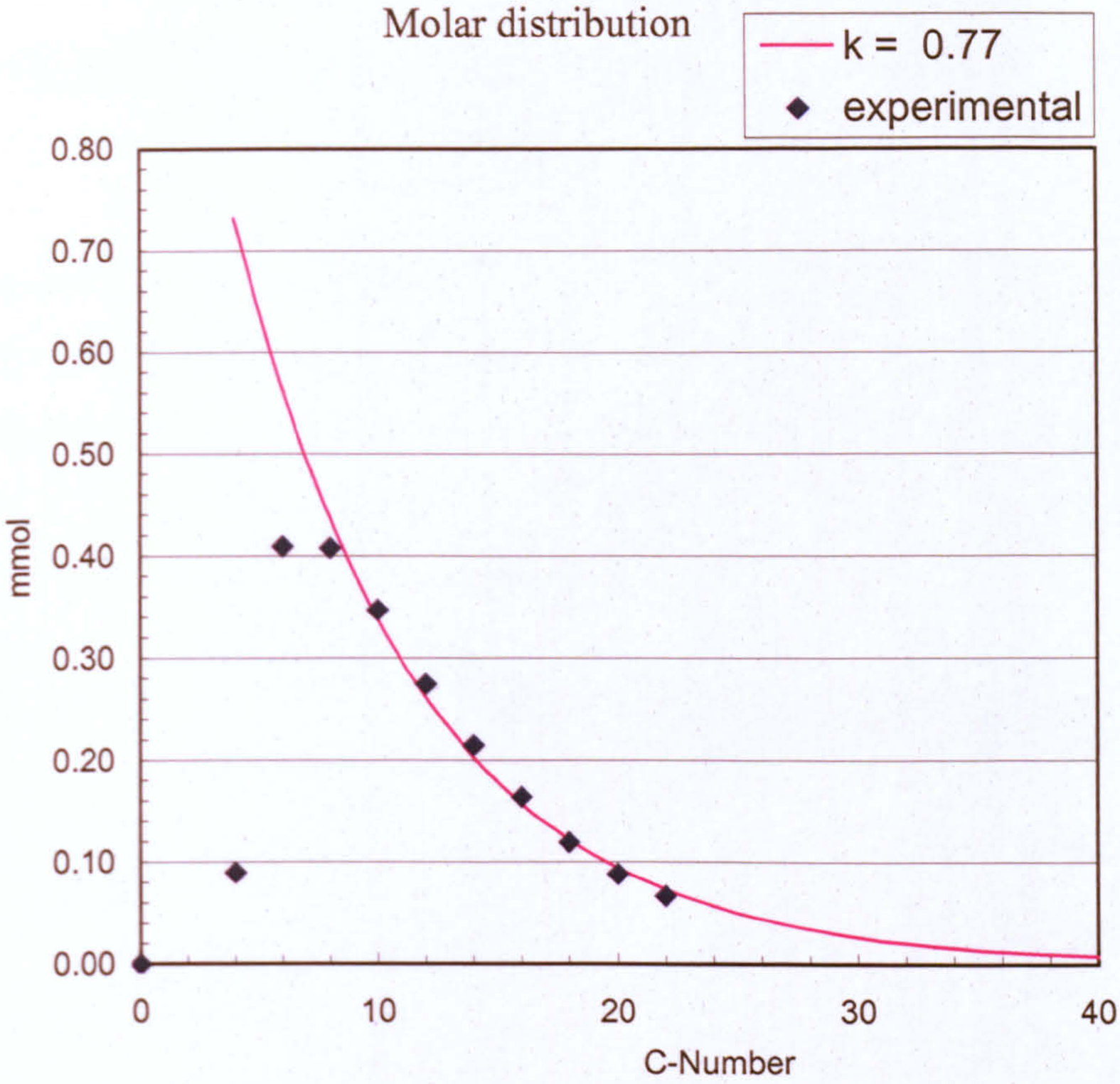

Figure 4.9 Fit for the Schulz-Flory distribution for (**2.9**)

Table 4.3 *k* values for ethylene oligomerisation runs with ligands (**2.9**), (**2.10**) and (**2.11**) with and without the presence of hydrogen

Ligand	H_2 (bar)	*k*
(2.9)	0	0.77
(2.9)	1	0.78
(2.10)	0	0.80
(2.10)	1	0.78
(2.11)	0	0.77
(2.11)	1	0.68

Between the ligands **(2.9)**, **(2.10)** and **(2.11)** there is very little difference in the *k* values at 12 bar ethylene pressure, indicating similar rates of propagation and termination leading to a similar distribution of oligomers.

The activities are in some cases higher than for the standard (**OMePNP**) catalyst. With **(2.9)** the activity is 531 g $mmol^{-1}$ h^{-1} at 12 bar ethylene and 1 bar hydrogen pressure. Changing the number of carbon atoms on the nitrogen **(2.10)** decreases the activity to 407 g $mmol^{-1}$ h^{-1}. The phenyl analogue **(2.11)** gives an activity of 89 g $mmol^{-1}$ h^{-1} at 12 bar ethylene, 1 bar hydrogen pressure, see Figure 4.10.

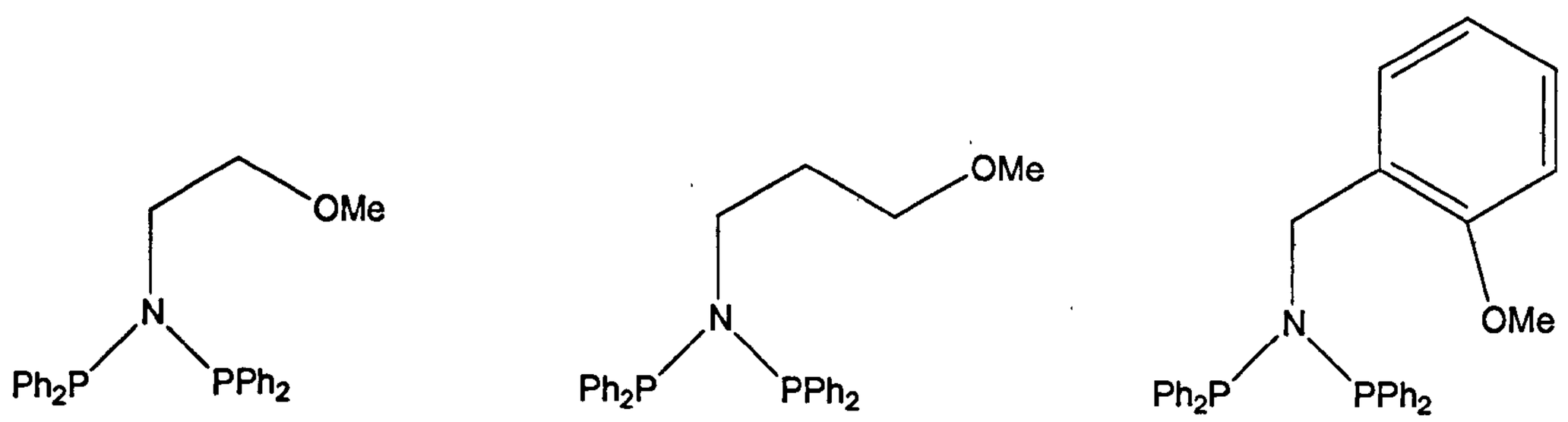

(2.9) **(2.10)** **(2.11)**

The presence of hydrogen in the catalytic runs for this series of ligands **(2.9)**, **(2.10)** and **(2.11)** has no effect on the selectivity. For **(2.11)** the hydrogen seems to decrease the activity; for **(2.9)** and **(2.10)** a small increase in activity is observed on addition of hydrogen, see Table 4.2.

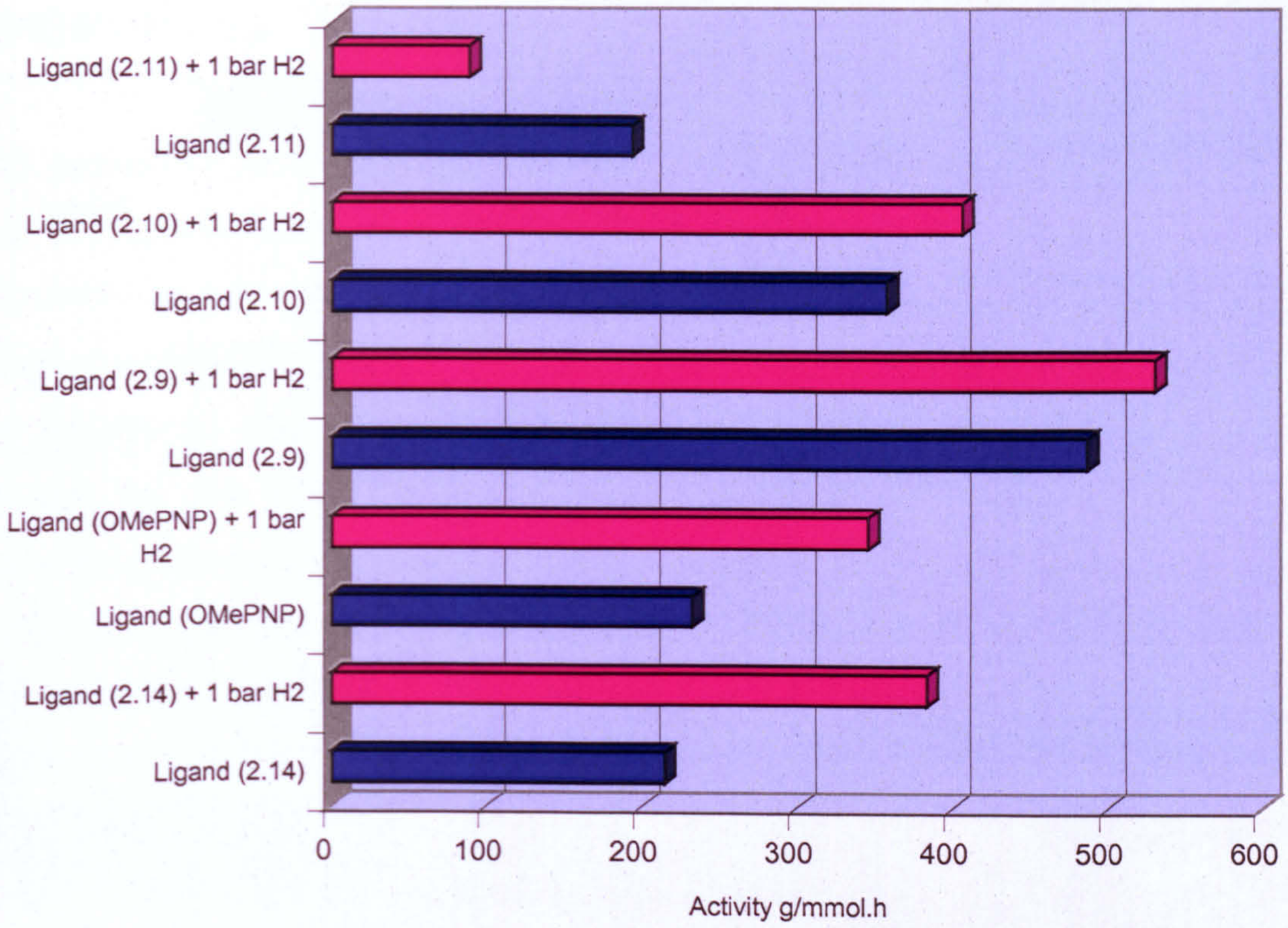

General conditions 300 eq MAO, 4 ml toluene, 2 μmol catalyst solution, 30 min, 80 °C, 12 bar ethylene pressure

Figure 4.10 Activities of the Cr catalysts with ligands (**2.14**), (**OMePNP**), (**2.9**), (**2.10**) and (**2.11**) with and without addition of hydrogen

4.3.2.1 Summary of results with PNP ligands (2.9), (2.10), (2.11), (2.14) and (OMePNP)

These results lead us to conclude that our initial postulate that four ortho-methoxy groups may not be necessary was partially correct. The activity for the catalyst with (**2.14**) with only two *ortho*-methoxy groups was higher than that for (**OMePNP**) although a decreased selectivity to 1-hexene was observed. The decrease in bulk of

(2.14) may increase the activity allowing easier access of ethylene to the metal centre, but the four *ortho*-methoxy groups in **(OMePNP)** seem to be necessary in order to keep the high selectivity.

The presence of the methoxy groups on the nitrogen substituent in ligands **(2.9)**, **(2.10)** and **(2.11)** was shown to give a Schulz-Flory distribution of oligomers instead of selectivity to 1-hexene but greater activities were observed. The lack of 1-hexene selectivity with **(2.9)**, **(2.10)** and **(2.11)** and the similarity of their *k* values suggests that the ligands are similar in their catalytic performance and the donor group on the nitrogen has little effect. This would be expected if the donor group is not involved in coordination to the metal centre, consistent with the dichloropalladium crystal structures in Chapter 3 that showed no M-O interaction. Their high activity may be due to the ease of access of the ethylene to the metal centre, which would then explain why the bulkiest ligand **(2.11)** has the lowest productivity.

A new ligand designed to combine these two properties **(4.15)**, has a non bulky group on the nitrogen and *ortho*-methoxy groups present. A study into the selectivity and activity of a catalyst using **(4.16)** (an analogue of **(2.14)** but with three methoxy groups) would also be of interest.

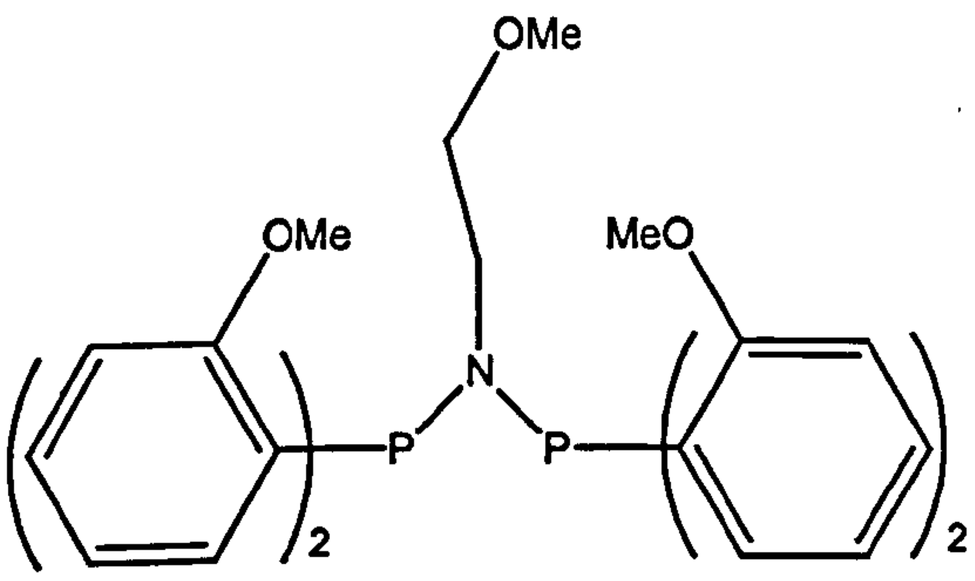

(4.15)

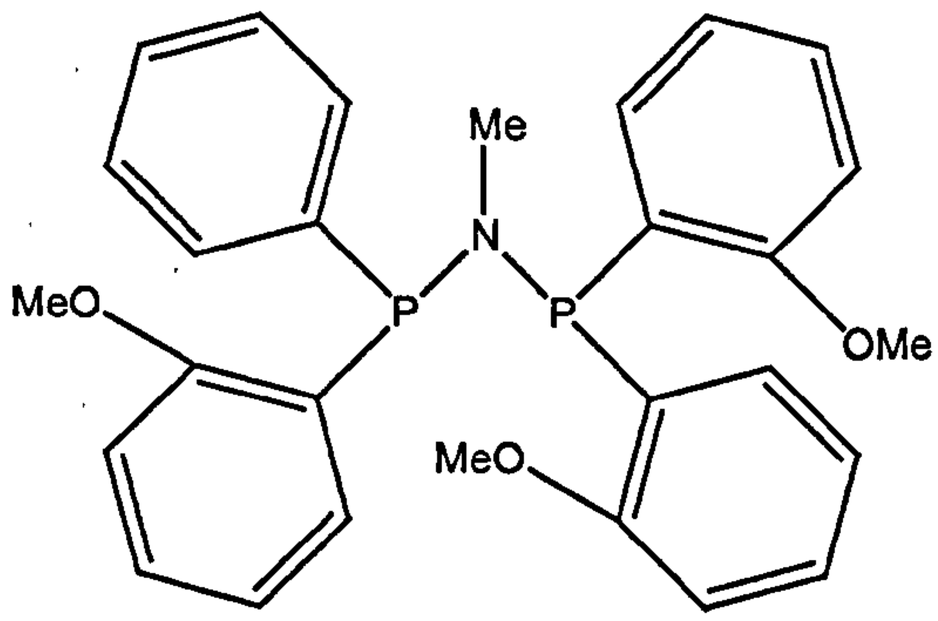

(4.16)

4.3.3 Comparison of Cr-catalysed ethylene oligomerisation with PNP ligands (2.12) and (2.15)

The two ligands (**2.12**) and (**2.15**) have no methoxy groups present (see Figure 4.1). The results for the 30 min catalytic runs are given in Figure 4.11 and Table 4.4.

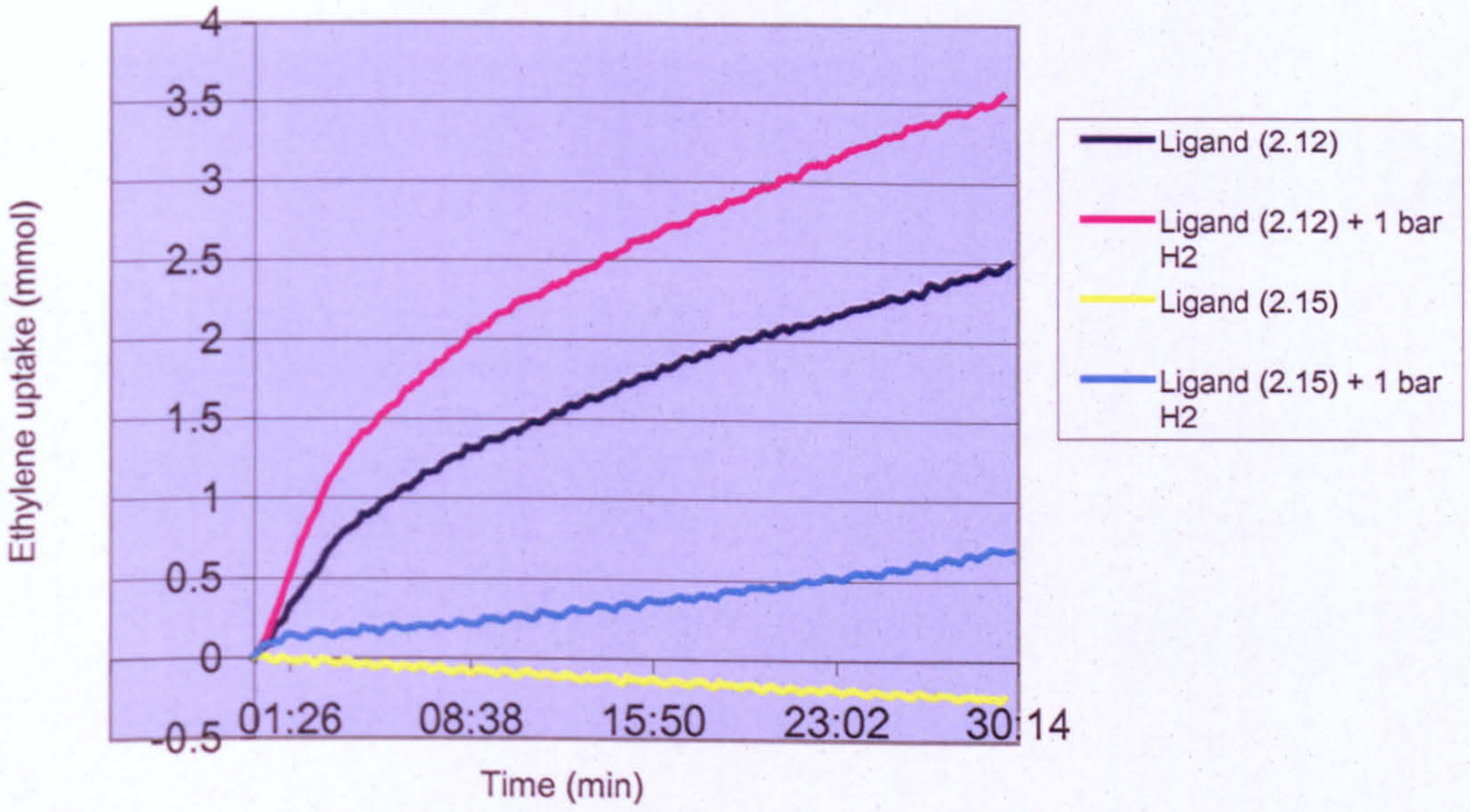

General conditions 300 eq MAO, 4 cm^3 toluene, 2 μmol catalyst solution, 30 min, 80 °C, 12 bar ethylene pressure

Figure 4.11 Uptake of ethylene for *Endeavor* Cr-catalysed ethylene oligomerisation runs

Table 4.4 Results for *Endeavor* Cr-catalysed ethylene oligomerisation runs

Ligand	H_2 (bar)	Yield (g/kg)	Productivity (g $mmol^{-1}$ h^{-1})	Selectivity (wt%)[a]	Product analysis (wt%)			
					C_4	C_6	C_8	C_{10}
(2.12)	0	13.6	71	80.3	2.1	12.5	14.6	13.2
(2.12)	1	69.0	380	94.5	2.8	15.8	13.2	16.4
(2.15)	0	17.7	92	79.4	2.6	12.7	14.8	13.2
(2.15)	1	6.6	34	84.1	3.2	19.7	19.0	12.8

[a] Selectivity to 1-hexene within C_6 fraction.

General conditions 300 eq MAO, 4 cm^3 toluene, 2 μmol catalyst solution, 30 min, 80 °C, 12 bar ethylene pressure

The Cr-catalysed ethylene oligomerisation runs with ligands **(2.12)** and **(2.15)** gives a Schulz-Flory distribution of oligomers, with very little C_6 product yielded (< 20%); the selectivity to 1-hexene within these fractions is between 80 to 95%. The *k* values for these catalytic runs are given in Table 4.5; little variation was observed when hydrogen was added.

Table 4.5 *k* values for ethylene oligomerisation runs with ligands **(2.12)** and **(2.15)** with and without the presence of hydrogen

Ligand	H_2 pressure (bar)	*k*
(2.12)	0	0.69
(2.12)	1	0.66
(2.15)	0	0.71
(2.15)	1	0.80

The activity with ligand (**2.12**) is 92 g $mmol^{-1}$ h^{-1} at 12 bar ethylene pressure, this decreases to 34 g $mmol^{-1}$ h^{-1} when 1 bar hydrogen is added. For (**2.15**) the activity is 71 g $mmol^{-1}$ h^{-1}, but on addition of hydrogen the activity increases to 380 g $mmol^{-1}$ h^{-1} (see Figure 4.12)

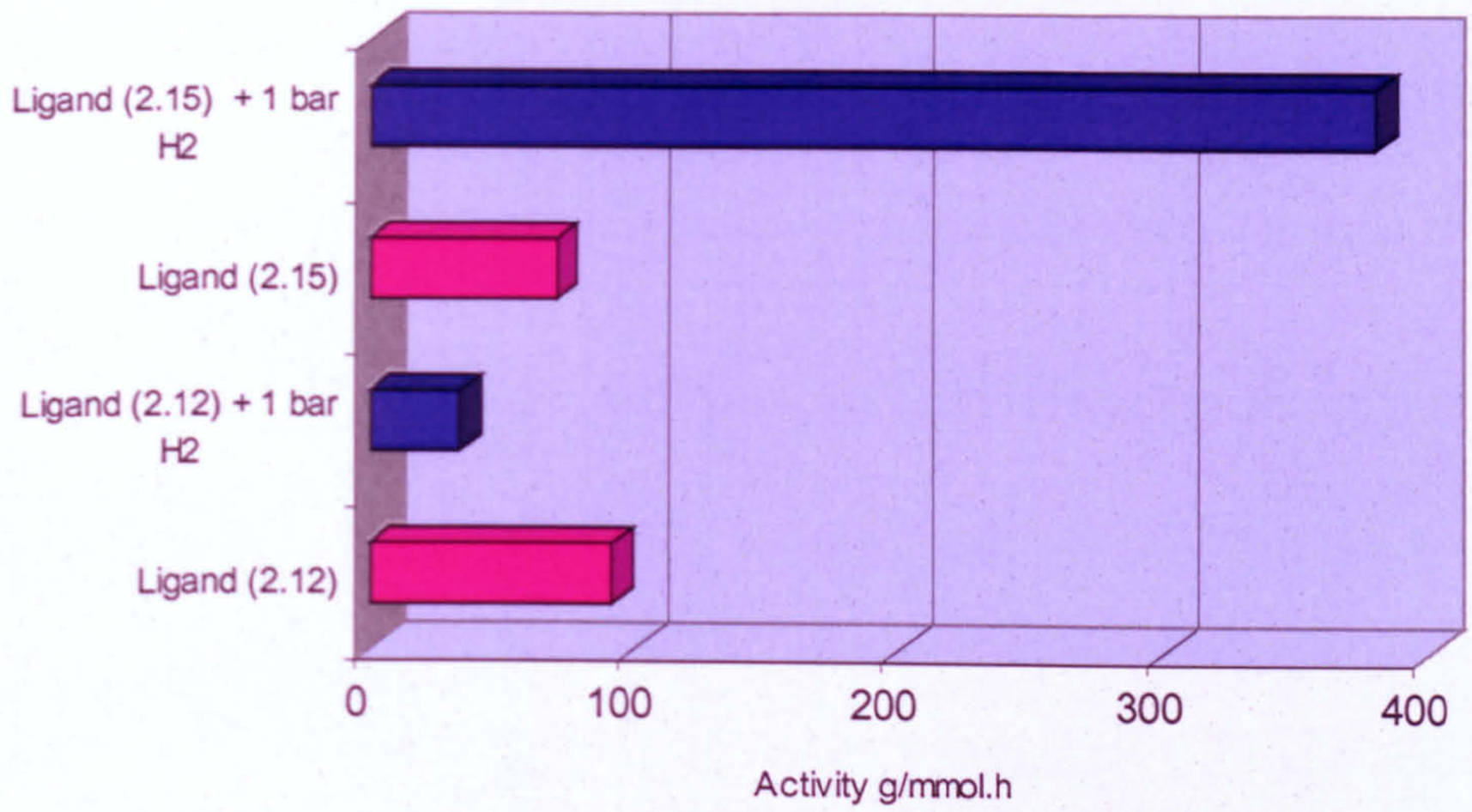

General conditions 300 eq MAO, 4 cm^3 toluene, 2 μmol catalyst solution, 30 min, 80 °C, 12 bar ethylene pressure

Figure 4.12 Activities of the Cr catalysts with ligands (**2.12**), and (**2.15**) at different pressures

4.3.3.1 Summary of results with PNP ligands (2.12) and (2.15)

These results show that the ligand with *ortho*-CF_3 groups (**2.12**) and the diphosphoramidite ligand (**2.15**) with no *ortho*-methoxy groups present are poor oligomerisation catalysts when complexed to chromium. This highlights the need for the *ortho*-anisyl groups on the PNP ligand in order to obtain trimerisation selectivity.

The recent work by Sasol on selective ethylene tetramerisation[117] would suggest that higher pressures of ethylene should be investigated with our PNP ligands.

4.4 Conclusion

The results for the Ni-catalysed ethylene polymerisation show the PNP ligand with *ortho*-chloro substituents **(2.13)** to be highly active, although only low molecular weight oligomers are produced. An increase in bulk of the ligand could help to switch the catalysis towards polymerisation. The diphosphoramidite ligand **(2.15)** has a lower activity with the same product distribution and is significant because it may be representative of a new class of diphosphine ligand for oligomerisation catalysis.

The results for Cr-catalysed ethylene trimerisation have highlighted the need for *ortho*-methoxy groups. The ligand with only two *ortho*-methoxy groups **(2.14)** gives a slightly greater activity but less selectivity to 1-hexene than the previously studied **(OMePNP)** ligand, with the ligands containing methoxy groups on the nitrogen substituent **(2.9)**, **(2.10)** and **(2.11)** yielding a Schulz-Flory distribution of oligomers. In some of these cases the activity has been shown to be greater than that for the standard ligand **(OMePNP)**. The ligands with no methoxy groups **(2.12)** and **(2.15)** also gave a Schulz-Flory distribution of oligomers with lower activities.

The interpretation of these results in terms of mechanism requires much work in the future. The results suggest that further investigation of structure-activity relationships with PNP ligands would be fruitful in both Ni- and Cr-based oligomerisation catalysts. For example the ligands below may combine high activity and high selectivity by building in the favourable structural components we have discovered.

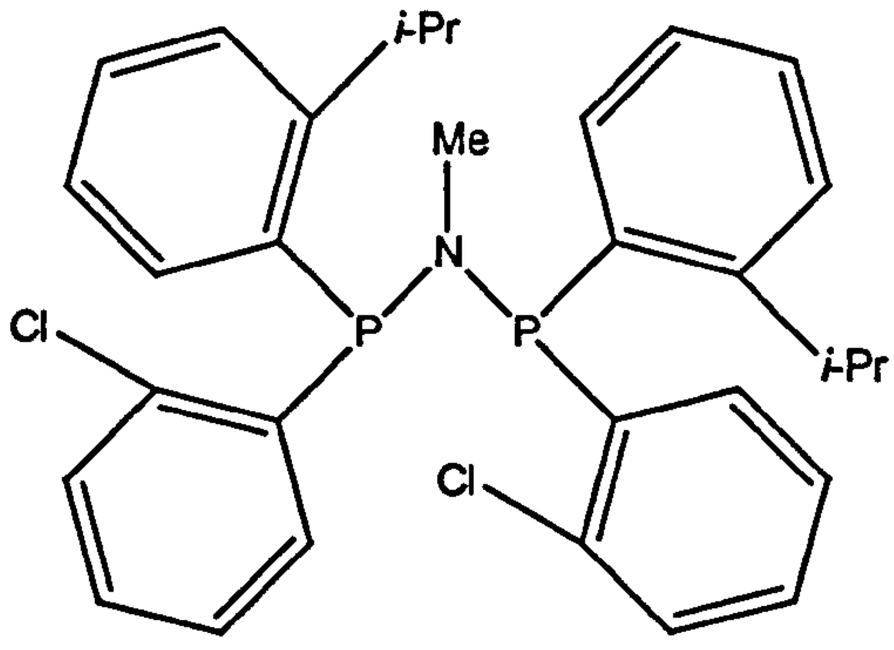

(4.14)

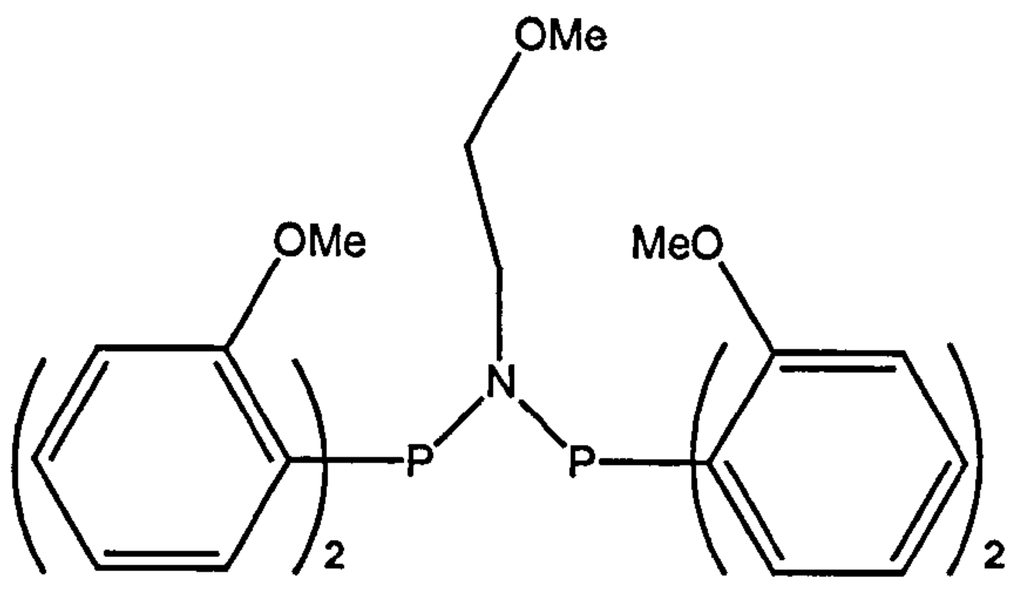

(4.15)

Finally, the catalysis results reported here with Ni and Cr produced some surprises. Previously the palladium complexes of PNP ligands have been shown to be highly active carbonylation catalysts[35] and it would therefore be of interest to investigate the coordination chemistry and catalytic properties of PNP ligands with other transition metals.

Chapter 5:

Experimental details

Experimental details

5.1 General experimental techniques

Unless otherwise stated, all reactions were carried out in a dry dinitrogen atmosphere using standard Schlenk techniques. Dry N_2-saturated solvents were collected from a Grubbs system using filtration through an alumina column impregnated with deoxygenated catalysts in flame and vacuum dried glassware.[125] Commercial reagents were used as supplied unless otherwise stated. NEt_3, PCl_3, Ph_2PCl were distilled prior to use.

After purification, all phosphines were stored under nitrogen at room temperature. All complexes were treated as air stable and thus stored in air at room temperature.

Starting materials prepared by literature methods were $(C_6H_5)_2PN(Me)P(C_6H_5)_2$ (2.5),[35] $(2\text{-}CH_3C_6H_4)_2P(CH_2)_nP(2\text{-}CH_3C_6H_4)_2$ n = 1–3,[35] $(2\text{-}ClC_6H_4)_2PCl$,[86] $[PtCl_2(1,5\text{-}COD)]$,[127] $[PtMe_2(1,5\text{-}COD)]$,[128] $[PtClMe(1,5\text{-}COD)]$,[129] and $[PdCl_2(NCPh)_2]$.[130] Racemic-9,9′-biphenanthryl-10,10′-diol and (*S*)-9,9′-biphenanthryl-10,10′-diol were kindly donated by Dr Richard Wingad. ((*o*-$OCH_3C_6H_4$)(C_6H_5))PN(Me)P((C_6H_5)(*o*-$OCH_3C_6H_4$)) was prepared by Philip Winder.

The Microanalytical Laboratory of the School of Chemistry, University of Bristol, carried out elemental analyses.

The Mass Spectrometry Service, University of Bristol, recorded Electron Impact, Chemical Ionisation, Electron Spray Ionisation and Fast Atom Bombardment on MD800, Quattro and Autospec spectrometers.

$^{31}P\{^1H\}$, $^{13}C\{^1H\}$, $^{19}F\{^1H\}$, ^1H NMR spectra were recorded by the author at ambient temperature of the probe unless otherwise stated, using deuterated solvent to provide the field/frequency lock. The following NMR spectrometers were used:

^1H NMR spectra	Jeol Δ300 (300 MHz) and Jeol Δ400 (400 MHz) with chemical shifts relative to high frequency of residual solvent.

$^{13}C\{^1H\}$ NMR spectra	Jeol Δ300 (75 MHz) and Jeol Δ400 (100.6 MHz) with chemical shifts relative to high frequency of residual solvent.
$^{31}P\{^1H\}$ NMR spectra	Jeol Δ300 (121.2 MHz) and Jeol Δ400 (161.9 MHz) with chemical shifts relative to high frequency of 85 % H_3PO_4.
$^{19}F\{^1H\}$ NMR spectra	Jeol Δ300 (282.6 MHz) with chemical shifts relative to high frequency of $CFCl_3$.

Crystal structure determinations were carried out by the author, Angharad Baber and Katie Heslop on SMART and APEX diffractometers.

5.2 Experimental detail for Chapter 2

5.2.1 Synthesis of $Cl_2PN(Me)PCl_2$ [4] (2.1)

Phosphorus trichloride was heated under reflux for 2 h to expel HCl gas, then distilled into an adjacent trap at – 78 °C and stored under nitrogen. Tetrachloroethane was saturated with nitrogen for 1 h and stored under nitrogen. Methylamine hydrochloride salt was heated to 35 °C under vacuum for 3 d and stored in a glove box.

Methylamine hydrochloride (5.00 g, 0.074 mol) was added to a 250 cm^3 round bottomed flask in a glove box. To this was added tetrachloroethane (40 cm^3) and phosphorus trichloride (26 cm^3, 0.296 mol) and the mixture was then refluxed with stirring at 170 °C for 3 d. The progress of the reaction was monitored by $^{31}P\{^1H\}$NMR. The reaction mixture was then allowed to cool and the excess phosphorus trichloride removed under vacuum. A second trap was then fitted and the tetrachloroethane solvent removed through to the main trap. The second trap was then surrounded by liquid

nitrogen and the desired product distilled over as a colourless oil (7.412 g, 0.0318 mol 43%).

Data:

δ_P (121 MHz; $CDCl_3$)	160.8 (s)
δ_H (300 MHz; $CDCl_3$)	3.24 (3H, s, CH_3)
δ_C (75 MHz; $CDCl_3$)	29.1 (s, CH$_3$)

5.2.2 Synthesis of $Cl_2PN(Et)PCl_2$ [4] (2.2)

The starting materials were purified and the experiment carried out as described previously for the synthesis of $Cl_2PN(Me)PCl_2$, using ethylamine hydrochloride salt (5.00 g, 0.0613 mol) and phosphorus trichloride (21.4 cm^3, 0.245 mol) in tetrachloroethane (32 cm^3). The desired product was obtained as a colourless oil (12.450 g, 0.0504 mol, 82%).

Data:

δ_P (121 MHz; $CDCl_3$)	164.8 (s)
δ_H (300 MHz; $CDCl_3$)	3.87 (2H, qt, J_{HH} 7.3 Hz, CH_2), 1.68 (3H, t, J_{HH} 7.2 Hz, CH_3)
δ_C (75 MHz; $CDCl_3$)	43.4 (t, J_{CP} 2.5 Hz, CH$_2$), 17.8 (s, CH$_3$)

5.2.3 Synthesis of $Cl_2PN(n\text{-}Pr)PCl_2$ (2.3)

The starting materials were purified and the experiment carried out as described previously for the synthesis of $Cl_2PN(Me)PCl_2$, using propylamine hydrochloride salt (5.00 g, 0.0523 mol) and phosphorus trichloride (18.3 cm^3, 0.209 mol) in tetrachloroethane (28 cm^3). The desired product was obtained as a colourless oil (12.266 g, 0.0470 mol, 89%).

Data:

δ_P (121 MHz; $CDCl_3$)	165.1 (s)
δ_H (300 MHz; $CDCl_3$)	3.70 – 3.65 (2H, m, CH_2), 1.89 (2H, qt, J_{HH} 7.5 Hz, CH_2), 0.94 (3H, t, J_{HH} 7.5 Hz, CH_3)
δ_C (75 MHz; $CDCl_3$)	50.3 (s, CH_2), 25.4 (s, CH_2), 11.8 (s, CH_3)

5.2.4 Synthesis of $Cl_2PN(i\text{-}Pr)PCl_2$ (2.4)

The starting materials were purified and the experiment carried out as described previously for the synthesis of $Cl_2PN(Me)PCl_2$, using isopropylamine (7.20 cm^3, 0.0846 mmol) and phosphorus trichloride (30.0 cm^3, 0.338 mol) in tetrachloroethane (44 cm^3). The desired product was obtained as a colourless oil (14.636 g, 0.0561 mol, 66%).

Data:

δ_P (121 MHz; $CDCl_3$)	170.5 (s)
δ_H (300 MHz; $CDCl_3$)	4.46 (1H, sept, J_{HH} 7.0 Hz, CH), 1.42 (6H, d, J_{HH} 6.8 Hz, C(CH_3)$_2$)
δ_C (75 MHz; $CDCl_3$)	53.7 (t, J_{CP} 13.1 Hz, NCH), 24.2 (t, J_{CP} 6.8 Hz, (CH_3)$_2$C)

5.2.5 Synthesis of $(C_6H_5)_2PN(Et)P(C_6H_5)_2$ (2.6)

Magnesium turnings (0.542 g, 0.0223 mol) were stirred under nitrogen overnight to activate the surface. THF (5 cm^3) was added to the magnesium with vigorous stirring and then bromobenzene (2.14 cm^3, 0.0203 mol) in THF (5 cm^3) was added dropwise over 5 min. The solution started to warm and was left to stir overnight with further addition of THF (5 cm^3). A 3-necked flask fitted with dropping funnel was then charged

with $Cl_2PN(Et)PCl_2$ (1.001 g, 4.06 mmol) in THF (15 cm^3) and cooled to – 78 °C. The Grignard solution was added to the dropping funnel and the flask rinsed with THF (5 cm^3) and added slowly over 30 min. The dropping funnel was then rinsed with THF (5 cm^3). The solution stirred for 3 h and monitored by $^{31}P\{^1H\}$ NMR. The solution was then allowed to warm slowly to room temperature and excess solvent removed under vacuum. CH_2Cl_2 (50 cm^3) and water (30 cm^3) was added to the resulting pale brown oily residue and the aqueous layer was extracted with CH_2Cl_2 (2 x 10 cm^3). The organic extracts were combined and dried over magnesium sulphate and then filtered under nitrogen and the solvent removed under vacuum, to leave a yellow oily residue. The residue was triturated with methanol (15 cm^3). The resulting fine white powder settled out and the methanol removed by cannular. The product was dried *in vacuo* yielding a white solid (0.526 g, 1.27 mmol, 31%).

Data:

δ_P (162 MHz; $CDCl_3$)	62.3 (s)
δ_H (400 MHz; $CDCl_3$)	7.45 – 7.18 (20H, m, Ar*H*), 3.28 – 3.24 (2H, m, CH_2), 0.81 (3H, t, J_{HH} 6.6 Hz, CH_3)
δ_C (100 MHz; $CDCl_3$)	139.6 (t, J_{CP} 12.3 Hz, *C*P), 132.7 (t, J_{CP} 22.3 Hz, *C*H), 128.7 (s, *C*H), 128.0 (t, J_{CP} 6.2 Hz, *C*H), 47.2 (t, $^2J_{CP}$ 11.5 Hz, *C*H_2), 16.7 (t, $^3J_{CP}$ 3.1 Hz, *C*H_3)
EI mass spectrum: *m/z*	413 (M^+)
Elemental analysis % (calc: $C_{26}H_{25}NP_2$)	C: 74.15 (75.53) H: 5.86 (6.09) N: 3.20 (3.39)

5.2.6 Synthesis of $(C_6H_5)_2PN(n\text{-}Pr)P(C_6H_5)_2$ (2.7)

Magnesium turnings (0.513 g, 21.09 mmol) were stirred under nitrogen overnight to activate the surface. THF (5 cm^3) was added to the magnesium with vigorous stirring and then bromobenzene (2.02 cm^3, 19.17 mmol) in THF (5 cm^3) was added dropwise

over 5 min. The solution started to warm and was left to stir overnight with further addition of THF (5 cm^3). A 3-necked flask fitted with dropping funnel was then charged with $Cl_2PN(n\text{-}Pr)PCl_2$ (0.911 g, 3.49 mmol) in THF (15 cm^3) and cooled to – 78 °C. The Grignard solution was added to the dropping funnel and the flask rinsed with THF (5 cm^3) and added slowly over 30 min. The dropping funnel was then rinsed with THF (5 cm^3). The solution was stirred for 3 h and monitored by $^{31}P\{^1H\}$ NMR. The solution was then allowed to warm slowly to room temperature and excess solvent removed under vacuum. CH_2Cl_2 (50 cm^3) and water (30 cm^3) was added to the resulting pale brown oily residue and the aqueous layer was extracted with CH_2Cl_2 (2 x 10 cm^3). The organic extracts were combined and dried over magnesium sulphate then filtered under nitrogen and the solvent removed under vacuum, to leave a yellow oily residue. The residue was triturated with methanol (10 cm^3). The resulting fine white powder settled out and the methanol removed by cannular. The product was dried *in vacuo* yielding a white solid (0.426 g, 0.977 mmol, 29%).

Data:

δ_P (162 MHz; $CDCl_3$)	63.0 (s)
δ_H (400 MHz; $CDCl_3$)	7.49 – 7.21 (20H, m, Ar*H*), 3.20 – 3.15 (2H, m, CH_2), 1.09 – 1.05 (2H, m, CH_2), 0.88 (3H, t, J_{HH} 7.1 Hz, CH_3)
δ_C (100 MHz; $CDCl_3$)	139.7 (t, J_{CP} 13.1 Hz, *C*P), 132.7 (t, J_{CP} 22.3 Hz, *C*H), 128.7 (s, *C*H), 128.0 (t, J_{CP} 6.2 Hz, *C*H), 54.8 (t, $^2J_{CP}$ 10.0 Hz, *C*H_2), 24.7 (t, $^3J_{CP}$ 2.3 Hz, *C*H_2), 22.3 (s, *C*H_3)
EI mass spectrum: *m/z*	427 (M^+)
Elemental analysis % (calc: $C_{27}H_{27}NP_2$)	C: 74.36 (75.86) H: 6.66 (6.37) N: 3.10 (3.28)

5.2.7 Synthesis of $(C_6H_5)_2PN(i\text{-}Pr)P(C_6H_5)_2$ (2.8)

Magnesium turnings (1.54 g, 0.0633 mol) were stirred under nitrogen overnight to activate the surface. THF (3 cm^3) was added to the magnesium with vigorous stirring and then bromobenzene (6.06 cm^3, 0.0575 mol) in THF (6 cm^3) was added dropwise over 5 min. The solution started to warm and was left to stir overnight with further addition of THF (3 cm^3). A 3-necked flask fitted with dropping funnel was then charged with $Cl_2PN(i\text{-}Pr)PCl_2$ (3.00 g, 0.0115 mol) in THF (15 cm^3) and cooled to – 78 °C. The Grignard solution was added to the dropping funnel and the flask rinsed with THF (5 cm^3) and added slowly over 30 min. The dropping funnel was then rinsed with THF (5 cm^3). The solution stirred for 3 h and monitored by $^{31}P\{^1H\}$ NMR. The solution was then allowed to warm slowly to room temperature and excess solvent removed under vacuum. CH_2Cl_2 (50 cm^3) and water (30 cm^3) was added to the resulting pale brown oily residue and the aqueous layer was extracted with CH_2Cl_2 (2 x 10 cm^3). The organic extracts were combined and dried over magnesium sulphate then filtered under nitrogen and the solvent removed under vacuum, to leave a brown oily residue. The residue was triturated with methanol (15 cm^3). The resulting fine white powder settled out and the methanol removed by cannular. The product was recrystallised from hot *iso*-propanol and dried *in vacuo* yielding a white solid (0.989 g, 2.31 mmol, 20%).

Data:

δ_P (162 MHz; $CDCl_3$)	50.0 (br)
δ_H (400 MHz; $CDCl_3$)	7.38 – 7.25 (20H, m, Ar*H*), 3.74 (1H, sept J_{HH} 6.6 Hz, C*H*), 1.14 (6H, d, J_{HH} 6.4 Hz, $C(CH_3)_3$)
δ_C (100 MHz; $CDCl_3$)	139.9 (t, J_{CP} 20.0 Hz, *C*P), 132.9 (t, J_{CP} 22.3 Hz, *C*H), 128.5 (s, *C*H), 128.0 (t, J_{CP} 5.4 Hz, *C*H), 51.9 (t, $^2J_{CP}$ 10.0 Hz, *C*H), 24.4 (t, $^3J_{CP}$ 6.9 Hz, *C*H_3)
CI mass spectrum: *m/z*	428 (M^+)
Elemental analysis % (calc: $C_{27}H_{27}NP_2$)	C: 73.89 (75.86) H: 6.32 (6.37) N: 3.21 (3.28)

5.2.8 Synthesis of $(C_6H_5)_2PN(CH_2CH_2OCH_3)P(C_6H_6)_2$ (2.9)

Triethylamine (3.15 cm^3, 0.0226 mol) was added dropwise to chlorodiphenylphosphine (4.06 cm^3, 0.0226 mol) in CH_2Cl_2 (20 cm^3) and the resulting orange solution was then stirred for 1 h at room temperature. 2-Methoxyethylamine (0.98 cm^3, 0.0113 mol) was then added dropwise and a precipitate formed. The reaction mixture was stirred for 1 h, then the solution filtered free of ammonium salts. The solvent was then removed *in vacuo* to leave a yellow residue that was triturated with MeCN (20 cm^3) to give (**2.9**) as a fine white powder in a purity of 90% by $^{31}P\{^1H\}$ NMR. The MeCN solution was set aside to crystallise at 0 °C, giving block like crystals (3.250 g, 7.345 mmol, 65%).

Data:

δ_P (162 MHz; $CDCl_3$)	64.9 (s)
δ_H (400 MHz; $CDCl_3$)	7.42 – 7.26 (20H, m, Ar*H*), 3.46 (2H, m, CH_2), 3.00 (3H, s, OCH_3), 2.89 (2H, t, J_{HH} 7.6 Hz, CH_2O)
δ_C (100 MHz; $CDCl_3$)	139.3 (t, J_{CP} 13.1 Hz, *C*P), 132.7 (t, J_{CP} 22.3 Hz, *C*H), 128.8 (s, *C*H) 128.1 (t, J_{CP} 6.1 Hz, *C*H), 71.9 (t, $^2J_{CP}$ CH_2), 58.5 (s, O*C*H$_3$) 51.2 (t, $^3J_{CP}$ 10.0 Hz, *C*H$_2$)
EI mass spectrum: *m/z*	443 (M^+)
Elemental analysis % (calc: $C_{27}H_{27}NOP_2$)	C: 73.30 (73.18) H: 6.14 (6.09) N: 3.16 (3.58)

Crystallographic data for (**2.9**): $C_{27}H_{27}NOP_2$, M = 443.46, monoclinic, space group *P2(1)/n*, a = 13.916(17), b = 10.186(10), c = 17.453(2) Å, V = 2348.6(5) Å^3, Z = 4, T = 173(2) K, μ = 0.204 mm^{-1}, 5373 independent reflections, R_{int} = 0.0282, R_1 = 0.0389, wR_2 = 0.0905.

5.2.9 Synthesis of $(C_6H_5)_2PN(CH_2CH_2CH_2OCH_3)P(C_6H_6)_2$ (2.10)

Triethylamine (3.15 cm^3, 0.0226 mol) was added dropwise to chlorodiphenylphosphine (4.06 cm^3, 0.0226 mol) in CH_2Cl_2 (50 cm^3) and the resulting orange solution was then stirred for 1 h at room temperature. 3-Methoxypropylamine (1.15 cm^3, 0.0113 mol) was then added dropwise and a precipitate formed. The reaction mixture was stirred for 1 h, then the solution filtered free of ammonium salts. The solvent was then removed *in vacuo* to leave an off-white residue that was triturated with MeCN (30 cm^3) giving **(2.10)** as a fine white powder with a purity of 92% by $^{31}P\{^1H\}$ NMR. The remaining solution was set aside to crystallise at 0 °C (2.580 g, 5.64 mmol, 50%).

Data:

δ_P (162 MHz; CD_2Cl_2)	63.4 (s)
δ_H (400 MHz; CD_2Cl_2)	7.60 – 7.34 (20H, m, Ar*H*), 3.44 – 3.32 (2H, m, NCH_2), 3.10 (3H, s, OCH_3), 3.02 (2H, t, J_{HH} 8.0 Hz, CH_2O), 1.38 (2H, br tt, J_{HH} 8.0 Hz, J_{HH} *ca.* 4 Hz, CH_2)
δ_C (100 MHz; CD_2Cl_2)	140.0 (t, J_{CP} 13.1 Hz, *C*P), 133.1 (t, J_{CP} 22.3 Hz, *C*H), 129.1 (s, *C*H) 128.4 (t, J_{CP} 6.2 Hz, *C*H), 70.6 (s, CH_2), 58.4 (s, CH_3), 50.7 (t, $^2J_{CP}$ 10.8 Hz, CH_2), 31.7 (t, $^3J_{CP}$ 3.1 Hz, CH_2)
EI mass spectrum: *m/z*	457 (M^+)
Elemental analysis % (calc: $C_{28}H_{29}NOP_2$)	C: 73.10 (73.51) H: 6.34 (6.39) N: 3.29 (3.06)

Crystallographic data for **(2.10)**: $C_{28}H_{29}NOP_2$, M = 457.46, orthorhombic, space group *P2(1)2(1)2(1)* $a = 9.303(3)$, $b = 9.712(4)$, $c = 26.806(10)$ Å, $V = 2421.8(15)$ $Å^3$, $Z = 4$, $T = 173(2)$ K, $\mu = 0.200$ mm^{-1}, 5550 independent reflections, $R_{int} = 0.1033$, $R_1 = 0.0653$, $wR_2 = 0.1045$.

5.2.10 Synthesis of $(C_6H_5)_2PN(CH_2(2\text{-}OCH_3)C_6H_4)P(C_6H_6)_2$ (2.11)

Triethylamine (3.15 cm^3, 0.0226 mol) was added dropwise to chlorodiphenylphosphine (4.06 cm^3, 0.0226 mol) in CH_2Cl_2 (50 cm^3) and the resulting orange solution was then stirred over 1 h at room temperature. 2-Methoxybenzylamine (1.47 cm^3, 0.0113 mol) was then added dropwise and a precipitate formed. The reaction mixture was stirred for 1 h, then the solution filtered free of ammonium salts. The solvent removed *in vacuo* to leave an off-white residue which was triturated with MeCN (50 cm^3) giving (**2.11**) as a fine white powder of 90% purity by $^{31}P\{^1H\}$ NMR. The remaining solution was set aside to crystallise at 0 °C (3.867 g, 7.60 mmol, 67%).

Data:

δ_P (162 MHz; $CDCl_3$)	58.8 (s)
δ_H (400 MHz; $CDCl_3$)	7.38 – 7.26 (20H, m, Ar*H*), 6.78 – 6.68 (4H, m, Ar*H*), 4.46 (2H, t, J_{PH} 9.2 Hz, CH_2), 3.68 (3H, s, OCH_3)
δ_C (100 MHz; $CDCl_3$)	157.4 (s, *C*O), 139.6 (t, J_{CP} 13.8 Hz, *C*P), 133.0 (t, J_{CP} 23.1 Hz, *C*H), 130.0 (s, *C*H), 128.5 (s, *C*H), 128.3 (s, *C*), 128.0 (s, *C*H), 127.9 (t, J_{CP} 6.2 Hz, *C*H), 120.0 (s, *C*H), 110.0 (s, *C*H), 54.9 (s, OCH_3), 49.7 (t, $^2J_{CP}$ 13.1 Hz, CH_2)
EI mass spectrum: *m/z*	505 (M^+)
Elemental analysis % (calc: $C_{32}H_{29}NOP_2$)	C: 76.03 (76.03) H: 5.60 (5.78) N: 2.97 (2.77)

5.2.11 Synthesis of $(2\text{-}CF_3C_6H_4)_2PN(Me)P(2\text{-}CF_3C_6H_4)_2$ (2.12)

n-Butyl lithium (9.7 cm^3, 1.6 M in hexanes, 15.5 mmol) was added dropwise over 20 min to a solution of 2-bromobenzotrifluoride (2.11 cm^3, 15.5 mmol) in diethyl ether (15

cm^3) at – 78 °C. This gave a yellow solution which was stirred for 10 min. Diethyl ether (5 cm^3) was then added to the reaction mixture at – 78 °C, followed by a solution of $Cl_2PN(Me)PCl_2$ (0.601 g, 2.59 mmol) in diethyl ether (15 cm^3), added dropwise over 10 min. The reaction mixture was stirred at – 78 °C for a further 10 min and then gradually allowed to warm to room temperature to give a mustard yellow suspension which was stirred at room temperature for a further 2 h. The suspension was then cooled to – 78 °C and dilute nitrogen saturated HCl (10 cm^3, 2.0 M) added. The solution was then allowed to warm to room temperature. Water (20 cm^3) was added and the mixture stirred for 30 min to give a white suspension of the product in the aqueous layer. The product was filtered off under nitrogen and dried *in vacuo* to give a white solid (1.103 g, 1.64 mmol, 87%).

Data:

δ_P (162 MHz; $CDCl_3$)	63.8 (dsept, J_{PF} 27.3 Hz)
δ_H (400 MHz; $CDCl_3$)	7.73 – 7.18 (16H, m, Ar*H*), 2.59 (3H, t, J_{PH} 2.9 Hz, CH_3)
δ_C (100 MHz; $CDCl_3$)	136.9 – 136.7 (m, *C*P), 134.9 (s, *C*H), 133.3 – 132.7 (m, *C*CF_3), 131.1 (s, *C*H), 129.8 (s, *C*H), 127.4 – 127.1 (m, *C*H), 124.6 (q, J_{CF} 275.3 Hz, *C*F_3), 32.8 (s, *C*H_3)
δ_F (282 MHz; $CDCl_3$)	- 56.70 (12F, br dd, J_{PF} *ca.* 31 Hz, J_{PF} *ca.* 34 Hz, CF_3)
EI mass spectrum: *m/z*	671 (M^+)
Elemental analysis % (calc: $C_{29}H_{19}F_{12}NP_2$)	C: 51.36 (51.88) H: 3.01 (2.85) N: 2.24 (2.09)

Crystallographic data for **(2.12)**: $C_{29}H_{19}F_{12}NP_2$, M = 671.39, orthorhombic, space group *Pca2(1)*, a = 22.226(5), b = 11.806(2), c = 21.415(7) Å, V = 5619(2) $Å^3$, Z = 8, T = 173(2) K, μ = 0.257 mm^{-1}, 12123 independent reflections, R_{int} = 0.1706, R_1 = 0.0727, wR_2 = 0.1415.

5.2.12 Synthesis of $(2\text{-}ClC_6H_4)_2PN(Me)P(2\text{-}ClC_6H_4)_2$ (2.13)

Triethylamine (11.5 cm^3, 82.8 mmol) and methylamine 2.0 M in THF (4.6 cm^3, 9.20 mmol) was added dropwise to a solution of chlorodi(*o*-chlorophenyl)phosphine (5.71 g, 18.4 mmol) in CH_2Cl_2 (40 cm^3). The reaction mixture turned clear orange and was left to stir over 2 h at room temperature, during which time a small quantity of precipitate formed. The solution was filtered and the solvent removed *in vacuo*, to leave a dark orange residue of 88% purity by $^{31}P\{^1H\}$ NMR (1.63 g, 3.034 mmol, 33%).

Data:

δ_P (121 MHz; $CDCl_3$)	36.3 (s)
CI mass spectrum: *m/z*	538 (M^+) 284 $(2\text{-}ClC_6H_4)_2PNH$)

The ligand **(2.13)** was of unsatisfactory purity.

5.2.13 Synthesis of $(2\text{-}OCH_3C_6H_4)(C_6H_5)PN(Me)P(C_6H_5)(2\text{-}OCH_3C_6H_4)$ (2.14)

o-Anisyl(chloro)phenylphosphine (0.03651 mol) was dissolved in CH_2Cl_2 (120 cm^3). Triethylamine (23.13 cm^3, 0.166 mol) and methylamine (9.13 cm^3, 0.01826 mol) were added dropwise over 10 minutes. The solution was heated under reflux for 24 h. The reaction mixture was filtered and the solvent removed *in vacuo* to yield a pink slurry/oil. The product was washed with MeOH (10 cm^3) and the resultant colourless precipitate was filtered off and dried *in vacuo* to yield the *rac* isomer in a 98:2 ratio.

Data:

δ_P (162 MHz; $CDCl_3$)	64.5 (s, major *rac* isomer), 62.9 (s, minor *meso* isomer)
δ_H (400 MHz; $CDCl_3$)	7.43 – 6.92 (18H, m, Ar*H*), 3.63 (6H, s, CH_3), 2.32 (3H, t, J_{PH} 3.0 Hz, CH_3) additional peaks assigned to minor *meso* isomer 3.61 (6H, s, CH_3), 2.37 (3H, t, J_{PH} 3.0 Hz, CH_3)
δ_C (100 MHz; CD_2Cl_2)	161.2 (t, J_{CP} 16.9 Hz, *C*P), 139.1 (s, *C*),

132.8 (s, *C*H), 132.7 (t, J_{CP} 21.5 Hz, *C*H), 130.6, (s, *C*H), 128.9 (s, *C*H), 128.2 (s, *C*H), 127.0 (t, J_{CP} 12.3 Hz, *C*P), 120.9, (s, *C*H), 110.9 (s, *C*H), 55.6 (s, CH_3), 33.5 (t, $^2J_{CP}$ 6.15 Hz, CH_3), some additional peaks assigned to minor meso isomer at 161.2 (t, J_{CP} 16.9 Hz, *C*P), 133.0 (s, *C*H), 132.3 (t, J_{CP} 21.5 Hz, *C*H), 130.8 (s, *C*H), 128.6 (s, *C*H), 120.8 (s, *C*H), 110.7 (s, *C*H), 55.5 (s, CH_3)

EI mass spectrum: *m/z* 459 (M^+)

5.2.14 Synthesis of ((*R*)-1,1′-bi-2-naphthoxo)PN(Me)P((*R*)-1,1′-bi-2-naphthoxo) (2.15)

(*R*)-1,1′-bi-2-naphthol (2.77 g, 9.675 mmol) was dried by azeotroping with toluene (3 x 10 cm^3) and then dissolved in toluene (60 cm^3). A solution of $Cl_2PN(Me)PCl_2$ (0.576 g, 2.47 mmol) in toluene (10 cm^3) was added dropwise at room temperature followed by triethylamine (1.5 cm^3, 10.75 mmol). The white reaction mixture was stirred overnight and then filtered, the solvent removed *in vacuo* to give a white solid. The product was washed with hexane (10 cm^3) and dried *in vacuo* (0.978 g, 1.482 mmol, 60%).

Data:

δ_P (162 MHz; CD_2Cl_2) 144.6 (s)

δ_H (400 MHz; CD_2Cl_2) 8.16 – 7.80 (8H, m, Ar*H*), 7.76 – 7.12 (16H, m, Ar*H*), 2.01 (3H, t, J_{PH} 3.4 Hz, CH_3)

δ_C (100 MHz; CD_2Cl_2) 150.4 (s, *C*), 149.4 (s, *C*), 133.2 (s, *C*) 132.9 (s, *C*), 132.1 (s, *C*), 131.4 (s, *C*), 131.2 (s, *C*H), 130.9 (s, *C*H), 128.9 (s, *C*H), 128.7 (s, *C*H), 127.2 (s, *C*H), 127.1

	(s, *C*H), 126.8 (s, *C*H), 126.7 (s, *C*H), 125.6 (s, *C*H), 125.3 (s, *C*H), 124.3 (s, *C*), 122.4 (s, *C*), 122.2 (s, *C*H), 122.0 (s, *C*H), 28.4 (s, CH_3)
FAB mass spectrum: *m/z*	660 (M^+)
Elemental analysis % (calc: $C_{41}H_{27}NO_4P_2$)	C: 73.22 (74.66) H: 4.44 (4.13) N: 2.27 (2.12)

5.2.15 Synthesis of ((*S*)-9,9′-biphenanthryl-10,10′-dioxo)PN(Me)P((*S*)-9,9′-biphenanthryl-10,10′-dioxo) (2.16)

(*S*)-9,9′-biphenanthryl-10,10′-diol (0.390 g, 1.01 mmol) was dried by azeotroping with toluene (4 x 3 cm^3) and then dissolved in toluene (20 cm^3). A solution of $Cl_2PN(Me)PCl_2$ (0.107 g, 0.459 mmol) in toluene (5 cm^3) was added dropwise at room temperature followed by triethylamine (0.32 cm^3, 2.30 mmol). The yellow reaction mixture was stirred overnight then filtered and solvent removed under vacuum. The resulting solid was washed with hexane (10 cm^3) and then dried *in vacuo* giving a yellow solid (0.315 g, 0.367 mmol, 79%).

Data:

δ_P (162 MHz; CD_2Cl_2)	147.0 (s)
δ_H (400 MHz; CD_2Cl_2)	8.91 – 8.61 (8H, m, Ar*H*), 8.01 – 7.19 (24H, m, Ar*H*), 1.60 (3H, t, J_{PH} 2.9 Hz, CH_3)
δ_C (100 MHz; CD_2Cl_2)	147.0 (s, *C*), 146.0 (s, *C*), 132.3 (s, *C*), 131.9 (s, *C*), 131.6 (s, *C*), 131.4 (s, *C*), 129.3 (s, *C*), 129.1 (s, *C*), 128.5 (s, *C*H), 128.4 (s, *C*H), 128.3 (s, *C*H), 128.3 (s, *C*H), 128.2 (s, *C*H), 128.0 (s, *C*H), 127.9 (s, *C*H), 127.8 (s, *C*H), 127.4 (s, *C*), 127.0 (s, *C*H), 126.8 (s, *C*H), 126.4 (s,

	*C*H), 126.0 (s, *C*H), 125.6 (s, *C*), 123.4 (s, *C*H), 123.2 (s, *C*H), 123.1 (s, *C*H), 123.1 (s, *C*H), 121.6 (s, *C*), 120.0 (s, *C*) 27.5 (s, CH_3)
FAB mass spectrum: *m/z*	860 (M^+)
Elemental analysis % (calc: $C_{57}H_{35}NO_4P_2.CD_2Cl_2$)	C: 73.75 (73.58) H: 4.60 (4.15) N: 1.41 (1.48)

5.2.16 Synthesis of a mixture of *rac* and *meso* (9,9′-biphenanthryl-10,10′-dioxo)PN(Me)P(9,9′-biphenanthryl-10,10′-dioxo) (2.17)

Racemic-9,9′-biphenanthryl-10,10′-diol (0.995 g, 2.57 mmol) was dried by azeotroping with toluene (4 x 5 cm^3) and then dissolved in toluene (30 cm^3). A solution of $Cl_2PN(Me)PCl_2$ (0.268 g, 1.15 mmol) in toluene (10 cm^3) was added dropwise at room temperature followed by triethylamine (0.80 cm^3, 5.75 mmol). The yellow reaction mixture was stirred overnight then filtered and solvent removed under vacuum. The resulting solid was washed with hexane (10 cm^3) and then dried *in vacuo* giving a yellow solid (0.811 g, 0.943 mmol, 82%).

Data:

δ_P (162 MHz; $CDCl_3$, 23 °C)	155.9 (br, major *meso* diastereomer) 147.1 (s, minor *rac* diastereomer)
δ_P (121 MHz; $CDCl_3$, – 55 °C)	169.5 (br), 151.0 (br, major *meso* diastereomer) 147.1 (s, minor *rac* diastereomer)
δ_H (400 MHz; $CDCl_3$)	Major *meso* diastereomer 8.88 – 8.46 (8H, m, Ar*H*), 7.97 – 7.16 (24H, m, Ar*H*), 2.29 (3H, t, J_{PH} 8.1 Hz, CH_3), additional peaks assigned to minor *rac* diastereomer 1.62 (3H, t, J_{PH} 2.9 Hz, CH_3)

FAB mass spectrum: *m/z*	860 (M^+)
Elemental analysis % (calc: $C_{57}H_{35}NO_4P_2.1.5CHCl_3$)	C: 68.62 (68.67) H: 3.57 (3.98) N: 1.37 (1.27)

Crystallographic data for **(2.17)**: $C_{58.5}H_{36.5}Cl_{4.5}NO_4P_2$, M = 1038.85, triclinic, space group *P-1*, a = 12.232(2), b = 17.076(3), c = 23.848(5) Å, V = 4751.7(16) Å^3, Z = 4, T = 173(2) K, μ = 0.397 mm^{-1}, 21719 independent reflections, R_{int} = 0.2026, R_1 = 0.0842, wR_2 = 0.2113.

5.3 Experimental detail for Chapter 3

5.3.1 Synthesis of [PtClMe(2-$CH_3C_6H_4$)$_2$PCH_2P(2-$CH_3C_6H_4$)$_2$] (3.1)

To a 50 cm^3 round bottomed Schlenk tube was added (2-$CH_3C_6H_4$)$_2$PCH_2P(2-$CH_3C_6H_4$)$_2$ (0.098 g, 0.222 mmol) in CH_2Cl_2 (3 cm^3). To this was added dropwise [PtClMe(1,5-COD)] (0.075 g, 0.212 mmol) in CH_2Cl_2 (2 cm^3). The solution was stirred for 2 h at room temperature. The solvent was then removed *in vacuo* to leave a cream solid that was triturated with pentane to give an off-white solid. The product was recrystallised from CH_2Cl_2 and pentane at 0 °C (0.051 g, 0.0742 mmol, 35%).

Data:

δ_P (121 MHz; $CDCl_3$)	- 33.2 (d, J_{PP} 31.4 Hz, J_{PtP} 3112.2 Hz, trans to Cl), - 26.0 (d, J_{PP} 31.4 Hz, J_{PtP} 1176.2 Hz, cis to Cl), - 61.1 (s, J_{PtP} 3102.2 Hz, [$PtCl_2$(2-$CH_3C_6H_4$)$_2$PCH_2P(2-$CH_3C_6H_4$)$_2$] impurity)
δ_H (400 MHz; $CDCl_3$)	7.75 – 7.11 (16H, m, Ar*H*), 4.46 (2H, dd, J_{PH} 8.1 Hz, J_{PH} 10.5 Hz, CH_2), 2.55 (6H, s, CH_3), 2.17 (6H, s, CH_3), 0.49 (3H, dd, J_{PH} 3.4 Hz, J_{PH} 8.3 Hz, J_{PtH} *ca.* 64 Hz,

	CH_3)
EI mass spectrum: *m/z*	671 (M^+ - CH_3)
Elemental analysis % (calc: $C_{30}H_{33}ClP_2Pt$)	C: 51.21 (52.52) H: 4.91 (4.85)

5.3.2 Synthesis of [PtClMe(2-$CH_3C_6H_4$)$_2$P(CH_2)$_2$P(2-$CH_3C_6H_4$)$_2$] (3.2)

To a 50 cm^3 round bottomed Schlenk tube was added (2-$CH_3C_6H_4$)$_2$P(CH_2)$_2$P(2-$CH_3C_6H_4$)$_2$ (0.030 g, 0.066 mmol) and CH_2Cl_2 (2 cm^3) and the mixture left to stir. To this was added dropwise [PtClMe(1,5-COD)] (0.022 g, 0.063 mmol) in CH_2Cl_2 (2 cm^3). The solution was stirred for 1 h at room temperature. The solvent was then removed *in vacuo* to leave a cream solid that was triturated with pentane to give an off-white solid. The product was recrystallised from CH_2Cl_2 and pentane at 0 °C (0.025 g, 0.0353 mmol, 56%).

Data:

δ_P (121 MHz; $CDCl_3$)	43.4 (d, J_{PP} 3.7 Hz, J_{PtP} 4250.2 Hz, trans to Cl), 46.4 (d, J_{PP} 3.7 Hz, J_{PtP} 1697.0 Hz, cis to Cl)
EI/CI mass spectrum: *m/z*	685 (M^+ - CH_3)
Elemental analysis % (calc: $C_{31}H_{35}ClP_2Pt$)	C: 52.49 (53.18) H: 5.41 (5.04)

Crystallographic data for (3.2x): $C_{30}H_{32}Cl_2P_2Pt$, M = 720.51, triclinic, space group *P-1*, a = 8.533(3), b = 18.090(7), c = 20.059(8) Å, V = 2827.2(19) Å^3, Z = 12, T = 173(2) K, μ = 5.283 mm^{-1}, 12863 independent reflections, R_{int} = 0.2670, R_1 = 0.0834, wR_2 = 0.2072.

5.3.3 Synthesis of [PtClMe(2-$CH_3C_6H_4$)$_2$P(CH_2)$_3$P(2-$CH_3C_6H_4$)$_2$] (3.3)

To a 50 cm^3 round bottomed Schlenk tube was added (2-$CH_3C_6H_4$)$_2$P(CH_2)$_3$P(2-$CH_3C_6H_4$)$_2$ (0.105 g, 0.224 mmol) and CH_2Cl_2 (4 cm^3) and the mixture stirred. To this was added dropwise [PtClMe(1,5-COD)] (0.075 g, 0.213 mmol) in CH_2Cl_2 (2 cm^3). The resulting solution was stirred for 2 d at room temperature and then cooled to 0 °C to crystallise the product. The solid was filtered off and dried *in vacuo* to yield an off white solid (0.140 g, 0.196 mmol, 96%).

Data:

δ_P (121 MHz; $CDCl_3$)	broad spectrum at room temperature ($w_{1/2}$ 278.2 Hz)
δ_P (121 MHz; $CDCl_3$, – 90 °C)	11.1 (br s, J_{PtP} 4229.6 Hz, $w_{1/2}$ 53.5 Hz, trans to Cl), 13.3 (br s, J_{PtP} 1700.8 Hz, $w_{1/2}$ 53.5 Hz, cis to Cl), 3.7 (s, J_{PtP} 3517.0 Hz, [$PtCl_2$(**2.3**)] impurity)
δ_H (300 MHz; $CDCl_3$, - 90 °C)	broad spectrum
EI/CI mass spectrum: *m/z*	699 (M^+ - CH_3)
Elemental analysis % (calc: $C_{32}H_{37}ClP_2Pt$)	C: 51.23 (53.82) H: 4.92 (5.22)

Crystallographic data for (**3.3**): $C_{32}H_{37}ClP_2Pt$, M = 714.10, monoclinic, space group *Pc*, a = 11.711(2), b = 9.141(16), c = 14.144(3) Å, V = 1432.6(4) Å^3, Z = 2, T = 173(2) K, μ = 5.122 mm^{-1}, 4832 independent reflections, R_{int} = 0.0539, R_1 = 0.0409, wR_2 = 0.0714.

5.3.4 Synthesis of [PtClMe(C_6H_5)$_2$PN(Me)P(C_6H_5)$_2$] (3.4)

To a 50 cm^3 round bottomed Schlenk tube was added the (C_6H_5)$_2$PN(Me)P(C_6H_5)$_2$ (0.100 g, 0.250 mmol) in CH_2Cl_2 (5 cm^3). To this was added dropwise [PtClMe(1,5-COD)] (0.084 g, 0.238 mmol) in CH_2Cl_2 (5 cm^3). The solution was stirred for 2 h at

room temperature. The solvent was then removed *in vacuo* to leave a cream solid that was triturated with pentane to give an off-white solid. The product was recrystallised from CH_2Cl_2 and pentane at 0 °C (0.0814 g, 0.126 mmol, 53%).

Data:

δ_P (121 MHz; $CDCl_3$)	35.1 (d, J_{PP} 31.2 Hz, J_{PtP} 4025.4 Hz, trans to Cl), 54.9 (d, J_{PP} 31.2 Hz, J_{PtP} 1338.9 Hz, cis to Cl)
δ_H (400 MHz; $CDCl_3$)	7.69 – 7.36 (20H, m, Ar*H*), 2.38, (3H, J_{PH} 8.8 Hz J_{PH} 10.8 Hz, CH_3) 0.45 (3H, dd, J_{PH} 3.2 Hz, J_{PH} 8.6 Hz, J_{PtH} *ca.* 60 Hz, CH_3)
EI mass spectrum: *m/z*	630 (M^+ - CH_3)
Elemental analysis % (calc: $C_{25}H_{23}Cl_2NP_2Pt$)	C: 45.65 (45.13) H: 4.14 (3.48) N: 2.30 (2.11)

Crystallographic data for **(3.4x)**: $C_{25}H_{23}Cl_2NP_2Pt$, M = 665.39, monoclinic, space group *P2(1)/n*, a = 9.315(3), b = 13.955(5), c = 19.198(7) Å, V = 2494.33(15) Å^3, Z = 4, T = 173(2) K, μ = 5.875 mm^{-1}, 5702 independent reflections, R_{int} = 0.0227, R_1 = 0.0297, wR_2 = 0.0899.

5.3.5 Synthesis of [PtCl(CH$_3$)(C$_6$H$_5$)$_2$PN(Et)P(C$_6$H$_5$)$_2$] (3.5)

To a 50 cm^3 round bottomed Schlenk tube was added **(2.6)** (0.043 g, 0.104 mmol) in CH_2Cl_2 (3 cm^3). To this was added dropwise [PtClMe(1,5-COD)] (0.035 g, 0.099 mmol) in CH_2Cl_2 (2 cm^3). The solution was stirred for 2 d at room temperature. The solvent was then removed *in vacuo* to leave a cream solid that was triturated with pentane to give an off-white solid. The product was recrystallised from CH_2Cl_2 and pentane at 0 °C (0.0457 g, 0.0693 mmol, 70%).

Data:

δ_P (121 MHz; $CDCl_3$)	35.2 (d, J_{PP} 34.4 Hz, J_{PtP} 4015.6 Hz, trans

	to Cl), 54.9 (d, J_{PP} 34.4 Hz, J_{PtP} 1358.4 Hz, cis to Cl)
δ_H (400 MHz; $CDCl_3$)	7.91 – 7.39 (20H, m, Ar*H*), 3.05 – 2.82 (2H, m, CH_2), 0.89 – 0.75 (3H, m, CH_3), 0.56 (3H, dd, J_{PH} 3.1 Hz, J_{PH} 8.4 Hz, J_{PtH} *ca.* 32 Hz, CH_3)
CI mass spectrum: *m/z*	644 (M^+ - CH_3)
Elemental analysis % (calc: $C_{27}H_{28}ClNP_2Pt$)	C: 47.65 (49.21) H: 4.14 (4.28) N: 2.30 (2.13)

Crystallographic data for (**3.5**): $C_{27}H_{28}ClNP_2Pt$, M = 659.00, monoclinic, space group *P2(1)/c*, a = 9.858(17), b = 9.469(19), c = 27.948(6) Å, V = 2608.7(9) Å^3, Z = 4, T = 173(2) K, μ = 5.619 mm^{-1}, 5980 independent reflections, R_{int} = 0.2043, R_1 = 0.0681, wR_2 = 0.1363.

5.3.6 Synthesis of [PtCl(CH_3)(C_6H_5)$_2$PN(*n*-Pr)P(C_6H_5)$_2$] (3.6)

To a 50 cm^3 round bottomed Schlenk tube was added (**2.7**) (0.100 g, 0.234 mmol) in CH_2Cl_2 (5 cm^3). To this was added dropwise [PtClMe(1,5-COD)] (0.078 g, 0.222 mmol) in CH_2Cl_2 (5 cm^3). The solution was stirred for 2 h at room temperature. The solvent was then removed *in vacuo* to leave a cream solid that was triturated with pentane to give an off-white solid. The product was recrystallised from CH_2Cl_2 and pentane at 0 °C (0.0554 g, 0.080 mmol, 36%).

Data:

δ_P (121 MHz; $CDCl_3$)	35.5 (d, J_{PP} 34.9 Hz, J_{PtP} 4015.7 Hz, trans to Cl), 55.1 (d, J_{PP} 34.9 Hz, J_{PtP} 1360.3 Hz, cis to Cl)
δ_H (400 MHz; $CDCl_3$)	7.80 – 7.25 (20H, m, Ar*H*), 2.84 – 2.66 (2H, br m, CH_2), 1.19 – 0.99 (2H, br m, CH_2), 0.58 – 0.30 (3H, br m, CH_3), 0.58 –

	0.30 (3H, br m, J_{PtP} *ca.* 70 Hz, CH_3) (overlapping signals)
CI mass spectrum: *m/z*	658 (M^+ - CH_3)
Elemental analysis % (calc: $C_{28}H_{30}ClNP_2Pt$)	C: 49.98 (49.97) H: 4.31 (4.49) N: 1.98 (2.08)

Crystallographic data for **(3.6x)**: $C_{27}H_{27}Cl_2NP_2Pt$, M = 693.44, monoclinic, space group *P2(1)/n*, a = 10.653(16), b = 18.690(4), c = 12.930(2) Å, V = 2554.0(8) Å^3, Z = 4, T = 173(2) K, μ = 5.740 mm^{-1}, 5856 independent reflections, R_{int} = 0.0913, R_1 = 0.0552, wR_2 = 0.1137.

5.3.7 Synthesis of [PtClMe(C_6H_5)$_2$PN(*i*-Pr)P(C_6H_5)$_2$] (3.7)

To a 50 cm^3 round bottomed Schlenk tube was added **(2.8)** (0.100 g, 0.234 mmol) in CH_2Cl_2 (5 cm^3). To this was added dropwise [PtClMe(1,5-COD)] (0.078 g, 0.222 mmol) in CH_2Cl_2 (5 cm^3). The solution was stirred for 2 h at room temperature. The solvent was then removed *in vacuo* to leave a cream solid that was triturated with pentane to give an off-white solid. The product was recrystallised from CH_2Cl_2 and pentane at 0 °C (0.0470 g, 0.0698 mmol, 31%).

Data:

δ_P (121 MHz; $CDCl_3$)	35.3 (d, J_{PP} 34.9 Hz, J_{PtP} 4017.1 Hz, trans to Cl), 55.0 (d, J_{PP} 34.9 Hz, J_{PtP} 1357.3 Hz, cis to Cl)
δ_H (400 MHz; $CDCl_3$)	8.05 – 7.33 (20H, m, Ar*H*), 3.65 – 3.46 (1H, m, C*H*), 0.65 (6H, d, J_{HH} 6.9 Hz, CH_3), 0.36 (3H, dd, J_{PH} 8.3 Hz, J_{PH} 2.9 Hz, J_{PtP} *ca.* 60 Hz, CH_3)
EI mass spectrum: *m/z*	658 (M^+ - CH_3)
Elemental analysis % (calc: $C_{28}H_{30}ClNP_2Pt$)	C: 49.18 (49.97) H: 4.45 (4.49) N: 2.17 (2.08)

Crystallographic data for **(3.7x)**: $C_{27}H_{27}Cl_2NP_2Pt$, M = 693.44, monoclinic, space group *P2(1)/c*, a = 20.382(3), b = 16.868(3), c = 14.996(2) Å, V = 5155.8(13) Å^3, Z = 4, T = 173(2) K, μ = 5.791 mm^{-1}, 11829 independent reflections, R_{int} = 0.1180, R_1 = 0.0406, wR_2 = 0.1107.

5.3.8 Synthesis of [PtClMe(C_6H_5)$_2$PN($CH_2CH_2OCH_3$)P(C_6H_5)$_2$] (3.8)

To a 50 cm^3 round bottomed Schlenk tube was added (**2.9**) (0.100 g, 0.225 mmol) in CH_2Cl_2 (5 cm^3). To this was added dropwise [PtClMe(1,5-COD)] (0.076 g, 0.215 mmol) in CH_2Cl_2 (5 cm^3). The solution was stirred for 1 h at room temperature. The solvent was then removed *in vacuo* to leave a cream solid that was triturated with pentane to give a white solid (0.117 g, 0.170 mmol, 79%).

Data:

δ_P (121 MHz; $CDCl_3$)	37.6 (d, J_{PP} 35.8 Hz, J_{PtP} 4011.9 Hz, trans to Cl), 56.7 (d, J_{PP} 35.8 Hz, J_{PtP} 1364.9 Hz, cis to Cl)
δ_H (400 MHz; $CDCl_3$)	7.83 – 7.37 (20H, m, Ar*H*), 3.02 – 2.98 (2H, m, CH_2), 2.86 – 2.95 (2H, m, CH_2), 2.79 (3H, s, CH_3), 0.44 (3H, dd, J_{PH} 8.3 Hz, J_{PH} 2.9 Hz, J_{PtP} *ca.* 62 Hz, CH_3)
EI mass spectrum: *m/z*	674 (M^+ - CH_3)
Elemental analysis % (calc: $C_{28}H_{30}ClNOP_2Pt$)	C; 48.94 (48.81) H: 4.47 (4.39) N: 2.02 (2.03)

5.3.9 Synthesis of $[PtClMe(C_6H_5)_2PN(CH_2CH_2CH_2OCH_3)P(C_6H_5)_2]$ (3.9)

To a 50 cm^3 round bottomed Schlenk tube was added (**2.10**) (0.080 g, 0.175 mmol) in CH_2Cl_2 (5 cm^3). To this was added dropwise [PtClMe(1,5-COD)] (0.059 g, 0.166 mmol) in CH_2Cl_2 (5 cm^3). The solution was stirred for 1 h at room temperature. The solvent was then removed *in vacuo* to leave a cream solid, which was triturated with pentane to give a white solid (0.074 g, 0.105 mmol, 63%).

Data:

δ_P (121 MHz; CD_2Cl_2)	36.3 (d, J_{PP} 34.9 Hz, J_{PtP} 4018.5 Hz, trans to Cl), 55.9 (d, J_{PP} 34.9 Hz, J_{PtP} 1361.2 Hz, cis to Cl)
δ_H (400 MHz; CD_2Cl_2)	7.79 – 7.50 (20H, m, Ar*H*), 3.03 (3H, s, CH_3), 2.98 – 2.92 (2H, m, CH_2), 2.90 (2H, t, J_{HH} 5.6 Hz, CH_2), 1.32 – 1.25 (2H, m, CH_2), 0.46 (3H, dd, J_{PH} 8.3 Hz, J_{PH} 3.2 Hz, J_{PtP} *ca.* 61 Hz, CH_3)
EI mass spectrum: *m/z*	688 (M^+ - CH_3)
Elemental analysis % (calc: $C_{29}H_{32}ClNOP_2Pt$)	C: 49.27 (49.54) H: 4.52 (4.59) N: 1.96 (1.99)

5.3.10 Synthesis of $[PtClMe(C_6H_5)_2PN(CH_2(2\text{-}OCH_3)C_6H_4)P(C_6H_5)_2]$ (3.10)

To a 50 cm^3 round bottomed Schlenk tube was added (**2.11**) (0.102 g, 0.202 mmol) in CH_2Cl_2 (5 cm^3). To this was added dropwise [PtClMe(1,5-COD)] (0.068 g, 0.192 mmol) in CH_2Cl_2 (5 cm^3). The solution was stirred for 1 h at room temperature. The solvent was then removed *in vacuo* to leave a cream solid, which was triturated with pentane to give a white solid (0.095 g, 0.126 mmol, 66%).

Data:

δ_P (121 MHz; $CDCl_3$)	37.4 (d, J_{PP} 35.4 Hz, J_{PtP} 4004.5 Hz, trans

	to Cl), 57.0 (d, J_{PP} 35.4 Hz, J_{PtP} 1378.9 Hz, cis to Cl)
δ_H (400 MHz; $CDCl_3$)	7.90 – 7.34 (20H, m, Ar*H*), 6.43 – 6.26 (4H, m, Ar*H*), 4.12 (2H, dd, J_{PH} 8.6 Hz, J_{PH} 10.8 Hz, CH_2), 3.25 (3H, s, CH_3), 0.38 (3H, dd, J_{PH} 3.2 Hz, J_{PH} 8.6 Hz, J_{PtH} *ca.* 60 Hz)
CI mass spectrum: *m/z*	736 (M^+ - CH_3)
Elemental analysis % (calc: $C_{33}H_{32}ClNOP_2Pt$)	C: 52.24 (52.77) H: 5.20 (4.29) N: 2.24 (1.86)

5.3.11 Synthesis of $[PdCl_2(C_6H_5)_2PN(CH_2CH_2OCH_3)P(C_6H_5)_2]$ (3.11)

To a 50 cm^3 round bottomed Schlenk tube was added (**2.9**) (0.050 g, 0.123 mmol) in CH_2Cl_2 (2 cm^3). To this was added dropwise $[PdCl_2(NCPh)_2]$ (0.041 g, 0.107 mmol) in CH_2Cl_2 (2 cm^3). The solution was stirred over 1 h at room temperature. The solvent was then removed *in vacuo* and the product was triturated with pentane and recrystallised using CH_2Cl_2 and Et_2O to give a yellow solid (0.022 g, 0.035 mmol, 33%).

Data:

δ_P (121 MHz; CD_2Cl_2)	32.6 (s)
δ_H (400 MHz; CD_2Cl_2)	7.98 – 7.57 (20H, m, Ar*H*), 3.13 – 3.10 (2H, m, CH_2), 3.08 – 3.02 (2H, m, CH_2), 2.81 (3H, s, CH_3)
ESI mass spectrum: *m/z*	(M^+ - Cl) 586.0
Elemental analysis % (calc: $C_{27}H_{27}Cl_2NOP_2Pd$)	C: 51.67 (52.24) H: 4.39 (4.38) N: 2.33 (2.26)

Crystallographic data for (**3.11**): $C_{27}H_{27}Cl_2NOP_2Pd$, M = 620.74, monoclinic, space group *P2(1)/c*, a = 9.400(11), b = 14.599(18), c = 18.850(2) Å, V = 2585(5) $Å^3$, Z = 4, T

= 173(2) K, μ = 1.070 mm^{-1}, 5944 independent reflections, R_{int} = 0.1633, R_1 = 0.0859, wR_2 = 0.1914.

5.3.12 Synthesis of $[PdCl_2(C_6H_5)_2PN(CH_2CH_2CH_2OCH_3)P(C_6H_5)_2]$ (3.12)

To a 50 cm^3 round bottomed Schlenk tube was added (**2.10**) (0.100 g, 0.219 mmol) in CH_2Cl_2 (3 cm^3). To this was added dropwise $[PdCl_2(NCPh)_2]$ (0.080 g, 0.208 mmol) in CH_2Cl_2 (3 cm^3). The solution was stirred for 1 h at room temperature. The solvent was then removed *in vacuo* and the product was triturated with pentane and recrystallised using CH_2Cl_2 and Et_2O to give a yellow solid (0.051 g, 0.080 mmol, 39%).

Data:

δ_P (121 MHz; CD_2Cl_2)	31.2 (s)
δ_H (400 MHz; CD_2Cl_2)	7.97 – 7.58 (20H, m, Ar*H*), 3.21 – 3.10 (2H, m, CH_2), 3.03 (3H, s, CH_3), 2.92 (2H, t, J_{HH} 5.6 Hz, CH_2), 1.37 – 1.30 (2H, m, CH_2)
ESI mass spectrum: *m/z*	(M^+ - Cl) 599.8
Elemental analysis % (calc: $C_{28}H_{29}Cl_2NOP_2Pd$)	C: 52.63 (52.98) H: 4.76 (4.60) N: 2.28 (2.21)

Crystallographic data for (**3.12**): $C_{28}H_{29}Cl_2NOP_2Pd$, M = 634.76, monoclinic, space group *P2(1)/c*, a = 9.468(17), b = 14.250(3), c = 20.607(4) Å, V = 2772.3(9) Å^3, Z = 4, T = 173(2) K, μ = 1.000 mm^{-1}, 6343 independent reflections, R_{int} = 0.0472, R_1 = 0.0341, wR_2 = 0.0736.

5.3.13 Synthesis of $[PdCl_2(C_6H_5)_2PN(CH_2(2\text{-}OCH_3)C_6H_4)P(C_6H_5)_2]$ (3.13)

To a 50 cm^3 round bottomed Schlenk tube was added (**2.11**) (0.100 g, 0.198 mmol) in CH_2Cl_2 (3 cm^3). To this was added dropwise $[PdCl_2(NCPh)_2]$ (0.072 g, 0.188 mmol) in CH_2Cl_2 (3 cm^3). The solution was stirred for 1 h at room temperature. The solvent was then removed *in vacuo* to leave an orange solid, which was triturated with pentane and recrystallised using CH_2Cl_2 and Et_2O to give a yellow solid (0.073 g, 0.107 mmol, 57%).

Data:

δ_P (121 MHz; CD_2Cl_2)	33.3 (s)
δ_H (400 MHz; CD_2Cl_2)	7.84 – 7.50 (20H, m, Ar*H*), 6.54 – 6.32 (4H, m, Ar*H*), 4.29 (2H, J_{PH} 10.0 Hz, CH_2), 3.19 (3H, s, CH_3)
EI/CI mass spectrum: *m/z*	(M^+ - Cl) 647.7
Elemental analysis % (calc: $C_{32}H_{29}Cl_2NOP_2Pd$)	C: 55.94 (56.28) H: 4.04 (4.28) N: 1.96 (2.05)

Crystallographic data for (**3.13**): $C_{32}H_{29}Cl_2NOP_2Pd$, M = 682.80, monoclinic, space group *P2(1)/n*, a = 11.617(2), b = 17.321(4), c = 15.305(3) Å, V = 2943.7(10) $Å^3$, Z = 4, T = 173(2) K, μ = 0.948 mm^{-1}, 6746 independent reflections, R_{int} = 0.0710, R_1 = 0.0327, wR_2 = 0.0631.

5.3.14 Attempted Synthesis of $[PtClMe\ (2\text{-}CF_3C_6H_4)_2PN(Me)P(2\text{-}CF_3C_6H_4)_2]$

To a 50 cm^3 round bottomed Schlenk tube was added [PtClMe(1,5-COD)] (0.025 g, 0.0709 mmol) and CH_2Cl_2 (2 cm^3) and the mixture left to stir. To this was added dropwise (**2.12**) (0.050 g, 0.0744 mmol) in CH_2Cl_2 (3 cm^3). The solution was stirred for 2 d at room temperature with $^{31}P\{^1H\}$ NMR monitoring. An insoluble solid crashed out suspected to be a polymer.

5.3.15 Synthesis of $[PdCl_2(2\text{-}CF_3C_6H_4)_2PN(Me)P(2\text{-}CF_3C_6H_4)_2]$ (3.14)

To a 50 cm^3 round bottomed Schlenk tube was added $[PdCl_2(NCPh)_2]$ (0.025 g, 0.0652 mmol) and CH_2Cl_2 (3 cm^3) and the mixture left to stir. To this was added dropwise **(2.12)** (0.046 g, 0.0685 mmol) dissolved in CH_2Cl_2 (3 cm^3). The solution was stirred for 2 d at room temperature and a yellow solid crashed out. The excess solvent was removed *in vacuo* to leave a cream solid which was triturated with pentane to give an off-white sparingly soluble solid (0.025 g, 0.0293 mmol, 45%).

Data:

δ_P (121 MHz; $CDCl_3$)	45.3 (m)
δ_H (400 MHz; $CDCl_3$)	7.72 – 7.13 (16H, m, Ar*H*), 2.57 (3H, t, J_{CP} 2.4 Hz, CH_3)
FAB mass spectrum: *m/z*	811 (M^+ - Cl), 671 (M^+ - $PdCl_2$)
Elemental analysis % (calc: $C_{29}H_{19}Cl_2F_{12}NP_2Pd$)	C: 41.39 (41.04) H: 2.36 (2.26) N: 1.55 (1.65)

5.3.16 Synthesis of $[PtCl_2(2\text{-}ClC_6H_4)_2PN(Me)P(2\text{-}ClC_6H_4)_2]$ (3.15)

To a 50 cm^3 round bottomed Schlenk tube was added **(2.13)** (0.200 g, 0.372 mmol) in CH_2Cl_2 (5 cm^3). To this was added dropwise $[PtCl_2(1,5\text{-COD})]$ (0.133 g, 0.355 mmol) in CH_2Cl_2 (5 cm^3). The solution was stirred for 2 h at room temperature. The solvent was then removed *in vacuo* to leave a cream solid, which was triturated with pentane, to give an off-white solid (0.121 g, 0.151 mmol, 42%).

Data:

δ_P (121 MHz; CD_2Cl_2)	42.8 (s, J_{PtP} 4100.3 Hz)
δ_H (400 MHz; CD_2Cl_2)	7.77 – 7.29 (16H, m, Ar*H*), 1.35 (3H, t, J_{PH} 7.3 Hz, CH_3)
CI mass spectrum: *m/z*	803 (M^+)
Elemental analysis % (calc:	C: 37.00 (37.39) H: 1.50 (2.38) N: 2.01

$C_{25}H_{19}Cl_6NP_2Pt$) (1.74)

5.3.17 Synthesis of [$PtMe_2(2\text{-}ClC_6H_4)_2PN(Me)P(2\text{-}ClC_6H_4)_2$] (3.16)

To a 50 cm^3 round bottomed Schlenk tube was added (**2.13**) (0.012 g, 0.0223 mmol) in CH_2Cl_2 (2 cm^3). To this was added dropwise [$PtMe_2$(1,5-COD)] (0.007 g, 0.0213 mmol) in CH_2Cl_2 (2 cm^3). The solution was stirred for 1 h at room temperature. The solvent was then removed *in vacuo* to leave a cream solid, which was triturated with pentane, to give an off-white solid (0.005 g, 0.007 mmol, 32%).

Data:

δ_P (121 MHz; CD_2Cl_2)	65.8 (s, J_{PtP} 2124.1 Hz)
δ_H (400 MHz; CD_2Cl_2)	7.48 – 7.13 (16H, m, Ar*H*), 1.30 (3H, t, J_{PH} 8.0 Hz, CH_3) 0.41 (6H, m, J_{PtH} 72.0 Hz)

5.3.18 Synthesis of [$PtCl_2$((*R*)-1,1′-bi-2-naphthoxo)PN(Me)P((*R*)-1,1′-bi-2-naphthoxo)] (3.17)

To a 50 cm^3 round bottomed Schlenk tube was added (**2.15**) (0.075 g, 0.114 mmol) in CH_2Cl_2 (3 cm^3). To this was added dropwise [$PtCl_2$(1,5-COD)] (0.0.041 g, 0.108 mmol) in CH_2Cl_2 (3 cm^3). The solution was for 1 h at room temperature. The solvent was then removed *in vacuo* to leave a cream solid, which was triturated with pentane, to give an off-white solid. The product was recrystallised from CH_2Cl_2 and Et_2O yielding a fine white powder (0.089 g, 0.0961 mmol, 89%).

Data:

δ_P (121 MHz; CD_2Cl_2)	51.1 (s, J_{PtP} 5125.7 Hz)
δ_H (400 MHz; CD_2Cl_2)	8.23 – 7.88 (8H, m, Ar*H*), 7.66 – 7.24

	(16H, m, Ar*H*), 2.08 (3H, t, J_{PH} 12.0 Hz, CH_3)
FAB mass spectrum: *m/z*	890(M^+ - Cl)

5.3.19 Synthesis of [$PtCl_2$((*S*)-9,9′-biphenanthryl-10,10′-dioxo)PN(Me)P((*S*)-9,9′-biphenanthryl-10,10′-dioxo)] (3.18)

To a 50 cm^3 round bottomed Schlenk tube was added (**2.16**) (0.050 g, 0.0581 mmol) in CH_2Cl_2 (2 cm^3). To this was added dropwise [$PtCl_2$(1,5-COD)] (0.021 g, 0.055 mmol) in CH_2Cl_2 (2 cm^3). The solution was stirred for 1 h at room temperature. The solvent was then removed *in vacuo* to leave a cream solid, which was triturated with pentane, to give a sparingly soluble white solid (0.017 g, 0.0151 mmol, 27%).

Data:

δ_P (121 MHz; CD_2Cl_2)	54.6 (s, J_{PtP} 5042.8 Hz)
δ_H (400 MHz; CD_2Cl_2)	8.99 – 8.36 (8H, m, Ar*H*), 8.11 – 6.33 (24H, m, Ar*H*), 1.76 (3H, br, CH_3)

5.4 Experimental details for Chapter 4

5.4.1 High throughput screening in a *Radleys GreenHouse* reactor at atmospheric ethylene pressure for ethylene polymerisation catalysis

In the glove box the metal precursor [$NiBr_2$(dme)] (2 mg, 0.0097 mmol) was massed into sample vials, to this was added the ligand (5 μmol) as a solution in toluene. The vials were then stirred and heated to 50 °C for 10 min, after which time MAO (200 eq, 4 ml solution in toluene) was added. The vials were subsequently massed. 24 filled

sample vials were then placed into the *GreenHouse* reactor, which was then closed and purged with ethylene outside the box. The reactor was left under atmospheric pressure of ethylene for 30 min. After this time the ethylene atmosphere was replaced by nitrogen by several pump-refill cycles, so terminating the run. The reactor was then transferred back into the glove box and sample vials remassed to determine polymer yield.

5.4.2 High throughput screening in an *Endeavor* reactor for ethylene polymerisation catalysis

In the glove box the metal precursor $NiBr_2dme$ (3.0 mg) was massed into schlenk tubes. To this was added the ligand to form a solution of the catalyst (1.25 mM in toluene). This catalyst solution was then heated with stirring to 50 °C for 45 min. The *Endeavor* reactor was set up and the eight vials massed prior to assembly. To this sealed system was initially added MAO (4 ml, 200 eq), this was then followed by the catalyst solution (4 ml) and toluene (4 ml). Each of the eight reaction vessels then contained 0.2 μmol catalyst solution and 100 μmol (200 eq) MAO. Each reactor vessel was then heated to 50 °C and ethylene added at a pressure according to the reaction conditions. A pressure of hydrogen gas was also added to some of the reaction vessels. The ethylene was added for 30 min and its uptake continually monitored, after 30 min or 17 mmol uptake of ethylene the reactors were depressurised. To each vial was then added 1 ml of a solution of nonane (0.5 mmol in methanol) and the sample sent for GC analysis. The remaining sample was allowed to dry in air and any polymer produced then massed and sent for analysis.

5.4.3 High throughput screening in an *Endeavor* reactor for ethylene trimerisation catalysis

In the glove box solutions of the catalyst were prepared by dissolving the ligands in a solution of the (*o*-tolyl)$CrCl_2.THF_3$ metal precursor in toluene to produce a 5mM solution of catalyst. The *Endeavor* reactor was set up and the eight reaction vessels massed prior to assembly. To this sealed system was initially added MAO (0.4 ml, 300 eq in toluene) to each reactor followed by TEAL (0.2 eq), the catalyst solution (0.4 ml) and toluene (0.6 ml). Each reactor vessel was then heated to 80 °C and ethylene added at a pressure according to the reaction conditions. A pressure of hydrogen gas was also added to some of the reaction vessels. The ethylene was added for 30 min and its uptake continually monitored, after 30 min or 17 mmol uptake of ethylene the reactors were depressurised. To each vial was then added 1 ml of a solution of nonane (0.5 mmol in methanol) and the sample sent for GC analysis. The remaining sample was allowed to dry in air and any polymer produced then massed and sent for analysis.

Appendices

A1. Crystal data and structure refinement for (2.9)

The author carried out this crystal structure determination under the supervision of Dr. J. Charmant.

Identification code	lillya	
Empirical formula	C27 H27 N O P2	
Formula weight	443.44	
Temperature	173(2) K	
Wavelength	0.71073 Å	
Crystal system	Monoclinic	
Space group	P2(1)/n	
Unit cell dimensions	a = 13.9163(17) Å	α = 90°
	b = 10.1858(10) Å	β = 108.311(8)°
	c = 17.453(2) Å	γ = 90°
Volume	2348.6(5) $Å^3$	
Z	4	
Density (calculated)	1.254 Mg/m^3	
Absorption coefficient	0.204 mm^{-1}	
F(000)	936	
Crystal size	1.20 x 0.70 x 0.30 mm	
θ range for data collection	1.64 to 27.47°	
Index ranges	-18<=h<=12, -13<=k<=9, -22<=l<=22	
Reflections collected	11517	
Independent reflections	5373 [R_{int} = 0.0282]	
Completeness to θ = 27.47°	99.8 %	
Absorption correction	Semi-empirical from equivalents	
Max. and min. transmission	0.940 and 0.769	
Refinement method	Full-matrix least-squares on F^2	
Data / restraints / parameters	5373 / 0 / 281	
Goodness-of-fit on F^2	S = 1.040	
R indices [for 4073 reflections with I>2σ (I)]	R_1 = 0.0389, wR_2 = 0.0905	
R indices (for all 5373 data)	R_1 = 0.0596, wR_2 = 0.0982	
Weighting scheme	$w^{-1} = \sigma^2(F_o^2) + (aP)^2 + (bP)$, where $P = [\max(F_o^2, 0) + 2F_c^2]/3$ a = 0.0435, b = 0.5149	
Largest diff. peak and hole	0.401 and -0.257 $eÅ^{-3}$	

A2. Crystal data and structure refinement for (2.10)

The author carried out this crystal structure determination under the supervision of Dr. J. Charmant.

Identification code	primrose	
Empirical formula	C28 H29 N O P2	
Formula weight	457.46	
Temperature	173(2) K	
Wavelength	0.71073 Å	
Crystal system	Orthorhombic	
Space group	P2(1)2(1)2(1)	
Unit cell dimensions	a = 9.303(3) Å	α = 90.000(3)°
	b = 9.712(4) Å	β = 90.000(18)°
	c = 26.806(10) Å	γ = 90.000(3)°
Volume	2421.8(15) $Å^3$	
Z	4	
Density (calculated)	1.255 Mg/m^3	
Absorption coefficient	0.200 mm^{-1}	
F(000)	968	
Crystal size	0.20 x 0.15 x 0.05 mm	
θ range for data collection	1.52 to 27.48°	
Index ranges	-12<=h<=12, -9<=k<=12, -34<=l<=34	
Reflections collected	17407	
Independent reflections	5550 [R_{int} = 0.1033]	
Completeness to θ = 27.48°	100.0 %	
Absorption correction	None	
Refinement method	Full-matrix least-squares on F^2	
Data / restraints / parameters	5550 / 0 / 401	
Goodness-of-fit on F^2	S = 0.861	
R indices [for 4003 reflections with I>2σ (I)]	R_1 = 0.0653, wR_2 = 0.1045	
R indices (for all 5550 data)	R_1 = 0.0946, wR_2 = 0.1160	
Weighting scheme	$w^{-1} = \sigma^2(F_o^2) + (aP)^2 + (bP)$, where $P = [\max(F_o^2, 0) + 2F_c^2]/3$	
	a = 0.0071, b = 0.0000	
Absolute structure (Flack) parameter	0.02(13)	
Largest diff. peak and hole	0.451 and -0.305 eÅ^{-3}	

A3. Crystal data and structure refinement for (2.12)

K. Heslop carried out this crystal structure determination under the supervision of Prof. A. G. Orpen.

Identification code	Sherlock (pca)	
Empirical formula	C29 H19 F12 N P2	
Formula weight	671.39	
Temperature	173(2) K	
Wavelength	0.71073 Å	
Crystal system	Orthorhombic	
Space group	Pca2(1)	
Unit cell dimensions	a = 22.226(5) Å	α = 90.000(5)°
	b = 11.806(2) Å	β = 90.000(6)°
	c = 21.415(7) Å	γ = 90.000(7)°
Volume	5619(2) $Å^3$	
Z	8	
Density (calculated)	1.587 Mg/m^3	
Absorption coefficient	0.257 mm^{-1}	
F(000)	2704	
Crystal size	0.01 x 0.05 x 0.30 mm	
θ range for data collection	1.72 to 27.50°	
Index ranges	-28<=h<=27, -11<=k<=15, -24<=l<=27	
Reflections collected	35412	
Independent reflections	12123 [R_{int} = 0.1706]	
Completeness to θ = 27.60°	99.9 %	
Absorption correction	Multiscan	
Refinement method	Full-matrix least-squares on F^2	
Data / restraints / parameters	12123 / 1 / 796	
Goodness-of-fit on F^2	S = 0.995	
R indices [for 2563 reflections with I>2σ (I)]	R_1 = 0.0727, wR_2 = 0.1415	
R indices (for all 5980 data)	R_1 = 0.2221, wR_2 = 0.1983	
Weighting scheme	$w^{-1} = \sigma^2(F_o^2) + (aP)^2 + (bP)$, where $P = [\max(F_o^2, 0) + 2F_c^2]/3$	
	a = 0.07820, b = 0.0000	
Largest diff. peak and hole	0.533 and –0.440 $eÅ^{-3}$	

A4. Crystal data and structure refinement for (2.17).2(CH_2Cl_2)

The author carried out this crystal structure determination under the supervision of Dr. J. Charmant.

Identification code	bluebell	
Empirical formula	C58.50 H36.50 Cl4.50 N O4 P2	
Formula weight	1038.85	
Temperature	173(2) K	
Wavelength	0.71073 Å	
Crystal system	Triclinic	
Space group	P-1	
Unit cell dimensions	a = 12.232(2) Å	α = 88.34(3)°
	b = 17.076(3) Å	β = 83.82(3)°
	c = 23.848(5) Å	γ = 73.65(3)°
Volume	4751.7(16) $Å^3$	
Z	4	
Density (calculated)	1.452 Mg/m^3	
Absorption coefficient	0.397 mm^{-1}	
F(000)	2132	
Crystal size	0.20 x 0.15 x 0.15 mm	
θrange for data collection	0.86 to 27.48°	
Index ranges	-15<=h<=15, -21<=k<=22, -30<=l<=30	
Reflections collected	54925	
Independent reflections	21719 [R_{int} = 0.2026]	
Completeness to θ = 27.48°	99.7 %	
Absorption correction	Multiscan	
Refinement method	Full-matrix least-squares on F^2	
Data / restraints / parameters	21719 / 0 / 1263	
Goodness-of-fit on F^2	S = 0.663	
R indices [for 6074 reflections with I>2σ (I)]	R_1 = 0.0842, wR_2 = 0.2113	
R indices (for all 21719 data)	R_1 = 0.2293, wR_2 = 0.2888	
Weighting scheme	$w^{-1} = \sigma^2(F_o^2) + (aP)^2 + (bP)$, where $P = [\max(F_o^2, 0) + 2F_c^2]/3$	
	a = 0.0626, b = 0.0000	
Largest diff. peak and hole	1.836 and -1.211 $eÅ^{-3}$	

A5. Crystal data and structure refinement for (3.2x)

A. Baber carried out this crystal structure determination under the supervision of Prof. A. G. Orpen. In view of the large difference in map residuals and the disorder in the Me/Cl site further refinement or repeat data collection is desirable.

Identification code	josh	
Empirical formula	C30 H32 Cl2 P2 Pt	
Formula weight	720.51	
Temperature	173(2) K	
Wavelength	0.71073 Å	
Crystal system	Triclinic	
Space group	P-1	
Unit cell dimensions	a = 8.533(3) Å	α = 69.179(7)°
	b = 18.090(7) Å	β = 83.689(7)°
	c = 20.059(8) Å	γ = 77.853(7)°
Volume	2827.2(19) $Å^3$	
Z	2	
Density (calculated)	1.693 Mg/m^3	
Absorption coefficient	5.283 mm^{-1}	
F(000)	1416	
Crystal size	0.2 x 0.18 x 0.15 mm	
θ range for data collection	1.33 to 27.53°	
Index ranges	-11<=h<=10, -23<=k<=23, -25<=l<=26	
Reflections collected	29849	
Independent reflections	12863 [R_{int} = 0.2670]	
Completeness to θ = 27.53°	98.7 %	
Absorption correction	None	
Refinement method	Full-matrix least-squares on F^2	
Data / restraints / parameters	12863 / 0 / 631	
Goodness-of-fit on F^2	S = 0.947	
R indices [for 5995 reflections with I>2σ (I)]	R_1 = 0.0834, wR_2 = 0.2072	
R indices (for all 12863 data)	R_1 = 0.1727, wR_2 = 0.2612	
Weighting scheme	$w^{-1} = \sigma^2(F_o^2) + (aP)^2 + (bP)$, where $P = [\max(F_o^2, 0) + 2F_c^2]/3$ a =0.0920, b = 0.0000	
Largest diff. peak and hole	2.799 and -5.348 $eÅ^{-3}$	

A6. Crystal data and structure refinement for (3.3)

K. Heslop carried out this crystal structure determination under the supervision of Prof. A. G. Orpen.

Identification code	malmo (sad)	
Empirical formula	C32 H37 Cl P2 Pt	
Formula weight	714.10	
Temperature	173(2) K	
Wavelength	0.71073 Å	
Crystal system	Monoclinic	
Space group	Pc	
Unit cell dimensions	a = 11.711(2) Å	α = 90°
	b = 9.1413(16) Å	β = 108.901(3)°
	c = 14.144(3) Å	γ = 90°
Volume	1432.6(4) $Å^3$	
Z	2	
Density (calculated)	1.655 Mg/m^3	
Absorption coefficient	5.122 mm^{-1}	
F(000)	708	
Crystal size	0.20 x 0.20 x 0.05 mm	
θ range for data collection	1.84 to 27.47°	
Index ranges	-15<=h<=13, -11<=k<=11, -15<=l<=18	
Reflections collected	9003	
Independent reflections	4832 [R_{int} = 0.0539]	
Completeness to θ = 27.47°	99.4 %	
Absorption correction	None	
Refinement method	Full-matrix least-squares on F^2	
Data / restraints / parameters	4832 / 62 / 283	
Goodness-of-fit on F^2	S = 0.952	
R indices [for 3688 reflections with I>2σ (I)]	R_1 = 0.0409, wR_2 = 0.0714	
R indices (for all 4832 data)	R_1 = 0.0678, wR_2 = 0.0781	
Weighting scheme	$w^{-1} = \sigma^2(F_o^2) + (aP)^2 + (bP)$, where $P = [\max(F_o^2, 0) + 2F_c^2]/3$ a = 0.0298, b = 0.0000	
Absolute structure (Flack) parameter	0.58(2)	
Largest diff. peak and hole	1.012 and -1.096 $eÅ^{-3}$	

A7. Crystal data and structure refinement for (3.4x)

The author carried out this crystal structure determination under the supervision of Dr. J. Charmant. In view of the large difference in map residuals and the disorder in the Me/Cl site further refinement or repeat data collection is desirable.

Identification code	gerbraa	
Empirical formula	C25 H23 Cl2 N P2 Pt	
Formula weight	665.39	
Temperature	173(2) K	
Wavelength	0.71073 Å	
Crystal system	Monoclinic	
Space group	P2(1)/n	
Unit cell dimensions	a = 9.3152(3) Å	α = 90°
	b = 13.9550(5) Å	β = 91.828(10)°
	c = 19.1979(7) Å	γ = 90°
Volume	2494.33(15) $Å^3$	
Z	4	
Density (calculated)	1.717 Mg/m^3	
Absorption coefficient	5.875 mm^{-1}	
F(000)	1256	
Crystal size	0.25 x 0.20 x 0.15 mm	
θ range for data collection	1.80 to 27.54°	
Index ranges	-12<=h<=10, -18<=k<=15, -24<=l<=19	
Reflections collected	15864	
Independent reflections	5702 [R_{int} = 0.0227]	
Completeness to θ = 27.54°	99.2 %	
Absorption correction	None	
Refinement method	Full-matrix least-squares on F^2	
Data / restraints / parameters	5702 / 0 / 280	
Goodness-of-fit on F^2	S = 0.598	
R indices [for 5008 reflections with I>2σ (I)]	R_1 = 0.0297, wR_2 = 0.0899	
R indices (for all 5702 data)	R_1 = 0.0360, wR_2 = 0.1018	
Weighting scheme	$w^{-1} = \sigma^2(F_o^2) + (aP)^2 + (bP)$, where $P = [\max(F_o^2, 0) + 2F_c^2]/3$	
	a = 0.0370, b = 0.0000	
Largest diff. peak and hole	0.821 and -1.944 $eÅ^{-3}$	

A8. Crystal data and structure refinement for (3.5)

The author carried out this crystal structure determination under the supervision of Dr. J. Charmant. In view of the large difference in map residuals further refinement or repeat data collection is desirable.

Identification code	geranium	
Empirical formula	C27 H28 Cl N P2 Pt	
Formula weight	658.98	
Temperature	173(2) K	
Wavelength	0.71073 Å	
Crystal system	Monoclinic	
Space group	P2(1)/c	
Unit cell dimensions	a = 9.8576(17) Å	α = 90°
	b = 9.4691(19) Å	β = 91.2°
	c = 27.948(6) Å	γ = 90°
Volume	2608.7(9) $Å^3$	
Z	4	
Density (calculated)	1.678 Mg/m^3	
Absorption coefficient	5.619 mm^{-1}	
F(000)	1288	
Crystal size	0.03 x 0.04 x 0.25 mm	
θ range for data collection	1.46 to 27.60°	
Index ranges	-11<=h<=12, -12<=k<=11, -36<=l<=29	
Reflections collected	16734	
Independent reflections	5980 [R_{int} = 0.2043]	
Completeness to θ = 27.60°	98.8 %	
Absorption correction	Multiscan	
Refinement method	Full-matrix least-squares on F^2	
Data / restraints / parameters	5980 / 0 / 291	
Goodness-of-fit on F^2	S = 0.890	
R indices [for 2563 reflections with I>2σ (I)]	R_1 = 0.0681, wR_2 = 0.1363	
R indices (for all 5980 data)	R_1 = 0.1984, wR_2 = 0.1741	
Weighting scheme	$w^{-1} = \sigma^2(F_o^2) + (aP)^2 + (bP)$, where $P = [\max(F_o^2, 0) + 2F_c^2]/3$	
Largest diff. peak and hole	4.091 and -1.898 $eÅ^{-3}$	

A9. Crystal data and structure refinement for (3.6x)

The author carried out this crystal structure determination under the supervision of Dr. J. Charmant. In view of the large difference in map residuals and the disorder in the Me/Cl site further refinement or repeat data collection is desirable.

Identification code	snowdrop	
Empirical formula	C27 H27 Cl2 N P2 Pt	
Formula weight	693.44	
Temperature	173(2) K	
Wavelength	0.71073 Å	
Crystal system	Monoclinic	
Space group	P2(1)/n	
Unit cell dimensions	a = 10.653(16) Å	α = 90°
	b = 18.69(4) Å	β = 96.92(15)°
	c = 12.93(2) Å	γ = 90°
Volume	2554(8) $Å^3$	
Z	4	
Density (calculated)	1.750 Mg/m^3	
Absorption coefficient	5.740 mm^{-1}	
F(000)	1320	
Crystal size	0.10 x 0.10 x 0.02 mm	
θ range for data collection	1.93 to 27.48°	
Index ranges	-13<=h<=13, -24<=k<=18, -16<=l<=14	
Reflections collected	17531	
Independent reflections	5856 [R_{int} = 0.0913]	
Completeness to θ = 27.48°	100.0 %	
Absorption correction	Multiscan	
Max. and min. transmission	1.000 and 0.723301	
Refinement method	Full-matrix least-squares on F^2	
Data / restraints / parameters	5856 / 0 / 134	
Goodness-of-fit on F^2	S = 0.896	
R indices [for 3676 reflections with I>2σ (I)]	R_1 = 0.0552, wR_2 = 0.1137	
R indices (for all 5856 data)	R_1 = 0.0963, wR_2 = 0.1227	
Weighting scheme	$w^{-1} = \sigma^2(F_o^2) + (aP)^2 + (bP)$, where $P = [\max(F_o^2, 0) + 2F_c^2]/3$	
	a = 0.0466, b = 0.0000	
Largest diff. peak and hole	3.482 and -3.627 $eÅ^{-3}$	

A10. Crystal data and structure refinement for (3.7x)

A. Baber carried out this crystal structure determination under the supervision of Prof. A. G. Orpen. In view of the large difference in map residuals and the disorder in the Me/Cl site further refinement or repeat data collection is desirable.

Identification code	cml27	
Empirical formula	C54 H54 Cl4 N2 P4 Pt2	
Formula weight	1386.85	
Temperature	173(2) K	
Wavelength	0.71073 Å	
Crystal system	Monoclinic	
Space group	P2(1)/c	
Unit cell dimensions	a = 20.382(3) Å	α = 90°
	b = 16.868(3) Å	β = 89.990(3)°
	c = 14.996(2) Å	γ = 90°
Volume	5155.8(13) $Å^3$	
Z	4	
Density (calculated)	1.787 Mg/m^3	
Absorption coefficient	5.791 mm^{-1}	
F(000)	2704	
Crystal size	0.15 x 0.08 x 0.04 mm	
θ range for data collection	1.57 to 27.51°	
Index ranges	-26<=h<=26, -21<=k<=21, -18<=l<=19	
Reflections collected	49014	
Independent reflections	11829 [R_{int} = 0.1180]	
Completeness to θ = 27.51°	99.7 %	
Absorption correction	None	
Refinement method	Full-matrix least-squares on F^2	
Data / restraints / parameters	11829 / 0 / 599	
Goodness-of-fit on F^2	S = 1.034	
R indices [for 7672 reflections with I>2σ (I)]	R_1 = 0.0406, wR_2 = 0.1107	
R indices (for all 11829 data)	R_1 = 0.0724, wR_2 = 0.1240	
Weighting scheme	$w^{-1} = \sigma^2(F_o^2) + (aP)^2 + (bP)$, where $P = [\max(F_o^2, 0) + 2F_c^2]/3$	
	a = 0.0543, b = 0.0000	
Largest diff. peak and hole	1.904 and -2.723 $eÅ^{-3}$	

A11. Crystal data and structure refinement for (3.11)

The author carried out this crystal structure determination under the supervision of Dr. J. Charmant. In view of the large difference in map residuals further refinement or repeat data collection is desirable.

Identification code	sunflower	
Empirical formula	C27 H27 Cl2 N O P2 Pd	
Formula weight	620.74	
Temperature	173(2) K	
Wavelength	0.71073 Å	
Crystal system	Monoclinic	
Space group	P2(1)/c	
Unit cell dimensions	a = 9.400(11) Å	α = 90°
	b = 14.599(18) Å	β = 91.53(2)°
	c = 18.85(2) Å	γ = 90°
Volume	2585(5) $Å^3$	
Z	4	
Density (calculated)	1.595 Mg/m^3	
Absorption coefficient	1.070 mm^{-1}	
F(000)	1256	
Crystal size	0.22 x 0.20 x 0.05 mm	
θ range for data collection	1.76 to 27.64°	
Index ranges	-12<=h<=6, -17<=k<=18, -24<=l<=24	
Reflections collected	15920	
Independent reflections	5944 [R_{int} = 0.1633]	
Completeness to θ = 27.64°	98.7 %	
Absorption correction	Multiscan	
Max. and min. transmission	1.000 and 0.625018	
Refinement method	Full-matrix least-squares on F^2	
Data / restraints / parameters	5944 / 0 / 308	
Goodness-of-fit on F^2	S = 0.981	
R indices [for 2688 reflections with I>2σ (I)]	R_1 = 0.0859, wR_2 = 0.1914	
R indices (for all 5944 data)	R_1 = 0.2072, wR_2 = 0.2446	
Weighting scheme	$w^{-1} = \sigma^2(F_o^2) + (aP)^2 + (bP)$, where $P = [\max(F_o^2, 0) + 2F_c^2]/3$	
	a = 0.1164, b = 0.0000	
Largest diff. peak and hole	2.248 and -1.534 $eÅ^{-3}$	

A12. Crystal data and structure refinement for (3.12)

The author carried out this crystal structure determination under the supervision of Dr. J. Charmant.

Identification code	hollyhock	
Empirical formula	C28 H29 Cl2 N O P2 Pd	
Formula weight	634.76	
Temperature	173(2) K	
Wavelength	0.71073 Å	
Crystal system	Monoclinic	
Space group	P2(1)/c	
Unit cell dimensions	a = 9.4675(17) Å	α = 90°
	b = 14.250(3) Å	β = 94.266(4)°
	c = 20.607(4) Å	γ = 90°
Volume	2772.3(9) $Å^3$	
Z	4	
Density (calculated)	1.521 Mg/m^3	
Absorption coefficient	1.000 mm^{-1}	
F(000)	1288	
Crystal size	0.25 x 0.12 x 0.10 mm	
θ range for data collection	1.74 to 27,51°	
Index ranges	-9<=h<=12, -17<=k<=18, -26<=l<=26	
Reflections collected	17771	
Independent reflections	6343 [R_{int} = 0.0472]	
Completeness to θ = 27.51°	99.3 %	
Absorption correction	Multiscan	
Max. and min. transmission	1.000 and 0.000	
Refinement method	Full-matrix least-squares on F^2	
Data / restraints / parameters	6343 / 0 / 428	
Goodness-of-fit on F^2	S = 0.961	
R indices [for 4607 reflections with I>2σ (I)]	R_1 = 0.0341, wR_2 = 0.0736	
R indices (for all 6343 data)	R_1 = 0.0628, wR_2 = 0.0842	
Weighting scheme	$w^{-1} = \sigma^2(F_o^2) + (aP)^2 + (bP)$, where $P = [\max(F_o^2, 0) + 2F_c^2]/3$	
	a = 0.0362, b = 0.0299	
Largest diff. peak and hole	0.666 and -0.531 $eÅ^{-3}$	

A13. Crystal data and structure refinement for (3.13)

The author carried out this crystal structure determination under the supervision of Dr. J. Charmant.

Identification code	crocus	
Empirical formula	C32 H29 Cl2 N O P2 Pd	
Formula weight	682.80	
Temperature	173(2) K	
Wavelength	0.71073 Å	
Crystal system	Monoclinic	
Space group	P2(1)/n	
Unit cell dimensions	a = 11.617(2) Å	α = 90°
	b = 17.321(4) Å	β = 107.09(3)°
	c = 15.305(3) Å	γ = 90°
Volume	2943.7(10) $Å^3$	
Z	4	
Density (calculated)	1.541 Mg/m^3	
Absorption coefficient	0.948 mm^{-1}	
F(000)	1384	
Crystal size	0.15 x 0.10 x 0.07 mm	
θ range for data collection	1.82 to 27.48°	
Index ranges	-14<=h<=15, -19<=k<=22, -19<=l<=14	
Reflections collected	20801	
Independent reflections	6746 [R_{int} = 0.0710]	
Completeness to θ = 27.48°	100.0 %	
Absorption correction	Multiscan	
Max. and min. transmission	1.000 and 0.000	
Refinement method	Full-matrix least-squares on F^2	
Data / restraints / parameters	6746 / 0 / 353	
Goodness-of-fit on F^2	S = 0.846	
R indices [for 4860 reflections with I>2σ (I)]	R_1 = 0.0327, wR_2 = 0.0631	
R indices (for all 6746 data)	R_1 = 0.0500, wR_2 = 0.0662	
Weighting scheme	$w^{-1} = \sigma^2(F_o^2) + (aP)^2 + (bP)$, where $P = [\max(F_o^2, 0) + 2F_c^2]/3$ a = 0.0133, b = 0.0000	
Largest diff. peak and hole	0.730 and -1.111 $eÅ^{-3}$	

References

References

1. R. J. Puddephatt, *Chem. Soc. Rev.*, 1983, 99
2. R. B. King, *Acc. Chem. Res.*, 1980, 243
3. R. Keat, L. M. Muir, K. W. Muir and D. S. Rycroft, *J. Chem. Soc., Dalton Trans.*, 1981, 2192
4. J. F. Nixon, *J. Chem. Soc.*, 1968, 2689
5. G. Ewart, A. P. Lane, J. McKechnie and D. S. Payne, *J. Chem. Soc.*, 1964, 1543
6. R. J. Cross, T. H. Green and R. Keat, *J. Chem. Soc., Dalton Trans.*, 1976, 1424
7. V. S. Reddy and K. V. Katti, *Inorg. Chem.*, 1994, **33**, 2698
8. V. S. Reddy, K. V. Katti and C. L. Barnes, *Inorg. Chem.*, 1995, **34**, 5483
9. Z. Fei, R. Scopelliti and P. J. Dyson, *J. Chem. Soc., Dalton Trans.*, 2003, 2772
10. M. R. I. Zubiri, H. L. Milton, D. J. Cole-Hamilton, A. M. Z. Slawin and J. D. Woollins, *Polyhedron*, 2004, **23**, 693
11. M. T. Reetz, S. R. Waldvogel, R. Goddard, *Tetrahedron Lett.*, 1997, **38**, 5967
12. S. M. Aucott, M. L. Clarke, A. M. Z. Slawin and J. D. Woollins, *J. Chem. Soc., Dalton Trans.*, 2001, 972
13. H. Noeth and L. Meinel, *Z. Anorg. Allg. Chem.*, 1967, **349**, 225
14. J. Ellermann, E. F. Hohenberger, W. Kehr, A. Purzer and G. Thiele, *Z. Anorg. Allg. Chem.*, 1980, **464**, 45
15. J. Ellermann and L. Mader, *Z. Naturforsch. Teil B*, 1980, **356**, 307
16. R. Uson, J. Fornies, R. Navarro, M. Tomas, C. Fortuno, J. I. Cebollada and A. J. Welch, *Polyhedron*, 1989, **8**, 1045
17. I. Bachert, I. Bartusseck, P. Braunstein, E. Guillon, J, Rose and G. Kickelbick, *J. Org. Chem.*, 1999, **580**, 257
18. I. Bachert, P. Braunstein, M. K. McCart, F. Fabrizi de Biani, F. Laschi, P. Zanello, G. Kickelbick and U. Schubert, *J. Org. Chem.*, 1999, **573**, 47

19. J. Ellermann and M. Lietz, *Z. Naturforsch. Teil B*, 1980, **35**, 64

20. P. Bhattacharyya and J. D. Woollins, *Polyhedron*, 1995, **14**, 3367

21. J. F. Nixon, *Chem. Comm.*, 1967, 669

22. R. Jefferson, J. F. Nixon, T. M. Painter, R. Keat and L. Stobbs, *J. Chem. Soc., Dalton Trans.*, 1973, 1414

23. Zh. K. Gorbatenko, I. T. Rozhdestvenskaya and N. G. Feshchenko, *Zh. Obshch. Khim.*, 1975, **45**, 2367

24. T. R. Johnson and J. F. Nixon, *J. Chem. Soc. A*, 1969, 2518

25. R. B. King and T. W. Lee, *Inorg. Chem.*, 1982, **21**, 319

26. M. S. Balakrishna, V. S. Reddy, S. S. Krishnamurthy, J. F. Nixon and J. C. T. R. Burkett St. Laurent, *Coord. Chem. Rev.*, 1994, **129**, 1

27. E. Hedberg, L. Hedberg and K. Hedberg, *J. Am. Chem. Soc.*, 1974, **96**, 4417

28. D. F. Clemens, M. L Caspar, D Rosenthal and R. Peluso, *Inorg. Chem.*, 1970, **9**, 960

29. W. Seidel and M. Alexiev, *Z. Anorg. Allg. Chem.*, 1978, **438**,68

30. W. Wiegrabe and H. Bock, *Chem. Ber.*, 1968, **101**, 1414

31. J. Ellermann and L. Mader, *Spectrochim. Acta. Part A*, 1981, **37**, 449

32. C. S. Browning, R. A. Burrow, D. H. Farrar and H. A. Mirza, *Inorg. Chim. Acta*, 1998, **27**, 112

33. C. S. Browning and D. H. Farrar, *J. Chem. Soc., Dalton Trans.*, 1995, 521

34. K. G. Gaw, M. S. Smith and A. M. Z. Slawin, *New J. Chem.*, 2000, **24**, 429

35. S. J. Dossett, A. Gillon, A. G. Orpen, J. S. Fleming, P. G. Pringle, D. F. Wass and M. D. Jones, *Chem. Commun.*, 2001, 699

36. E. Drent and P. H. M. Budzelaar, *Chem. Rev.*, 1996, **96**, 663

37. S. J. Dossett, *World Pat. Appl.*, 1997, 97/37765 (to BP Chemicals)

38. S. J. Dossett, *World Pat. Appl.*, 2000, 00/06299 (to BP Chemicals)

39. S. J. Dossett, J. S. Fleming and P. G. Pringle, *World Pat. Appl.*, 2000, 00/03803 (to BP Chemicals)

40. G. K. Barlow, J. D. Boyle, N. A. Cooley, T. Ghaffar and D. F. Wass, *Organometallics*, 2000, **19**, 1470

41. N. A. Cooley, S. M. Green, D. F. Wass, K. Heslop, A. G. Orpen and P. G. Pringle, *Organometallics*, 2001, **20**, 4769

42. G. J. P. Britovsek, V. C. Gibson, D. F. Wass, *Angew. Chem. Int. Ed.*, 1999, **38**, 429

43. S. D. Ittel, L. K. Johnson and M. Brookhart, *Chem. Rev.*, 2000, **100**, 1169

44. A. Hoehn, F. Lippert and E. Schauss, *World Pat. Appl.*, 1996, 96/37522 (to BASF)

45. M. Brookhart, J. Felgman, E. Hauptman and E. F. McCord, *World Pat. Appl.*, 1998, 98/47934 (to DuPont)

46. P. W. N. M. van Leeuwen, P. C. J. Kamer, J. N. H. Reek and P. Diekes, *Chem. Rev.*, 2000, **100**, 2741

47. E. Y. –X. Chen, T. J. Marks, *Chem. Rev.*, 2000, **100**, 1391

48. A. Carter, S. A. Cohen, N. A. Cooley, A. Murphy, J. Scutt and D. F. Wass, *Chem. Commun.*, 2002, 858

49. W. K. Reagen, T. M. Pettijohn and J. W. Freeman, *US Pat.*, 1996, US 5 523 507, (to Phillips Petroluem Company)

50. T. Agapie, S. J. Schofer, J. A. Labinger and J. E. Bercaw, *J. Am. Chem. Soc.*, 2004, **126**, 1304

51. T. Ohkuma, M. Kitamura and R. Noyori, *Catalytic Asymmetric Synthesis*, 2nd edn., VCH Publishers Inc., New York, 2000, 1

52. R. Halterman, *Comprehensive Asymmetric Catalysis*, Springer, Berlin, 1999, **1**, 183

53. W. S. Knowles and M. J. Sabacky, *Chem. Commun.*, 1968, 1445

54. W. S. Knowles, *Acc. Chem. Res.*, 1983, **16**, 106

55. L. Horner, H. Siegel and H. Büthe, *Angew. Chem. Int. Ed.*, 1968, **7**, 942

56. T. P. Dang and H. B. Kagan, *Chem. Commun.*, 1971, 481

57. H. B. Kagan and T. P. Dang, *J. Am. Chem. Soc.*, 1972, **94**, 6429

58. I. V. Komarov and A. Börner, *Angew. Chem. Int. Ed.*, 2001, **40**, 1197

59. W. Chen. J. Xiao, *Tetrahedron Lett.*, 2001, **42**, 2897

60. M. Ostermeier, J. Priess and G. Helmchen, *Angew. Chem. Int. Ed.*, 2002, **41**, 612

61. Q. Zeng, H. Liu, X. Cui, A. Mi, Y. Jiang, X. Li, M. C. K. Choi and A. S. C. Chan, *Tetrahedron: Asymmetry*, 2002, **13**, 115

62. K. Junge, G. Oehme, A. Monsees, T. Riermeier, U. Dinderdissed and M. Beller, *Tetrahedron Lett.*, 2002, **43**, 4977

63. C. Claver, E. Fernandez, A. Gillon, K. Heslop, D. J. Hyett, A. Martorell, A. G. Orpen and P. G. Pringle, *Chem. Commun.*, 2000, 961

64. M. T. Reetz and G. Mehler, *Angew. Chem. Int. Ed.*, 2000, **39**, 3889

65. R. Hulst, N. K. de Vries and B. L. Feringa, *Tetrahedron: Asymmetry*, 1994, **5**, 699

66. M. van den Berg, A. J. Minnaard, R. M. Haak, M. Leeman, E. P. Schudde, A. Meetsma, B. L. Feringa, A. H. M. de Vries. C. E. P. Maljaars, C. E. Willans, D. Hyett, J. A. F. Boogers, H. J. W. Henderickx and J. G. de Vries, *Adv. Synth. Catal.*, 2003, **345**, 308

67. C. E. Willans, J. M. C. A. Mulders, J. G. de Vries and A. H. M. de Vries, *J. Org. Chem.*, 2003, **687**, 494

68. A. H. M. de Vries, A. Meetsma and B. L. Feringa, *Angew. Chem. Int. Ed.*, 1996, **35**, 2374

69. A. van Rooy, D. Burgers, P. C. J. Kamer and P. W. N. M. van Leeuwen, *Recl. Trav. Chim. Pays-Bas*, 1996, **115**, 492

70. Y. H. Choi, J. H. Y. Choi, H. Y. Yang and Y. H. Kim, *Tetrahedron: Asymmetry*, 2002, **13**, 801

71. M. van den Berg, R. M. Haak, A. J. Minnaard, A. H. M. de Vries, J. G. de Vries and B. L. Feringa, *Adv. Synth. Catal.*, 2002, **9**, 344

72. X. Jia, R. Guo, X. Yao and A. S. C. Chan, *Tetrahedron Lett.*, 2002, **43**, 5541

73. A. W. van Ziji, L. A. Arnold, A. J. Minnaard and B. L. Feringa, *Adv. Synth. Catal.*, 2004, **346**, 413

74. C. G. Frost, J. Howarth and J. M. J. Williams, *Tetrahedron: Asymmetry*, 1992, **3**, 1089

75. B. M. Trost and D. L. van Vranken, *Chem. Rev.*, 1996, 395

76. B. M. Trost and M. L. Crawley, *Chem Rev.*, 2003, **103**, 2921

77. G. Helmchen, *J. Organomet. Chem.*, 1999, **576**, 203

78. R. M. Magid, *Tetrahedron*, 1980, **36**, 1901

79. B. Breit and P. Demel, *Modern Organocopper Chemistry*, Wiley-VCH, Weinheim, 2002, 210

80. A. S. E. Karlström and J. –E, Bäckvall, *Modern Organocopper Chemistry*, Wiley-VCH, Weinheim, 2002, 259

81. H. Malda, A. W. van Zijl, L. A. Arnold and B. L. Feringa, *Org. Lett.*, 2001, **3**, 1169

82. L. A. Arnold, R. Imbos, A. Mandoli, A. H. M de Vries, R. Naasz and B. L. Feringa, *Tetrahedron*, 2000, **56**, 2865

83. G. Calabrò, D. Drommi, G. Bruno and F. Faraone, *J. Chem. Soc., Dalton Trans.*, 2004, 81

84. D. F. Wass, *World Pat. Appl.*, 2002, 02/04119, (to BP Chemicals)

85. J. F. Nixon, *Chem. Commun.*, 1967, 669

86. A. A. Shvets, O. A. Moiseeva and O. A. Osipov, *Zh. Obshch. Khim.*, 1978. **48**, 232

87. T. S. Ventatakrishnan, M. Nethaji and S. S. Krishnamurthy, *Current Science*, 2003, **85**, 969

88. D. J. Hyett, Ph.D Thesis, University of Bristol, 1999

89. C. A. Tolman, *Chem. Rev.*, 1977, **77**, 313

90. P. Dierkes and P. W. N. M. van Leeuwen, *J. Chem. Soc., Dalton Trans.*, 1999, 1519

91. L. Deng, P. M. Margl and T. Ziegler, *J. Am. Chem. Soc.*, 1997, **119**, 1094

92. L. Deng, T. K. Woo, L. Cavallo, P. M. Margl and T. Ziegler, *J. Am. Chem. Soc.*, 1997, **119**, 6177

93. K. Zeigler, E. Holtzkamp, H. Breil and H. Martin, *Angew. Chem. Int. Ed.*, 1955, **67**, 541

94. G. Natta, *Angew. Chem.*, 1956, **68**, 393

95. M. Bochmann, *J. Chem. Soc., Dalton Trans.*, 1996, 255

96. L. L. Böhm, *Angew. Chem. Int. Ed.*, 2003, **42**, 5010

97. V. C. Gibson and D. F. Wass, *Chemistry in Britain*, 1999, 20

98. V. C. Gibson and S. K. Spitzmesser, *Chem, Rev.*, 2003, **103**, 283

99. L. K. Johnson, C. M. Killiam and M. Brookhart, *J. Am. Chem. Soc.*, 1995, **117**, 6414

100. V. C. Gibson, A. Tomov. D. F. Wass, A. J. P. White and D. J. Williams, *J. Chem. Soc., Dalton Trans.*, 2002, 2261

101. D. F. Wass, *World Pat. Appl.*, 2001, 01/10876, (to BP Chemicals)

102. T. R. Younkin, E. F. Connor, J. I. Henderson, S. K. Friedrich, R. H. Grubbs and D. A. Bansleben, *Science*, 2000, **287**, 460

103. P. J. Flory, *J. Am. Chem. Soc.*, 1936, 1877

104. P. J. Flory, *J. Am. Chem. Soc.*, 1940, **62**, 1561

105. G. V. Schulz, *Z. Phy. Chem. Abt. B.*, 1935, **30**, 379

106. G. V. Schulz, *Z. Phy. Chem. Abt. B.*, 1939, **43**, 25

107. J. Skupińska, *Chem. Rev.*, 1991, **91**, 613

108. W. Keim, R. F. Mason, H. C. Chung, P. Glockner, *US Pat.*, 1972, 3647914 (to Shell Oil Company)

109. W. Keim, B. Hoffmann, R. Lodewick, M. Peuckert, G. Schmitt, J. Fleischhauer and U. Meier, *J. Mol. Catal.*, 1979, **6**, 79

110. M. Peuckert and W. Keim, *J. Mol. Catal.*, 1984, **22**, 289

111. W. Keim, F. H. Kowaldt, R. Goddard and C. Krüger, *Angew. Chem. Int. Ed.*, 1978, **17**, 466

112. W. Keim, *Angew. Chem. Int. Ed.*, 1990, **29**, 235

113. W. Keim, A. Behr, B. Limbäcker and C. Krüger, *Angew. Chem. Int. Ed.*, 1983, **22**, 503

114. S. A. Svejda and M Brookhart, *Organometallics*, 1999, **18**, 65

115. C. M. Killian, L. K. Johnson and M. Brookhart, *Organometallics*, 1997, **16**, 2005

116. V. C. Gibson, C. M. Halliwell, N. J. Long, P. J. Oxford, A. M. Smith, A. J. P. White and D. J. Williams, *J. Chem. Soc., Dalton Trans.*, 2003, 918

117. K. Blann, J. T. Dixon, and D. de Wet-roos, *World Pat. Appl.*, 2004, 04/056480, (to Sasol Technology (PTY) Limited)

118. D. S. McGuinness, P. Wasserscheid, W. Keim, C. Hu, U. Englert, J. T. Dixon and C. Grove, *Chem. Commun.*, 2003, 334

119. D. S. McGuinness, P. Wasserscheid, W. Keim, D. Morgan, J. T. Dixon, A. Bollmann, H. Maumela, F. Hess and U. Englert, *J. Am. Chem. Soc.*, 2003, **125**, 5272

120 R. D. Köhn, M. Haufe, G. Kociok-Köhn, S. Grimm, P. Wasserscheid and W. Keim, *Angew. Chem. Int. Ed.*, 2000, **39**, 4337

120. J. R. Briggs, *Chem. Commun.*, 1989, 674

121. D. J. Temple, L. K. Johnson, R. L. Huff, P. S. White and M. Brookhart, *J. Am. Chem. Soc.*, 2000, **122**, 6686

122. G. J. P. Britovsek, S. Mastroianni, G. A. Solan, S. P. D. Baugh, C.

Redshaw, V. C. Gibson, A. J. P. White, D. J. Williams and M. R. J. Elsegood, *Chem. Eur. J.*, 2000, **6**, 2221

123. B. Cornils and W. A. Herrmann, *Applied Homogeneous Catalysis with Organometallic Compounds*, Wiley-VCH, Weinheim, Vol 1, 245

124. M. van Meurs and S. K. Spitzmesser, *Personal communication*

125. A. B. Pangborn, M. A. Giardello, R. H. Grubbs, R. K. Rosen and F. J. Timmers, *Organometallics*, 1996, **15**, 1518

126. J. X. McDermott, J. F. White and G. Whitesides, *J. Am. Chem. Soc.*, 1976, **98**, 6521

127. E. Costa, P. Pringle and M. Ravetz, *Inorg. Synth.*, 1997, **31**, 284

128. H. C. Clark and L. E. Manzer, *J. Organomet. Chem.*, 1973, 411

129. M. S. Kharasch, R. C. Seyler and F. R. Mayo, *J. Am. Chem. Soc.*, 1938, **60**, 882